TMEM67 is required for the maintenance of the perinuclear actin cap.

Submitted by Anastasia Toynbee to the University of Exeter
as a thesis for the degree of
Masters by Research in Biological Sciences
in September 2018.

Signature……

Acknowledgements

Huge thanks must go firstly to the Dawe and Jourdain groups for teaching me everything I know in the lab. In particular to Lauren Adams and Connor Horton for not only their help in the lab, but also for the ongoing moral support and coffee runs. Additionally, thanks to the previous Dawe lab members Ben Meadows, Amy Barker and Kat Curry upon who's hard work this thesis was built. Isabelle Jourdain is thanked for providing the GFP-TMEM67 plasmids, as well as all her support as my second supervisor. Finally, Helen, thank you for being an incredibly supportive supervisor, not only throughout my Master's, but throughout all my time at Exeter. Thank you also for being incredibly patient as I wrote this thesis at a frustratingly slow pace.

Thanks must also go to the rest of the 211 lab, especially Sam for keeping everything going so smoothly, Tina for keeping me entertained in the hours spent locked away in the cell culture room, and Andy for always keeping everyone laughing. Thanks also to the Harmer lab for their loan of the SnapGene software, and the Chilton lab for their input on the results at lab meetings.

The results in this thesis would not be possible without Colin Johnson who provided the MKS cell lines studied, Kate Heesom for running the mass spectrometry for the GFP-Trap® data, the Exeter Bioimaging team, Christian and Ana, for preparing the SEM samples and teaching me how to use the microscope, and Konrad Engel, at the University of Rostock for kindly sharing the FilaQuant software used in this thesis.

Lastly, enormous gratitude goes to my family, Mum, Dad, Robb and Jess for never-ending support and providing home comforts when they were sorely needed, and to Adam for his many, many, many hours spent proofreading, making cups of tea, and listening to me go on and on about cilia and questioning what it all means. You've been a saint.

Abstract

Meckel-Gruber syndrome (MKS) is a genetically heterogeneous disease characterised by the phenotypic triad of occipital encephalocele, polycystic kidneys, and polydactyly. MKS is classified as a ciliopathy as mutations to the MKS proteins result in dysfunction to the primary cilium. Recent research has expanded the aetiology of MKS, as increasing evidence for non-ciliary roles for the MKS proteins are uncovered. Evidence includes their presence at focal adhesions and a role in controlling extracellular matrix (ECM) morphology. The relative contributions of ciliary and non-ciliary cellular phenotypes to the clinical presentations of MKS are not currently known. This thesis identifies ECM-dependent aberrations to the perinuclear actin cap in MKS patient cells lacking the MKS type 3 transmembrane protein TMEM67, likely contributing to migration defects previously identified in patient cells. Furthermore, GFP-Trap analysis identifies a number of myosins as potential binding partners of TMEM67; a previously unreported association. Analysis of these binding partners reports the top biological processes for TMEM67 as myosin-motor activity and actin-based movement, adding to the potential non-ciliary roles of the protein already reported. By expanding our understanding of the role of ciliopathy proteins outside of the cilium, we better comprehend the aetiology of the diseases, providing an opportunity to find new therapeutic interventions.

Table of Contents

List of tables

List of illustrations

Abbreviations

ACAFA	Actin cap-associated focal adhesion
BBS	Bardet-Biedl Syndrome
CNS	Central Nervous System
ECM	Extracellular matrix
IFT	Intraflagellar Transport
JBTS	Joubert Syndrome
LINC	Linker of Nucleoskeleton and Cytoskeleton
MKS	Meckel Gruber Syndrome
NPHP	Nephronophthisis

1 Introduction

1.1 Ciliopathies: rare disorders of human development

The cilium is a highly conserved, microtubule-based organelle found on almost all cells in the human body. There are two types of cilium: motile and primary, the latter on which this thesis focuses (Mitchison and Valente, 2017). Reflective of their wide distribution throughout the body, defects in motile and primary cilia have a broad spectrum of effects. Defects in cilium formation or function cause a recognizable cluster of syndromes called ciliopathies (Hildebrandt *et al.*, 2011).

The link between defects in motile cilia at the cellular level and patients' resulting clinical presentation is straightforward: in humans, motile cilia are required for sperm motility and for generating fluid flow in a number of tissues, including in the respiratory tract, the fallopian tubes, and within the ventricular system (Mitchison and Valente, 2017). Patients with defects affecting the motility of cilia can therefore present with an inability to remove mucus from the lungs due to aberrant movement of cilia in the respiratory tract, as well infertility in men and women as a result of immotile sperm and aberrant fluid flow in the fallopian tubes, respectively. Situs inversus is also seen in about 50% of patients with mutations affecting motile cilia due to the importance of a motile cilium directing fluid flow and left-right asymmetry in the node during embryonic development (Leigh *et al.*, 2009). Loss of cilium motility is the key factor in the pathogenicity of ciliopathies stemming from defects in motile cilia, and thus the cellular basis of disease is clear.

Conversely, mutations in proteins comprising the primary cilia have a much more convoluted link to phenotype of primary ciliopathies for a few reasons. Firstly, there is large phenotypic overlap across the primary ciliopathies (Table 1.1).

Table 1.1 The phenotypic overlap of ciliopathies (Gerdes *et al.,* 2009; Norris and Grimes, 2012; GARD, 2018). '✓' represents that the phenotype is frequently reported. Due to universal lethality in MKS syndrome, usually during early embryonic development, '?' denotes phenotypes which may be present but cannot be established as they would develop during later developmental stages.

	MKS	BBS	JBTS	Jeune	NPHP	OFD	LCA	SLS	Alström	COACH
Cleft palate	✓									
Skeletal dysplasia	✓			✓		✓				✓
Situs inversus	✓	✓	✓		✓	✓		✓		
Retinopathy	?	✓	✓	✓	✓		✓	✓	✓	
Polydactyly	✓	✓	✓	✓		✓				
Obesity	?	✓	✓						✓	
Cognitive defects	?	✓	✓		✓	✓	✓			✓
Renal disease	✓	✓	✓	✓	✓	✓		✓		
Hepatic disease	✓	✓	✓	✓	✓	✓		✓		✓
Encephalocele	✓									
Cerebellar hypoplasia		✓	✓		✓					✓
Deafness	?								✓	

MKS = Meckel Gruber Syndrome, BBS = Bardet Biedl Syndrome, JBTS = Joubert Syndrome, NPHP = Nephronophthisis, OFD = Orofaciodigital Syndrome, LCA = Leber Congenital Amaurosis, SLS = Sjögren-Larsson Syndrome.

This broad spectrum of phenotypes in primary ciliopathies is reflective of the primary cilium's wide expression throughout the body: virtually every cell type in the human body has a primary cilium at some stage of its cell cycle (Malicki and Johnson, 2017). The primary cilium also has a number of different functions and thus mutation can affect many cellular processes. The cilium is often referred to as the cell's antenna due to its multi-faceted role sensing both mechanical and chemical stimuli (Singla and Reiter, 2006). In addition to these sensory roles, the primary cilium also has a vital role regulating a number of key signalling pathways in development (reviewed in detail in Malicki and Johnson, 2017; Wheway *et al.*, 2018). Thus, dysfunction or malformation of the primary cilium has far ranging, and often severe developmental consequences. The second difficulty in linking the pathogenic mutation to phenotype in primary ciliopathies is the fact that mutations in the same gene can result in clinically distinct diseases. It has been suggested that the type and location of mutation in the gene could determine the ciliopathy, and that the mutational load across the ciliary proteome could contribute to the reduced penetrance and clinical variability of the ciliopathies (Iannicelli *et al.*, 2010; Novarino *et al.*, 2011). For example, mutations in *TMEM67* have been linked to Meckel Gruber Syndrome (MKS; Smith *et al.*, 2006), Joubert Syndrome (JBTS; Baala *et al.*, 2007), Nephronophthisis (NPHP; Otto *et al.*, 2009), and COACH (Brancati *et al.*, 2009). Studies have linked missense mutations falling between exons 8 to 15 of *TMEM67* with MKS, especially when in conjunction with a truncating mutation, whereas mutations in other parts of the gene have been linked more closely

to JBTS (Iannicelli *et al.*, 2010). *TMEM67* can also act as a modifier to the clinical presentation of Bardet-Biedl Syndrome (BBS; Leitch *et al.*, 2008).

The third difficulty in linking genotype to phenotype in primary ciliopathies is the increasing evidence of extraciliary roles of primary ciliopathy proteins. This will be the primary focus of this thesis and will be discussed in detail later.

1.2 MKS is a lethal ciliopathy

The present study focuses on MKS. One of the most severe ciliopathies, MKS is universally lethal, usually during early embryonic development (Salonen, 1984). MKS is typically characterised by the phenotypic triad of polycystic kidneys (97.7% of cases), occipital encephalocele (83.8%), and polydactyly (typically post-axial; 87.3%), however, as summarised in Table 1.1, much wider phenotypic variability is seen (Barisic *et al.*, 2015). Additional phenotypes often observed include skeletal defects, hepatic fibrosis, cleft palate, abnormalities of the central nervous system, heart defects, and abnormal genitalia development (Fraser and Lytwyn, 1981; Salonen, 1984). The leading cause of death is pulmonary hypoplasia, but liver and kidney failure have also been reported (Kheir *et al.*, 2012).

MKS is autosomal recessive, and as such has variable incidence with higher incidence in regions were consanguineous marriage is commonplace. In Gujurat Indians the carrier rate is reported as 1 in 18, with 1 per 1300 births affected. In Belgians and

Bedouins in Kuwait, a carrier rate of 1 in 30 is reported, with 1 in 3,500 births affected (Parelkar *et al.*, 2013). Typical global statistics for MKS affected births are estimated between 1 in 9,000 and 1 in 140,000 (Salonen, 1984).

MKS is a genetically heterogeneous condition, with 14 causative genes identified at the time of writing this thesis; see Table 1.2 for full details.

Table 1.2 MKS causative genes. Gene name in bold refers to the commonly used protein name.

MKS locus	Gene name(s)	Identification of gene as MKS locus
MKS1	***MKS1*** *BBS13*	(Kyttälä *et al.*, 2006)
MKS2	***TMEM216*** *JBTS2* *CORS2*	(Valente *et al.*, 2010)
MKS3	***TMEM67*** *JBTS6* *NPHP11*	(Smith *et al.*, 2006)
MKS4	***CEP290*** *KIAA0373* *3H11AG* *JBTS5* *SLSN6* *LGA10* *BBS14* *NPHP6*	(Baala *et al.*, 2007)
MKS5	***RPGRIP1L*** *KIAA1005* *JBTS7* *NPHP8*	(Delous *et al.*, 2007)
MKS6	***CC2D2A*** *KIAA1345*	(Tallila *et al.*, 2008)
MKS7	***NPHP3***	(Bergmann *et al.*, 2008)

	NPH3 *RHPD*	
MKS8	***TCTN2*** *TECT2*	(Shaheen *et al.*, 2011)
MKS9	***B9D1*** *MKSR1*	(Hopp *et al.*, 2011)
MKS10	***B9D2*** *MKSR2*	(Dowdle *et al.*, 2011)
MKS11	***TMEM231*** *JBTS20*	(Shaheen *et al.*, 2013)
MKS12	***KIF14***	(Filges *et al.*, 2014)
MKS13	***TMEM107***	(Shaheen *et al.*, 2015)
n/a	***CSPP1***	(Shaheen *et al.*, 2014)

1.2.1 Genotype-phenotype relationships in MKS

There is very limited knowledge of genotype-phenotype correlations in MKS. As previously mentioned, the extensive phenotypic variability and genetic heterogeneity of MKS makes it difficult to link the underlying genetic mutation in patients to their clinical presentation. However, there are some observable patterns in genotype-phenotype correlation. While occipital encephalocele, polydactyly and polycystic kidneys are the most commonly observed malformations associated with MKS, forming the classic diagnostic triad, only occipital encephalocele and polycystic kidneys are near universally present: the incidence of polydactyly varies with mutation (Szymanska *et al.*, 2012). Polydactyly is rarely observed in *TMEM67* patients. Szymanska *et al.,* (2012) observed polydactyly in only 3/19 *TMEM67* patients: this was much lower than the incidence of polydactyly in *RPGRIP1L* and *CC2D2A* patients (n = 4/6). Conversely, polydactyly is a near-obligatory feature of *MKS1,* being

observed in 10/12 patients in a study by Khaddour *et al.*, (2007). Polydactyly stems from a disruption to the Hedgehog (Hh) signalling pathway during embryogenesis (Ehlen *et al.*, 2006). The variable presence of polydactyly in *TMEM67* patients, compared to the near obligatory presence in *MKS1* and other genotypes suggests that loss of *TMEM67* is less disruptive to the Hh pathway than other mutations. Central nervous system (CNS) malformations are also less frequent in *TMEM67* patients than in *MKS1* patients, with occipital encephalocele, bone dysplasia defects, cleft palate, and *situs* defects frequently associated with *MKS1* mutations (Consugar *et al.*, 2007; Khaddour *et al.*, 2007). *TMEM67* mutations are often associated with hepatic involvement (Brancati *et al.*, 2009; Otto *et al.*, 2009). While these patterns might help to narrow down the potential mutant genotype, providing a subset of genetic targets of interest, the phenotypes are still non-specific and thus genetic screening is required to confirm the mutation.

The wide range of phenotypes in MKS patients, and the lack of clear genotype-phenotype correlations led to the hypothesis that the presence of modifier alleles may be influencing disease presentation. Indeed, many modifiers have now been identified in MKS contributing to the wide and variable phenotypes observed in not just MKS, but all the ciliopathies. For example, it has been shown that *MKS1, TMEM67,* and *CEP290* have been shown to have epistatic effects on mutations in BBS (Leitch *et al.*, 2008).

1.3 The ciliary roles of MKS proteins

Most work on the biological function of MKS proteins thus far has focussed on their role in assembly and function of cilia.

1.3.1 Ciliogenesis

The primary cilium is a microtubule-based organelle, projecting from the apical cell surface. The 'back-bone' of the cilium, called the axoneme, consists of a ring of nine outer microtubule doublets, and functions as a scaffold for a number of protein complexes, in addition to acting as a "rail-road" for microtubule-based transport (in this context, known as intraflagellar transport (IFT; Rosenbaum and Witman, 2002).

Cilia are complex organelles, and their assembly is carried out in a series of highly regulated steps: a combination of cell cycle regulation, vesicle trafficking and IFT must be tightly controlled. Primary cilia are only found on cells in the quiescent state and are resorbed before the cells enter the S phase of the cell cycle (Avasthi and Marshall, 2012). It has been suggested that there is bidirectional crosstalk between the cell cycle and ciliogenesis, as cell lines with proliferation abnormalities (such as rapidly dividing cancer cells) often lack cilia, and cell lines with ciliary defects often have issues with cell division and cystogenesis (hence the presence of cystic kidneys caused by cells with IFT defects; Hassounah *et al.*, 2012; Hassounah *et al.*, 2013; Emoto *et al.*, 2014; Menzl *et al.*, 2014; Nobutani *et al.*, 2014)

The first step of ciliogenesis involves the docking of a centrosome to the membrane at the apical cell surface. In unciliated cells, the centrosome is usually attached to the nucleus at the centre of the cell. Centrosome migration to the apical cell surface is a two-step process. First, the centrosome moves around the nucleus until it is sitting at its apical surface. It has not been established whether the centrosome moves independently of the nucleus or remains attached and the nucleus itself rotates to orientate the centrosome. Once orientated correctly, the centrosome then migrates from the nucleus to the apical cell surface (Barker *et al.,* 2015).

In order to dock to the apical cell surface and support ciliogenesis, the mother centriole must undergo a maturation process, and acquire a number of distal and sub-distal appendages (Vorobjev and Chentsov, 1982). Maturation of the mother centriole occurs as a number of sequential protein recruitments and without these appendages, the centrosome migrates to the apical surface but cannot dock, as the appendages facilitate the association between the mother centriole and the ciliary vesicle (Sorokin, 1962; Garcia-Gonzalo and Reiter, 2012; Tanos *et al.*, 2013).

After association with the ciliary vesicle, the axoneme begins to extend from the mother centriole, bending the vesicle membrane. Through the translocation and fusion of secondary vesicles, the ciliary vesicle grows as the axoneme is extended, becoming the ‘ciliary sheath’. The sheath then fuses with the plasma membrane, thus externalising the primary cilium, and the once internal ciliary sheath becomes the

periciliary membrane (Sorokin, 1962). Extension of the axoneme from the mother centriole (termed the basal body when involved in ciliogenesis) is supported by IFT (Rosenbaum and Witman, 2002; Scholey, 2003).

1.3.2 All MKS proteins localise to the primary cilium

MKS was first reported by Johann Friedrich Meckel in 1822. It was first linked to ciliary dysfunction over 180 years later in 2006 when *MKS1*, encoding a component of the flagellar apparatus, and *TMEM67* were identified as causative genes (Kyttälä *et al.*, 2006; Smith *et al.*, 2006). Since this link was made, many further genes have been identified that cause MKS, all of which localise to the primary cilium. Mutation or loss of these genes results in aberrations to function or formation of the primary cilium.

1.3.3 The transition zone

Organelles are typically enclosed within their own lipid bilayer, creating unique compartments that are isolated from the cytosol. This allows functionally specialised processes to occur without the risk of affecting other cellular processes. Enclosure by membranes allows organelles to maintain a distinct complex of proteins that facilitates their unique function (Alberts *et al.*, 2002). The cilium however, as an extension of the cell membrane, is not fully enclosed in its own compartment. Thus, to allow the specialised function of the cilium, a ciliary gate is present at the bottom of the axoneme, which acts as a diffusion barrier, preventing the free migration of cytosolic

proteins into the cilium. The ciliary gate was first observed by transmission electron microscopy of cross sections of the cilium, and was observed to form during early ciliogenesis, before IFT extends the axoneme (Gibbons and Grimstone, 1960; Ringo, 1967). Two sub-regions comprise the ciliary gate: the transition zone and the transition fibres.

Transition fibres are involved in anchoring the basal body to the plasma membrane, and correspond to the distal appendages (Anderson, 1972). IFT52's localization to the transition fibres also suggests a role in the docking of IFT proteins and translocation of these and their associated motor proteins into the cilium (Deane *et al.*, 2001). It has been suggested that these fibres act as a pore complex, functioning as a selective barrier to diffusion, similar to the nuclear pore (Rosenbaum and Witman, 2002). The complete structure and composition of these fibres is still to be elucidated, as well as their complete function, and as such further proteins associated with the fibres, and by extension the primary cilium and its associated disorders are likely to be discovered.

The transition zone is characterised by Y-links and the ciliary necklace. While these fundamental structural components are conserved, the appearance of the transition zone can vary between species and even cell type (Fisch and Dupuis-Williams, 2011). Y-links, so called because of their shape, form an attachment between the ciliary membrane and the microtubule doublets (Gilula and Satir 1972). Until recently, the

proteins composing these Y-links, as well as their arrangement into the Y-shaped structure was not known. However, recent developments in super resolution microscopy have allowed the ultrastructure of this complex to be revealed (Yang *et al.*, 2015; Shi *et al.*, 2017).

Transition zone proteins can be split into the MKS/JTBS module and the NPHP module (Figure 1.1; Chih *et al.*, 2012; Dowdle *et al.*, 2011; Garcia-Gonzalo *et al.*, 2011; Sang *et al.*, 2011; Williams *et al.*, 2011). The MKS/JBTS module consists of the three tectonic proteins TCTN1, TCTN2 and TCTN3, the three B9 domain-containing proteins B9D1, B9D2, and MKS1, coiled-coil proteins CEP290, CC2D2A and AHI1, and the transmembrane proteins TMEM17, TMEM67, TMEM107, TMEM216 and TMEM231 (and possibly also TMEM237 and TMEM218; Chih *et al.,* 2012; Garcia-Gonzalo *et al.,* 2011; Sang *et al.,* 2011; Lambacher *et al.*, 2016; Roberson *et al.*, 2015; Garcia-Gonzalo and Reiter, 2017). The NPHP complex consists of the core complex NPHP1, NPHP4, and RPGRIP1L, with the remaining network of NPHP5, NPHP8, ATXN10, INVS, NEK8 variably associated at different times (Mollet *et al.*, 2005; Arts *et al.*, 2007; Sang *et al.,* 2011; Garcia-Gonzalo and Reiter, 2017). The NPHP complex is found close to the axoneme, with NPHP4 binding to the microtubule doublets (Mollet *et al.,* 2005; Garcia-Gonzalo and Reiter, 2017). The MKS/JBTS complex sits closer to the ciliary membrane, consistent with the presence of multiple transmembrane proteins in this cluster (Yang *et al.*, 2015; Garcia-Gonzalo and Reiter, 2017).

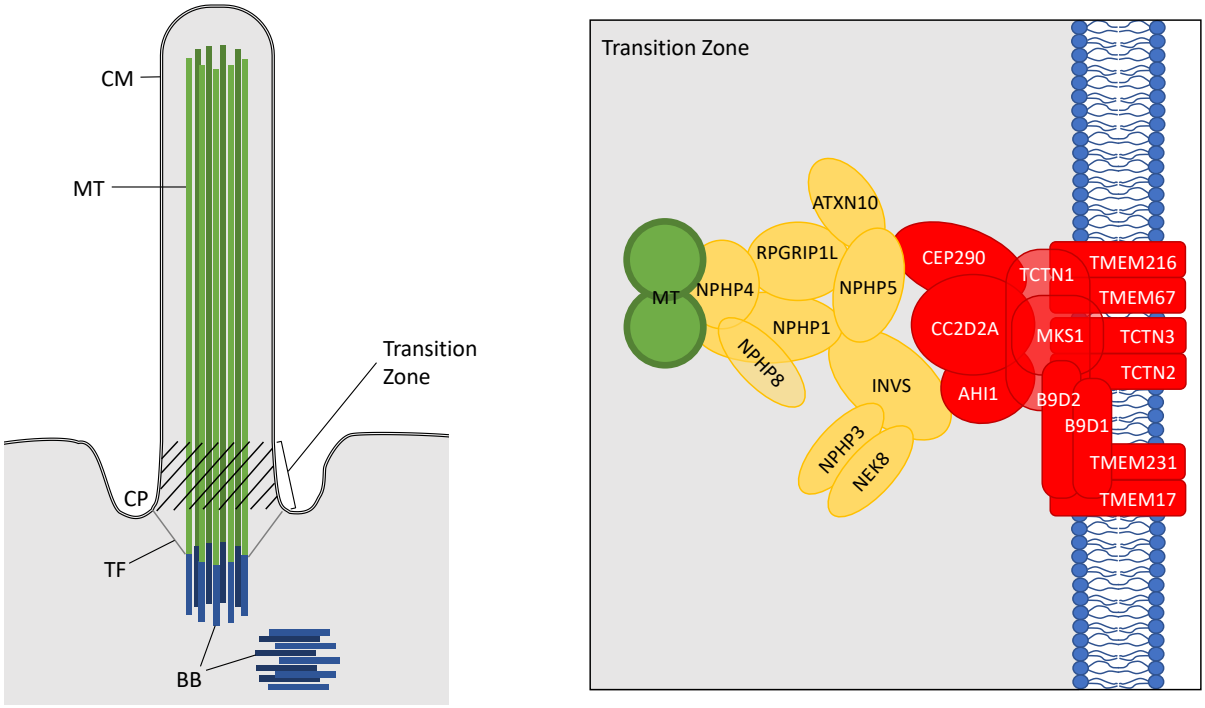

Figure 1.1 The transition zone is a complex of proteins, including the MKS/JTBS module (red) and the NPHP module (yellow). CM = ciliary membrane, MT = microtubule, CP = ciliary pocket, TF = transition fibre, BB = basal body.

CEP290, part of the MKS/JTBS complex, binds to other MKS proteins CC2D2A and TCTN1, but also binds NPHP protein NPHP5, forming a point of attachment between the two complexes. CEP290 is essential for the formation of the MKS module, and its loss results in a breakdown of the ultrastructure of the transition zone, and a leaky ciliary gate (Li *et al.*, 2016). CEP290 is localised to the transition zone by RPGRIP1L, which appears to be the key modulator of both NPHP and MKS/JTBS modules (Jensen *et al.*, 2015).

Most MKS proteins localize to the transition zone, however, mutations or loss of function in these proteins have varying phenotypic effects, often varying between species, and even cell type.

1.3.4 MKS proteins are required for ciliogenesis

A large number of studies have investigated MKS homologues and their effects on ciliogenesis, showing that MKS proteins are required for normal ciliogenesis to occur. Table 1.3 summarises the known localisation and roles of these proteins at the cilia.

Table 1.3 The ciliary localisation and roles of MKS proteins. TZ = transition zone; BB = basal body; AX = axoneme; CS = centriolar satellites

MKS protein	Localisation	Ciliary role
MKS1	BB TZ	Required for basal body docking and ciliogenesis (Dawe *et al.*, 2007b); component of the transition zone (Williams *et al.*, 2011); mediates Hedgehog and Wnt signalling (Wheway *et al.*, 2013; Goetz *et al.*, 2017).
TMEM216	AX BB TZ	Required for ciliogenesis through centrosome docking (Valente *et al.*, 2010); component of the transition zone (Williams *et al.,* 2011); modulates Wnt signalling through phosphorylation of Dishevelled (Valente *et al.,* 2010).
TMEM67	AX TZ	Regulates ciliary number (Tammachote *et al.*, 2009); required for centrosome migration to apical membrane and ciliogenesis (Dawe *et al.,* 2007b); component of the transition zone (Williams *et al.,* 2011); essential for phosphorylation of non-canonical Wnt receptor ROR2 (Abdelhamed *et al.*, 2015).

CEP290	BB CS TZ	Centrosomal protein involved in ciliary assembly and ciliary trafficking (Coppieters *et al.*, 2010); component of the transition zone (Williams *et al.,* 2011); required for normal Hedgehog signalling (Hynes *et al.*, 2014).
RPGRIP1L	AX BB TZ	Establishment of left/right asymmetry and patterning of neural tube and limbs (Vierkotten *et al.*, 2007); controls ciliary length (Gerhardt *et al.*, 2015); component of the transition zone (Williams *et al.,* 2011); controls ciliary proteasomal activity (Gerhardt *et al.,* 2015).
CC2D2A	BB TZ	Component of the transition zone (Williams *et al.,* 2011); essential for assembly of subdistal appendages (Veleri *et al.*, 2014); required for Hedgehog signalling (Chih *et al.*, 2012).
NPHP3	TZ	Required for normal ciliary development and function (Nauli *et al.*, 2003); inhibits disheveled-1-induced canonical Wnt signalling activity; may also function in the control of non-canonical Wnt signalling (Bergmann *et al.*, 2008).
TCTN2	AX BB TZ	Part of the tectonic-like complex of the transition zone (Garcia-Gonzalo *et al.*, 2011); required for Hedgehog signalling (Reiter and Skarnes, 2006).
B9D1	BB TZ	Part of the tectonic-like complex of the transition zone (Dowdle *et al.*, 2011); regulates ciliary length and number, but not essential for ciliogenesis (Roberson *et al.*, 2015); required for Hedgehog signalling (Chih *et al.,* 2012).
B9D2	TZ	Part of the tectonic-like complex of the transition zone (Williams *et al.,* 2011).
TMEM231	TZ	Part of the tectonic-like complex of the transition zone; regulates ciliary length and number, but not essential for ciliogenesis (Roberson *et al.,* 2015); required for Hedgehog signalling (Chih *et al.,* 2012).
KIF14	AX	Microtubule motor protein crucial for ciliogenesis and IFT (Scholey, 2008; Filges *et al.*, 2014).
TMEM107	TZ	Component of the transition zone; required for ciliogenesis and Hedgehog signalling (Shaheen *et al.*, 2015).

CSPP1	BB	Centrosome and spindle-pole associated protein; required for cilium formation and Hedgehog signalling; required for ciliary localisation of RPGRIP1L (Shaheen *et al.*, 2014).

In order for ciliogenesis to occur, the basal body must dock with the apical cell membrane; a process which requires the transition fibres. IFT must then extend the axoneme; a process requiring the effective compartmentalisation of the cilium. Thus, mutations in the MKS proteins which form the transition zone, and are essential for the compartmentalisation of the cilium, result in abnormal ciliogenesis.

The relationship between MKS proteins and ciliogenesis is not straight forward. Some of the published data are conflicting, thus making the elucidation of these proteins' properties complicated. Focusing on *TMEM67* as an example (as it is the gene of interest in this thesis), *in vitro* knockdown of the gene in mouse cell lines has been shown to result in a failure of the basal body to dock to the apical cell surface, and thus prevent ciliogenesis (Dawe *et al.,* 2007b; Valente *et al.,* 2010). However, in contrast to these cell culture studies, reduction of *TMEM67 in vivo* has shown no interference with basal body localisation: in the *Wpk* MKS type 3 rat, longer cilia have been observed in some cell types, as well as centriole overduplication and multiple cilia (Tammachote *et al.,* 2009). Furthermore, tissue-specific ciliogenesis defects have been reported, with fewer cilia in the kidney tubules of *TMEM67*-null mice and ciliogenesis defects in an inner medullary collecting duct (IMCD3) cell line with

TMEM67 knocked down. However, replicating this in mouse embryonic fibroblasts (MEF) resulted in no ciliogenesis defects, indicating tissue specific roles of TMEM67 in ciliogenesis (Garcia-Gonzalo *et al.*, 2011). These seemingly contradictory results are not singular to *TMEM67*: knockdown of *MKS1* in mouse cell lines has been shown to result in the failure of basal body docking (Dawe *et al.,* 2007b; Valente *et al.,* 2010), while an *in vivo* study in the *Mks1*^{krc} mutant mouse model reported normal apical localisation of basal bodies, and tissue-dependent defects to ciliogenesis, indicating that the ciliogenesis defect is not due to the failure of basal-body docking, but rather for the extension of the cilia (Weatherbee *et al.*, 2009). Tissue-specific roles of the MKS proteins provide one explanation for the conflicting reports of ciliogenesis in MKS mutants, however the presence of alternate pathways in ciliogenesis which have mediating or modifying effects *in vivo* could also contribute. Further research into these potential alternate pathways is required to unravel their contribution to ciliopathy.

In summary, many MKS proteins are required for ciliogenesis, and it is clear that their roles are tissue- or organism-specific, but the data are incomplete. In contrast, there is broad agreement that MKS proteins play key roles in regulating a major function of primary cilia: developmental signalling.

1.3.5 The primary cilium is a signalling hub during embryonic development

The primary cilium was first identified as an important regulator of vertebrate development when IFT machinery was linked to Hedgehog (Hh) signalling (Huangfu

et al., 2003). Since this discovery, a number of other important developmental pathways have been linked to the primary cilium, including the Wnt pathway.

The Hedgehog pathway

The Hh pathway is involved in determining cell fate and regulating tissue patterning during early development. There are three mammalian analogs of Hh: Sonic (Shh), Indian (Ihh), and Desert (Dhh). Hh signalling relies on the two transmembrane receptors, Patched1 (Ptch1) and Smoothened (Smo), and results in the activation of Gli transcription factors. In the absence of Hh signalling, Gli transcription factors are in their repressor form, and Ptch1 maintains Smo in its inactive state. When one of the Hh ligands binds to Ptch1, it translocates along the ciliary membrane, onto the membrane of the main body of the cell. Smo moves into the cilium, and this allows activation of Gli transcription factors and their translocation to the nucleus (Briscoe and Thérond, 2013; Nozawa *et al.*, 2013; Rimkus *et al.*, 2016).

The Hh pathway is one of the key regulators of mammalian development, and disruptions to Hh signalling can give rise to severe developmental abnormalities (Briscoe and Thérond, 2013). Between the three Hh homologues, Shh plays the most critical role, being involved in the patterning of multiple systems during development, including the brain midline, limb bud, spinal cord, thalamus, lungs and teeth. During the development of the limb bud, the concentration of Shh is responsible for the patterning of digits, whereby the amount of Shh and the timing of exposure during

development specifies digit identity (Briscoe and Thérond, 2013). In humans, the gradient of Shh decreases from the posterior to anterior side of the limb bud: from the little finger down to the thumb (which develops independently of Shh). An absence of Shh therefore results in only the digit on the farthest anterior position developing (the thumb in humans), as this is the only Shh-independent digit (Ehlen *et al.*, 2006). Conversely, the overexpression of Shh results in polydactyly: the presence of extra digits.

Hh signalling is dependent on the effective compartmentalisation of the primary cilium and the function of the transition zone. It thus follows that mutation to the transition zone results in phenotypes indicative of affected Hh signalling, for example the polydactyly and CNS malformations observed in MKS. As summarised above in Table 1.3, many of the MKS proteins are required for Hh signalling due to their role at the transition zone.

The Wnt pathway

The Wnt pathway is involved in cell fate determination and body axis patterning during development. Wnt proteins activate three different pathways (although there is overlap between all): one canonical pathway, and two non-canonical pathways (the planar cell polarity (PCP) pathway, and the Wnt/calcium pathway; Nusse and Clevers, 2017). All three pathways are instigated by the binding of a Wnt ligand to a Frizzled receptor but culminate in different actions: the canonical pathway regulates gene transcription, the

PCP pathway regulates the cytoskeleton, while the Wnt/Calcium pathway regulates the amount of intracellular calcium (Yu *et al.*, 2012; Dijksterhuis *et al.*, 2015). Intracellular calcium levels are important regulators of proteins such as cdc42, essential for ventral patterning, and cell morphology and migration.

The Wnt pathway was originally linked with cilia when the PCP proteins Inversin and Dishevelled were identified at the basal body, followed by the discovery that the knockdown of a number of other ciliary-associated genes resulted in hyperactivated canonical Wnt signalling (Otto *et al.*, 2003; Watanabe *et al.*, 2003; Simons *et al.*, 2005). However, there have also been several studies disputing the link between cilia and the Wnt pathways: normal Wnt signalling has been reported in zebrafish *ift88* mutants lacking cilia, and loss of primary cilia or defects in retrograde IFT did not have any effect on the response of mouse embryos to Wnt ligands (Huang and Schier, 2009; Ocbina *et al.*, 2009).

It has been suggested that these seemingly conflicting results could be due to spatio-temporal differences in Wnt signalling throughout development, but also tissue-specific function and localisation of proteins (Wallingford and Mitchell, 2011). In addition, May-Simera and Kelley, (2012) suggested that the cilia-independent Wnt responsiveness reported by Huang and Schier (2009) and Ocbina *et al.* (2009) could be explained if the basal body and transition zone were key modulators of Wnt

signalling. While the cilia could be absent, if the basal body and surrounding structures remained intact, this could allow a degree of Wnt signalling to continue.

1.3.6 Defects in the transition zone result in aberrant signalling

As covered above, the transition zone consists of a complex of the MKS proteins and is required in order to allow the specialisation of the cilium. The transition zone functions like a selective sieve at the base of the cilium, preventing the movement of unwanted proteins from the cell body into the cilium, as well as having roles in recruiting and trafficking proteins destined for the cilium into the organelle. Mutations in transition zone proteins can therefore have profound consequences on the cilium-dependent signalling pathways. For example, the transition zone protein TCTN2 (mutations in which result in MKS type 8) is required for the targeting of Smo to the primary cilium in a tissue-specific manner (Garcia-Gonzalo *et al.,* 2011). Knockdown of *Tctn2* in mouse studies resulted in a tissue-dependent reduction in Smo and thus a reduction in the levels of Hh activity (Garcia-Gonzalo *et al.*, 2011; Sang *et al.*, 2011). MKS protein B9D1 is also essential for Smo localisation to the cilia (Dowdle *et al.,* 2011; Garcia-Gonzalo *et al.,* 2011). It is not known whether an interaction between Smo and the transition zone facilitates its entry to the cilium, but it is apparent that the transition zone is important for the regulation of Hh signalling. Furthermore, as transition zone components are recruited in a series of hierarchical steps, mutation in core transition zone-assembling proteins can have knock on effects on signalling

pathways (which the individual protein may not have on its own). For example, RPGRIP1L has been reported to be the key transition zone protein, which is required for the localisation of all other transition zone proteins (Huang *et al.*, 2011; Williams *et al.*, 2011). Thus, mutation to RPGRIP1L would result in aberrant Hh signalling due to the subsequent loss of TCTN2 and B9D1 at the transition zone. This hierarchical recruitment suggests how mutations in different transition zone proteins can result in overlapping phenotypes.

1.4 The non-ciliary roles of MKS proteins

The ciliopathies have significant overlap in both clinical presentation (see Table 1.1) and cellular basis: mutations in different genes result in different disorders with similar phenotypes as all mutations affect the same organelle – the primary cilium. However, as the ciliopathies are all clinically distinct conditions, the question arises of how does ciliary dysfunction result in so many different diseases?

As touched on earlier, the identity of the mutated gene and the function of the affected protein is a leading factor: for example complete loss of cilium formation versus impairment of a specific ciliary pathway receptor will have varying degrees of impact on development. A second factor is the mutational load of ciliopathy genes and the presence of modifying alleles, which both affect clinical presentation (Iannicelli *et al.*, 2010; Novarino *et al.*, 2011). A third factor, and the factor that this thesis investigates, is the extra-ciliary role of ciliopathy proteins, and how these contribute to pathogenicity.

Increasingly, non-ciliary roles of ciliopathy proteins are being identified. Cilia are known to have a role in cell-cycle control, as they sequester the centrosome apparatus needed for cell division (Quarmby and Parker, 2005; Plotnikova *et al.*, 2009). Additionally, ciliopathy proteins have been linked to the DNA damage response pathway, cell growth and cancer (where disruption to the Hh and Wnt pathways have been linked to tumour-promotion), mitochondria, autophagy, and cytoskeleton organisation (Dawe *et al.*, 2007b; Böttinger, 2010; O'Toole *et al.*, 2010; Valente *et al.*, 2010; Adams *et al.*, 2012; Chaki *et al.*, 2012; Polakis, 2012; Hoff *et al.*, 2013; Hanna and Shevde, 2016; Pampliega and Cuervo, 2016; Walz, 2017). Many MKS proteins have been shown to have non-ciliary localisations. While localisation cannot be used to assign a definitive function, there are several lines of functional evidence to indicate that at least some MKS proteins have extra-ciliary roles (summarised in Table 1.4).

Table 1.4 Evidence of non-ciliary roles for MKS proteins.

MKS protein	Non-ciliary role or localisation (if reported)
MKS1	Localises to centrosome in non-ciliated cells (Bialas *et al.*, 2009).
TMEM216	Required for distribution of Filamin A (Valente *et al.,* 2010).
TMEM67	Interacts with Filamin A (Adams *et al.,* 2012); interacts with Nesprin 2 (Dawe *et al.,* 2007b); localises to actin cytoskeleton (Adams *et al.,* 2012), the cell surface of polarised cells (Dawe *et al.,* 2007b), and to focal adhesions (Meadows, 2017); required for ROR2 phosphorylation (Abdelhamed *et al.*, 2015) and ECM organisation (Meadows, 2017); localises to endoplasmic reticulum (Wang, Tytell and Ingber, 2009).
CEP290	Localises to centrosome (Coppieters *et al.*, 2010).
RPGRIP1L	Present throughout the cytoplasm during cell division (Delous *et al.*, 2007).
CC2D2A	Not reported

NPHP3	Not reported
TCTN2	Not reported
B9D1	Localises to centrosome in non-ciliated cells (Bialas *et al.,* 2009)
B9D2	Localises to centrosome in non-ciliated cells (Bialas *et al.,* 2009)
TMEM231	Not reported
KIF14	Involved in processes including vesicle transport, chromosome segregation, mitotic spindle formation, cytokinesis, apoptosis (Zhu *et al.*, 2005; Carleton *et al.*, 2006; Singel *et al.*, 2014); regulates cell cycle progression, cell growth, cell spreading, focal adhesion dynamics, and cell migration (Ahmed *et al.*, 2012; Xu *et al.*, 2014).
TMEM107	Not reported
CSPP1	Regulates cell-cycle progression, spindle organisation, microtubule organisation, and cytokinesis (Patzke *et al.*, 2005; Patzke, Stokke and Aasheim, 2006).

A common non-ciliary role of the MKS proteins is involvement in cytoskeletal-related processes. Indeed, a number of actin-binding proteins were identified as being required for ciliogenesis in two functional genomics screens (Kim *et al.*, 2010; Wheway *et al.*, 2015) and the key function of the actin cytoskeleton in ciliogenesis has recently been established. Actin remodelling has been identified as a regulator of ciliogenesis, and many actin regulatory proteins localise to the cilium. Actin has been linked to the regulation of ciliogenesis in at least three distinct ways (green arrows, Figure 1.2). Firstly, actin localises a number of proteins to the cilium that negatively control cilium length (arrow 1, Figure 1.2). One such protein is histone deacetylase 6 (HDAC6), targeted to the cilium by death inducer obliterator (Dido3). The amount of both proteins negatively correlates with cilium length (de Diego *et al.*, 2014). Secondly, actin is

thought to play a role in regulating vesicle transport to the cilium (arrow 2, Figure 1.2), and thus blocking the rapid vesicle transport that ciliogenesis requires (Kim *et al.,* 2015). Thirdly, F-actin polymerisation has been linked to the disassembly of cilia through YAP/TAZ activation (arrow 3, Figure 1.2). YAP/TAZ activity is involved in the growth of organs, tissue regeneration, and cell proliferation (Piccolo *et al.*, 2014). Through the actomyosin cytoskeleton, YAP/TAZ functions as a transcriptional regulator that responds to tension changes in a cell's microenvironment (Dupont *et al.*, 2011). On a hard substrate, YAP/TAZ localizes to the nucleus, whereas on soft substrates, YAP/TAZ re-localises to the cytoplasm, where its transcriptional activity is thus inhibited (Dupont *et al.,* 2011). The knockdown of YAP/TAZ facilitates ciliogenesis, whereas its hyperactivation prevents ciliogenesis, and meaning that rigidity in a cell's microenvironment, as well as cortical tension from the cytoskeleton are important regulators of ciliogenesis.

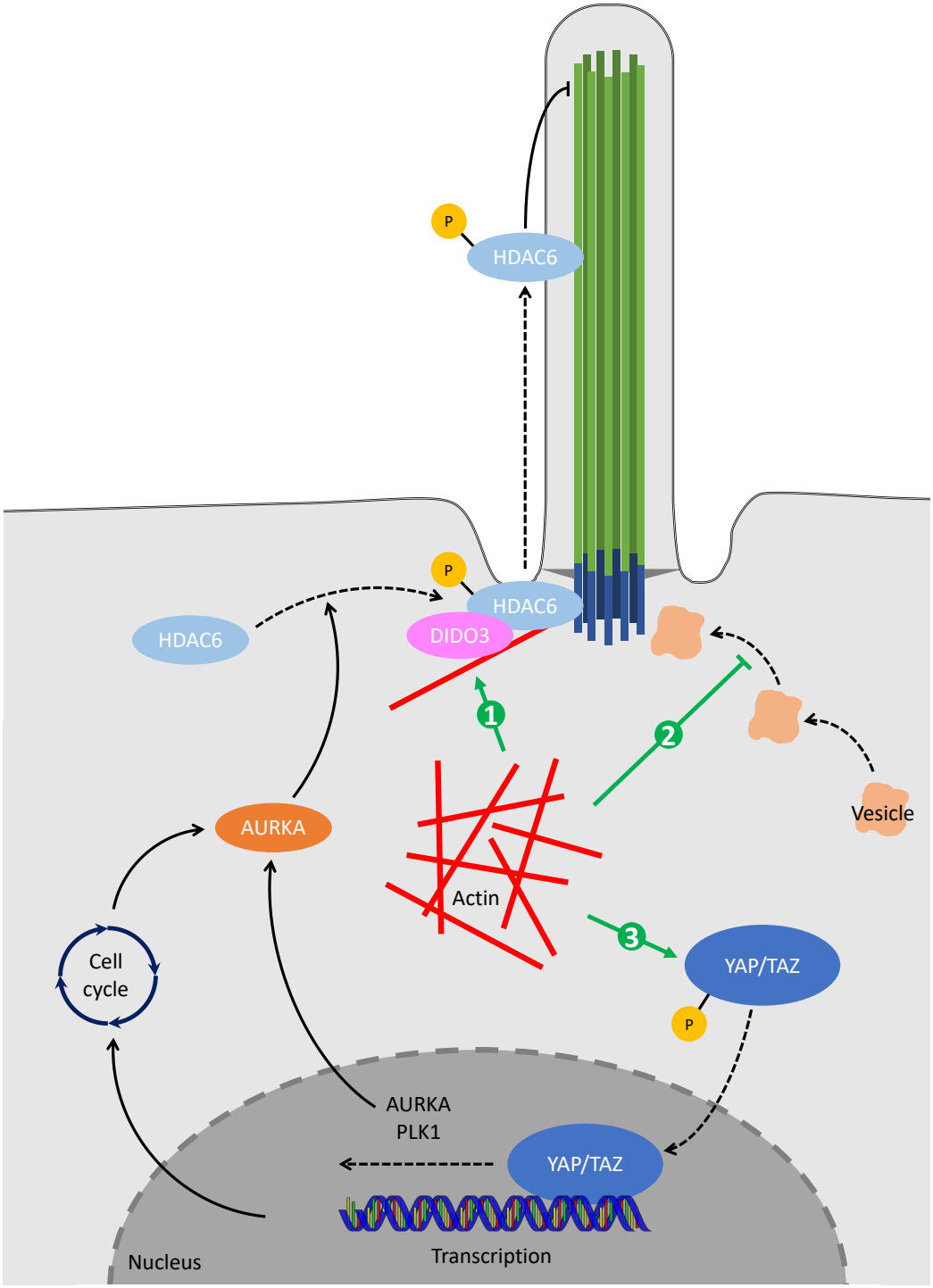

Figure 1.2 Actin affects ciliogenesis in at least three distinct mechanisms.

Defects to the actin cytoskeleton have been observed in MKS cells (Dawe *et al.*, 2009; Valente *et al.*, 2010; Adams *et al.*, 2012). In *TMEM67* patient cells, actin bundle density is markedly increased four days after plating the cells compared to levels observed in

non-diseased cells (McIntosh, 2016). In *TMEM216* patient cells, dense actin bundles have been seen as quickly as 40 minutes after plating (McIntosh, 2016). Actin defects have been reported in other ciliopathies, including BBS (Hernandez-Hernandez *et al.*, 2013), suggesting a general role of ciliopathy proteins in the regulation of the actin cytoskeleton.

The cytoskeletal roles of MKS proteins summarised in Table 1.4 could therefore result in ciliogenesis defects as a downstream factor of altered cortical or extracellular tension, rather than the ciliogenesis defect arising only as a result of a compromised transition zone.

1.5 The cytoskeleton and cell migration

This thesis investigates the impact of the loss of MKS type 3 protein TMEM67 on the actin cytoskeleton. The cytoskeleton is the network of filaments and tubules extending throughout the cytoplasm of the cell. It has multiple functionalities, for example providing the structural shape of the cell, protecting the cell from deformation, acting as the railroad for intracellular transport, facilitating whole cell migration, and roles in mitosis and meiosis (reviewed thoroughly in Fletcher and Mullins, 2010). Cytoskeletal components also form specialised structures, such as cilia. A cytoskeleton is universally present across eukaryotes and prokaryotes, but the composition of the cytoskeleton varies (Löwe and Amos, 2009). The eukaryotic cytoskeleton is comprised of three main types of structure: actin filaments, microtubules, and intermediate

filaments. This thesis focuses on the actin cytoskeleton, which is discussed in more detail below. Microtubules and intermediate filaments will not be discussed in detail, but are reviewed thoroughly in Fletcher and Mullins, (2010).

Present in almost all eukaryotic cells (the one reported exception being nematode sperm; Roberts and Stewart, 1997), actin has diverse roles, for example muscle contraction, apoptosis, adhesion, cytokinesis, whole cell locomotion, vesicle and organelle trafficking, maintenance of cell and nuclear shape, and signalling, amongst many others (Le Clainche and Carlier, 2008; Khatau *et al.*, 2009; Pollard and Cooper, 2009). Three main actin isoforms have been identified in vertebrates: α, β, and γ (Gunning *et al.*, 1983). α actin, or skeletal actin, is part of the contractile apparatus in skeletal muscle, while β and γ are the components of the cytoskeleton (NCBI, 2018). β and γ actin assemblies form various structures within the cell, including filamentous dendritic actin in the leading edge of a migrating cell, the cortical actin network, the circumferential actin belt (or adhesion belt), and stress fibres. Stress fibres form the foundation of contractile forces within a cell (Pellegrin and Mellor, 2007).

Actin exists in two principle forms: as a globular monomer (G-actin), and as a polymeric filament (F-actin). Filamentous actin is highly dynamic and the formation of filaments happens in three phases: nucleation, elongation, and steady state (see Pollard and Cooper, 1986; Pollard *et al.*, 2000; Stricker *et al.*, 2010; Wen and Janmey, 2011 for reviews on actin biochemistry and cytoskeletal mechanics). The first step in

formation of F-actin is nucleation, where three G-actin monomers associate into a trimer. This trimer is energetically unfavourable, and therefore elongation occurs in order to make a more stable structure (Winder and Ayscough, 2005). F-actin is asymmetric with a plus end and a minus end, with different dynamic states. The plus end of the actin filament has faster dynamics than the minus end, and as such when there is an excess of free G-actin, the monomers associate at the plus end of the filament and the filament grows in length. When the volume of G-actin reaches a 'critical concentration', F-actin reaches the steady state, where there is no net growth of the filament: polymerisation and the plus end, and monomer disassembly at the minus end are happening at the same rate. This is also known as actin treadmilling (Winder and Ayscough, 2005).

Numerous actin-binding proteins (ABPs) facilitate actin's various cellular roles. See Table 1.5 for an overview of the main classes of ABPs.

Table 1.5 Function of the main classes of ABPs (reviewed in Winder and Ayscough, 2005).

Function of ABP	Protein
Nucleation of G-actin	Arp2/3; formins; WASP
Nucleotide exchange	profilin
Actin capping/sequestration	thymosins
Depolymerisation and severing	ADF/cofilin
Bundlers and crosslinkers	*Microvilli:* fimbrin; scruin; villin; espin *Filopodia and stress fibres:* fascin; α-actinin
Crosslinkers	filamin; spectrin; transgelin
Cytoskeletal linkers	*Actin to intermediate filaments:* spectrin

	Actin to intermediate filaments and microtubules: plectin; BPAG; MACF; MAP2 *Actin to microtubules:* tau
Actin-based motility and contraction	myosins
Rulers and stabilisers	adducin; caldesmon; nebulins; tropomyosin
Anchors to membranes and membrane proteins	α-actinin; annexin II; α-catenin; BPAG; dystrophin; ERM proteins; plectin; spectrin; Sla2; talin; tensin; utrophin; vinculin
Sidebinders and signallers	IQGAP; Abp1; cortactin; coronin; drebrin; ENA/VASP
Branch formation	Arp2/3; WASP/SCAR/WAVE

1.5.1 The cytoskeleton during crawling motility

One of the major roles for the cytoskeleton is cell migration (Fletcher and Mullins, 2010). Whole cell locomotion is a fundamental process during development and maintenance of multicellular organisms: early in embryonic development, tissue formation requires the carefully orchestrated migration of precursor cells to specific locations, then throughout multicellular life, wound healing and immune response are key processes to survival that rely on cell migration (Friedl and Gilmour, 2009).

There are several modes of cell migration. While many unicellular eukaryotes propel themselves by cilia and flagella, cell migration in multicellular eukaryotes is more complex, although flagella-driven propulsion is present, such as in sperm motility (Ridley *et al.*, 2003). Cell motility in eukaryotic cells is largely pushed by cytoskeletal-driven changes in cell shape, with two main forms: crawling motility and blebbing

motility. While blebbing motility occurs independently from the actin cytoskeleton (Blaser *et al.*, 2006), crawling motility depends on the protrusion and retraction of actin. The present study focuses on crawling motility in MKS cells, and so the mechanics of blebbing and other forms of motility will not be covered but are reviewed in (Paluch and Raz, 2013).

Crawling motility in a 2-D environment can be broken down into four stages: protrusion, adhesion, traction, and de-adhesion/tail retraction (Mitchison and Cramer, 1996). During the protrusion phase, rapid actin polymerisation at the leading edge of the cell drives the lamellipodium forwards. Adhesion of the cell to the external environment is required for lamellipodial protrusion to be converted into cell traction (Ridley *et al.*, 2003). Adhesion occurs through focal adhesions; integrin-containing, multiprotein complexes which couple the actin cytoskeleton to the extracellular matrix (ECM; Vicente-Manzanares and Horwitz, 2011). Focal adhesion dynamics also play a central role during cell locomotion. In the leading edge of lamellipodia small adhesions form, containing integrins, talin, paxillin and vinculin. These immature adhesions are called focal complexes (Wozniak *et al.*, 2004). Many focal complexes are transient: the dynamic protrusion and withdrawal of the actin in the leading edge means many focal complexes do not mature and are disassembled. However, in the net-protrusion of the leading edge, some adhesions mature into the larger and more stable focal adhesion. During maturation, focal adhesions sequentially recruit additional proteins, such as zyxin and tensin, (Zaidel-Bar *et al.*, 2004). Through attachment to mature focal

adhesions, the actin cytoskeleton can exert force onto the ECM, generated by myosin activity, and in this way generate the traction needed for migration (Burridge and Guilluy, 2016).

Focal adhesions remain stationary with respect to the ECM, and as a cell migrates forwards they arrive closer to the rear of a cell. In order for tail retraction, mature focal adhesions at the trailing edge of a migrating cell must be disassembled. The rate of deadhesion of a cell is often the limiting factor in migration speed, with cell types that migrate faster forming weaker adhesions (Mitchison and Cramer, 1996).

While the actin cytoskeleton is the main driver of crawling motility in cells, microtubules have also been implicated in the process, as destruction of microtubules was found to inhibit protrusive lamellipodial activity in fibroblasts (Bershadsky *et al.*, 1996). Disrupting microtubules has also been shown to activate the small GTPase Rho, resulting in increased focal adhesion size, as well as enhancing the phosphorylation of the focal adhesion-associated proteins paxillin and FAK (Bershadsky *et al.,* 1996). Dynamic instability of microtubules also aids cell migration by allowing cells to rapidly remodel the cytoskeleton and focal adhesions, and microtubule inhibitors have been shown to hinder whole cell locomotion, and prevent migrating cells from effectively retracting their trailing edges, or tails (Yang *et al.*, 2010; Kaverina and Straube, 2011; Ganguly *et al.*, 2012). Microtubules also play a supporting and regulatory role to the actin cytoskeleton during migration, by transporting membrane vesicles to the leading

edge to help facilitate lamellipodial extension, by regulating actin polymerisation and controlling force-projection, and by aiding the disassembly of focal adhesions at the rear of the cell (Kaverina and Straube, 2011).

1.5.2 Organisation of actin in migrating cells

The reorganisation of the actin cytoskeleton provides the driving force for crawling migration, through the protrusion of the actin-rich lamellipodium at the leading edge, and the retraction of the tail at the cell rear. In a migrating cell, actin is organised into different structures which produce the two key functions required of the cytoskeleton for migration: pushing at the leading edge and pulling at the trailing edge (Figure 1.3; Mitchison and Cramer, 1996). As well as the actin structures in Figure 1.3, another type of specialised stress fibre is required for cell migration: perinuclear actin (Maninová *et al.*, 2014; Maninová and Vomastek, 2016; Maninová, Caslavsky and Vomastek, 2017).

Figure 1.3 provides an overview of the different types of actin structure found in a migrating cell.

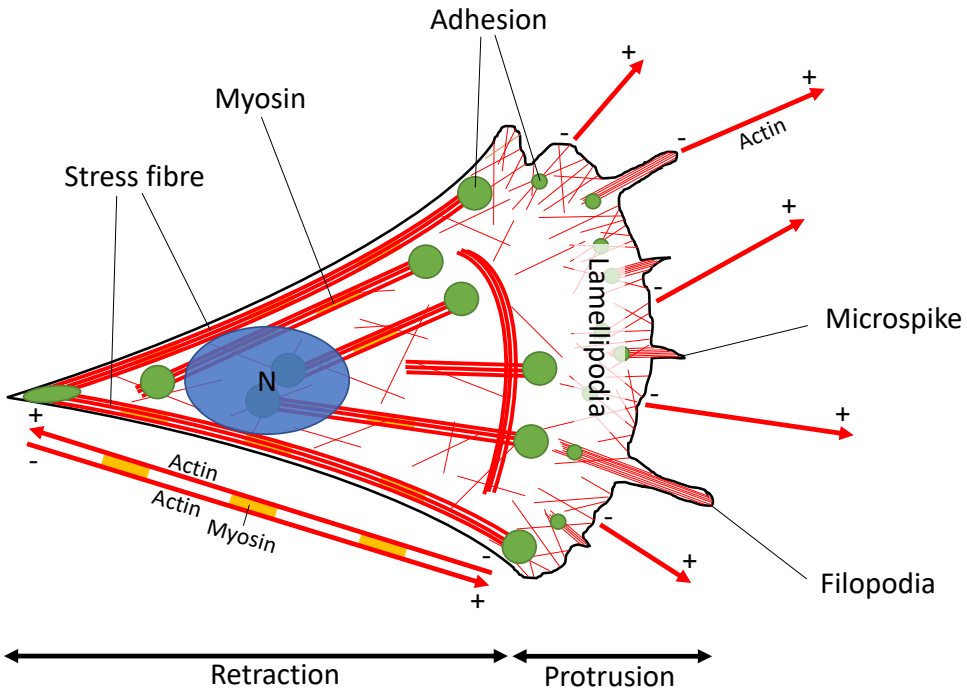

Figure 1.3 Representation of actin cytoskeleton in a migrating cell. Protrusion of the cell at the leading edge is facilitated by the lamellipodium: a meshwork of actin filaments, which push the cell edge forward through actin polymerisation at the + end. Retraction at the trailing edge is facilitated by the stress fibres. Actin stress fibres form bipolar bundles with myosin (yellow), allowing the contractibility required for retraction, shown by the red arrows underneath the cell. + and - indicate the polymerisation direction of the fibres. Focal adhesions are shown in green.

1.5.3 The perinuclear actin cap is vital for directed cell migration

Perinuclear actin cap fibres were first observed in rat fibroblasts in 1979, and were described as a sheath of highly organised actin over the top of the nucleus (Zigmond *et al.*, 1979). Later on, Khatau *et al.*, (2009) used confocal microscopy to observe the actin cap in MEFs, describing the cap as 'thick actin filament bundles organised into a curved shell or cap above the nucleus'. Actin cap fibres are aligned in the direction of cell orientation, terminating in specialised focal adhesions (actin cap-associated focal

adhesions, or ACAFAs) at either end of the fibre at the cell peripheries (Figure 1.4). ACAFAs are physically and functionally distinct from other conventional focal adhesions. ACAFAs have a distinct morphology: they are larger and more elongated than conventional focal adhesions, due to higher levels of tension exerted by the actin cap fibres (Kim *et al.*, 2012). Whereas other focal adhesions are distributed throughout a cell's basal surface, ACAFAs are restricted to the cell periphery (Kim *et al.,* 2012).

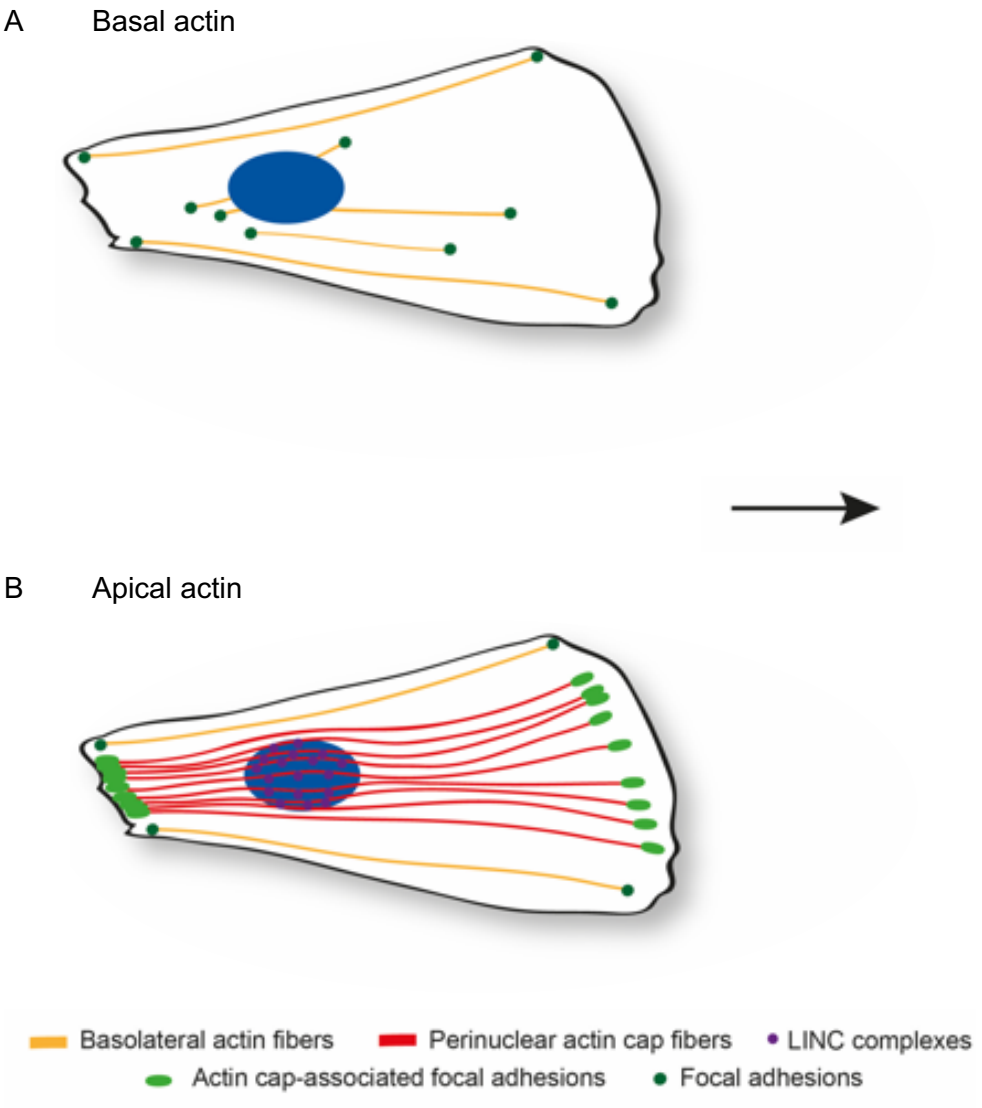

Figure 1.4 Apical view of a migrating fibroblast. (a) Basolateral actin lies under the nucleus. (b) Perinuclear actin cap fibres cover the nucleus like a cap, orientated in the direction of migration. Arrow indicates direction of migration.

Perinuclear actin cap fibres are highly dynamic, more so than other types of stress fibre (Khatau *et al.*, 2009). Association with Linker of Nucleoskeleton and Cytoskeleton (LINC) complexes help to stabilise cap fibres (Maninová *et al.*, 2017). The LINC complex is a protein complex spanning across both inner and outer membranes of the nucleus. It is comprised of a KASH domain, a SUN domain, and nesprin (Starr and Fridolfsson, 2010; Figure 1.5).

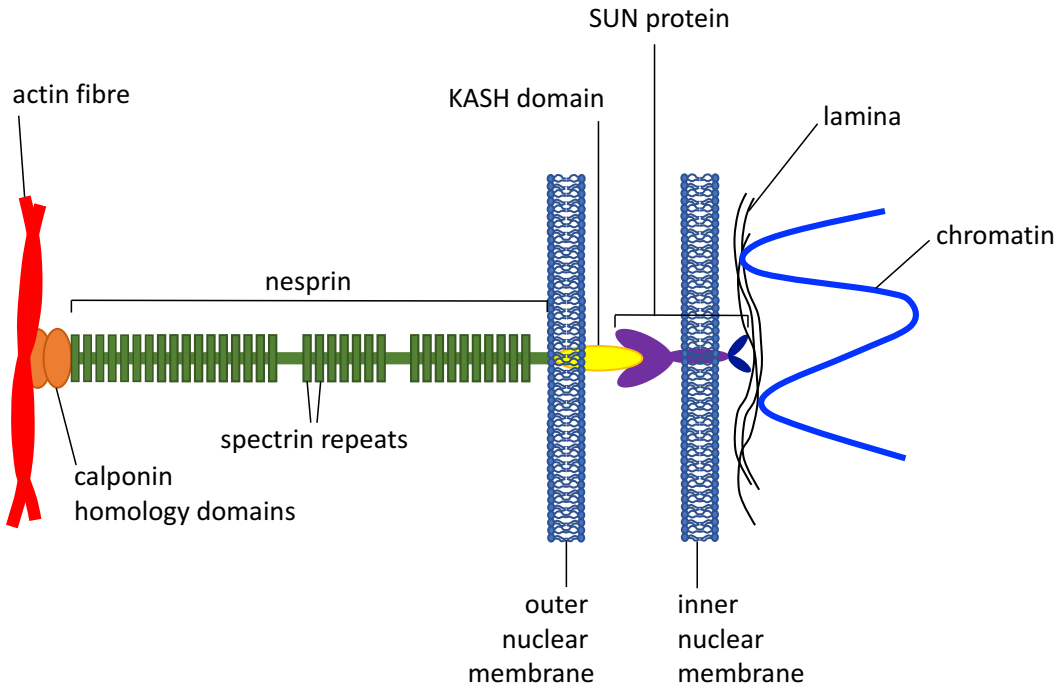

Figure 1.5 The LINC complex bridges both the inner and outer nuclear membranes, and provides the link between the perinuclear actin cap and the nucleus.

This SUN-KASH nuclear bridge and its role in nuclear positioning was first identified in the model organism *Caenorhabditis elegans* presenting with mispositioned nuclei and defects in nuclear migration (Horvitz and Sulston, 1980; Sulston and Horvitz, 1981). The LINC complex not only anchors the nucleus to the actin cytoskeleton (see

Figure 1.5), but also to the microtubule cytoskeleton and intermediate filaments, all of which are important for nuclear positioning (Starr and Han, 2002; Toivola *et al.*, 2005; Ralston *et al.*, 2006; Zhang *et al.*, 2007; Zhou *et al.*, 2009). Disruption of LINC complexes therefore results in nucleus mispositioning (Horvitz and Sulston, 1980; Sulston and Horvitz, 1981). As well as their function in LINC complexes, the SUN-KASH proteins have been shown to be important to a number of processes outside of linking the cytoskeleton to the nucleus, including function in the global reorganisation of the cytoskeleton and associated organelle movement, centriole attachment to the nuclear envelope, movement of telomeres during meiosis, and a variety of other processes (see Starr and Fridolfsson, 2010 for a review of the many roles of SUN-KASH proteins).

At their N-terminus, the LINC complex SUN proteins interact directly with the lamina (Figure 1.5), and it has been suggested that this interaction leads to regulation of gene expression (Alam *et al.*, 2016). LINC complexes provide a direct link between the lamina and the actin cap, and the actin cap fibres in turn terminate at the ACAFAs. These ACAFAs contain cell surface transmembrane receptors such as integrins, which associate with the ECM, and thus actin cap fibres provide a means of transmitting extracellular mechanical signals directly to the nucleus (Dechat *et al.*, 2008; Wang, Tytell and Ingber, 2009). As such, mechanical forces applied at the cell surface could promote the chemical conversion of signals at the nucleus. How the LINC complex is coupled to perinuclear actin cap fibres is not known. This connection

could either be direct, with actin fibres binding to the actin-binding domains at the N-termini of certain isoforms of nesprin-1 and nesprin-2; or indirect, through association with ABPs such as fascin, amphiphysin-2, and FHOD1, which are able to bind to spectrin repeats of nesprins (Maninová, Caslavsky and Vomastek, 2017).

Alongside the actin structures described in Figure 1.3, the perinuclear actin cap plays a vital role during cell migration (Khatau *et al*, 2012). Nuclear positioning and orientation are tightly regulated during cell migration: as a cell polarises, the nucleus moves towards the back of the cell, and is orientated to align in the direction of migration (Gomes *et al.*, 2005; Luxton *et al.*, 2010). This nuclear reorientation is controlled by the perinuclear actin cap, and disruption to the structure of the cap affects both nuclear reorientation and cell migration (Brosig *et al.*, 2010). The actin cap can be disrupted by both destabilising the formation of the actin fibres, or by disrupting the LINC complexes (Khatau *et al.*, 2009; Maninová and Vomastek, 2016). Disruption of the actin cap results in a change in cell morphology, and a decrease in the rate of cell migration (Khatau *et al.*, 2012).

1.5.4 Emerging evidence suggests that the actin cytoskeleton and cell migration are compromised in ciliopathies

During embryonic development, cells undergo a series of complex steps that will ultimately define their position and role during organogenesis. Cell migration is a fundamental part of this developmental chain of events, as cell lineages move from one part of the embryo to another (such as the migration of neural crest cells during

early development). Defects to cell migration during embryogenesis therefore have severe and potentially lethal results, and are responsible for a multitude of human syndromes. Heart septation defects, neuronal migration disorders such as Lissencephaly, craniofacial disorders, Hirschsprung's disease and numerous other disorders all result from a defect in cell migration (Kurosaka and Kashina, 2008).

Alterations to cellular migration have also been linked to ciliopathies. Inversin (linked to NPHP type 2) has been identified as having a role in cell migration, through transcriptional regulation of Wnt signalling and other pathways controlling the organisation of the cytoskeleton (Veland *et al.*, 2013). Additionally, loss of the intraflagellar transport protein Ift88 disrupts the polarisation and migration of cells, independently of cilia function (Jones *et al.*, 2012; Boehlke *et al.*, 2015). Mutation in BBS-associated proteins *Bbs4*- and *Bbs6*- result in cellular migration defects, with cells unable to form lamellipodial and filopodial extensions. These migratory defects arose from disrupted actin stress fibre formation and over-abundant focal adhesions stemming from upregulated levels of RhoA (a small GTPase required for actin organisation and myosin contractibility; Hernandez-Hernandez *et al.*, 2013).

Comparable cellular phenotypes to those observed in BBS have been discovered in MKS cells. RhoA is upregulated in MKS cells, with corresponding defects to the actin cytoskeleton and migratory defects (Dawe *et al.*, 2009; Valente *et al.*, 2010; McIntosh, 2016; Dawe lab, unpublished). However, while increased focal adhesions were

observed in BBS cells, focal adhesions in MKS cells have altered morphology and decreased levels of a number of adhesion proteins (Meadows, 2017). Additional migratory defects have recently been observed in MKS cells, adding to the evidence of extra-ciliary roles of MKS proteins. Loss of TMEM67 results in the loss of collective cell migration, with individual cells migrating faster, but with reduced directionality. Conversely, loss of TMEM216 leads to a reduction in cell migration speed (Dawe lab, unpublished). Aberrant nuclear rotation has also been observed in migrating cells lacking TMEM67, with the nucleus and centrosome being unaligned with the direction of cell polarisation and migration (Dawe lab, unpublished). Nuclear rotation and migratory defects are consistent with the aberrations to the actin cytoskeleton noted in the same *TMEM67* cell line in Dawe *et al.,* 2009, suggesting that the actin cap (which controls nucleus position during cell migration) could be disrupted in these cells.

These non-ciliary roles suggest that ciliopathy proteins have multiple functionalities within the cell, and supports the idea that the variety of distinct pathologies of ciliopathies could be a result of other non-ciliary roles of the mutated proteins. However, there is limited information on how cell migration impacts on ciliopathy, and in most cases the reason for the migration defect is unknown. It is not known whether the migration defects are due to the loss of cilia and altered ciliary signalling, or whether the root of the defect is extra-ciliary. Additionally, MKS has recently been linked to defects in the cell's extracellular environment (Meadows, 2017). The

extracellular environment and associated signalling is crucial to cell migration, and therefore to what extent the environment surrounding the cell contributes to the altered migration needs to be considered.

1.6 Migrating animal cells are surrounded by the extracellular matrix

The ECM is formed from a collection of extracellular molecules secreted by surrounding cells. The ECM not only functions as a physical scaffold for surrounding cells, but it also has an important role in cell-cell communication, cell differentiation, migration, gene expression, and acts as a repository for a number of growth factors (Rozario and DeSimone, 2010). In mammals, the ECM can be split into three major classes: structural proteins (including the collagens, fibrillins and elastin); other non-structural proteins (including fibronectin, laminins, integrins); and proteoglycans. The roles of collagen, fibronectin and laminin, as well as the organisation and function of the ECM are discussed in more detail in the following sections (see Hynes and Naba, (2012) for a thorough review of the other ECM components and their function).

1.6.1 Collagen

Collagen is the most abundant protein type in the human body, forming around 25-35% of its protein content (Di Lullo *et al.*, 2002). It is the main structural protein forming connective tissue in humans, and is subsequently found mainly in fibrous tissues, including ligaments, skin, and tendons. At a molecular level, three single polypeptide chains twist together into a helical structure to form ‘tropocollagen’. Many

tropocollagens then associate to form fibrils, and many fibrils come together to form a collagen fibre. This structure gives collagen a high tensile strength of between 0.2 and 0.86 GPa, around half the tensile strength of spider silk, allowing collagen to act as the main structural component in the human body (Griffiths and Salanitri, 1980; Svensson *et al.*, 2010). To date, 26 collagen types have been identified, with collagen Type I being the most abundant collagen in humans, making up around 90% of the collagen content (Di Lullo *et al.*, 2002; Gelse *et al.*, 2003; Avila Rodríguez *et al.*, 2018). The roles of the five most abundant collagens are laid out in Table 1.6.

Table 1.6 Functions of the five most abundant collagens in the human body (reviewed in Gelse *et al.*, 2003).

Collagen	Function
Type I	Skin; tendon; organs; bone
Type II	Cartilage
Type III	Reticulate
Type IV	Basal lamina
Type V	Cell surfaces; hair; placenta

1.6.2 Laminin

Laminins are important glycoproteins of the ECM and are the main constituent of the basal lamina, regulating cell differentiation, migration, and adhesion (Timpl *et al.*, 1979). Laminin is a heterotrimeric protein, consisting of an alpha, beta and gamma monomer (Figure 1.6). The three monomers associate to form a wind turbine-shaped structure, with the three individual monomers separately forming three short arms,

then associating into a long, coiled body (Aumailley *et al.*, 2005; Domogatskaya *et al.*, 2012). The arms bind to other laminin molecules, allowing the formation of laminin sheets, while the coiled body binds to cells, forming the points of attachment between tissues and the basement membrane. There are five alpha laminin variants, four beta, and three gamma, which combine to form different variations, named according to their arrangement; for example, alpha-5, beta-2 and gamma-1 monomers form Laminin-521 (Aumailley *et al.,* 2005).

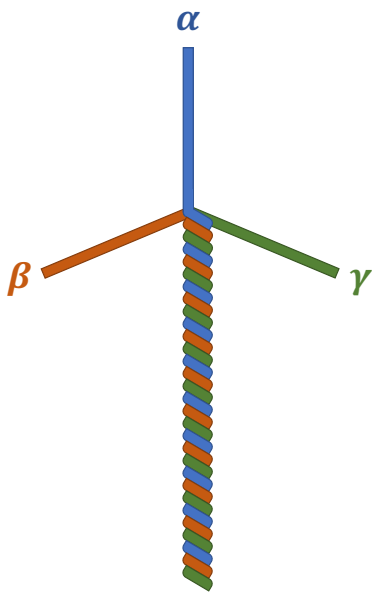

Figure 1.6 The heterotrimeric structure of laminin.

1.6.3 Fibronectin

Fibronectin is a high-molecular weight, multifunctional glycoprotein. There are two forms: the insoluble form synthesised by fibroblasts is a major constituent of the ECM, and a soluble form produced by hepatocytes is a major protein component of blood plasma. Alternative splicing of fibronectin mRNA creates upwards of 20 fibronectin

variants in humans, which vary both spatially and temporally across development and aging (Schwarzbauer *et al.*, 1983; Ffrench-Constant and Hynes, 1989).

In the ECM, fibronectins bind to other ECM components, including collagens, fibrins, and integrins. Fibronectins play major roles in cell migration, adhesion, growth, and differentiation, are major regulators of wound healing, and are required for embryonic development (reviewed in Hynes and Yamada, 1982).

1.6.4 Organisation of the extracellular matrix

In animals, the ECM includes the basement membrane and the interstitial matrix. The basement membrane is a sheet-like deposition of associated ECM molecules on which epithelial, mesothelial, or endothelial cells sit (Liotta *et al.*, 1980; Jayadev and Sherwood, 2017). It separates these cells from the body's connective tissue, both functioning as an anchor between these cell sheets and the looser connective tissue, but also as a mechanical barrier, preventing the invasion of malignant cells into deeper layers of tissue (Liotta *et al.,* 1980). The four main basement membrane components are collagen IV (see Table 1.6), laminin, nidogen, and perlecan (Paulsson *et al.*, 1992; LeBleu *et al.*, 2007). Collagen IV is the major constituent of the basement membrane, and laminin is the most abundant non-collagenous component (LeBleu *et al.*, 2007). Self-assembly of a collagen IV superstructure, and of laminin heterotrimers into integrin-associated polymers form the basement membrane scaffold. Nidogen and

perlecan stabilise the scaffold by bridging the networks. Basement membrane tissue specificity is generated through association of additional minor components to this core four (LeBleu *et al.*, 2007).

The interstitial matrix consists of gels of polysaccharide molecules and fibrous proteins, which amalgamate in the spaces between tissues, and act as a buffer to compressional stress (Frantz *et al.*, 2010).

1.6.5 The extracellular matrix and cell migration

As covered in section 1.5.1, in order for a cell to migrate, it must adhere to its extracellular environment: adhesion is regulated by cell surface receptors, of which the major class is the integrins (Harburger and Calderwood, 2009). The cell must also polarise and have contractile force generated by the cytoskeleton (DiMilla *et al.*, 1991). Net migration occurs when the contractile forces overcome the adhesive forces (DiMilla *et al.*, 1991). Eukaryotic cell migration is driven through cytoskeletal changes and ECM-integrin binding. A number of ECM qualities have a direct effect on cell migration, including ECM rigidity, ECM concentration, protein composition, and ligand concentration (Palecek *et al.*, 1997).

ECM rigidity varies between cell types due to the balance of collagen and elastin within the matrix: this is one of the ways in which protein composition can influence cell

migration. Cells migrate slower on more rigid matrices, due to the relationship between the ECM stiffness and cell spreading (Pelham and Wang, 1997). Like a water droplet falling onto a surface, when a cell hits a substrate, it passively deforms and spreads. Similar to surface tension in a water droplet, a cell's cortical tension holds them in a spherical shape. This cortical tension is driven by acto-myosin contractile tension (Vicente-Manzanares *et al.*, 2009; Clark *et al.*, 2014; Chugh *et al.*, 2017). When a cell is not migrating, its cortical tension is large, and therefore the force it exerts on the substrate is large. A softer substrate deforms more in response to these forces than a more rigid substrate, reducing the resultant force against the cell, and under these circumstances cells are not able to maintain the high tensions required for spreading. This results in less cell spreading on a softer substrate compared to a harder substrate (Lange and Fabry, 2013); see Figure 1.7.

As shown in Figure 1.7, on a more rigid matrix a cell spreads more, thus increasing the volume of engaged cell-matrix adhesions. This results in a decrease in migration speed as there are more adhesive forces for the cell to overcome (DiMilla *et al.*, 1991; Metzner *et al.,* 2007). Cell migration directed by ECM rigidity gradients is known as durotaxis. Through mechanosensing, whereby the cell responds to differences in applied forces, cells usually migrate from a low to a high rigidity (Pelham and Wang, 1997).

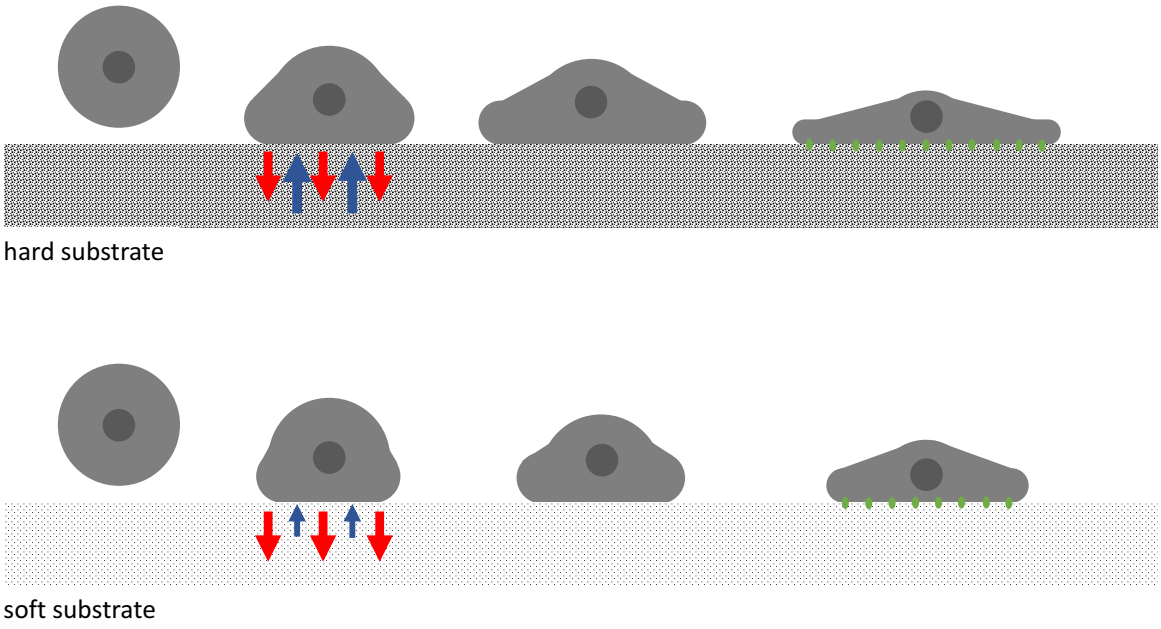

Figure 1.7 Cells spread less on softer substrates due to increased deformation of a soft substrate in response to a cell's cortical tension.

As well as the physical properties of matrix proteins, the second way in which protein composition of the ECM affects cell migration is the individual properties of matrix proteins: different matrix proteins affect cell adhesion and migration speed in different cell types (Strachan and Condic, 2003). For example, on matrices containing high laminin concentrations, cranial neural crest cells migrate faster than trunk neural crest cells due to the two cell types' alternate regulation of ECM receptor expression (Strachan and Condic, 2003).

Concentration of ECM also affects cell migration. Migration speed follows a normal distribution with increasing ECM concentration, whereby an intermediate concentration favours fastest migration speeds (Palecek *et al.*, 1997). At high levels of ECM concentration, cell detachment rate is low due to a high number of engaged cell adhesion sites, whereas at very low ECM concentrations, there are few adhesion sites and the lamellae are unstable – both conditions hamper migration. Fastest migration is therefore present on intermediate ECM concentrations, where adhesion and detachment are balanced (Palecek *et al.*, 1997). Cell migration directed through cells sensing and responding to ECM concentration gradients is known as haptotaxis: cells migrate away from regions of low ECM concentration, where cell adhesion is weak, to areas of higher ECM concentration (Wen *et al.*, 2015).

The above ECM properties influence different cell types to varying degrees, and have direct implications on vertebrate development (Rozario and DeSimone, 2010). For example, neural crest cell migration is a highly coordinated process, and ECM has been identified as an important regulator of this process. Unique to vertebrates, neural crest cells are a temporary group of cells which arise during development from the embryonic ectoderm and then differentiate into numerous cell types, including connective tissue, craniofacial cartilage, craniofacial bone, melanocytes, neurons, and glia. Individual ECM components have been identified as supporting different migratory behaviours, for example, laminin α5 has been suggested to be important for

restricting cell migration into controlled lanes (Strachan and Condic, 2003; Coles *et al.*, 2006; Rozario and DeSimone, 2010).

Recently a link between loss of cilia and defects to the ECM has been uncovered. Giantin, a Golgi protein, is required for ECM assembly, with rodent models with loss-of-function mutations in the protein showing extensive defects in ECM secretion and/or assembly (Katayama *et al.*, 2011). Giantin is also required for normal ciliary function (Asante *et al.*, 2013; Bergen *et al.*, 2017). Similar phenotypes have been observed in MKS, with loss of MKS type 3 protein TMEM67 resulting in changes to the secretion levels of a number of ECM proteins (Meadows, 2017).

1.6.6 Loss of MKS protein TMEM67 results in defects to the ECM

The following study focuses on TMEM67. Sometimes referred to as Meckelin, TMEM67 is a 995-amino acid protein encoded by the *TMEM67* gene, located at 8q22.1 in the human genome (Smith *et al.*, 2006). TMEM67 was originally implicated in MKS (Smith *et al.* 2006), but has since also been linked to BBS (as a modifier; Leitch *et al.*, 2008), COACH (Brancati *et al.*, 2009), JTBS (Delous *et al.*, 2007), and NPHP (Otto *et al.*, 2009). Mutations in *TMEM67* are the most common cause of MKS (Szymanska *et al.*, 2012). *In situ* hybridisation in human embryos has revealed that *TMEM67* is expressed in the kidney, liver, retina, hindbrain, developing sphenoid bone, and the brain midline, with strong expression in the developing digits (Dawe *et al.,* 2007). TMEM67 is a component of the transition zone, and is required for centriole

migration to the apical membrane during ciliogenesis (Dawe *et al.*, 2007b; Yang *et al.*, 2015; Shi *et al.*, 2017). Loss of the protein therefore disrupts ciliogenesis and cell types lacking the protein have significantly fewer cilia (Dawe *et al.,* 2007b).

The cytoplasmic region at the C terminus of TMEM67 interacts with Filamin A (encoded by the *FLNA* gene; Adams *et al.*, 2012). Filamin A is an ABP which facilitates cross-linking of actin filaments (see Table 1.5), and aids anchoring of membrane proteins to the actin cytoskeleton, and is therefore an important protein in the remodelling of the actin cytoskeleton during cell migration. Knockdown of both *FLNA* and *TMEM67* results in abnormal basal body positioning, loss of ciliogenesis, aberrant remodelling of the actin cytoskeleton, deregulation of RHOA and hyperactivation of canonical Wnt signalling (Dawe *et al.,* 2009; Adams *et al.*, 2012; McIntosh, 2016). The C-terminal coiled-coil domain of TMEM67 interacts with a structural maintenance of chromosomes (SMC) domain at the N terminus of Nesprin-2 (Dawe *et al.,* 2009). A component of the LINC complex, Nesprin typically localises to the outer nuclear membrane (see Figure 1.5). However, knockdown of *TMEM67* results in the aberrant re-localisation of Nesprin-2 to actin stress fibres and remodelling of the actin cytoskeleton (McIntosh, 2016).

Recent research has also identified TMEM67 as a focal adhesion protein, required for the organisation of adhesions, probably through recruitment or retention of other adhesion proteins (Meadows, 2017). Analysis of focal adhesions of *TMEM67* patient

cells revealed major alterations to the adhesome and associated morphological differences to adhesion patterning. As well as altered expression in adhesion-associated genes, *TMEM67* patient cells also exhibit altered ECM gene expression, with cell-derived matrix (CDM) isolated from *TMEM67* patient cells containing reduced levels of collagen IV and laminin (Meadows, 2017). While TMEM67 is the most well studied of the MKS proteins, there are still large gaps in our understanding of its function, including its role at focal adhesions.

1.7 Summary and scope of thesis

Until recently, the primary cilium was thought by many people to be a vestigial organelle. However, it is now known to be a key regulator in a number of key developmental pathways, with the loss of formation or function of primary cilia being linked to a number of inherited diseases (Waters and Beales, 2011). Originally, research focused on the loss of ciliary function and how this linked to pathogenicity, however, this raised the question of how loss of function of a single organelle could result in multiple clinically distinct diseases. Recent studies highlighting the extra-ciliary roles of ciliopathy proteins provides an answer: ciliopathy proteins have much wider roles in the cell than purely cilia-related functions.

This study builds on previous research linking the loss of TMEM67 to aberrant actin organisation, and to defects in cellular migration and ECM deposition (Dawe *et al.,* 2009; Adams *et al.,* 2012; McIntosh, 2016; Meadows, 2017; Dawe lab, unpublished).

We investigate whether the cellular migration defect and nuclear rotation during cell migration observed in *TMEM67* patient fibroblasts stems from a reorganisation of the perinuclear actin cap through the visualisation of the actin cytoskeleton in migrating cells. We also investigate the relationship between the ECM and the actin cytoskeleton, testing if the defects to the extracellular environment previously characterised in *TMEM67* patient cells are linked to the cytoskeletal abnormalities. In addition, we investigate TMEM67 function by studying the effects of six clinically relevant mutations across the protein on the actin cytoskeleton, and identify some novel binding partners of the protein. By detangling which regions of TMEM67 are important for particular functions, we aim to uncover more about the potential role of TMEM67 in the pathology of ciliopathies. In this study, we conclude that loss of TMEM67 results in a loss of the actin cap during cell migration, and uncover a novel role of TMEM67 in myosin motor activity.

2 Materials and Methods

2.1 Cell culture

hTERT immortalised *TMEM67* [c.653G>T]+[c.755T>C] fibroblasts from human neonates and non-diseased, age-matched control fibroblasts (obtained from Colin Johnson, Leeds Institute for Molecular Medicine) were grown in Dulbecco's Modified Eagle's Medium: Nutrient Mixture F-12 (DMEM-F12), supplemented with 20% Fibroblast Growth Medium (FGM; AMS Biotech), 10% foetal bovine serum (FBS) and 1% G418. Cells were cultured at 37 °C with 5% CO_2, and split to sub-passage in TrypLE Express (Gibco) when approximately 70% confluent in a T-25 flask. All cells used were between passages 12 and 20.

2.2 Isolation of cell-derived matrix

To isolate cell-derived matrix, cells were incubated on sterile glass coverslips for four days at 37 °C with 5% CO_2 post confluency. Cells were lysed using 20 mM NH_4OH in 0.5% Triton X-100-PBS for four minutes, and residual matrix was washed in PBS (Ca^-/Mg^-, Gibco) twice to ensure complete removal of NH_4OH. All coated coverslips were plated with fibroblasts immediately after the removal of fibroblasts.

2.3 Scanning electron microscopy

Cells were grown on coverslips in 4-well plates for the indicated times and fixed for 1 hour in 2% glutaraldehyde + 2.5% formaldehyde in 100 mM sodium cacodylate (pH 7.2). Cells were dehydrated in a series of ethanol concentrations, up to 100% ethanol. The samples were processed using the chemical drying agent Hexamethyldisilizane (HMDS). The samples were splutter coated and imaged at ×4000 using a Jeol JSM-6390LV Scanning Electron Microscope.

2.4 Surface coating with extracellular matrix proteins

Purified laminin, fibronectin, collagen I and collagen IV matrix proteins were obtained from Sigma-Aldrich: collagen I solution from rat tail (product code C3867), collagen IV derived from human placenta (product code C5533), human plasma fibronectin (product code F2006), laminin derived from human placenta (product code L6274). Sterile glass coverslips were coated overnight at 3 °C. All components were used at 10 µg ml^{-1}, diluted in PBS (Ca^{-}/Mg^{-}, Gibco) for laminin and fibronectin and 0.02 N acetic acid for collagen I and collagen IV. All coated coverslips were plated with fibroblasts immediately after the coating incubation.

Recombinant laminins were obtained from Biolamina: LAMscreen™ laminin isoform kit (product code KT202-1). All recombinant laminins were used at 10 µg ml^{-1} diluted in DPBS (Ca^{+}/Mg^{+}, Gibco) according to the manufacturer's instructions, and incubated on coverslips overnight at 3 °C. All coated coverslips were plated with fibroblasts immediately after the coating incubation.

2.5 Wound assays

Fibroblasts were grown on coverslips pre-coated in matrix proteins for four days at 37 °C with 5% CO_2 until a monolayer formed. A wound was induced using p200 pipette tip to scratch across centre of coverslip, and cells were incubated for a further 12 hours at 37 °C to allow migration into the wound. Cells were fixed and processed for fluorescence imaging immediately. Only cells with clear morphology indicating migration into the wound were quantified.

2.6 Immunofluorescence and cell staining

Cells were grown on 13 mm #1.5 glass coverslips in 4-well plates for the indicated times and fixed in paraformaldehyde (PFA) for 20 minutes at room temperature (see Supplementary Table 1 for PFA concentrations, and antibody and stain dilutions). After fixation, cells were permeabilised in 0.5% Triton X-100-PBS for five minutes, followed by 0.1% Triton X-100-PBS for five minutes, and then blocked in 1% Bovine Serum Albumin in PBS-0.1% Triton X-100-PBS (AbDil) for 20 minutes at room temperature. After blocking, cells were incubated with primary antibodies or AlexaFluor 594 phalloidin diluted in AbDil at room temperature for one hour (20 minutes for phalloidin) in a fluorescence chamber. Secondary antibodies were used at 1:500 dilutions in AbDil and were incubated for 30 minutes at room temperature. DAPI was used at 1 µg ml^{-1} and was incubated for two minutes at room temperature. Coverslips were mounted in Vectashield mounting medium, sealed with clear nail varnish and stored at -20 °C until quantification. Immunofluorescence images were taken using a Zeiss Axio Observer Z1 inverted microscope equipped with a 40x 1.3 NA oil objective, controlled by AxioVision software (Carl Zeiss). Images were acquired by a CoolSnap HQ2 camera (Photometrics) and processed in Fiji (ImageJ).

2.7 siRNA knockdown

Non-diseased control fibroblasts were cultured in a T-25 flask until 70-80% confluent before being trypsinised and centrifuged. The Amaxa Nucleofector electroporation device was used for transfection, using transfection kit R (Lonza). 400pmol of *tmem67* siRNA (Dharmacon ontarget plus smartpool L-016511-01-0005) was added to the pellet with 80 µl of transfection reagent (containing 65 µl nucleofector solution R and 15 µl supplement 1). This cell suspension was loaded into an electroporation cuvette

(Lonza) and electroporated with program D-023. The cells were immediately transferred to coverslips in a 4-well plate and left to grow for five days before a wound assay was performed.

2.8 Sequencing

Plasmid purification was performed by Miniprep (QIAGEN® QIAprep®) using the manufacturer's recommended protocol. Eurofins Genomics TubeSeq service was used for sequencing plasmids. Following Eurofins' sample submission guidelines, all sample concentrations contained 50-100 nl μl^{-1} of plasmid DNA. See Supplementary Table 2 for sequencing primers used. Alignments were analysed using SnapGene® (v.2.6.2).

2.9 Plasmid transfection

HA-TMEM67 plasmids were all made by Katerina Szymanska and were provided by Colin Johnson (Leeds Institute for Molecular Medicine). Transfection of *TMEM67* fibroblasts and age-matched controls with HA-TMEM67 plasmids was performed using electroporation. The Amaxa Nucleofector electroporation device was used for transection, using transfection kit R (Lonza). For each transfection, a T-25 flask of cells at 70 % confluency were spun down and resuspended in 80 µl of transfection buffer, containing 65 µl nucleofector solution R, 15 µl supplement 1, and 1 µg of plasmid DNA. This cell suspension was loaded into an electroporation cuvette (Lonza) and electroporated with program D-023. Post-electroporation, the cells were immediately transferred into a T-25 flask with 3ml of fresh media. Cells were grown for four days before being fixed for IF.

2.10 GFP trap

GFP-TMEM67-N1 FL (full length TMEM67 protein) and GFP-TMEM67-N1 ΔECL (TMEM67 lacking the large N terminal extracellular loop) plasmids were transfected into 3T3 cells as described above. Triplicate repeats were performed for each plasmid in the initial run, and the experiment was replicated for a second run to pool two separate datasets for each plasmid. The transfected cells were seeded into 10 cm dishes and left to grow for two days in media. To extract TMEM67, the media were removed and the cells were lysed on ice using a lysis buffer of 1% Nonidet NP-40, 130mM NaCl, and 20mM Tris pH8. A cell scraper was used to harvest all the ECM components from each plate. The resultant extracts were rotated at 4 °C for 30 minutes before centrifugation. The lysate was removed and incubated with GFP-trap_A beads overnight at 4 °C according to the manufacturer's specification. The bead solution was frozen at -80 °C in preparation for mass spectrometry (MS). DAVID Bioinformatics Resources 6.8 was used to annotate the gene list produced from the MS data.

2.11 Western blot

A polyacrylamide gel was made using 10% acrylamide. Whole cell lysate and immunoprecipitate samples were run on the gel using SDS-PAGE then transferred to a methanol-activated PVDF membrane overnight at 30 V. The membrane was blocked in PBS with 5% Marvel milk powder (Premier Foods Group) under continuous rotation for one hour at room temperature. Post-blocking, the membrane was incubated with anti-GFP primary antibody for one hour at room temperature with continuous rotation, washed x3 in PBS 0.1% Tween, and incubated in secondary antibody for 60 minutes under rotation at room temperature. Antibodies were diluted in PBS 2.5% Marvel milk

powder as described in Supplementary Table 1. To visualise protein, the membrane was treated with Amersham ECL Western Blotting Detection Reagent (GE Healthcare Life Sciences, Cat #RPN2106) and exposed to X-ray film (Super RX, FujiFilm).

2.12 Image analysis and statistical analysis

For SEM analysis of the ECM, images were randomly taken across the samples from three independent experiments and quantified. Significance between the number of images displaying a fibrillar and non-fibrillar matrix between MKS patient and non-diseased control cells was determined using Chi Squared test.

The number of bundles in the perinuclear actin cap were quantified using two methods. First, data were quantified according to the published literature (Woroniuk *et al.*, 2018; Andrew Porter, personal communication). Briefly, Z-stacks were acquired, and the plane of focus just above the nucleus identified using the DAPI and Phalloidin channels. In most cases the cables were distinct enough to count manually by eye. Where this was not possible, 2 pixel line scans were drawn across the widest part of the nucleus, orthogonal to the longest axis nucleus, and the peaks of the line intensity plot were quantified. Two different researchers performed the analysis, and the information from both counts was combined to increase the robustness of the data. In an independent second approach, images from the same slides were acquired using a Zeiss LSM 880 confocal microscope equipped with AiryScan. The actin cap was identified as above, and bundles were analysed using FilaQuant software (Matschegewski *et al.*, 2012; generously shared by Konrad Engel, University of Rostock) according to the User Guide. The analysis pipeline is summarised in Figure 3.3a. The same conclusions were obtained using both methods.

Fluorescence intensity measurements were performed using linescan analysis in ImageJ and mean pixel intensity (a measure of brightness and therefore an indirect measure of F-actin levels) was calculated. For these analyses, the staining conditions, microscope objective, and camera exposures (based on the brightest images to ensure non-saturating exposure conditions for the whole dataset) were the same, and all measurements were made on unprocessed images. In each individual image, total fluorescence (sum of all grey levels) was measured by linescan and mean intensity recorded. Background fluorescence was measured at three points in each image, averaged, and subtracted from each data point. Three bundles per actin cap were measured and 50 cells were quantified per cell line.

Numerical and statistical analyses were performed using Excel (Microsoft Corporation), and Prism (GraphPad). For all data, the Shapiro–Wilk test, which estimates the variance of the sample, was used to assess normality. This test exhibits high power, meaning that reliable conclusions can be drawn even with a small number of observations. Where the test statistic was smaller than the critical threshold, the assumption of a normal distribution was rejected and non-parametric testing methods used for those samples.

For comparison of actin cap organisation and florescence intensity measurements in fibroblasts plated on their own matrices or on specific ECM components, the data were not normally distributed and thus the non-parametric Mann–Whitney test was used to compare *TMEM67* or *tmem67*-silenced cells to the control. For analysis of actin cap organisation in cells plated onto purified laminin isoforms the data were not normally

distributed and thus the non-parametric Kruskal–Wallis test was used. Since multiple groups were to be compared to a single control, Dunn's post-hoc correction for multiple comparisons was used to determine which groups were significantly altered. For analysis of actin cap bundles in cells expressing HA-TMEM67 variants, the Kruskal–Wallis test with Dunn's post hoc was used for the same reason.

Mass spectrometry data were aligned to the human proteome using SEQUEST, corrected for false-discovery rate, and analysed according to the workflow summarised in Figure 3.10. Functional annotation clustering was performed using the online DAVID resource (https://david.ncifcrf.gov/).

3 Results

3.1 *TMEM67* patient fibroblasts synthesise a morphologically and biochemically altered cell matrix

Previous research into the ECM of *TMEM67* patient fibroblasts revealed aberrant levels of a number of matrix associated proteins (Meadows, 2017). Tandem Mass Tag Mass Spectrometry (TMT MS) undertaken by Meadows (2017) revealed that compared to age-matched, non-diseased control fibroblasts, *TMEM67* patient fibroblasts secreted decreased levels of a number of important ECM proteins, including laminins, collagens, fibronectin, fibrillins 1 and 2, and thrombospondin 1 and 2.[1] These proteins showed a decrease in representation compared to non-diseased control cells, from 12-70% (Figure 3.1a). In order to establish the effect of these altered protein levels on ECM architecture, we utilised an immortalised human embryonic cell line from a patient with MKS, who was compound heterozygous for the missense and truncating mutations [c.653G>T]+[c.755T>C] in *TMEM67.* These *TMEM67* patient cells produce reduced levels of the TMEM67 protein (Dawe *et al.*, 2009). *TMEM67* patient fibroblasts were left to grow for four days on glass coverslips to allow secretion of ECM proteins. The cells were stripped, leaving this cell-derived matrix (CDM) intact, and the matrix was fixed for analysis by scanning electron microscopy (SEM).

[1] The Tandem Mass Tag Mass Spectrometry data in this section was performed by Ben Meadows as part of his PhD at the University of Exeter (awarded 2017). Data relevant to this thesis was filtered out of the main dataset by A. Toynbee (author of this thesis) to identify which ECM proteins would be most relevant to investigate in relation to the present study.

Micrographs revealed that *TMEM67* patient fibroblasts secrete an altered CDM, with the loss of the thick ECM depositions seen in non-diseased control cell CDM (Figure 3.1b). Only 21% of images of the patient fibroblasts scored as having a fibrillar matrix, compared to 86% of the non-diseased control cells (*TMEM67* patient cells: n = 52 images taken over 3 experiments; non-diseased control cells: n = 43 images taken over 3 experiments; $p < 0.05$, Chi Squared test).

A

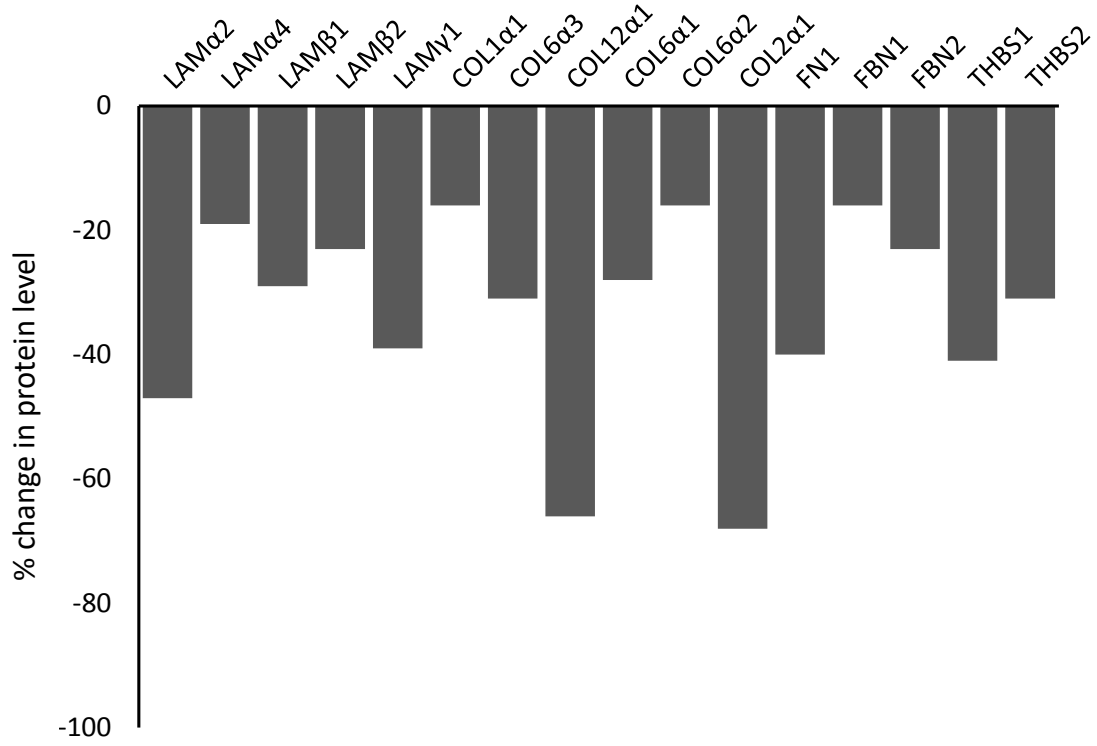

B

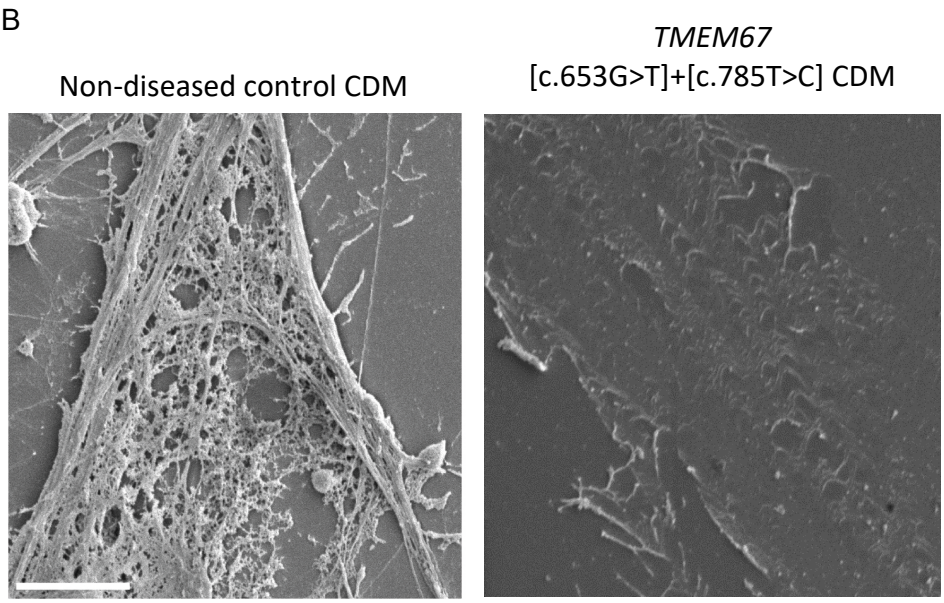

Figure 3.1 *TMEM67* patient fibroblasts secrete a biochemically and morphologically altered cell matrix. (a) TMT MS of *TMEM67* patient CDM showing % decrease in protein level of the ECM compared to age-matched, non-diseased control fibroblasts. A number of other structural ECM components were not identified or not significantly changed compared to the control. TMT MS sample prepared by B. Meadows, and data extracted from dataset by me. (b) SEM of a four day control CDM versus a four day *TMEM67* patient CDM. Scale bar = 5 μm.

3.2 SEM analysis reveals *TMEM67* patient fibroblasts do not degrade the ECM

The ECM morphology defect could be due to either assembly failure or to excess ECM degradation by matrix metalloproteinases. To identify whether the aberrant ECM morphology arises because *TMEM67* patient cells alter ECM architecture post-secretion, the cells were plated on a control CDM and the matrix was observed after four days.

Using the same method as in section 3.1, non-diseased control fibroblasts were plated on glass coverslips and left to produce matrix for four days. The cells were then

stripped, leaving their CDM isolated on the coverslip, and *TMEM67* patient fibroblasts were plated on top and left for a further four days. The *TMEM67* patient cells were removed and the residual matrix fixed for SEM. SEM analysis revealed that *TMEM67* patient fibroblasts did not cause visible degradation to the ECM, as the characteristic thick control CDM was still observable (Figure 3.2, right, white arrow head). 75% of images scored as having a fibrillar matrix (n = 61 cells, images taken over 3 experiments) and this was not a significant difference compared to the non-diseased fibroblast matrix quantified in section 3.1 ($p > 0.05$, chi squared test). Concurrent with the data presented in Figure 3.1a, these data suggest that the altered ECM architecture observable by SEM is either due to decreased levels of protein secretion or a failure to assemble or anchor the matrix (thus leaving it soluble in media), and not due to degradation post-secretion. This result also provided a control for future ECM experiments, by confirming that *TMEM67* patient cells would not degrade the ECM environment to an extent that would interfere with data interpretation. Furthermore, in many cases, two distinct layers of ECM could be observed that presumably correspond to the initial layer of CDM (Figure 3.2 right panel, white arrow head) with subsequent depositions lying on top (Figure 3.2 right panel, black arrow head). This suggests that when given a scaffold ECM, *TMEM67* fibroblasts regained the ability to synthesise CDM effectively. Similarly, the CDM of the control cells plated on the *TMEM67* CDM (Figure 3.2 left panel) appeared visibly thinner than it appeared in Figure 3.1b.

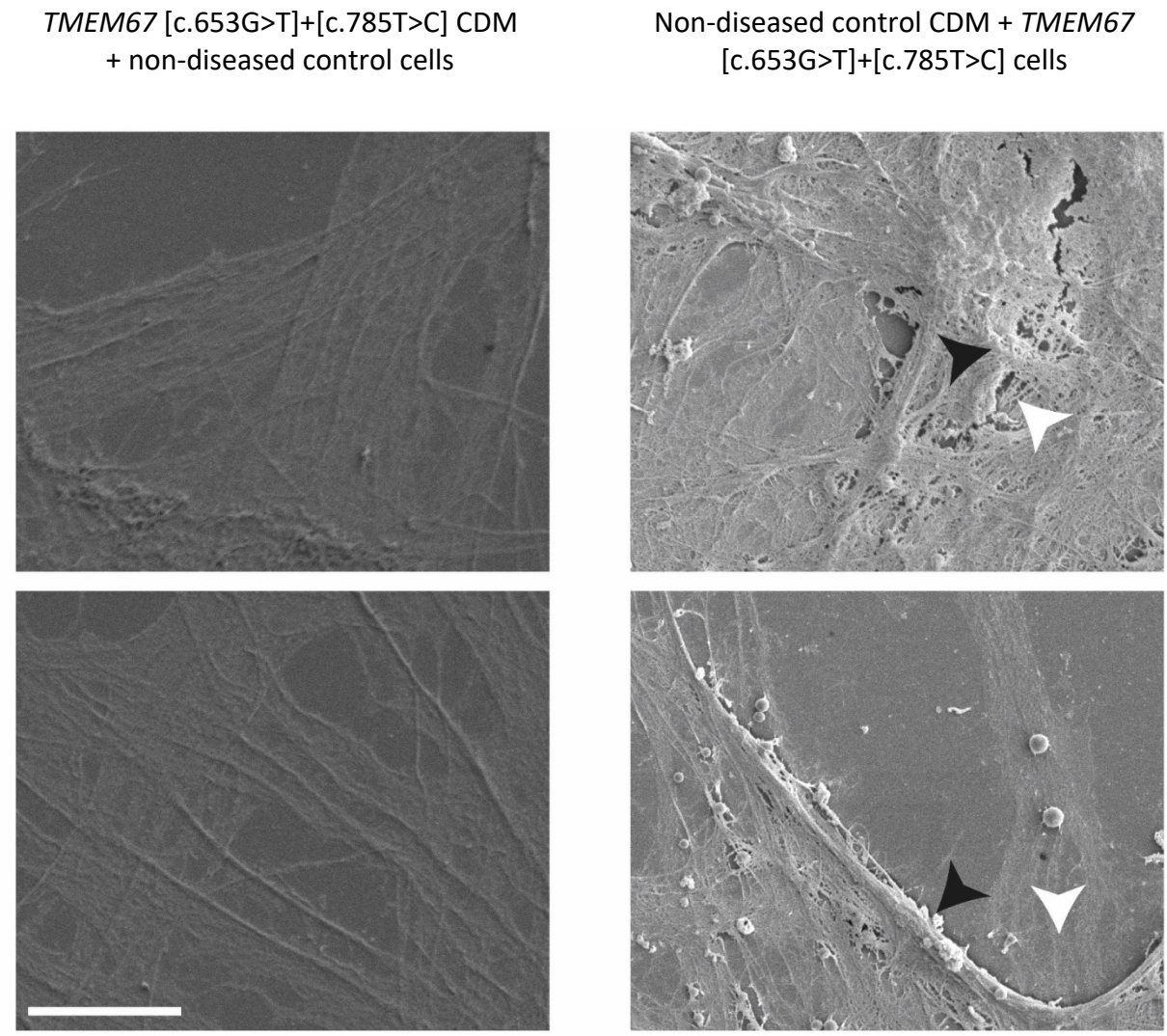

Figure 3.2 *TMEM67* patient cells do not degrade the ECM and are able to assemble matrix when plated onto a control matrix scaffold. White arrow head indicates the underlying control CDM; black arrowhead indicates the overlying *TMEM67* CDM. Scale bar = 5 μm.

Taken together, these data indicate that several important qualities of the ECM are disrupted in *TMEM67* patient fibroblasts, including protein composition, ECM morphology and density, and therefore likely ECM rigidity. As discussed in section 1.6.5, ECM qualities impact multiple cellular processes, including cell migration. Cell migration defects have been observed in MKS patient cells (Dawe lab, unpublished), but the molecular cause is unknown. We hypothesised that the altered ECM

composition is a contributing factor to the migration phenotype, and therefore sought to investigate how ECM composition impacts cell migration in MKS patient cells compared with age-matched controls.

3.3 TMEM67 is required for the correct organisation of the perinuclear actin cap

TMEM67 patient fibroblasts migrate more quickly than control fibroblasts *in vitro*, but take the same length of time to close the wound in a scratch assay due to a loss of directionality (Dawe lab, unpublished). The nuclear–centrosome axis is also affected in MKS patient fibroblasts (Dawe lab, unpublished). One structure that is vital for the maintenance of directionality during cell migration is the perinuclear actin cap, which is also responsible for the orientation of the nucleus (Brosig *et al.*, 2010). As the actin cytoskeleton is known to be disrupted in the MKS patient cell line used in this thesis (Dawe *et al.,* 2009; Adams *et al.,* 2012; McIntosh, 2016) we postulated that a disruption to the perinuclear actin cap could underlie the directionality defect in *TMEM67* patient fibroblasts.

In order to investigate this hypothesis, fibroblasts were grown to confluency for four days; the time at which previous actin defects in *TMEM67* patient cells have been observed (McIntosh, 2016), and the time corresponding to the SEM analyses above. A scratch assay was performed by introducing a wound through the cell monolayer using a pipette tip, and the cells were left to migrate into the wound for 12 hours. The

cells were then fixed and F-actin and DNA were labelled with fluorescent phalloidin and DAPI, respectively. Phase contrast was used to view cell morphology, and only cells with clear polarised morphology that were migrating into the wound were imaged. Actin on the basal cell surface appeared similar in the two cell types (Figure 3.3b and d, compare the control cells in the left panels with the MKS patient cells in the right panels). In contrast, the apical actin cap in *TMEM67* patient fibroblasts had fewer bundles visible (Figure 3.3b, compare the top right insets). We quantified this using two independent methods of actin bundle quantification (Matschegewski *et al.*, 2012; Woroniuk *et al.*, 2018; Figure 3.3c) and observed similar results with each. Compared to the age-matched control fibroblasts, *TMEM67* patient fibroblasts had significantly fewer actin bundles in the perinuclear actin cap (Figure 3.3c; Mann–Whitney Test, $p < 0.0001$). The mean number of bundles in the cap of *TMEM67* fibroblasts was 4.7 ± 0.3 (linescan analysis) and 4.1 ± 0.7 (FilaQuant analysis) compared to 9.4 ± 0.4 (linescan analysis) and 9.1 ± 1.5 (FilaQuant analysis) in the control fibroblasts (n = at least 150 cells per cell line, over three independent experiments). Complete loss of the actin cap was frequently observed in cells with wide and ruffled lamellopodia; a characteristic phenotype of *TMEM67* patient cells (McIntosh, 2016). To distinguish between reduced bundle numbers of unchanged thickness (i.e. reduced total actin) and increased actin bundling and therefore fewer but thicker bundles (i.e. unchanged total actin), we imaged the phalloidin-stained actin cap under constant camera conditions and quantified fluorescence intensity of individual actin bundles by linescan analysis. There was no significant difference in fluorescence intensity of bundles within the actin

cap when patient cells were compared to controls (3850 ± 169 versus 4223 ± 145, n = 50 cells from three independent experiments per condition; Mann–Whitney test, p = 0.08). Therefore, it is unlikely that the reduction in actin cap bundle number seen in patient cells is a result of increased actin bundling, and instead may indicate that there is less F-actin between the apical surface of the nucleus and the plasma membrane.

siRNA-mediated silencing of *tmem67* in non-diseased control fibroblasts confirmed the link between TMEM67 and the actin cap. Control fibroblasts were transfected with *tmem67* siRNA and a scratch assay carried out, following the same method as above. Successful knockdown was judged by immunofluorescence and Western blotting using an anti-TMEM67 antibody (Figure 3.3d bottom right insets, and Figure 3.3f) and only cells which were clearly polarised but with low levels of TMEM67 fluorescence were analysed. Similar results were observed to those from the patient cells (Figure 3.3d, compare the top right insets). WT cell + *tmem67* siRNA fibroblasts had significantly fewer actin bundles in the perinuclear actin cap, compared to age-matched control + control siRNA (Figure 3.3e). Once again, we quantified the number of actin bundles within the cap using both linescan analysis and FilaQuant software and found that quantification method did not make a significant difference to the results (Figure 3.3e, n = at least 150 cells per cell line, over three independent experiments). The mean number of bundles in the actin cap of the cells treated with *tmem67* siRNA was 6.5 ± 0.5 (Mann–Whitney test, $p < 0.0001$, linescan analysis) and 5.5 ± 1.1 (Mann–

Whitney test, $p < 0.0001$, FilaQuant analysis) compared to 9.5 ± 0.6 (linescan analysis) and 9.6 ± 1.9 (FilaQuant analysis) in the fibroblasts treated with control siRNA.

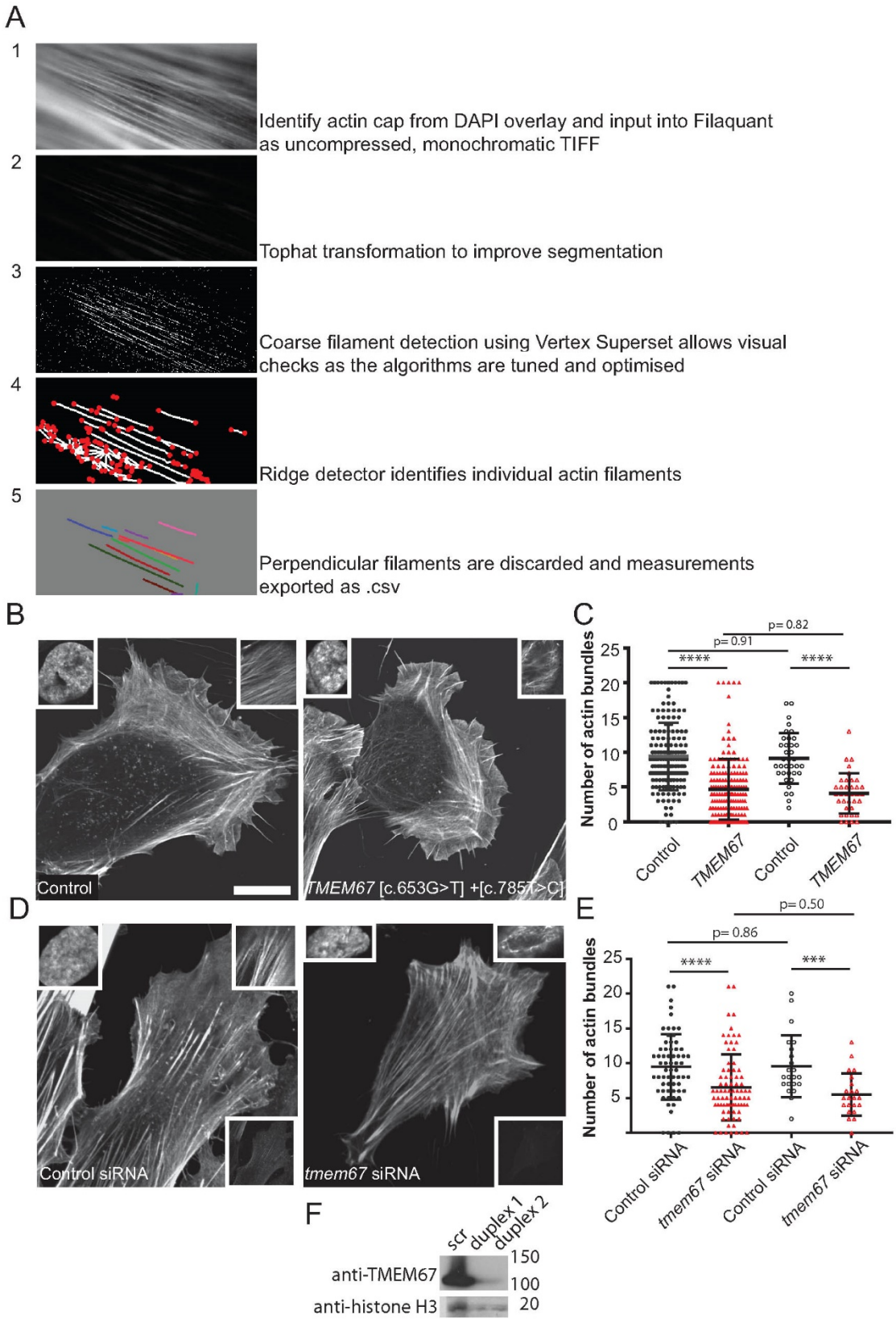

Figure 3.3 TMEM67 is required for the maintenance of the perinuclear actin cap in polarised migrating fibroblasts. (a) Workflow showing stages of the FilaQuant bundle quantification software. (b, d) Basolateral F-actin staining using phalloidin in control cells (left panels), TMEM67 patient cells (b, right panel) and tmem67 siRNA treated cells (d, right panel). Scale bar = 20 μm. The position of the actin cap was identified from the nucleus image (DAPI, top left inset in all panels), and the phalloidin image captured (top right inset in all panels). (c, e) Quantification of the number of bundles in the perinuclear cap in each condition, expressed as mean ± s.e.m. In both graphs the first two columns are derived from manual line-scan analysis of the actin cap, and the second two columns represent quantification obtained using FilaQuant software. See methods for details. Note that method of quantification does not affect the results. **** $P < 0.0001$, *** $P < 0.001$, Mann–Whitney test. (f) and (d, bottom right inset) tmem67 siRNA effectively reduces cellular TMEM67 as determined by Western blotting (f) and anti-TMEM67 immunofluorescence (d).

3.4 Plating cells onto laminin rescues the formation of the perinuclear actin cap in *TMEM67* patient fibroblasts

As it is known that ECM environment has profound effects on cellular migration and the actin cap, we thus investigated the role of individual matrix proteins in the formation of the perinuclear actin cap. As laminin, collagen and fibronectin levels were all shown to be reduced in the TMT MS data presented in Figure 3.1a, these ECM proteins were identified as targets for further investigation. Glass coverslips were coated in four different commercially available purified matrix proteins: collagen I, collagen IV, fibronectin and laminin. Equal concentrations of each protein were used, at 10 μg ml^{-1}: the concentration determined experimentally by our laboratory to be sufficient for effective coverage (Meadows, 2017). Equal numbers of *TMEM67* patient fibroblasts were seeded onto each of the matrix proteins and left to grow to confluency for four days. A scratch assay was performed following the same method used in section 3.3,

and the actin cap was examined (Figure 3.4; n = 170–200 cells per condition, from three independent experiments). ECM composition did not affect formation of the actin cap in control cells (Figure 3.4a, top right insets and Figure 3.4c, closed symbols; mean bundle number 9.3 ± 0.8 to 10.0 ± 0.9 derived from pooled linescan and FilaQuant data). However, when patient fibroblasts were plated on laminin, the appearance of the actin cap was rescued (Figure 3.4 compare a and b, top right insets of "laminin" panels) and the number of bundles in the actin cap (8.5 ± 0.6, Figure 3.4c open squares) was restored to that seen in the control cells (9.3 ± 0.7, Figure 3.4c closed squares; Mann–Whitney test, $p > 0.05$). In contrast, there was no change in actin cap appearance or actin bundle number observed in *TMEM67* patient fibroblasts on any other ECM type compared to the patient fibroblasts on their own CDM (collagen 1: 4.1 ± 0.4; collagen IV: 4.3 ± 0.5; fibronectin: 4.6 ± 0.5), nor in the control cells on any ECM protein compared to that of control cells on their own CDM (Supplementary Figure 1).

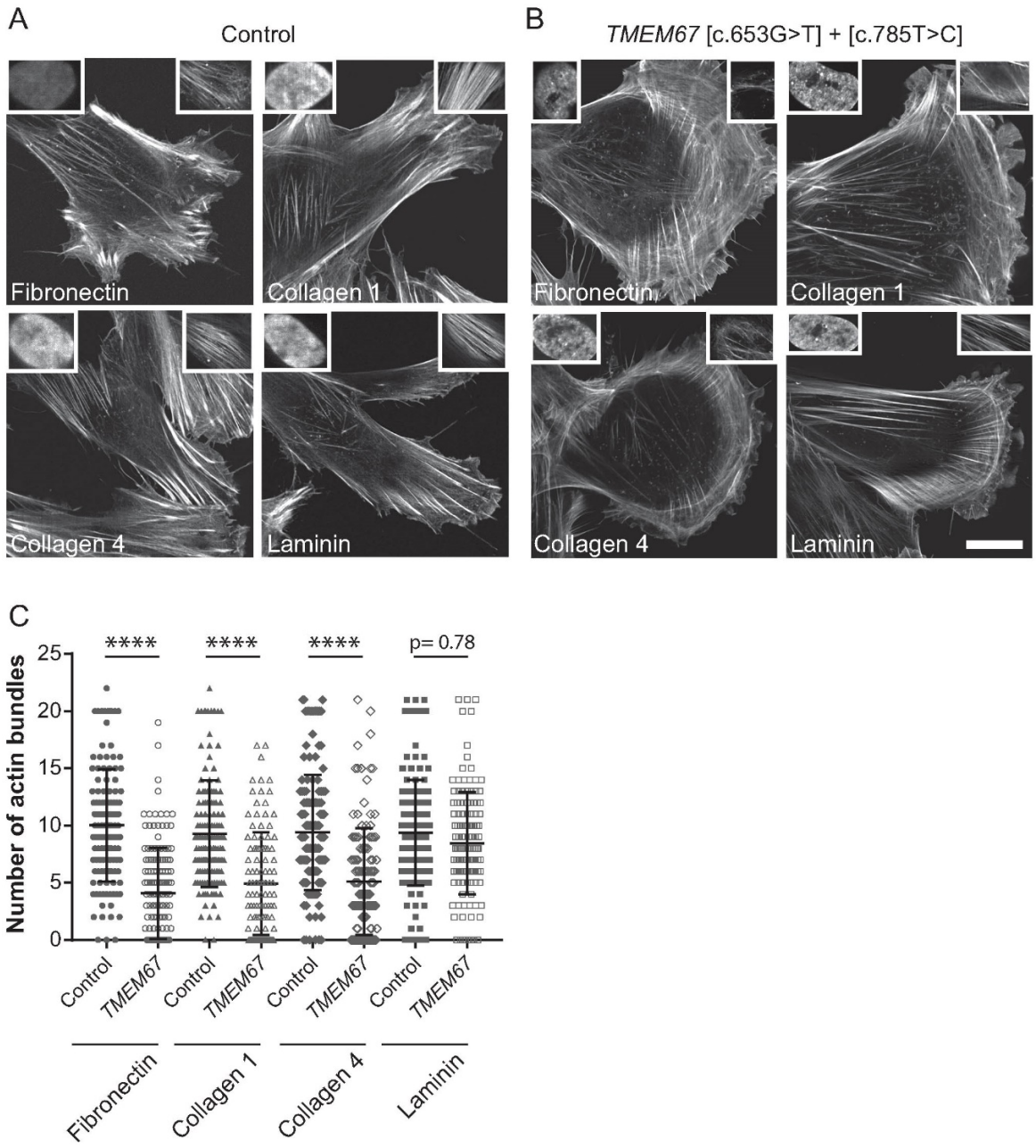

Figure 3.4 Laminin restores actin cap formation in *TMEM67* patient cells. (a, b) Basolateral F-actin staining using phalloidin in control cells (a), and *TMEM67* patient cells (b), plated onto purified ECM components as indicated. Scale bar = 20μm. The position of the actin cap was identified from the nucleus image (DAPI, top left inset in all panels), and the phalloidin image captured (top right inset in all panels). (c) Quantification of the number of bundles in the perinuclear cap in control cells (filled shapes) and *TMEM67* patient cells (open shapes) plated as indicated. Graph represents mean ± s.e.m of at least 170 cells per condition, from three independent experiments. Note that the number of actin cap bundles when cells are plated onto Laminin is indistinguishable in control and patient cells. **** $P < 0.0001$, Mann–Whitney test.

3.5 All combinations of laminin isoforms tested rescue the formation of the perinuclear actin cap

To narrow down the root of the laminin rescue, we asked whether there was a specific laminin isoform that would rescue cap formation. The TMT MS data shows that laminins α2, α4, β1, β2 and γ1 are all greatly reduced in the *TMEM67* cell CDM (Figure 3.1a). We plated fibroblasts on commercially available recombinant forms of laminin (BioLamina), with eight different combinations of alpha, beta and gamma chains (Table 3.1).

Table 3.1 Combinations of laminin chains tested.

α	β	γ
1	1	1
	2	
2	1	
	2	
4	1	
	2	
5	1	
	2	

TMEM67 patient fibroblasts were left for four days to grow to confluency, and a scratch assay was performed, following the same method used in section 3.3. Cells were left to migrate into the wound for 12 hours, before being fixed and stained for F-actin and the nucleus. Fluorescent imaging of the actin cap revealed that for all laminin combinations tested (Table 3.1), there was no significant difference between the

number of bundles in *TMEM67* fibroblast actin caps on the recombinant laminins and WT cells on their own CDM.

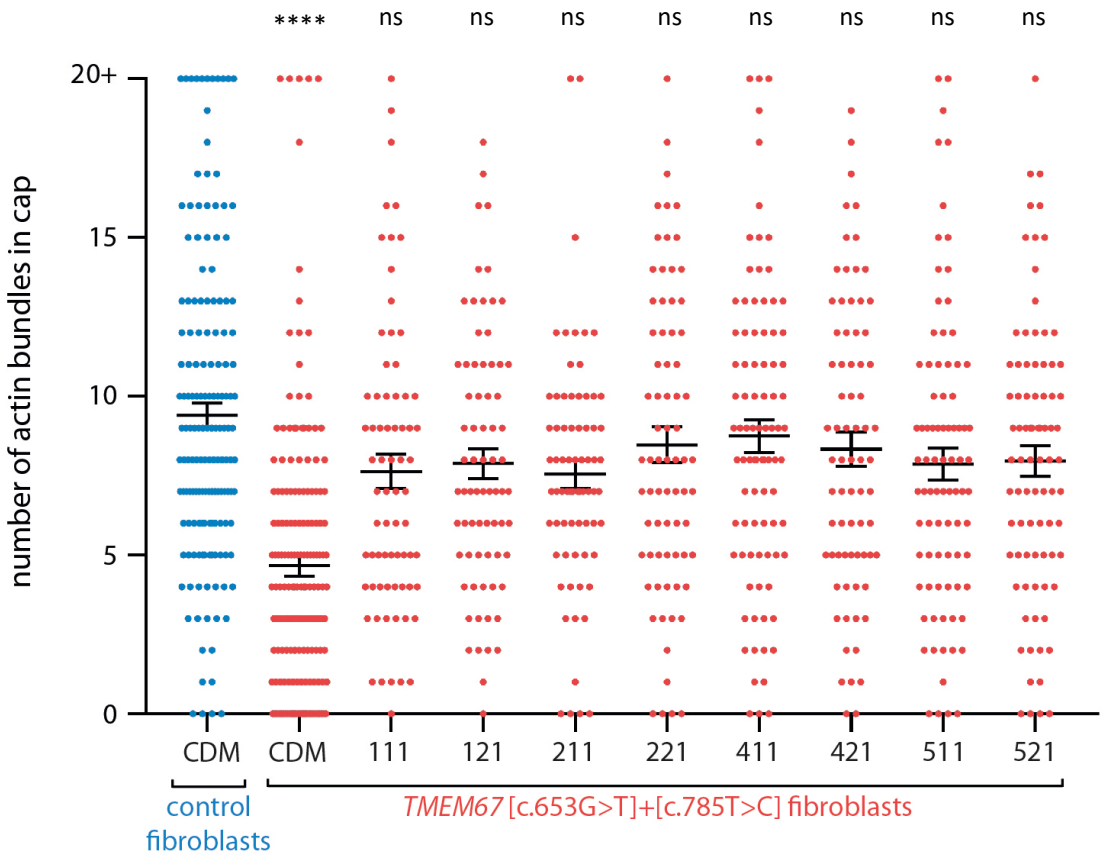

Figure 3.5 All laminin isoforms tested rescue the perinuclear actin cap in *TMEM67* patient fibroblasts. There was no significant difference in the number of actin bundles in the cap in *TMEM67* patient fibroblasts compared to non-diseased control fibroblasts on their own CDM (blue). Graph represents mean ± s.e.m of at least 150 cells for cells on CDM and at least 70 cells on recombinant Laminins, from three independent experiments. **** $P < 0.0001$, Mann–Whitney test, ns = not significant; all red datasets (patient cells) have been compared to blue dataset (non-diseased control cells).

There were no commercially available laminins with an alternate gamma isoform at the time of investigation. As such, we were not able to establish whether this rescue is due to the presence of laminin $\gamma 1$, which was found to be the second most decreased

laminin in the *TMEM67* matrix (Figure 3.1a). There were no overall trends between the presence or absence of any alpha or beta isoforms, lending further support to the hypothesis that the rescue may be a gamma chain-dependent phenomenon.

3.6 TMEM67 is a transmembrane protein, with a large extracellular loop at the N terminus

TMEM67 is the best studied of the MKS proteins, however there are still large gaps in the understanding of its structure and function. There are two main splice variants of TMEM67. Isoform 1 of TMEM67 is the canonical isoform, consisting 995 amino acids (Uniprot: Q5HYA8-1; Supplementary Figure 2). At the time of writing, there are 10 identified TMEM67 isoforms available on Uniprot, where isoform 1 and 2 are confirmed, and isoforms thereafter are computationally predicted. Only Isoform 1 has experimental data available (UniProt: Q5HYA8). There are conflicting data on the membrane-folding structure of TMEM67. Originally reported as having seven transmembrane regions (Smith *et al.*, 2006), other sources have reported only three (Dawe *et al.*, 2009), while at time of writing UniProt reports six (UniProt ID: Q5HYA8; UniProt Consortium, 2018). To better understand the membrane-folding architecture of TMEM67, Isoform 1 was put into transmembrane helix predictor TMHMM Server (v. 2.0). It was predicted that TMEM67 contains seven transmembrane domains with a large extracellular loop towards the N terminus (Figure 3.6). Six of these domains match with the six transmembrane regions predicted by UniProt, but UniProt does not report the N-terminal transmembrane region between amino acids 7–29. For the model in the present study, we have included the seventh domain.

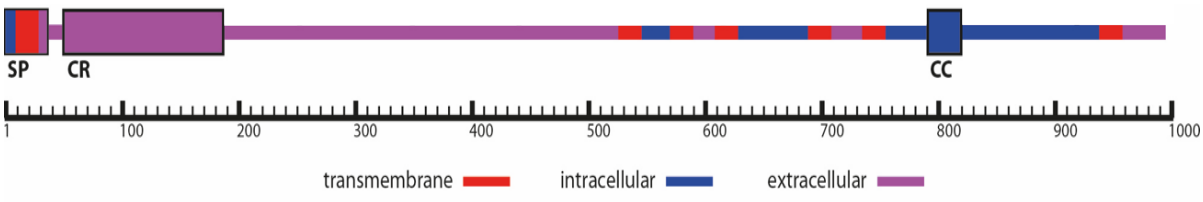

Figure 3.6 The predicted structure of TMEM67. Ruler indicates amino acid position. SP = signal peptide, CR = cysteine-rich domain, CC = coiled-coil domain.

The lack of consensus over the presence of a transmembrane domain between amino acids 7–29 does not impact the structure of the regions under investigation in this study: the large extracellular domain at the N terminus is universally predicted in all databases and source literature.

To date, the functional understanding of TMEM67 has been restricted to the protein's intracellular interactions: the function of the large extracellular loop containing the cysteine-rich repeat region has not been elucidated. So far we have shown that TMEM67 is required for the maintenance of the perinuclear actin cap in migrating cells, and that loss of TMEM67 corresponds to a loss of the actin cap which could be restored by plating cells on laminin. Previous work from our laboratory has shown that TMEM67 is a novel focal adhesion protein required for ECM organisation (Meadows, 2017). Therefore, we hypothesized that TMEM67 might provide a link between actin cap-associated focal adhesions and the ECM and, more specifically, that this might be mediated by the large N-terminal extracellular loop (Figure 3.6).

To test this hypothesis, we studied the effects of three clinically relevant mutations present in the N-terminal extracellular loop of TMEM67 (p.M252T, p.L349S and

p.R440Q) on actin cap formation. We expect that mutations effecting the formation or function of the extracellular loop will have a significant negative impact on the formation of the actin cap if our hypothesis that TMEM67 functions as a link between the actin cap and the ECM is correct. We also studied three further mutations in regions across TMEM67, two in intracellular loops of the protein, and one in a transmembrane region (p.R549C, p.C615R and p.F919del), in order to test the importance of these regions for actin cap formation.

Table 3.2 Plasmid sequencing for TMEM67 allelic series. All variants are derived from ciliopathy patient sequences and are reported as pathogenic.

Plasmid name	Codon change	Amino acid change	Mutation	Diseases reported	Reference
252	c.755T>C	p.Met252Thr	Missense	MKS JBTS NPHP	Consugar *et al.,* 2007; Otto *et al.,* 2009; Tallila *et al.,* 2009; Iannicelli *et al.,* 2010; Chaki *et al.,* 2011; Bachmann-Gagescu *et al.,* 2015
349	c.1046T>C	p.Leu349Ser	Missense	MKS JBTS NPHP COACH	Khaddour *et al.,* 2007; Iannicelli *et al.,* 2010; Chaki *et al.,* 2011; Bachmann-Gagescu *et al.,* 2015
440	c.1319G>A	p.Arg440Gln	Missense	MKS COACH	Consugar *et al.,* 2007; Khaddour *et al.,* 2007; Brancati *et al.*, 2009; Tallila *et al.,* 2009; Iannicelli *et al.,* 2010
549	c.1645C>T	p.Arg549Cys	Missense	MKS	Szymanska *et al.,* 2012; Zhang *et al.,* 2015
615	c.1843T>C	p.Cys615Arg	Missense	JBTS NPHP	Gunay-Agun *et al.,* 2009; Chaki *et al.,* 2011; Bachmann-Gagescu *et al.,* 2015
919	c.2754_2756 delCTT	p.Phe919del	In-frame deletion	MKS	Adams *et al*., 2012

Primers used for sequencing can be found in Supplementary Table 2.

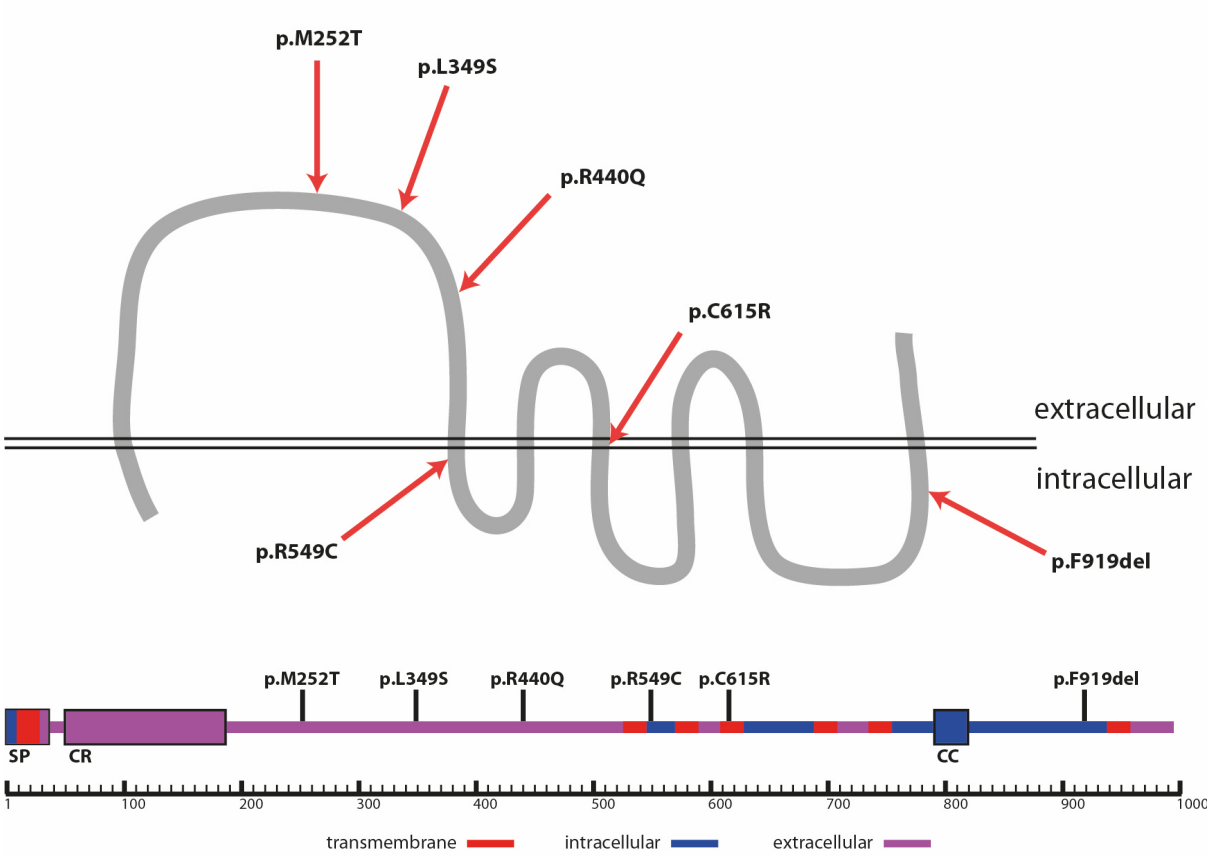

Figure 3.7 The six mutations in TMEM67 tested span across the protein. Ruler indicates amino acid position. SP = signal peptide, CR = cysteine-rich domain, CC = coiled coil domain.

3.7 Mutations that affect actin cap formation are associated with Meckel-Gruber syndrome

To ascertain which regions of TMEM67 are required for the maintenance of the perinuclear actin cap, we transfected *TMEM67* patient fibroblasts with plasmids carrying the HA-tagged forms of the TMEM67 mutants in Table 3.2, with an HA-only plasmid as a control. The fibroblasts were plated onto glass coverslips and left to grow to confluency for four days. Following the same protocol as previous scratch assays, the cell monolayer was scratched and cells were left to migrate into the wound for 12

hours before fixing and staining for IF microscopy. Transfected cells were identified using immunofluorescence with an anti-HA antibody. Analysis of the actin cap demonstrated that the cap was disrupted in all but one of the TMEM67 variants, with significantly fewer actin bundles compared to *TMEM67* patient fibroblasts transfected with wild-type HA-TMEM67 (Figure 3.8, graph represents pooled linescan and FilaQuant data from 100 cells per condition, over 3 experiments, $P < 0.0001$ to $P < 0.001$, Kruskal–Wallis test with Dunn's post hoc analysis). Actin bundle number in *TMEM67* fibroblasts transfected with an HA-only plasmid (3.9 ± 0.3) was indistinguishable compared to *TMEM67* patient cells (no transfection, 4.1 ± 0.7), confirming the HA-plasmid was not having any influence on the results. However, the C615R variant was able to rescue actin cap formation to the same extent as the non-diseased control HA-TMEM67 construct. This is the only variant tested that has a mutation within a predicted transmembrane domain, perhaps pointing to a less deleterious effect on specific aspects of TMEM67 function. In support of this, TMEM67 C615R is the only construct tested that is associated with Joubert syndrome and nephronophthisis, but not the neonatal lethal Meckel-Gruber syndrome, although other non-Meckel-Gruber syndrome-associated variants would need to be assessed to further test this idea.

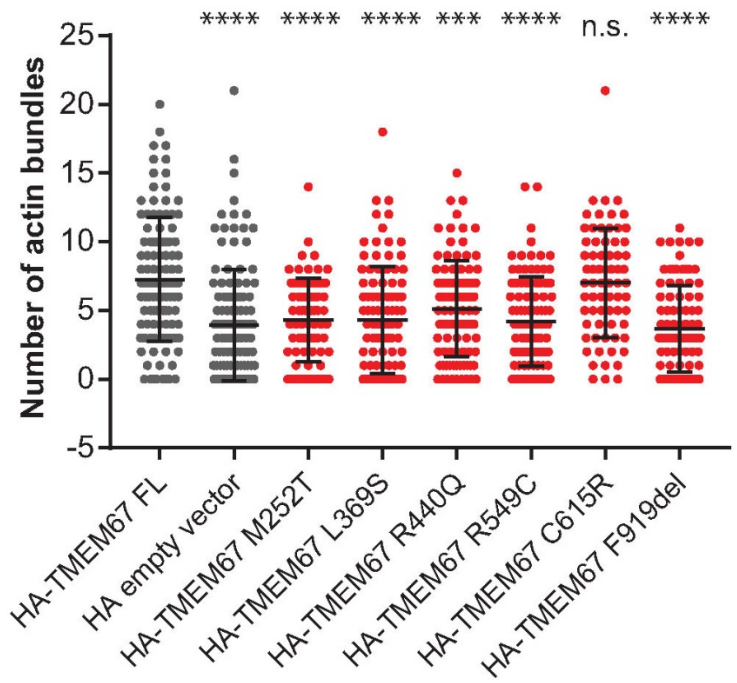

Figure 3.8 Mutations affecting actin cap formation are all associated with Meckel-Gruber syndrome. *TMEM67* patient cells were transfected with a series of HA-tagged constructs that model clinically relevant TMEM67 mutations, and their ability to restore actin cap formation assessed. The graph shows quantification of the number of bundles in the perinuclear cap in each condition, expressed as mean ± s.e.m of at least 100 cells per condition, from three independent experiments. Grey bars indicate control transfections with full length wild-type (FL) HA-tagged TMEM67 or vector only. Red bars indicate clinically relevant TMEM67 mutations. Note that only the C615R construct, which models a mutation associated with Joubert Syndrome and Nephronophthisis but not Meckel-Gruber syndrome, can rescue actin cap formation to the same extent as non-diseased control TMEM67. **** $P < 0.0001$ and *** $P < 0.001$, Kruskal–Wallis test with Dunn's post hoc analysis.

However, the rescue of the actin cap in variant 615 could also be a reflection of the contribution of multiple factors regulating the actin cap. For example, the extracellular environment can affect the actin cytoskeleton, and reduced ECM levels can result in a dysregulation to the actin cap. This rescue of cap fibres observed in variant 615 could potentially be as a result of an intermediate phenotype, whereby the actin fibres themselves are not disrupted directly, but the aberrations to the ECM phenotype are

still in place (or vice versa), resulting in a partial increase in actin fibres in these variants, but not a full increase to control levels. To further investigate this hypothesis in the future, the ECM produced by these variants could be visualised by SEM to establish the effects of mutation in these regions on ECM architecture.

3.8 GFP-trap of TMEM67 suggests a role of the protein in organising membrane-actin cytoskeleton linkages at adhesion sites

In order to explore the hypothesis that the N-terminal extracellular loop (ECL) of TMEM67 could provide a link between actin cap-associated focal adhesions and the ECM further, we utilised a GFP-tagged mutant TMEM67 lacking this ECL: TMEM67 ΔECL. To investigate the function of this ECL, we compared binding partners of TMEM67 full length and TMEM67 ΔECL using a GFP-Trap® to isolate the target proteins and their binding partners, followed by mass spectrometry to identify the proteins pulled out. The TMEM67 full length and TMEM67 ΔECL constructs were cloned into a pEGFP-N1 plasmid, 3T3 fibroblasts were transfected with these plasmids, and the cells left to grow to 60% confluency. A GFP-only plasmid was used as a control. As we hypothesised TMEM67 to interact with the ECM, we harvested the cells and the ECM, and incubated the resultant extracts with Chromotek GFP-Trap® beads to isolate the GFP-TMEM67 constructs and their binding partners. The constructs were successfully detected by western blot in both the whole cell lysate sample and the precipitate from post-incubation with 10% GFP-Trap® beads (Figure 3.9). Protein concentration was markedly increased in the 10% bead sample compared to the whole cell lysate in both repeats (A and B), demonstrating that

incubation with the GFP-Trap® beads successfully concentrated the tagged GFP-TMEM67 constructs.

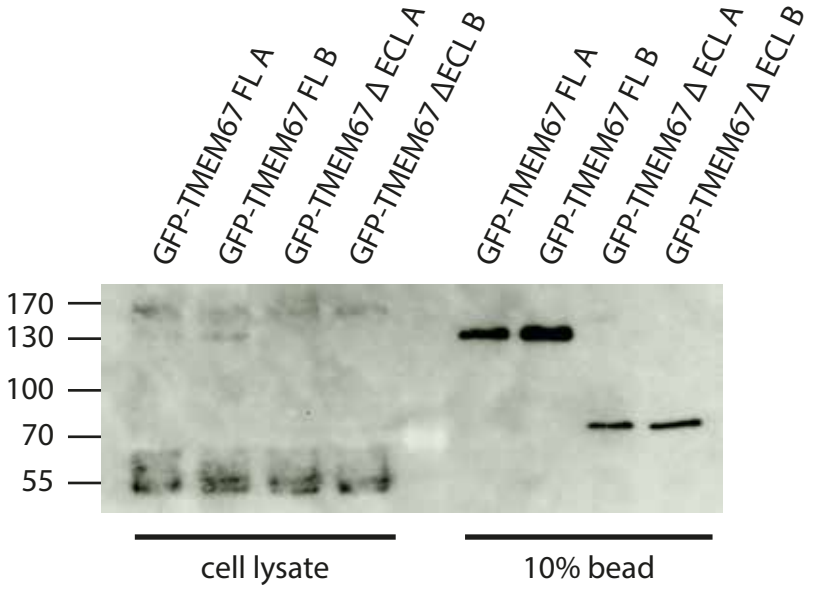

Figure 3.9 Western blot confirming successful concentration of GFP-TMEM67 full length (FL) and GFP-TMEM67 ΔECL after incubation with GFP-Trap® beads compared to in the whole cell lysate, in two separate repeats (A and B).

Initial data obtained from the mass spectrometry of our protein lysate were filtered according to the process illustrated in Figure 3.10 to produce a list of high-confidence hits to be taken forward for further analysis. Both GFP-TMEM67 full length and GFP-TMEM67 ΔECL were compared against a negatives list from our GFP-only control to remove any non-specific hits. Proteins detected exclusively in GFP-TMEM67 or GFP-TMEM67 ΔECL samples were considered true positives, as were proteins in the negatives list that had at least a 2.5-fold increase in score. Data from two independent replicates were pooled, and proteins appearing in both lists were considered high-confidence double-positive hits that represent putative GFP-TMEM67 (n = 352) or

GFP-TMEM67 ΔECL (n = 525) interacting proteins (see Supplementary Table 3 for the full double positive lists for GFP-TMEM67 and GFP-TMEM67 ΔECL). 179 double positives were shared between GFP-TMEM67 and GFP-TMEM67 ΔECL, while 173 proteins that were identified in the full length TMEM67 samples were lost in the ΔECL mutant. TMEM67 itself and known TMEM67-interacting protein Nesprin were double positives, suggesting that our approach had been successful at pulling down TMEM67-associated proteins (Dawe *et al.,* 2009). Proteins known to interact with TMEM67 at the ciliary transition zone were not identified, however this can be attributed to the fact that the fibroblasts used for the GFP-Trap® were in a cycling culture and therefore non-ciliated. This supports the idea of TMEM67 having multiple functions within the cell with distinct cilium-independent roles, as it appears to interact with a unique set of proteins outside the context of the cilium. This is a proof-of-principal that GFP-Trap® is a good tool for studying TMEM67 associated proteins. In the future, a more thorough GFP-Trap® investigation could be completed with cells at different cell cycle stages to better elucidate TMEM67s protein-protein interactions as they change throughout the cell cycle.

Functional annotation clustering using DAVID 6.8 software (Huang *et al.,* 2009a; Huang *et al.,* 2009b) revealed that our initial hypothesis for TMEM67 functioning at actin cap-associated focal adhesions as an interactor with the ECM is unlikely. While ECM proteins were enriched in the TMEM67 samples, grouping by cellular compartment (GOTERM_CC_5) placed ‘basement membrane’ at 14th position and

'proteinaceous extracellular matrix' in 15th (Figure 3.11a). Grouping by biological process (GOTERM_BP_5) placed 'proteoglycan formation' in 8th, and 'extracellular matrix organisation' at 15th (Figure 3.11b). Three collagens were identified (12α1, 3α1, 4α1), together with fibulin-2, laminin α3, and the non-integrin 37/67-kDa laminin receptor Rpsa. All but collagen IVα1 and laminin α3 were found associated with the ΔECL mutant, suggesting that the N-terminal ECL is not required for linkage with the ECM, as these would have been otherwise absent in our mutant. Laminin α3 was not available for the actin cap studies described above at the point of investigation, and so its role in actin cap formation could not be determined within this thesis.

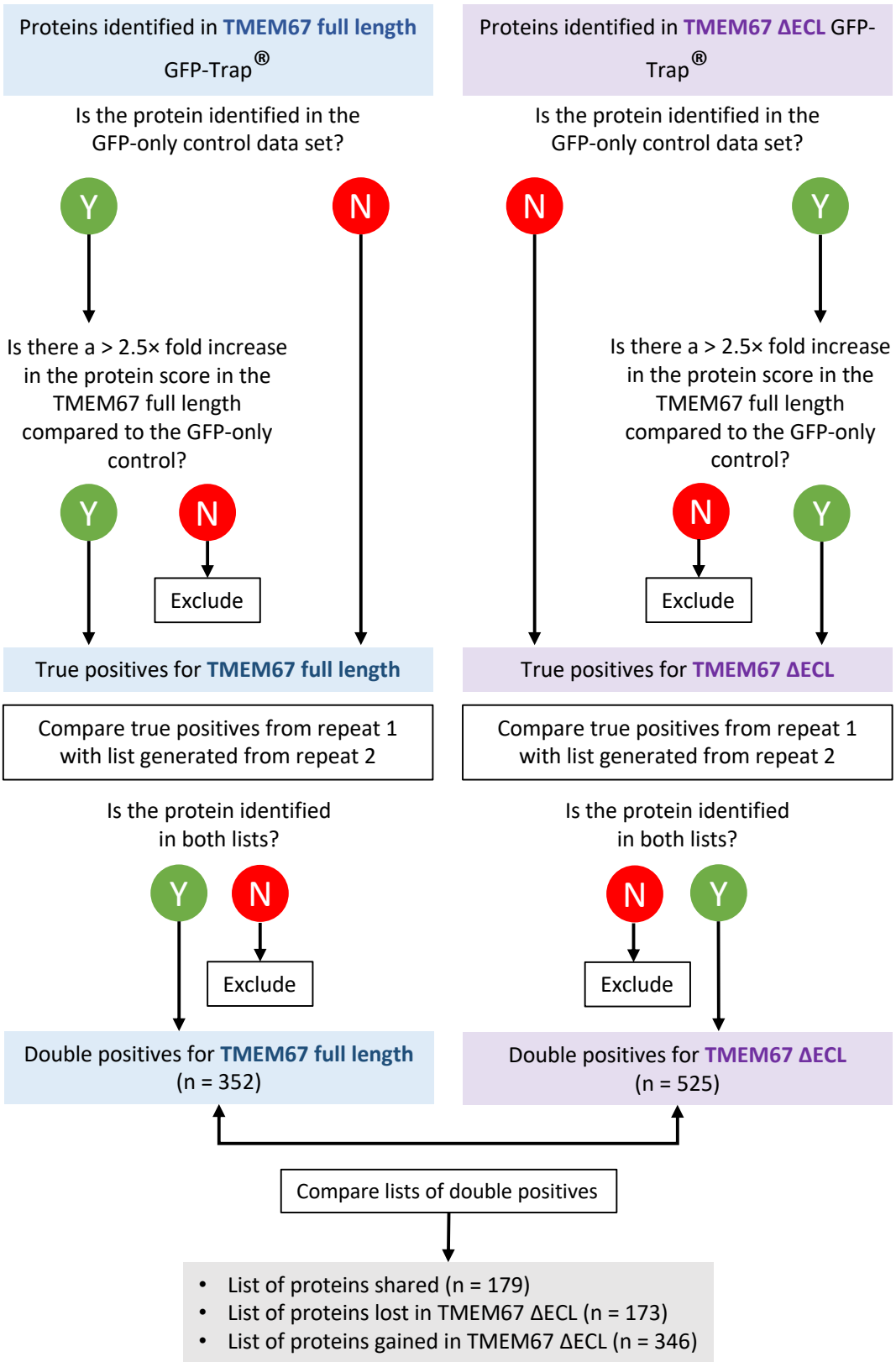

Figure 3.10 Filtering steps taken on GFP-trap data for the TMEM67 full length sample (blue) and the TMEM67 ΔECL sample (purple) to produce list of high confidence, double positive hits. The double positive lists for the two variants were then compared to investigate function of the N-terminal ECL of TMEM67.

A

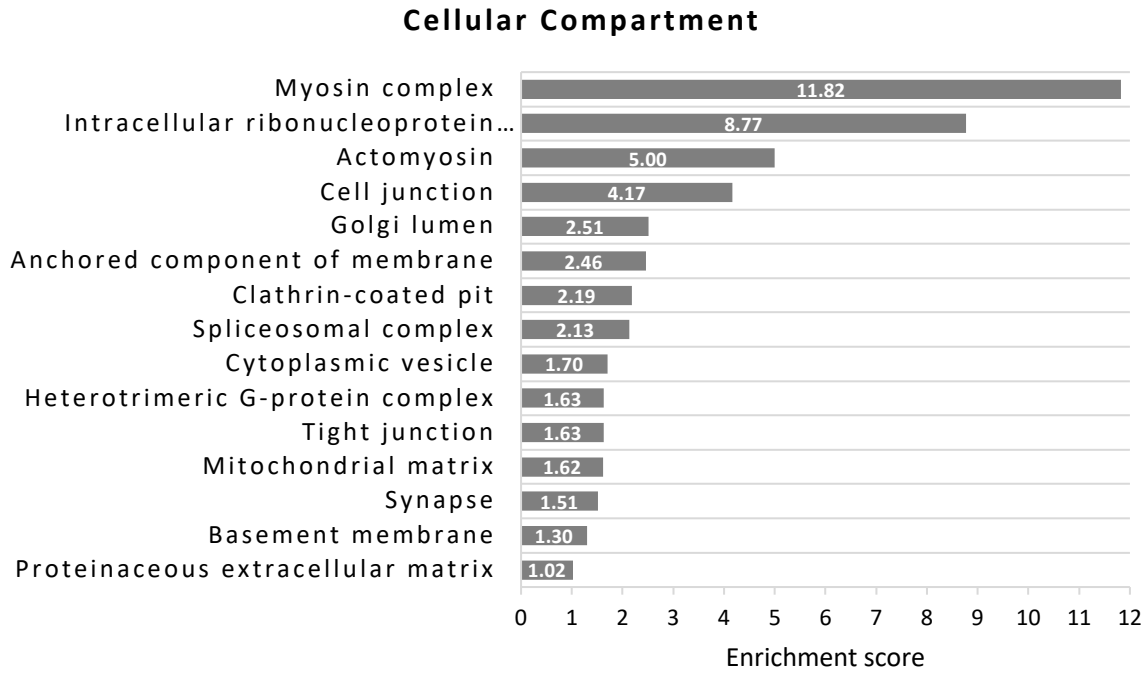

B

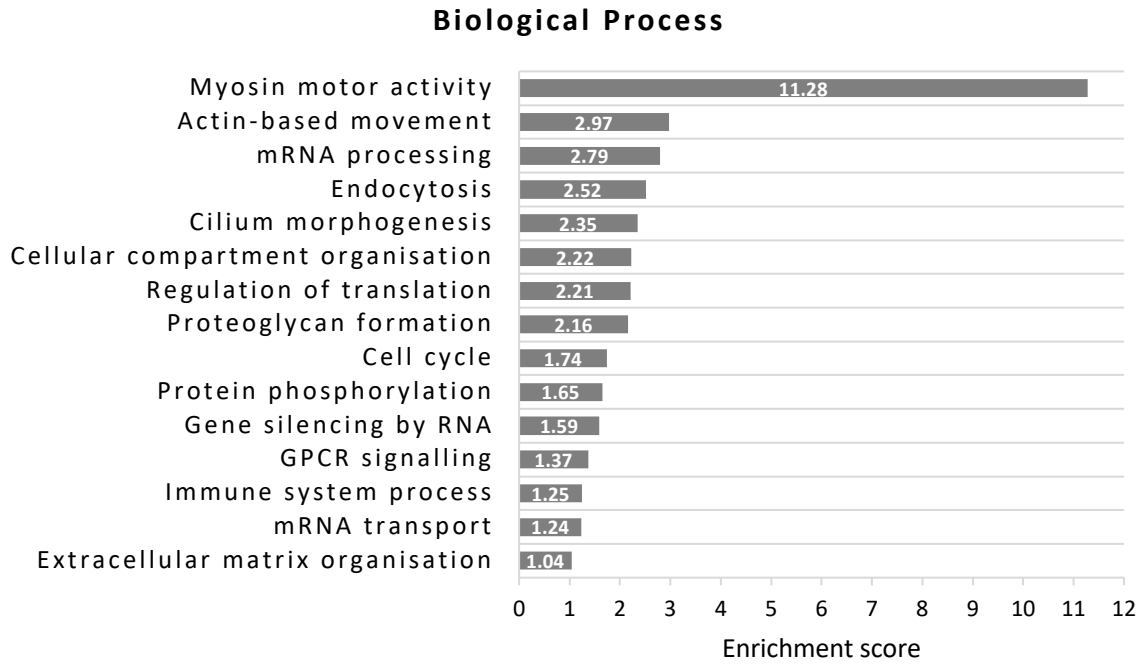

Figure 3.11 Clustering of GFP-trap data by (a) Cellular Compartment (CC) and (b) Biological Process (BP) sheds light on function of TMEM67. For both analyses, acto-myosin roles for TMEM67 came out as the top function.

Actin- and myosin-related functions were the most significant hits for both cellular compartment and biological process clustering (Figure 3.11). Within the top 15 hits for biological process was also cilium morphogenesis, cellular compartment organisation, G protein-coupled receptor (GPCR) signalling and protein phosphorylation that, alongside actin-related functions, align with previous described cellular roles for TMEM67 (Smith *et al.*, 2006; Dawe *et al.*, 2007b; Avasthi *et al.*, 2012; Abdelhamed *et al.*, 2015) and provide confidence that our GFP-Trap® approach had been successful.

Most enriched were proteins involved in the biological process 'myosin motor activity', and cellular compartment myosin complex, with enrichment scores of 11.28 and 11.82, respectively. Further examination of the myosin cluster revealed many different classes of motor protein were identified (Table 3.3), including all three conventional non-muscular class II myosins, the minus end-directed motor myosin VI, and several class I myosins, which can all form dynamic links between the actin cytoskeleton and the plasma membrane/intracellular vesicles.

As well as these well-characterised myosins, the dataset also contained several less studied unconventional myosins. Myosin XVIIIa is related to Myosin II, but is a weak motor that probably functions as a tether as it can link transmembrane receptors to the cytoskeleton (Masters, Kendrick-Jones and Buss, 2017). Myosin X is important for filopodia formation, binds integrins, and facilitates their transport at filopodia tips (Zhang *et al.*, 2004), while myosin VIIa's role in linking adhesion proteins to the

cytoskeleton is also well described in processes such as cell spreading and migration (Tuxworth *et al.*, 2001), where it may also function as a tension sensor (Nyitrai and Geeves, 2004).

Table 3.3 Myosins (a) shared, (b) lost, and (c) gained between TMEM67 full length and TMEM67 ΔECL constructs

(a) Myosins shared

Myosin	Gene name
Unconventional myosin-Ib	Myo1b
Unconventional myosin-Ic	Myo1c
Unconventional myosin-Id	Myo1d
Unconventional myosin-Ie	Myo1e
Unconventional myosin-VI	Myo6
Unconventional myosin-X	Myo10
Unconventional myosin-XVIIIa	Myo18a
Myosin-9	Myh9
Myosin-10	Myh10
Myosin-14	Myh14
Myosin regulatory light chain 12B	Myl12b
Myosin light polypeptide 6	Myl6

(b) Myosins lost in TMEM67 ΔECL

Myosin	Gene name
Myosin-11	Myh11
Unconventional myosin-Va	Myo5a
Unconventional myosin-VIIa	Myo7a
Myosin light chain 6b	Myl6b

(c) Myosin gained in TMEM67 ΔECL

Myosin	Gene name
Unconventional myosin-IXb (Fragment)	Myo9b

The majority of these myosins (13/18) were shared between the full length *TMEM67* and the ΔECL mutant, however, Myosin-11, the unconventional myosins Va and VIIa, and myosin light chain 6b were lost. *TMEM67* ΔECL also gained an association with motor myosin IXb, which has a RhoGAP domain and may function in the regulation of actin organisation via negative feedback of Rho signalling (van den Boom *et al.*, 2007). As a minority of myosin associations (4/18) were lost with the deletion of TMEM67's N-terminal ECL, this suggests that this region of the protein plays only a slight role for myosin association. The most likely candidate for myosin association is the C-terminal coiled-coil domain, which is known to associate with other actin binding proteins (Dawe *et al.,* 2009; Adams *et al.,* 2012).

Biological processes 'mRNA processing', 'endocytosis', and 'regulation of translation' have not been previously linked to *TMEM67* function, and appeared 3rd, 4th, and 7th most enriched protein clusters respectively in this dataset. This appears consistent with some of the functions of the myosins listed in in Table 3.3, specifically Myosin-10, which is involved in the stabilisation of collagen I mRNAs, Myosin-Ic which has a nuclear isoform which associates with RNA polymerase I and II to help initiate transcription, and Myosin-VI, which has been implicated in clathrin-mediated endocytosis (Masters, Kendrick-Jones and Buss, 2017). Concurrently, mutations in *TMEM67* have been reported to lead to nuclear morphology defects (Dawe *et al.,* 2009).

Taking these results together, we hypothesise a potential role for TMEM67 in organising or regulating membrane-actin cytoskeleton linkages at adhesion sites, where it could be tethered by myosin XVIII and possibly aids tension sensing through myosin VIIa and the contractile myosin IIs. There was no clear relationship between mutation of the first extracellular loop and loss of a particular gene ontology group, making it difficult to draw any conclusions about the function of this region of TMEM67, despite its obvious importance for the development of ciliopathy. Within the scope of this thesis it was not possible to validate the potential myosin–TMEM67 interaction suggested by our GFP-trap® data. In order to draw a more conclusive hypothesis on the role of TMEM67, an alternate method, such as co-immunoprecipitation of the protein should be performed in order to confirm these early indicators.

4 Discussion

4.1 Summary

This thesis builds upon several lines of research from the Dawe research group into the extra-ciliary roles of TMEM67. Outside of the ciliation defect, our laboratory group has characterised numerous cellular abnormalities directly linked to the loss of TMEM67, including defective ECM production, alterations to the adhesome, loss of directed cell migration, widespread alterations to the actin cytoskeleton and associated signalling pathway RhoA, and alterations to Golgi and nucleus morphology (Dawe *et al.,* 2009; McIntosh, 2016; Meadows, 2017; Dawe lab, unpublished observations). In this thesis, it has been shown that loss of TMEM67 results in a defective perinuclear actin cap, which is the most likely cause of the loss of directionality in migrating *TMEM67* patient cells. Additionally, we characterised potential novel interactions between TMEM67 and a number of myosins which localise to focal adhesions. Together, we hypothesise a possible role of TMEM67 in organising or tethering membrane–actin cytoskeleton linkages at adhesion sites.

4.2 Link between extra-ciliary functions of TMEM67 and the cellular phenotypes observed

4.2.1 TMEM67-associated defects in the ECM could contribute to the increased speed of migrating patient cells

SEM analysis of the *TMEM67* patient cell ECM revealed dramatically different architecture compared to the ECM secreted by non-diseased cells, reflective of the decreased protein levels in the matrix characterised previously (Meadows, 2017). Reciprocal plating of *TMEM67* cells on WT matrix and WT cells on *TMEM67* matrix and subsequent imaging of the resultant matrix revealed that *TMEM67* patient cells

do not degrade the matrix, despite higher expression levels of matrix metallopeptidases (Meadows, 2017). We were therefore confident that increased metallopeptide secretion was not a factor effecting observed ECM phenotypes continuing forward, and instead we are confident that our observations are canonically *TMEM67* mutation related.

The ECM plays a number of important biological functions to the cell. It provides both structural and biochemical support to the cell, facilitating cell adhesion, communication, and differentiation, and is vital for growth and wound healing (Rozario and DeSimone, 2010). The ECM also sequesters a number of important growth factors (Rozario and DeSimone, 2010). It thus follows that disruption to the ECM would have widespread cellular, as well as developmental, consequences. At the cellular level, a number of physical and biochemical qualities of the ECM directly impact migration (Palecek *et al.*, 1997; Strachan and Condic, 2003; Lange and Fabry, 2013; Wen *et al.*, 2015), and the defects to the matrix observed with loss of TMEM67 could help explain some of the migration defects observed in *TMEM67* patient cells. The data presented in Figure 3.1 highlight that the protein levels of the *TMEM67* CDM are disrupted compared to WT levels, and that there is an overall decrease in production of ECM proteins leading to visible architectural differences in the CDM. As well as a reduction in overall ECM concentration, reduced protein levels in the CDM are likely to have knock-on effects on matrix rigidity, as reductions in collagens and altered balances of proteins change the physical properties of the matrix (DiMilla *et al.*, 1993; Strachan and Condric, 2003). As loss of TMEM67 results in quite major aberrations to the ECM (Meadows, 2017), it seems likely that this could be contributing to the migration defect in patient fibroblasts.

There are two separate defects in migration linked to the loss of TMEM67: 1) cells migrate *faster*, and 2) cells migrate with *reduced directionality*. The aforementioned ECM qualities are likely to be a key influencer to the increase in speed of the *TMEM67* cells. Speed of cell migration is mostly dictated by one factor: the number of engaged adhesions (DiMilla *et al.,* 1991; Lange and Fabry, 2013). For a cell to migrate, adhesions must be made at the front of the cell to stabilise the extending lamellipodium, and adhesions must be disassociated at the rear of the cell to allow retraction of the tail. Tension on the actin cytoskeleton from the dynamic formation and turnover of these adhesions is the main driver of cell migration (DiMilla *et al.*, 1991; DiMilla *et al.*, 1993; Metzner *et al.*, 2007). With high numbers of engaged adhesions, the rate at which de-adhesion at the cell rear occurs becomes a limiting factor to speed of migration. However, with too few engaged adhesions, the lamellipodium is not stable and there is less tension through the actin cytoskeleton, hampering forward movement (DiMilla *et al.*, 1991; DiMilla *et al.*, 1993). The changes observed in the ECM as a result of the loss of TMEM67 are likely to contribute to the migration defects in patient cells. Firstly, with the low ECM concentration found with *TMEM67* patient cells, there are fewer sites for ECM-cell attachment directly resulting in fewer engaged adhesions. As a result, the adhesive force the cell needs to overcome in order to generate movement is reduced, and this could partly explain the faster migration speeds observed in *TMEM67* patient fibroblasts. Changes in ECM concentration and protein composition are likely to influence matrix rigidity, and as shown in the model in Figure 1.7, matrix rigidity can also influence the number of engaged adhesions due to changes in cell cortical tension and resultant cell spreading. On more rigid substrates, there is more resultant force exerted on the cell from the matrix, which facilitates cell spreading, thus increasing the number of cell-matrix adhesions. The

present study did not directly investigate the rigidity of the CDM produced by *TMEM67* patient cells, and so conclusions on the effect of differences in rigidity of the patient cell CDM on the migration defects cannot be drawn, however, from our knowledge of matrix properties and the alterations to protein level, it could tentatively be suggested that the ECM produced by *TMEM67* patient fibroblasts would be less rigid: collagens provide tensile strength and provide resistance to deformation, and increased collagen concentration has been directly linked to increased matrix rigidity (Yunoki *et al.*, 2011; Li *et al.*, 2017). As collagen production is reduced in *TMEM67* patient cells, it follows that the ECM would be less rigid.

The image however is not this simple: while these physical matrix properties can influence migration speed, the factor that underpins migration speed is the number of engaged adhesions. Therefore, we cannot reliably link the physical matrix properties alone to migration speed unless there is no other factor influencing the engagement of adhesions. This is not the case in MKS type 3: TMEM67 has been shown to be a focal adhesion protein, where loss of the protein results in major changes to the adhesome (Meadows, 2017). Therefore, it could be the case that the matrix produced by *TMEM67* patient cells is more rigid, but reduced numbers of functional adhesions result in faster migration, up until the point where the lamellipodia become unstable. Testing the rigidity of the matrix produced by *TMEM67* patient fibroblasts using atomic force microscopy to analyse the deformation of the matrix will help to classify which factors are contributing to the migration abnormalities.

4.2.2 TMEM67 is required for maintenance of the perinuclear actin cap

Loss of TMEM67 has been shown to result in decreased directionality during cell migration, a rotating nucleus and a mispositioned centrosome (Dawe lab, unpublished observations). The data presented in this thesis suggest that this directionality defect is due to a failure to assemble or maintain the perinuclear actin cap.

The actin cytoskeleton is organised into a highly complex three-dimensional structure (see Figure 1.3). While there are a number of tools for image analysis, problems with blurring and imaging-related artefacts can arise due to high throughput automation methods or the structure of the filaments. The latter particularly comes into play when actin filaments pass through different focal planes, which when imaged by two-dimensional microscopy methods often exhibit blurring. As the perinuclear actin cap is formed of actin filaments terminating at the basal surface and moving up to the apical plane (see Figure 1.4), it therefore poses a challenge for automated analysis. In addition, limited research thus far has investigated the number of actin bundles in the actin cap, with the majority of studies only quantifying the presence, absence or disruption of the actin cap (Khatau *et al.*, 2009; Kim *et al.*, 2012; Maninová and Vomastek, 2016; Thakar and Carroll, 2017). A limitation of these studies is the use of discontinuous grouping systems: where does the boundary lie between ‘presence’ and ‘disruption’ of the actin cap? A quality of the actin caps of MKS patient cells observed in this study was well organised actin bundles in the cap, but larger gaps between bundles, or fewer bundles in the cap and thus it is difficult to draw the distinction between actin cap presence and disruption. In order to overcome both of these limitations to the analysis of the actin cap, we used a continuous quantification method by quantifying the number of actin bundles in the nuclear area, and also used two quantification methodologies, one manual (linescan analysis; Woroniuk *et al.,* 2018),

and one automated approach (FilaQuant anaysis; Matschegewski *et al.,* 2012) to increase the robustness of our data.

Perinuclear actin cap fibres hold more tension than other basal actin stress fibres (Kim *et al.*, 2012). In order to accommodate this tension and stabilise the perinuclear actin cap, actin cap-associated focal adhesions are elongated and larger than normal focal adhesions (Kim *et al.*, 2012). Disruption to these specialised focal adhesions results in the breakdown of the actin cap. Disruption to the LINC complexes, which tether the actin cap fibres to the nucleus also results in the breakdown of the cap (Khatau *et al.*, 2012). TMEM67 associates with both LINC complexes and focal adhesions (Khatau *et al.*, 2012; Meadows, 2017). Thus, if TMEM67 is involved in actin binding at both locations, loss of the protein could result in a potential decrease in tension held at these adhesion points, and cause a breakdown of the actin cap.

The perinuclear actin cap is also affected by the ECM. On softer substrates, the cap is not present, as the fibres are not able to hold enough tension through their focal adhesions for the fibres to stabilise (Kim *et al.,* 2012). Following our hypothesis that the *TMEM67* matrix would be less rigid than a control matrix due to reduced expression of collagens, it follows that the physical ECM properties could be contributing to our actin cap phenotype. If this were the case, we would expect the plating of cells on collagen matrices to rescue the actin cap. However, our data show that only laminin rescued the cap, with no significant increase of actin cap fibres on any other matrix protein tested, including collagen I and IV. This therefore suggests that the altered physical properties of the *TMEM67* patient cell matrix are not the major influence on our observed cap phenotype.

We have shown that laminin rescues actin cap appearance, but within the scope of this thesis it wasn't possible to test whether the directionality defect was rescued. However, as the cap is integral to the maintenance of directed cell migration, we hypothesise that a rescue would be likely. A point for further examination would therefore be to test the directionality of migrating fibroblasts in live culture on laminin. The substrate-specific differences in cap rescue in *TMEM67* patient cells suggest that the underlying defect for the directionality defect is not physical properties: i.e., it is not driven by the overall decrease in ECM. As integrins are substrate-specific and are a major component of focal adhesions (Vicente-Manzanares and Horwitz, 2011), it follows that our substrate-specific actin cap rescue could be a result of defects to a specific integrin in *TMEM67* fibroblasts, reversible by the presence of extra-cellular laminin.

While our data suggest that the defective ECM is not the main underlying cause of the actin cap defect, the aberrant matrix could affect engagement of adhesions. Fewer engaged adhesions as a result of the lower levels of ECM produced by *TMEM67* patient cells, as well as defects to the overall structure of adhesions observed with loss of TMEM67 could both be contributing to the loss of actin cap fibres observed in patient cells.

4.2.3 TMEM67 may function in organising or recruiting membrane-actin cytoskeleton linkages at focal adhesions through an interaction with myosin

Based on our initial data, we originally hypothesised that TMEM67 functioned in the coupling of the actin cytoskeleton to the ECM at focal adhesions, where TMEM67 is known to localise (Meadows, 2017). TMEM67 associates with filamin A, an actin

binding protein, at its intracellular C-terminal coiled-coil domain. Based on the structure of the protein, we hypothesised that the N-terminal extracellular loop could be the point of association with ECM proteins.

To establish whether the N-terminal ECL of TMEM67 does indeed bind with the ECM, we performed a GFP-Trap® on GFP-TMEM67 and a mutant GFP-TMEM67 which lacks this N-terminal ECL. Interestingly, while ECM proteins were enriched in the TMEM67 samples, 'proteinaceous extracellular matrix' and 'extracellular matrix organisation' were included at the bottom of our cellular compartment and biological process lists respectively (Figure 3.11). Additionally, all but two of the ECM proteins identified in our GFP-TMEM67 dataset were also found in our GFP-TMEM67 ΔECL mutant, suggesting that this domain is not required for linkage with the ECM, as otherwise we could have expected all ECM proteins to be absent in our mutant dataset.

Our findings instead suggest that instead of TMEM67 functioning as a linker with the ECM, it could potentially be involved with organising or regulating membrane-actin linkages at adhesion sites through association with a number of myosins. Table 4.1 summarises the function of the myosins identified by our GFP-trap®.

Table 4.1 Summary of the functions of myosins (a) shared, (b) lost, and (c) gained between TMEM67 full length and TMEM67 ΔECL constructs. Protein function summarised from UniProtKB, the Human Genome Database, and (Masters *et al.*, 2017).

(a) Myosins shared

Myosin class	Myosin	Gene name	Protein function
Class I	Unconventional myosin-Ib	Myo1b	Can directly associate with membranes. Is required for directed cell migration. Involved in neurite outgrowth and vesicular transport.
Class I	Unconventional myosin-Ic	Myo1c	Can directly associate with membranes. Multiple transcript variants encoding different isoforms identified, with variety of functions, including exocytosis, hair cell adaptation, regulation of actin organisation during cell migration. A nuclear isoform associates with RNA polymerase I to promote transcription activity.
Class I	Unconventional myosin-Id	Myo1d	Can directly associate with membranes. Required for membrane trafficking to apical domain in polarised epithelial cells, and for maintenance of rotational planar cell polarity in ciliated tracheal and ependymal cells.
Class I	Unconventional myosin-Ie	Myo1e	Can directly associate with membranes. Functions in intracellular movement and membrane trafficking. Is required for normal kidney function. Tail domain crosslinks actin filaments.
Class II	Myosin-9	Myh9	Conventional non-muscular class II myosin. Functions in cytokinesis, cell shape, secretion and capping, and cytoskeleton reorganisation, focal adhesion formation (in the periphery but not the centre of spreading cells), and lamellipodial extension during cell spreading.
Class II	Myosin-10	Myh10	Conventional non-muscular class II myosin. Functions in cytokinesis, cell shape, secretion and capping, cytoskeleton reorganisation, focal adhesion formation (in the centre but not the periphery of spreading cells), and lamellipodial retraction during cell spreading. Involved with LARP6 in the stabilization of type I collagen mRNAs for CO1A1 and CO1A2.
Class II	Myosin-14	Myh14	Conventional non-muscular class II myosin.

			Functions in cytokinesis, cell shape, secretion and capping.
Class VI	Unconventional myosin-VI	Myo6	Reverse-direction motor protein. Functions in vesicular membrane trafficking, cell migration, structural integrity of Golgi apparatus, clathrin-mediated endocytosis in polarized epithelial cells. Regulator of F-actin dynamics, and has an important role in anchoring plasma membrane domains to actin filaments.
Class X	Unconventional myosin-X	Myo10	Binds to integrins, mediates cargo transport along actin filaments. Regulates cell shape, cell spreading and cell adhesion. Stimulates the formation and elongation of filopodia.
Class XVIII	Unconventional myosin-XVIIIa	Myo18a	Binds GOLPH3, linking the Golgi to the cytoskeleton and influencing Golgi membrane trafficking. Regulates retrograde flow of actomyosin in lamellipodia. Facilitates cell-cell contact.
n/a	Myosin regulatory light chain 12B	Myl12b	Myosin regulatory subunit that plays an important role in regulation of both smooth muscle and non-muscle cell contractile activity via its phosphorylation. Phosphorylation triggers actin polymerization in vascular smooth muscle. Implicated in cytokinesis, receptor capping, and cell locomotion.
n/a	Myosin light polypeptide 6	Myl6	Regulatory light chain of myosin.
n/a	Myosin phosphatase Rho-interacting protein	Mprip	Targets myosin phosphatase to the actin cytoskeleton. Required for the regulation of the actin cytoskeleton by RhoA and ROCK1.

(b) Myosins lost in TMEM67 ΔECL

Myosin class	Myosin	Gene name	Protein function
Class II	Myosin-11	Myh11	Major contractile protein in smooth muscle.
Class V	Unconventional myosin-Va	Myo5a	High duty ratio motor. Functions in cytoplasmic vesicle transport and anchorage, spindle-pole alignment and mRNA translocation.

Class VII	Unconventional myosin-VIIa	Myo7a	Tension generator/sensor or anchor for membrane receptors. Can bind to adhesion proteins and the cytoskeleton, facilitating cell-cell and cell-matrix adhesion, with important functions in cell spreading, migration, and phagocytosis. Functions in opsin transport in cilia, potentially maintaining selection barrier.
n/a	Myosin light chain 6b	Myl6b	Alkali light chain expressed in both slow-twitch skeletal muscle and in non-muscle tissue.

(c) Myosin gained in TMEM67 ΔECL

Myosin class	Myosin	Gene name	Protein function
Class IX	Unconventional myosin-IXb (Fragment)	Myo9b	Functions in the regulation of cell migration through RhoA GTPase activation.

It was not possible within the scope of this thesis to establish whether these TMEM67-myosin interactions are direct or indirect, or validate these possible interactions using an alternate methodology. Therefore, further experiments to validate these interactions using a second approach, for example, co-immunoprecipitation should be performed to gain confidence in this data.

Common qualities of these myosins is their ability to bind to membranes, and their presence at adhesions. As TMEM67 is a transmembrane protein that has been observed to localise at adhesions (Meadows, 2017), a possible point of contact between TMEM67 and these myosins could be at these adhesion points. The sole class VI myosin identified in our GFP-trap® data is a regulator of F-actin dynamics and has an important role in anchoring plasma membrane domains to actin filaments, and the Class VII myosin is known to bind adhesion proteins and the cytoskeleton. All three

non-muscular class II myosins were found, and these also have important roles in focal adhesion dynamics (Masters *et al.*, 2017).

Loss of TMEM67 has also been found to result in thicker actin stress fibres, and TMEM67 mislocalises to these actin bundles in patient fibroblasts (Dawe *et al.*, 2009; Adams *et al.*, 2012; McIntosh, 2016). The presence of thicker actin stress fibres in *TMEM67* patient cells has been hypothesised to be due to hyperactive RhoA (Dawe *et al.,* 2009; McIntosh, 2016), however, an association between TMEM67 and myosins could provide an additional explanation: myosins are important regulators of actin dynamics, for example, controlling actin bundling. Aberrant localisation of TMEM67 to actin could result in irregular myosin activity at stress fibres, potentially resulting in changes to stress bundle architecture, as observed.

At the transition zone, TMEM67 interacts with a number of other proteins linked with MKS (see Figure 1.1), however, none of these were identified in our GFP-trap® data. This is likely due to the fact that the cells from which GFP-TMEM67 was isolated were not ciliated, and there is no evidence that the transition zone complex exists outside of the primary cilium. The only two known interacting proteins of TMEM67 outside of the cilium, Nesprin and Filamin A, were both found in our GFP-trap® data. Nesprin was found on the final double positive list, however Filamin A was identified in the original list of proteins from the GFP-Trap® but excluded from the true positives list (see Figure 3.10 for a schematic of the filtering steps) as it was also found in the GFP-only control dataset. There are an expanding number of extra-ciliary roles for ciliopathy proteins being reported (Quarmby and Parker, 2005; Dawe *et al.*, 2007b; Plotnikova *et al.*, 2009; Böttinger, 2010; O'Toole *et al.*, 2010; Valente *et al.*, 2010; Adams *et al.*, 2012;

Chaki *et al.*, 2012; Polakis, 2012; Hoff *et al.*, 2013; Hanna and Shevde, 2016; Pampliega and Cuervo, 2016; Walz, 2017). The molecular basis of these are as yet not well understood, but there are several pieces of evidence to indicate that ciliopathy proteins have different binding partners in different cellular contexts. For example, CEP290, one of the causative genes for MKS, is a component of the transition zone but also localises to the centrosome and nucleus in a cell cycle-dependent manner, and interacts with a number of centriolar satellite proteins and the transcription factor ATF4 independently from its function at the transition zone (Sayer *et al.*, 2006; Kim *et al.*, 2008; Stowe *et al.*, 2012). These extra-ciliary interacting complexes have also been found in other ciliopathy proteins, including BBS proteins which interact with the Exocyst, Flotillins, and Aldolase B amongst others (Oeffner *et al.*, 2008; Novas *et al.*, 2015). This supports the hypothesis of cilium-independent roles of TMEM67, suggesting that the potential myosin-TMEM67 interaction happens independently of the protein's role at the transition zone, and thus explains why we did not identify the transition zone proteins in our GFP-trap® from non-ciliated cells. In order to further explore this hypothesis, a more thorough GFP-Trap® investigation could be completed with cells at different cell cycle stages to better elucidate TMEM67s protein-protein interactions as they change throughout the cell cycle.

4.3 Proposed model for TMEM67's role at ACAFAs and future work

We hypothesise that TMEM67 could function as a potential linker between the actin cytoskeleton and the plasma membrane at focal adhesions through an association, either direct or indirect, with various myosins. Figure 4.1 summarises our hypothesised function of TMEM67 at ACAFAs based on the results in this thesis. In normal focal adhesions (Figure 4.1a), alpha and beta integrin subunits (light and dark orange

respectively) associate with a number of proteins (the adhesome: shown as a cluster of green ellipses) and form a link between the ECM proteins (shown in grey) and the actin cytoskeleton (shown in red). Multiple integrins cluster to form a mature focal adhesion. We hypothesise that TMEM67 (Figure 4.1b; shown in black), a transmembrane protein, is functioning as a tether between myosins and the plasma membrane at these adhesion points. TMEM67 is required for the maintenance of the actin cap and thus directed cell migration. Loss of the TMEM67 protein has been found to result in alterations to the adhesome (Meadows, 2017) and we have demonstrated a loss of the actin cap in this thesis (Figure 4.1c). This results in a loss of directed cell migration, likely due to failure to correctly align, and subsequently maintain the alignment of the nucleus.

In order to test this hypothesis, the localisation of the myosins identified by the GFP-trap® in non-diseased control cells and *TMEM67* patient cells could be investigated by immunofluorescence: do myosins localise to the perinuclear actin cap in non-diseased control cells? If yes, where do they localise in our MKS patient cells? In addition, the HA-TMEM67 plasmids used in this study could give insight into potential myosin binding regions of TMEM67 by investigating whether any of the mutations in the intracellular regions of the protein abrogate myosin binding. CRISPR-Cas9 non-homologous end joining-based gene knockout of variety of target myosins identified in our GFP-trap® (Table 3.3) followed by protein pull down assays using TMEM67 as the bait protein could allow us to better understand the potential relationship between TMEM67 and associated myosins. For example, this would allow us to probe myosin-binding hierarchy: are specific myosin–TMEM67 interactions required for further myosin–myosin interactions, or do myosins bind to TMEM67 independently?

Functional studies of these knockouts will help to identify the role of myosins in the pathogenicity of MKS – it could be hypothesised that similar cellular phenotypes as seen in *TMEM67* patient cells would be observed when we knock out the myosins identified in our GFP-trap® if our model in Figure 4.1 is correct.

A

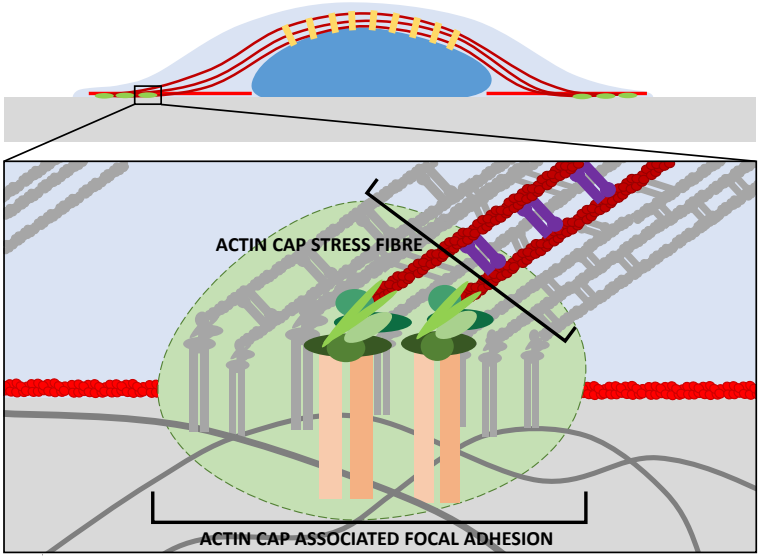

B

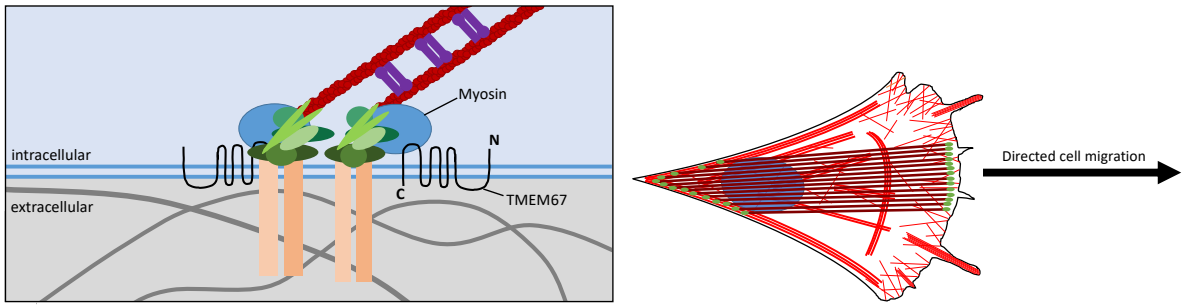

C

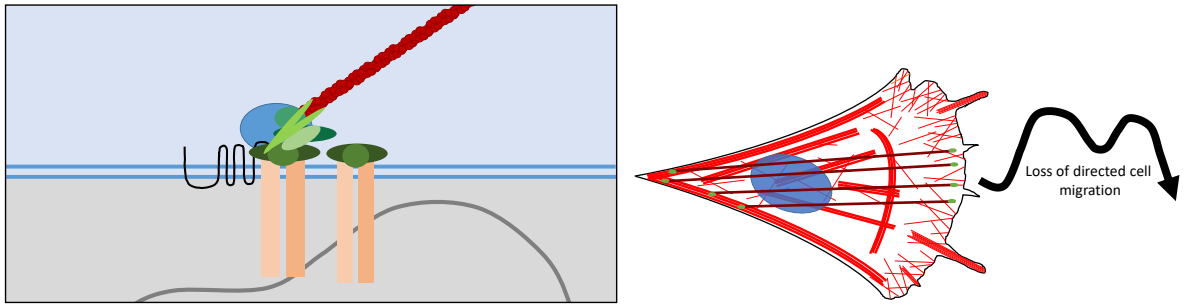

Figure 4.1 Potential model for the function of TMEM67. (a) Structure of a normal focal adhesion, showing alpha and beta integrin subunits (light and dark orange respectively) associating with a number of proteins (the adhesome: cluster of green) and forming a link between the ECM proteins (grey) and the actin cytoskeleton (red). (b) TMEM67 (black), a transmembrane protein, may function as a tether between myosins (blue) and the plasma membrane at these adhesion points. TMEM67 is required for the maintenance of the actin cap and directed cell migration. (c) Loss of TMEM67 protein results in alterations to the adhesome and a loss of the actin cap. This results in a loss of directed cell migration.

In addition, in order to improve understanding of the membrane-folding architecture of TMEM67, recent advances in cryo-electron microscopy of membrane proteins could be utilised (Thonghin *et al.,* 2018). As previously mentioned, there are conflicting reports of the number of transmembrane regions in TMEM67 (Smith *et al.,* 2006; Dawe *et al.,* 2009; UniProt Consortium, 2018), and uncovering the protein's structure could help to shed some light on the functions of the different internal and external domains.

4.4 Extra-ciliary roles of MKS proteins help explain the clinical presentation of severe ciliopathy

While it explains some, the ciliary roles of MKS proteins cannot account for the full spectrum of phenotypes observed in patients. The link between the underlying cellular defects and polydactyly is easy to link to the primary cilium: cilia and IFT are required for Hh signalling (Huangfu *et al.*, 2003), which is responsible for the patterning of the digits (Ehlen *et al.*, 2006). Disruption to the cilium in MKS is therefore likely to disrupt the Hh concentration and thus result in the polydactyly observed in patients. The other key MKS phenotypes are more difficult to link directly to a defect in the primary cilium, but the recently uncovered extra-ciliary roles of TMEM67 help to explain these.

The primary cilium has important roles in renal cystogenesis: modelling of total loss of cilia, structural abnormalities of cilia, and disruptions to the protein composition of ciliary membranes have all shown to produce fibrocystic kidneys (Bialas *et al.*, 2009; Weatherbee *et al.*, 2009; Cui *et al.*, 2011; Garcia-Gonzalo *et al.*, 2011; Ma *et al.*, 2017). Defects to the cilium's mechanosensory and chemosensory functions were thought to be main contributors to the renal cyst phenotype in ciliopathies, however the extra-ciliary defects presented in this thesis could also contribute to the phenotype. The differences in ECM production are likely to contribute to polycystic kidneys as the ECM serves several functions during branching morphogenesis. The balance of ECM proteins and matrix metallopeptidases are important regulators of the tissue development, and the ECM also acts as an important reservoir for a number of morphogenesis molecules (Shah *et al.*, 2004). Furthermore, cell-ECM attachment and subsequent migration and cellular mechanotransduction are also required during kidney morphogenesis (Shah *et al.,* 2004). In this thesis we have described alterations to the ECM of *TMEM67* patient cells and actin cytoskeletal defects. The latter, coupled with TMEM67's potential function at focal adhesions are likely to impair the cell's mechanotransduction pathways. Taken together, it follows that these cellular phenotypes associated with the loss of TMEM67 are likely to affect kidney development and contribute to the polycystic kidneys observed as one of the hallmarks of MKS.

The third phenotype of the MKS diagnostic triad, occipital encephalocele, could also be influenced by the migration and ECM defect observed in MKS patient cells. Encephalocele occurs due to a failure to completely close the neural tube during development: a process dependent on cell adhesion and migration, and the loss of

directed cell migration and major changes to the cell adhesome associated with the loss of TMEM67 are likely to affect this tightly controlled process.

4.5 Cell migration and ciliopathy: an emerging link

Aberrations to stress fibres and focal adhesions, as well as defective cell migration have been linked to other ciliopathies. Identically to our *TMEM67* patient cells, Jones *et al.*, (2012) reported that oak ridge polycystic kidney (Tg737$^{orpk/orpk}$; ORPK) mouse cells (model of polycystic kidney disease) migrate faster than non-diseased control cells but with reduced directionality, as well as migrating individually instead of as a monolayer as the control cells do. However, they also found that Tg737$^{orpk/orpk}$ cells have reduced actin stress fibres and smaller focal adhesions compared to non-diseased control cells, unlike *TMEM67* patient cells, which have more prominent actin stress fibres, but no significant difference in adhesion size (Jones *et al.,* 2012; Meadows, 2017). The Jones *et al.* (2012) study concluded that defects to the primary cilium results in alterations to the actin cytoskeleton and focal adhesion assembly, which leads to impaired directional migration. However, the data from this thesis, taken in conjunction with that previously published from our laboratory provide an alternate conclusion to the cytoskeletal, adhesion, and migration defects: if the differences Jones *et al.* reported in *Tg737*$^{orpk/orpk}$ cells were due to the defect to the structure of the cilium, then it would follow that we would see the same cellular phenotypes in our MKS cells (and indeed in cells from other ciliopathies) as they all intrinsically have defects to the cilium. As this is not the case, this supports our hypothesis of dual functionality of ciliopathy proteins influencing different cellular phenotypes. Indeed, cilium independent roles IFT proteins *IFT88* (the gene mutated in the *ORPK* mouse) and IFT20 have been reported (Finetti *et al.*, 2009; Boehlke *et al.*, 2015).

The data presented in this thesis suggest that the migration defect observed in the *ORPK* mouse could be due to the loss of the actin cap as the directionality defect observed is the same as in our *TMEM67* cells. However, as the underlying actin stress fibre phenotypes of these cell types are different, it is unlikely that the mechanism of disruption is the same. As Jones *et al.* have reported decreased levels of basal actin stress fibres, it's likely that the loss of actin cap would be due to this same defect as actin cap fibres are specialised stress fibres and are more responsive to disruption than basal stress fibres (Khatau *et al.*, 2009). From this, we can hypothesise that the extra-ciliary functions of the ciliopathy proteins do not interact in the same way they do at the cilium, that is, they do not come together to form a complex outside of the cilium in the same way they form the transition zone complex at the cilium for example. Supporting this theory, we did not identify IFT88 in our GFP-Trap as an interactor of TMEM67.

Migration and cytoskeletal defects have also been reported in the ciliopathy BBS (Hernandez-Hernandez *et al.*, 2013). Bbs4- and Bbs6-decifient cells exhibit poor migration, with delayed wound closure, and an over-abundance of apical actin aggregates (Hernandez-Hernandez *et al.*, 2013). This, taken together with the data presented in this thesis and from Jones *et al.,* (2012) covered above suggest a general role for ciliopathy proteins in cell migration. It is not currently known whether there are ECM defects in BBS cells, however loss of cilia and resultant defects to the ECM have been linked in rodent models with loss-of-function mutations in the protein Giantin (Katayama *et al.*, 2011), as well as in MKS cells (Meadows, 2017), and so a pertinent point of future study would be to investigate the ECM in BBS. Conversely to *TMEM67*

cells which migrate faster, BBS cells migrate slower, which further supports the hypothesis that the extraciliary roles of ciliopathy proteins do not function together in a complex like they do at the cilium.

4.6 Conclusion

While once thought to be a vestigial organelle, the primary cilium is now recognised as a key player in vertebrate development. After the discovery that its dysfunction resulted in disruption to several key development pathways, research was focused on the proteins of the primary cilium and how their mutation affected the organelle and the subsequent knock-on effects on ciliary signalling. How mutation to one organelle could result in multiple clinically distinct diseases was thought to be due to the severity of the mutation and the degree to which it disrupted ciliary signalling, but the discovery of dual functionality of a number of ciliopathy proteins provided a new mechanism of pathology: extra-ciliary secondary roles of cilia-associated proteins could contribute to the phenotypes. This thesis has characterised the underlying directionality defect of *TMEM67* patient cells, finding an ECM-dependent loss of the perinuclear actin cap associated with the loss of TMEM67. We have also identified a potential TMEM67–myosin association, and taking our data together we hypothesise a role for TMEM67 as an organiser or tether of myosin-actin assemblages at ACAFAs, expanding its role beyond the cilium.

The continued identification of multi-faceted roles for these ciliopathy proteins will help towards therapeutic advances for the treatment of ciliopathy, however, it also raises a number of questions. What are the relative contributions of the ciliary and non-ciliary phenotypes to the clinical presentation of ciliopathy? Is dysfunction of the cilium the

key cellular phenotype, or is this a downstream consequence of another defect, such as aberrations to the actin cytoskeleton, ECM, or loss of cell polarity? How could we disentangle these? It is clear that cilia, the actin cytoskeleton, and the ECM are linked but as of now, it is not clear how. Continued investigation of the extra-ciliary roles of ciliopathy proteins will allow these questions to be answered, and not only facilitate better understanding of the pathology of ciliopathies and allow the development of effective treatments for these diseases, but will also deepen our understanding of human development.

5 Bibliography

Abdelhamed, Z.A., Natarajan, S., Wheway, G., Inglehearn, C.F., Toomes, C., Johnson, C.A., and Jagger, D.J. (2015). The Meckel-Gruber syndrome protein TMEM67 controls basal body positioning and epithelial branching morphogenesis in mice via the non-canonical Wnt pathway. *Disease Models & Mechanisms*, 8(6), pp. 527–541.

Adams, M., Simms, R.J., Abdelhamed, Z., Dawe, H.R., Szymanska, K., Logan, C. V., Wheway, G., Pitt, E., Gull, K., Knowles, M.A., Blair, E., Cross, S.H., Sayer, J.A. and Johnson, C.A. (2012). A meckelin-filamin a interaction mediates ciliogenesis. *Human Molecular Genetics*, 21(6), pp. 1272–1286.

Ahmed, S.M., Thériault, B.L., Uppalapati, M., Chiu, C.W.N., Gallie, B.L., Sidhu, S.S. and Angers, S. (2012). KIF14 negatively regulates Rap1a-Radil signaling during breast cancer progression. *The Journal of Cell Biology*, 199(6), pp. 951–967.

Alam, S.G., Zhang, Q., Prasad, N., Li, Y., Chamala, S., Kuchibhotla, R., Kc, B., Aggarwal, V., Shrestha, S., Jones, A.L., Levy, S.E., Roux, K.J., Nickerson, J.A. and Lele, T.P. (2016). The mammalian LINC complex regulates genome transcriptional responses to substrate rigidity. *Scientific Reports*, 6, 38063.

Alberts, B., Johnson, A., Lewis, J., Raff, M., Roberts, K., and Walter, P. (2002). *Molecular Biology of the Cell*. 4th ed. [ebook] New York: Garland Science. doi: 10.1002/bmb.2003.494031049999.

Anderson, R.G.W. (1972). The three-dimensional structure of the basal body from the rhesus monkey oviduct. *Journal of Cell Biology*, 54(2), pp. 246–265.

Arts, H.H., Doherty, D., van Beersum, S.E.C., Parisi, M.A., Letteboer, S.J.F., Gorden, N.T., Peters, T.A., Märker, T., Voesenek, K., Kartono, A., Ozyurek, H., Farin, F.M., Kroes, H.Y., Wolfrum, U., Brunner, H.G., Cremers, F.P.M., Glass, I.A., Knoers, N.V.A.M., (2007). Mutations in the gene encoding the basal body protein RPGRIP1L, a nephrocystin-4 interactor, cause Joubert syndrome. *Nature Genetics*, 39(7), pp. 882–888.

Asante, D., MacCarthy-Morrogh, L., Townley, A.K., Weiss, M.A., Katayama, K., Palmer, K.J., Suzuki, H., Westlake, C.J., Stephens, D.J. (2013). A role for the Golgi matrix protein giantin in ciliogenesis through control of the localization of dynein-2. *Journal of Cell Science*, 126(22), pp. 5189–5197.

Aumailley, M., Bruckner-Tuderman, L., Carter, W.G., Deutzmann, R., Edgar, D., Ekblom, P., Engel, J., Engvall, E., Hohenester, E., Jones, J.C.R., Kleinman, H.K., Marinkovich, M.P., Martin, G.R., Mayer, U., Meneguzzi, G., Miner, J.H., Miyazaki, K., Patarroyo, M., Paulsson, M., Quaranta, V., Sanes, J.R., Sasaki, T., Sekiguchi, K., Sorokin, L.M., Talts, J.F., Tryggvason, K., Uitto, J., Virtanen, I., Von Der Mark, K., Wewer, U.M., Yamada, Y., Yurchenco, P.D. (2005). A simplified laminin nomenclature. *Matrix Biology*, 24, pp. 326–332.

Avasthi, P., Marley, A., Lin, H., Gregori-Puigjane, E., Shoichet, B.K., Zastrow, M.V., Marshall, W.F. (2012). A chemical screen identifies class A G-protein coupled receptors as regulators of cilia. *ACS Chemical Biology*, 7(5), pp. 911–919.

Avasthi, P. and Marshall, W.F. (2012). Stages of ciliogenesis and regulation of ciliary length. *Differentiation*, 83(2), pp. S30–S42.

Avila Rodríguez, M.I., Rodríguez Barroso, L.G. and Sánchez, M.L. (2018). Collagen: A review on its sources and potential cosmetic applications. *Journal of Cosmetic Dermatology*, 17(1), pp. 20–26.

Baala, L., Audollent, S., Martinovic, J., Ozilou, C., Babron, M.-C., Sivanandamoorthy, S., Saunier, S., Salomon, R., Gonzales, M., Rattenberry, E., Esculpavit, C., Toutain, A., Moraine, C., Parent, P., Marcorelles, P., Dauge, M.-C., Roume, J., Le Merrer, M., Meiner, V., Meir, K., Menez, F., Beaufrère, A.-M., Francannet, C., Tantau, J., Sinico, M., Dumez, Y., MacDonald, F., Munnich, A., Lyonnet, S., Gubler, M.-C., Génin, E., Johnson, C.A., Vekemans, M., Encha-Razavi, F., Attié-Bitach, T. (2007). Pleiotropic effects of CEP290 (NPHP6) mutations extend to Meckel syndrome. *American Journal of Human Genetics*, 81(1), pp. 170–179.

Barisic, I., Boban, L., Loane, M., Garne, E., Wellesley, D., Calzolari, E., Dolk, H., Addor, M.-C., Bergman, J.E.H., Braz, P., Draper, E.S., Haeusler, M., Khoshnood, B., Klungsoyr, K., Pierini, A., Queisser-Luft, A., Rankin, J., Rissmann, A., Verellen-Dumoulin, C. (2015). Meckel–Gruber Syndrome: a population-based study on prevalence, prenatal diagnosis, clinical features, and survival in Europe. *European Journal of Human Genetics*, 23(6), pp. 746–752.

Bergen, D.J.M., Stevenson, N.L., Skinner, R.E.H., Stephens, D.J., Hammond, C.L. (2017). The Golgi matrix protein giantin is required for normal cilia function in zebrafish. *Biology Open*, 6(8), pp. 1180–1189.

Bergmann, C. Fliegauf, M., Brüchle, N.O., Frank, V., Olbrich, H., Kirschner, J., Schermer, B., Schmedding, I., Kispert, A., Kränzlin, B., Nürnberg, G., Becker, C., Grimm, T., Girschick, G., Lynch, S.A., Kelehan, P., Senderek, J., Neuhaus, T.J., Stallmach, T., Zentgraf, H., Nürnberg, P., Gretz, N., Lo, C., Lienkamp, S., Schäfer, T., Walz, G., Benzing, T., Zerres, K., Omran, H. (2008). Loss of nephrocystin-3 function can cause embryonic lethality, Meckel-Gruber-like syndrome, situs inversus, and renal-hepatic-pancreatic dysplasia. *American Journal of Human Genetics*, 82(4), pp. 959–970.

Bershadsky, A., Chausovsky, A., Becker, E., Lyubimova, A., and Geiger, B., (1996). Involvement of microtubules in the control of adhesion-dependent signal transduction. *Current Biology*, 6(10), pp. 1279–1289.

Bialas, N.J., Inglis, P.N., Li, C., Robinson, J.F., Parker, J.D.K., Healey, M.P., Davis, E.E., Inglis, C.D., Toivonen, T., Cottell, D.C., Blacque, O.E., Quarmby, L.M., Katsanis, N., and Leroux, M.R. (2009). Functional interactions between the ciliopathy-associated Meckel syndrome 1 (MKS1) protein and two novel MKS1-related (MKSR) proteins. *Journal of Cell Science*, 122(5), pp. 611–624.

Blaser, H., Reichman-Fried, M., Castanon, I., Dumstrei, K., Marlow, F.L., Kawakami, K., Solnica-Krezel, L., Heisenberg, C.-P., and Raz, E. (2006). Migration of zebrafish primordial germ cells: a role for myosin contraction and cytoplasmic flow. *Developmental Cell*, 11(5), pp. 613–627.

Boehlke, C., Janusch, H., Hamann, C., Powelske, C., Mergen, M., Herbst, H., Kotsis, F., Nitschke, R., and Kuehn, E.W. (2015). A Cilia Independent Role of Ift88/Polaris during Cell Migration. *PLOS ONE*, 10(10), e0140378.

Boisvieux-Ulrich, E., Lainé, M.-C. and Sandoz, D. (1990). Cytochalasin D inhibits basal body migration and ciliary elongation in quail oviduct epithelium. *Cell and Tissue Research*, 259(3), pp. 443–454.

van den Boom, F., Düssmann, H., Uhlenbrock, K., Abouhamed, M., & Bähler, M. (2007). The Myosin IXb motor activity targets the myosin IXb RhoGAP domain as cargo to sites of actin polymerization. *Molecular Biology of the Cell*, 18(4), pp. 1507–1518.

Böttinger, E.P. (2010). Lights on for aminopeptidases in cystic kidney disease. *The Journal of Clinical Investigation*. 120(3), pp. 660–663.

Brancati, F., Iannicelli, M., Travaglini, L., Mazzotta, A., Bertini, E., Boltshauser, E., D'Arrigo, S., Emma, F., Fazzi, E., Gallizzi, R., Gentile, M., Loncarevic, D., Mejaski-Bosnjak, V., Pantaleoni, C., Rigoli, L., Salpietro, C.D., Signorini, S., Stringini, G.R., Verloes, A., Zabloka, D., Dallapiccola, B., Gleeson, J.G. and Valente, E.M. (2009). MKS3/TMEM67 mutations are a major cause of COACH Syndrome, a Joubert Syndrome related disorder with liver involvement. *Human Mutation*, 30(2), pp. E432–E442.

Briscoe, J. and Thérond, P.P. (2013). The mechanisms of Hedgehog signalling and its roles in development and disease. Nature Reviews Molecular Cell Biology, 14(7), pp. 416–429.

Brosig, M., Ferralli, J., Gelman, L., Chiquet, M. and Chiquet-Ehrismann, R. (2010). Interfering with the connection between the nucleus and the cytoskeleton affects nuclear rotation, mechanotransduction and myogenesis. *International Journal of Biochemistry and Cell Biology*, 42, pp. 1717–1728.

Burridge, K. and Guilluy, C. (2016). Focal adhesions, stress fibers and mechanical tension. *Experimental Cell Research*, 343(1), pp. 14–20.

Carleton, M., Mao, M., Biery, M., Warrener, P., Kim, S., Buser, C., Marshall, C.G., Fernandes, C., Annis, J. and Linsley, P.S. (2006). RNA interference-mediated silencing of mitotic kinesin KIF14 disrupts cell cycle progression and induces cytokinesis failure. *Molecular and Cellular Biology*, 26(10), pp. 3853–3863.

Chaki, M., Airik, R., Ghosh, A.K., Giles, R.H., Chen, R., Slaats, G.G., Wang, H., Hurd, T.W., Zhou, W., Cluckey, A., Gee, H.Y., Ramaswami, G., Hong, C.-J., Hamilton, B.A., Červenka, I., Ganji, R.S., Bryja, V., Arts, H.H., van Reeuwijk, J., Oud, M.M., Letteboer, S.J.F., Roepman, R., Husson, H., Ibraghimov-Beskrovnaya, O.,

Yasunaga, T., Walz, G., Eley, L., Sayer, J.A., Schermer, B., Liebau, M.C., Benzing, T., Le Corre, S., Drummond, I., Janssen, S., Allen, S.J., Natarajan, S., O'Toole, J.F., Attanasio, M., Saunier, S., Antignac, C., Koenekoop, R.K., Ren, H., Lopez, I., Nayir, A., Stoetzel, C., Dollfus, H., Massoudi, R., Gleeson, J.G., Andreoli, S.P., Doherty, D.G., Lindstrad, A., Golzio, C., Katsanis, N., Pape, L., Abboud, E.B., Al-Rajhi, A.A., Lewis, R.A., Omran, H., Lee, E.Y.-H.P., Wang, S., Sekiguchi, J.M., Saunders, R., Johnson, C.A., Garner, E., Vanselow, K., Andersen, J.S., Shlomai, J., Nurnberg, G., Nurnberg, P., Levy, S., Smogorzewska, A., Otto, E.A. and Hildebrandt, F. (2012). Exome Capture Reveals ZNF423 and CEP164 Mutations, Linking Renal Ciliopathies to DNA Damage Response Signaling. *Cell*, 150(3), pp. 533–548.

Chih, B., Liu, P., Chinn, Y., Chalouni, C., Komuves, L.G., Hass, P.E., Sandoval, W. and Peterson, A.S. (2012). A ciliopathy complex at the transition zone protects the cilia as a privileged membrane domain. *Nature Cell Biology*, 14(1), pp. 61–72.

Chugh, P., Clark, A.G., Smith, M.B., Cassani, D.A.D., Dierkes, K., Ragab, A., Roux, P.P., Charras, G., Salbreux, G. and Paluch, E.K., (2017). Actin cortex architecture regulates cell surface tension. *Nature Cell Biology*, 19(6), pp. 689–697.

Clark, A.G., Wartlick, O., Salbreux, G. and Paluch, E.K. (2014). Stresses at the Cell Surface during Animal Cell Morphogenesis. *Current Biology*, 24, pp. R484–R494.

Coles, E.G., Gammill, L.S., Miner, J.H. and Bronner-Fraser, M. (2006). Abnormalities in neural crest cell migration in laminin α5 mutant mice. *Developmental Biology*, 289(1), pp. 218–228.

Consugar, M.B., Kubly, V.J., Lager, D.J., Hommerding, C.J., Wong, W.C., Bakker, E., Gattone, V.H., Torres, V.E., Breuning, M.H. and Harris, P.C. (2007). Molecular diagnostics of Meckel–Gruber syndrome highlights phenotypic differences between MKS1 and MKS3. *Human Genetics*, 121(5), pp. 591–599.

Coppieters, F., Lefever, S., Leroy, B.P. and De Baere, E. (2010). CEP290, a gene with many faces: mutation overview and presentation of CEP290base. *Human Mutation*, 31(10), pp. 1097–1108.

Cui, C., Chatterjee, B., Francis, D., Yu, Q., SanAgustin, J.T., Francis, R., Tansey, T., Henry, C., Wang, B., Lemley, B., Pazour, G.J. and Lo, C.W. (2011). Disruption of Mks1 localization to the mother centriole causes cilia defects and developmental malformations in Meckel-Gruber syndrome. *Disease Models & Mechanisms*, 4(1), pp. 43–56.

Dawe, H.R., Adams, M., Wheway, G., Szymanska, K., Logan, C. V., Noegel, A.A., Gull, K. and Johnson, C.A. (2009). Nesprin-2 interacts with meckelin and mediates ciliogenesis via remodelling of the actin cytoskeleton. *Journal of Cell Science*, 122(15), pp. 2716–2726.

Dawe, H.R., Smith, U.M., Cullinane, A.R., Gerrelli, D., Cox, P., Badano, J.L., Blair-Reid, S., Sriram, N., Katsanis, N., Attie-Bitach, T., Afford, S.C., Copp, A.J., Kelly, D.A., Gull, K. and Johnson, C.A. (2007b). The Meckel-Gruber Syndrome proteins

MKS1 and meckelin interact and are required for primary cilium formation. *Human Molecular Genetics*, 16(2), pp. 173–186.

Deane, J.A., Cole, D.G., Seeley, E.S., Diener, D.R. and Rosenbaum, J.L. (2001). Localization of intraflagellar transport protein IFT52 identifies basal body transitional fibers as the docking site for IFT particles. Current Biology, 11(20), pp. 1586–1590. Dechat, T., Pfleghaar, K., Sengupta, K., Shimi, T., Shumaker, D.K., Solimando, L., and Goldman, R.D. (2008). Nuclear lamins: major factors in the structural organization and function of the nucleus and chromatin. *Genes and Development*, 22(7), pp. 832–853.

Delous, M., Baala, L., Salomon, R., Laclef, C., Vierkotten, J., Tory, K., Golzio, C., Lacoste, T., Besse, L., Ozilou, C., Moutkine, I., Hellman, N.E., Anselme, I., Silbermann, F., Vesque, C., Gerhardt, C., Rattenberry, E., Wolf, M.T.F., Gubler, M.C., Martinovic, J., Encha-Razavi, F., Boddaert, N., Gonzales, M., Macher, M.A., Nivet, H., Champion, G., Berthélémé, J.P., Niaudet, P., McDonald, F., Hildebrandt, F., Johnson, C. a, Vekemans, M., Antignac, C., Rüther, U., Schneider-Maunoury, S., Attié-Bitach, T. and Saunier, S. (2007). The ciliary gene RPGRIP1L is mutated in cerebello-oculo-renal syndrome (Joubert syndrome type B) and Meckel syndrome. *Nature Genetics*, 39(7), pp. 875–881.

Di Lullo, G.A., Sweeney, S.M., Korkko, J., Ala-Kokko, L. and San Antonio, J.D. (2002). Mapping the ligand-binding sites and disease-associated mutations on the most abundant protein in the human, type I collagen. *Journal of Biological Chemistry*, 277(6), pp. 4223–4231.

Dijksterhuis, J.P., Baljinnyam, B., Stanger, K., Sercan, H.O., Ji, Y., Andres, O., Rubin, J.S., Hannoush, R.N. and Schulte, G. (2015). Systematic Mapping of WNT-FZD Protein Interactions Reveals Functional Selectivity by Distinct WNT-FZD Pairs. *Journal of Biological Chemistry*, 290(11), pp. 6789–6798.

DiMilla, P.A., Barbee, K. and Lauffenburger, D.A. (1991). Mathematical model for the effects of adhesion and mechanics on cell migration speed. *Biophysical Journal*, 60(1), pp. 15–37.

DiMilla, P.A., Stone, J.A., Quinn, J.A, Albelda, S.M. and Lauffenburger, D.A. (1993). Maximal migration of human smooth muscle cells on fibronectin and type IV collagen occurs at an intermediate attachment strength. *The Journal of Cell Biology*, 122(3), pp.729–737.

de Diego, A.S., Alonso Guerrero, A., Martínez-A, C., and van Wely, K.H.M. (2014). Dido3-dependent HDAC6 targeting controls cilium size. Nature Communications, 5, 3500.

Domogatskaya, A., Rodin, S. and Tryggvason, K. (2012). Functional Diversity of Laminins. *Annual Review of Cell and Developmental Biology*, 28(1), pp. 523–553.

Dowdle, W.E., Robinson, J.F., Kneist, A., Sirerol-Piquer, M.S., Frints, S.G.M., Corbit, K.C., Zaghloul, N.A., Zaghloul, N.A., van Lijnschoten, G., Mulders, L., Verver, D.E., Zerres, K., Reed, R.R., Attié-Bitach, T., Johnson, C.A., García-Verdugo, J.M.,

Katsanis, N., Bergmann, C. and Reiter, J.F. (2011). Disruption of a ciliary B9 protein complex causes Meckel syndrome. *American Journal of Human Genetics*, 89(1), pp. 94–110.

Dupont, S., Morsut, L., Aragona, M., Enzo, E., Giulitti, S., Cordenonsi, M., Zanconato, F., Le Digabel, J., Forcato, M., Bicciato, S., Elvassore, N. and Piccolo, S. (2011). Role of YAP/TAZ in mechanotransduction. *Nature*, 474, pp. 179–183.

Ehlen, H.W., Buelens, L.A. and Vortkamp, A. (2006). Hedgehog signaling in skeletal development. *Birth Defects Research, Part C: Embryo Today: Reviews*, 78(3), pp. 267–279.

Emoto, K., Masugi, Y., Yamazaki, K., Effendi, K., Tsujikawa, H., Tanabe, M., Kitagawa, Y. and Sakamoto, M. (2014). Presence of primary cilia in cancer cells correlates with prognosis of pancreatic ductal adenocarcinoma. *Human Pathology*, 45(4), pp. 817–825.

Ffrench-Constant, C. and Hynes, R.O. (1989). Alternative splicing of fibronectin is temporally and spatially regulated in the chicken embryo. *Development*, 106, pp. 375–388.

Filges, I., Nosova, E., Bruder, E., Tercanli, S., Townsend, K., Gibson, W.T., Röthlisberger, B., Heinimann, K., Hall, J.G., Gregory-Evans, C.Y., Wasserman, W.W., Miny, P. and Friedman, J.M. (2014). Exome sequencing identifies mutations in KIF14 as a novel cause of an autosomal recessive lethal fetal ciliopathy phenotype. *Clinical Genetics*, 86(3), pp. 220–228.

Finetti, F., Paccani, S.R., Riparbelli, M.G., Giacomello, E., Perinetti, G., Pazour, G.J., Rosenbaum, J.L. and Baldari, C.T. (2009). Intraflagellar transport is required for polarized recycling of the TCR/CD3 complex to the immune synapse. *Nature Cell Biology*, 11, pp. 1332–1339.

Fisch, C. and Dupuis-Williams, P. (2011). Ultrastructure of cilia and flagella - back to the future! *Biology of the Cell*, 103(6), pp. 249–270.

Fletcher, D.A. and Mullins, R.D. (2010). Cell mechanics and the cytoskeleton. *Nature*, 463, pp. 485–492.

Frantz, C., Stewart, K.M. and Weaver, V.M. (2010). The extracellular matrix at a glance. *Journal of Cell Science*, 123(24), pp. 4195–4200.

Fraser, F.C. and Lytwyn, A. (1981). Spectrum of anomalies in the Meckel syndrome, or: “Maybe there is a malformation syndrome with at least one constant anomaly”. *American Journal of Medical Genetics*, 9(1), pp. 67–73.

Friedl, P. and Gilmour, D. (2009). Collective cell migration in morphogenesis, regeneration and cancer. *Nature Reviews Molecular Cell Biology*, 10(7), pp. 445–457.

Ganguly, A., Yang, H., Sharma, R., Patel, K.D. and Cabral, F. (2012). The role of microtubules and their dynamics in cell migration. *Journal of Biological Chemistry*, 287(52), pp. 43359–43369.

Garcia-Gonzalo, F.R., Corbit, K.C., Sirerol-Piquer, M.S., Ramaswami, G., Otto, E.A., Noriega, T.R., Seol, A.D., Robinson, J.F., Bennett, C.L., Josifova, D.J., García-Verdugo, J.M., Katsanis, N., Hildebrandt, F. and Reiter, J.F. (2011). A transition zone complex regulates mammalian ciliogenesis and ciliary membrane composition. *Nature Genetics*, 43(8), pp. 776–784.

Garcia-Gonzalo, F.R. and Reiter, J.F. (2012). Scoring a backstage pass: mechanisms of ciliogenesis and ciliary access. *The Journal of Cell Biology*, 197(6), pp. 697–709.

Garcia-Gonzalo, F.R. and Reiter, J.F. (2017). Open Sesame: How transition fibers and the transition zone control ciliary composition. *Cold Spring Harbor Perspectives in Biology*, 9(2), a028134.

Gelse, K., Pöschl, E. and Aigner, T. (2003). Collagens - Structure, function, and biosynthesis. *Advanced Drug Delivery Reviews*, 55(12), pp. 1531–1546.

Gerhardt, C., Lier, J.M., Burmühl, S., Struchtrup, A., Deutschmann, K., Vetter, M., Leu, T., Reeg, S., Grune, T. and Rüther, U. (2015). The transition zone protein Rpgrip1l regulates proteasomal activity at the primary cilium. *The Journal of Cell Biology*, 210(1), pp. 115–133.

Gibbons, I.R. and Grimstone, A.V. (1960). On Flagellar Structure in Certain Flagellates. *The Journal of Cell Biology*, 7(4), pp. 697–716.

Goetz, S.C., Bangs, F., Barrington, C.L., Katsanis, N. and Anderson, K.V. (2017). The Meckel syndrome- associated protein MKS1 functionally interacts with components of the BBSome and IFT complexes to mediate ciliary trafficking and hedgehog signaling. *PLOS ONE*, 12(3), e0173399.

Gomes, E.R., Jani, S., Gundersen, G.G. (2005). 'Nuclear Movement Regulated by Cdc42, MRCK, Myosin, and Actin Flow Establishes MTOC Polarization in Migrating Cells'. *Cell*, 121(3), pp 451–463.

Griffiths, J.R. and Salanitri, V.R. (1980). The strength of spider silk. Journal of Materials *Science*, 15(2), pp. 491–496.

Gunning, P., Ponte, P., Okayama, H., Engel, J., Blau, H. and Kedesi, L. (1983). Isolation and Characterization of Full-Length cDNA Clones for Human α-, β-, and γ-Actin mRNAs: Skeletal but Not Cytoplasmic Actins Have an Amino-Terminal Cysteine that Is Subsequently Removed. *Molecular and Cellular Biology*, 3(5), pp. 787–795.

Hanna, A. and Shevde, L.A. (2016). Hedgehog signaling: modulation of cancer properies and tumor mircroenvironment. *Molecular Cancer*, [online] 15(24). Available at https://doi.org/10.1186/s12943-016-0509-3 [Accessed 29/04/2019].

Harburger, D.S. and Calderwood, D.A. (2009). Integrin signalling at a glance. Journal of Cell *Science*, 122, pp. 159–163.

Hassounah, N.B., Bunch, T.A. and McDermott, K.M. (2012). Molecular pathways: the role of primary cilia in cancer progression and therapeutics with a focus on Hedgehog signaling. *Clinical Cancer Research*, 18(9), pp. 2429–2435.

Hassounah, N.B., Nagle, R., Saboda, K., Roe, D.J., Dalkin, B.L. and McDermott, K.M. (2013). Primary cilia are lost in preinvasive and invasive prostate cancer. *PLOS ONE*, 8(7), e68521.

Hernandez-Hernandez, V., Pravincumar, P., Diaz-Font, A., May-Simera, H., Jenkins, D., Knight, M. and Beales, P.L. (2013). Bardet–Biedl syndrome proteins control the cilia length through regulation of actin polymerization. *Human Molecular Genetics*, 22(19), pp. 3858–3868.

Hildebrandt, F., Benzing, T. and Katsanis, N. (2011). Ciliopathies. *New England Journal*. 364(16), pp. 1533–1543.

Hoff, S., Halbritter, J., Epting, D., Frank, V., Nguyen, T.-M.T., van Reeuwijk, J., Boehlke, C., Schell, C., Yasunaga, T., Helmstädter, M., Mergen, M., Filhol, E., Boldt, K., Horn, N., Ueffing, M., Otto, E.A., Eisenberger, T., Elting, M.W., van Wijk, J.A.E., Bockenhauer, D., Sebire, N.J., Rittig, S., Vyberg, M., Ring, T., Pohl, M., Pape, L., Neuhaus, T.J., Elshakhs, N.A.S., Koon, S.J., Harris, P.C., Grahammer, F., Huber, T.B., Kuehn, E.W., Kramer-Zucker, A., Bolz, H.J., Roepman, R., Saunier, S., Walz, G., Hildebrandt, F., Bergmann, C. and Lienkamp, S.S. (2013). ANKS6 is a central component of a nephronophthisis module linking NEK8 to INVS and NPHP3. *Nature Genetics*, 45(8), pp. 951–956.

Hopp, K., Heyer, C.M., Hommerding, C.J., Henke, S.A., Sundsbak, J.L., Patel, S., Patel, P., Consugar, M.B., Czarnecki, P.G., Gliem, T.J., Torres, V.E., Rossetti, S. and Harris, P.C. (2011). B9D1 is revealed as a novel Meckel syndrome (MKS) gene by targeted exon-enriched next-generation sequencing and deletion analysis. *Human Molecular Genetics*, 20(13), pp. 2524–2534.

Horvitz, H.R. and Sulston, J.E. (1980). Isolation and Genetic Characterization of Cell-Lineage Mutants of the Nematode Caenorhabditis elegans. *Genetics*, 96(2), pp. 435–454.

Huang, L., Szymanska, K., Jensen, V.L., Janecke, A.R., Innes, A.M., Davis, E.E., Frosk, P., Li, C., Willer, J.R., Chodirker, B.N., Greenberg, C.R., McLeod, D.R., Bernier, F.P., Chudley, A.E., Müller, T., Shboul, M., Logan, C. V., Loucks, C.M., Beaulieu, C.L., Bowie, R. V., Bell, S.M., Adkins, J., Zuniga, F.I., Ross, K.D., Wang, J., Ban, M.R., Becker, C., Nürnberg, P., Douglas, S., Craft, C.M., Akimenko, M.A., Hegele, R.A., Ober, C., Utermann, G., Bolz, H.J., Bulman, D.E., Katsanis, N., Blacque, O.E., Doherty, D., Parboosingh, J.S., Leroux, M.R., Johnson, C.A. and Boycott, K.M. (2011). TMEM237 is mutated in individuals with a Joubert syndrome related disorder and expands the role of the TMEM family at the ciliary transition zone. *American Journal of Human Genetics*, 89(6), pp. 713–730.

Huang, P. and Schier, A.F. (2009). Dampened Hedgehog signaling but normal Wnt signaling in zebrafish without cilia. *Development*, 136(18), pp. 3089–3098.

Huangfu, D., Liu, A., Wakeman, A.S., Murcia, N.S., Niswander, L. and Anderson, K. V. (2003). Hedgehog signalling in the mouse requires intraflagellar transport proteins. *Nature*, 426(6), pp. 83–87.

Hynes, A.M., Giles, R.H., Srivastava, S., Eley, L., Whitehead, J., Danilenko, M., Raman, S., Slaats, G.G., Colville, J.G., Ajzenberg, H., Kroes, H.Y., Thelwall, P.E., Simmons, N.L., Miles, C.G. and Sayer, J.A. (2014). Murine Joubert syndrome reveals Hedgehog signaling defects as a potential therapeutic target for nephronophthisis. *Proceedings of the National Academy of Sciences of the United States of America*, 111(27), pp. 9893–9898.

Hynes, R.O. and Naba, A. (2012). Overview of the matrisome - An inventory of extracellular matrix constituents and functions. *Cold Spring Harbor Perspectives in Biology*, 4(1), pp. 1–17.

Hynes, R.O. and Yamada, K.M. (1982). Fibronectins: Multifunctional modular glycoproteins. *Journal of Cell Biology*, 95(2), pp. 369–377.

Iannicelli, M., Brancati, F., Mougou-Zerelli, S., Mazzotta, A., Thomas, S., Elkhartoufi, N., Travaglini, L., Gomes, C., Luigi Ardissino, G., Bertini, E., Boltshauser, E., Castorina, P., D'Arrigo, S., Fischetto, R., Leroy, B., Loget, P., Bonnière, M., Starck, L., Tantau, J., Gentilin, B., Majore, S., Swistun, D., Flori, E., Lalatta, F., Pantaleoni, C., Penzien, J., Grammatico, P., the International JSRD Study Group, the I.J.S., Dallapiccola, B., Gleeson, J.G., Attie-Bitach, T. and Valente, E.M. (2010). Novel TMEM67 mutations and genotype-phenotype correlates in meckelin-related ciliopathies. *Human Mutation*, 31(5), pp. E1319–E1331.

Jayadev, R. and Sherwood, D.R. (2017). Basement membranes. *Current Biology*, 27(6), pp. R207–R211.

Jensen, V.L., Li, C., Bowie, R. V, Clarke, L., Mohan, S., Blacque, O.E. and Leroux, M.R. (2015). Formation of the transition zone by Mks5/Rpgrip1L establishes a ciliary zone of exclusion (CIZE) that compartmentalises ciliary signalling proteins and controls PIP2 ciliary abundance. *The EMBO Journal*, 34(20), pp. 2537–2556.

Jones, T.J., Adapala, R.K., Geldenhuys, W.J., Bursley, C., AbouAlaiwi, W.A., Nauli, S.M. and Thodeti, C.K. (2012). Primary cilia regulates the directional migration and barrier integrity of endothelial cells through the modulation of Hsp27 dependent actin cytoskeletal organization. *Journal of Cellular Physiology*, 227(1), pp. 70–76.

Katayama, K., Sasaki, T., Goto, S., Ogasawara, K., Maru, H., Suzuki, K. and Suzuki, H. (2011). Insertional mutation in the Golgb1 gene is associated with osteochondrodysplasia and systemic edema in the OCD rat. *Bone*, 49(5), pp. 1027–1036.

Kaverina, I. and Straube, A. (2011). Regulation of cell migration by dynamic microtubules. *Seminars in Cell and Developmental* Biology, 22, pp. 968–974.

Khaddour, R., Smith, U., Baala, L., Martinovic, J., Clavering, D., Shaffiq, R., Ozilou, C., Cullinane, A., Kyttälä, M., Shalev, S., Audollent, S., d'Humières, C., Kadhom, N., Esculpavit, C., Viot, G., Boone, C., Oien, C., Encha-Razavi, F., Batman, P.A., Bennett, C.P., Woods, C.G., Roume, J., Lyonnet, S., Génin, E., Le Merrer, M., Munnich, A., Gubler, M.-C., Cox, P., Macdonald, F., Vekemans, M., Johnson, C.A. and Attié-Bitach, T. (2007). Spectrum of MKS1 and MKS3 mutations in Meckel syndrome: a genotype-phenotype correlation. *Human Mutation*, 28(5), pp. 523–524.

Khatau, S.B., Hale, C.M., Stewart-Hutchinson, P.J., Patel, M.S., Stewart, C.L., Searson, P.C., Hodzic, D. and Wirtz, D. (2009). A perinuclear actin cap regulates nuclear shape. *Proceedings of the National Academy of Sciences*, 106(45), pp. 19017–19022.

Khatau, S.B., Kusuma, S., Hanjaya-Putra, D., Mali, P., Cheng, L., Lee, J.S.H., Gerecht, S., Wirtz, D. and Kreplak, L. (2012). The Differential Formation of the LINC-Mediated Perinuclear Actin Cap in Pluripotent and Somatic Cells. *PLOS ONE*, 7(5), e36689.

Kheir, A.E.M., Imam, A., Omer, I.M., Hassan, I.M.A., Elamin, S.A., Awadalla, E.A., Gadalla, M.H. and Hamdoon, T.A. (2012). Meckel-Gruber syndrome: A rare and lethal anomaly. *Sudanese Journal of Paediatrics*, 12(1), pp. 93–96.

Kim, D.-H., Khatau, S.B., Feng, Y., Walcott, S., Sun, S.X., Longmore and G.D., Wirtz, (2012). Actin cap associated focal adhesions and their distinct role in cellular mechanosensing. *Scientific Reports*, 2, 55.

Kim, J., Lee, J.E., Heynen-Genel, S., Suyama, E., Ono, K., Lee, K., Ideker, T., Aza-Blanc, P. and Gleeson, J.G. (2010). Functional genomic screen for modulators of ciliogenesis and cilium length. *Nature*, 464(7291), pp. 1048–1051.

Kim, J., Jo, H., Hong, H., Kim, M.H., Kim, J.M., Lee, J.-K., Heo, W.D., and Kim, J. (2015). Actin remodelling factors control ciliogenesis by regulating YAP/TAZ activity and vesicle trafficking. *Nature Communications*, 6, 6781.

Kim, J., Krishnaswami, S.R., and Gleeson, J.G. (2008). CEP290 interacts with the centriolar satellite component PCM-1 and is required for Rab8 localization to the primary cilium. *Human Molecular Genetics*, 17, pp. 3796–3805.

Kurosaka, S. and Kashina, A. (2008). Cell biology of embryonic migration. *Birth Defects Research: Part C, Embryo Today: Reviews*, 84(2), pp. 102–122.

Kyttälä, M., Tallila, J., Salonen, R., Kopra, O., Kohlschmidt, N., Paavola-Sakki, P., Peltonen, L. and Kestilä, M. (2006). MKS1, encoding a component of the flagellar apparatus basal body proteome, is mutated in Meckel syndrome. *Nature Genetics*, 38(2), pp. 155–157.

Lambacher, N.J., Bruel, A.-L., Van Dam, T.J.P., Szymańska, K., Slaats, G.G., Kuhns, S., Mcmanus, G.J., Kennedy, J.E., Gaff, K., Wu, K.M., Van Der Lee, R., Burglen, L., Doummar, D., Rivière, J.-B., Faivre, L., Attié-Bitach, T., Curd, A., Peckham, M., Giles, R.H., Johnson, C.A., Huynen, M.A., Thauvin-Robinet, C. and Blacque, O.E. (2016). TMEM107 recruits ciliopathy proteins to subdomains of the ciliary transition zone and causes Joubert syndrome. *Nature Cell Biology*, (18), pp. 122–131.

Lange, J.R. and Fabry, B. (2013). Cell and tissue mechanics in cell migration. *Experimental Cell Researc*h, 319(16), pp.2418–2423.

Le Clainche, C. and Carlier, M.F. (2008). Regulation of Actin Assembly Associated With Protrusion and Adhesion in Cell Migration. *Physiological Reviews*, 88(2), pp. 489–513.

LeBleu, V.S., MacDonald, B. and Kalluri, R. (2007). Structure and Function of Basement Membranes. *Experimental Biology and Medicine*, 232(9), pp. 1121–1129.

Leigh, M.W., Pittman, J.E., Carson, J.L., Ferkol, T.W., Dell, S.D., Davis, S.D., Knowles, M.R. and Zariwala, M.A. (2009). Clinical and genetic aspects of primary ciliary dyskinesia/Kartagener syndrome. *Genetics in Medicine*, 11(7), pp. 473–487.

Leitch, C.C., Zaghloul, N.A., Davis, E.E., Stoetzel, C., Diaz-Font, A., Rix, S., Alfadhel, M., Lewis, R.A., Eyaid, W., Banin, E., Dollfus, H., Beales, P.L., Badano, J.L. and Katsanis, N. (2008). Hypomorphic mutations in syndromic encephalocele genes are associated with Bardet-Biedl syndrome*. Nature Genetics*, 40(4), pp. 443–448.

Li, C., Jensen, V.L., Park, K., Kennedy, J., Garcia-Gonzalo, F.R., Romani, M., De Mori, R., Bruel, A.-L., Gaillard, D., Doray, B., Lopez, E., Rivière, J.-B., Faivre, L., Thauvin-Robinet, C., Reiter, J.F., Blacque, O.E., Valente, E.M. and Leroux, M.R. (2016). MKS5 and CEP290 Dependent Assembly Pathway of the Ciliary Transition Zone. *PLOS Biology*. 14(3), p. e1002416.

Li, H., Xu, B., Zhou, E.H., Sunyer, R. and Zhang, Y. (2017). Multiscale Measurements of the Mechanical Properties of Collagen Matrix. *ACS Biomaterials Science & Engineering*, 3(11), pp. 2815–2824.

Liotta, L.A., Tryggvason, K., Garbisa, S., Hart, I., Foltz, C.M. and Shafie, S. (1980). Metastatic potential correlates with enzymatic degradation of basement membrane collagen. *Nature*, 284(5751), pp. 67–68.

Löwe, J. and Amos, L.A. (2009). Evolution of cytomotive filaments: The cytoskeleton from prokaryotes to eukaryotes. *International Journal of Biochemistry and Cell Biology*, 41(2), pp. 323–329.

Luxton, G.W.G., Gomes, E.R., Folker, E.S., Vintinner, E. and Gundersen, G.G. (2010). Linear Arrays of Nuclear Envelope Proteins Harness Retrograde Actin Flow for Nuclear Movement. *Science*, 329(5994), pp. 956–959.

Ma, M., Gallagher, A.R. and Somlo, S. (2017). Ciliary mechanisms of cyst formation in polycystic kidney disease. Cold Spring Harbor Perspectives in Biology, 9(11). a028209.

Malicki, J.J. and Johnson, C.A. (2017). The Cilium: Cellular Antenna and Central Processing Unit. *Trends in Cell Biology*, 27(2), pp.126–140.

Maninová, M., Caslavsky, J. and Vomastek, T. (2017). The assembly and function of perinuclear actin cap in migrating cells. *Protoplasma*, 254(3), pp. 1207–1218.

Maninová, M., Iwanicki, M.P. and Vomastek, T. (2014). Emerging role for nuclear rotation and orientation in cell migration. *Cell Adhesion & Migration*, 8(1), pp. 42–48.

Maninová, M. and Vomastek, T. (2016). Dorsal stress fibers, transverse actin arcs, and perinuclear actin fibers form an interconnected network that induces nuclear movement in polarizing fibroblasts. *FEBS Journal*, 283(20), pp. 3676–3693.

Masters, T.A., Kendrick-Jones, J. and Buss, F. (2017). Myosins: Domain Organisation, Motor Properties, Physiological Roles and Cellular Functions. *Handbook of Experimental Pharmacology*, 235, pp. 77–122.

Matschegewski, C., Staehlke, S., Birkholz, H., Lange, R., Beck, U., Engel, K., and Nebe, J. B. (2012). Automatic Actin Filament Quantification of Osteoblasts and Their Morphometric Analysis on Microtextured Silicon-Titanium Arrays. *Materials*, 5(7), pp. 1176–1195.

May-Simera, H.L. and Kelley, M.W. (2012). Cilia, Wnt signaling, and the cytoskeleton. *Cilia*, 1(1).

McIntosh, K.V. (2016). *The extra-ciliary roles of Meckel-Gruber Syndrome proteins*. Doctoral Thesis, University of Exeter, Exeter, United Kingdom

Meadows, B. (2017). *Unravelling the Cell Adhesion Defect in Meckel Gruber Syndrome*. University of Exeter, Exeter, United Kingdom

Menzl, I., Lebeau, L., Pandey, R., Hassounah, N.B., Li, F.W., Nagle, R., Weihs, K. and McDermott, K.M. (2014). Loss of primary cilia occurs early in breast cancer development. *Cilia*, 3(1).

Metzner, C., Raupach, C., Paranhos Zitterbart, Z., and Fabry B. (2007). Simple model of cytoskeletal fluctuations. *Physical Review E*, 76(2), 021925.

Mirvis, M., Stearns, T. and James Nelson, W. (2018). Cilium structure, assembly, and disassembly regulated by the cytoskeleton. *The Biochemical Journal*, 475(14), pp. 2329–2353.

Mitchison, H.M. and Valente, E.M. (2017). Motile and non-motile cilia in human pathology: from function to phenotypes. *Journal of Pathology*, 241(2), pp. 294–309.

Mitchison, T.J. and Cramer, L.P. (1996). Actin-Based Cell Motility and Cell Locomotion. *Cell*, 84, pp. 371–379.

Mollet, G., Silbermann, F., Delous, M., Salomon, R., Antignac, C. and Saunier, S. (2005). Characterization of the nephrocystin/nephrocystin-4 complex and subcellular localization of nephrocystin-4 to primary cilia and centrosomes. *Human Molecular Genetics*, 14(5), pp. 645–656.

Nauli, S.M., Alenghat, F.J., Luo, Y., Williams, E., Vassilev, P., Li, X., Elia, A.E.H., Lu, W., Brown, E.M., Quinn, S.J., Ingber, D.E. and Zhou, J. (2003). Polycystins 1 and 2 mediate mechanosensation in the primary cilium of kidney cells. *Nature Genetics*, 33(2), pp. 129–137.

NCBI (2018). *ACTA1 actin, alpha 1, skeletal muscle [Homo sapiens (human)]*, 2018. Available at: https://www.ncbi.nlm.nih.gov/gene?Db=gene&Cmd=ShowDetailView&TermToSearch=58 (Accessed: 10 December 2017).

Nobutani, K., Shimono, Y., Yoshida, M., Mizutani, K., Minami, A., Kono, S., Mukohara, T., Yamasaki, T., Itoh, T., Takao, S., Minami, H., Azuma, T. and Takai, Y. (2014). Absence of primary cilia in cell cycle-arrested human breast cancer cells. *Genes to Cells*, 19(2), pp. 141–152.

Novarino, G., Akizu, N. and Gleeson, J.G. (2011). Modeling human disease in humans: the ciliopathies. *Cell*, 147(1), pp. 70–79.

Novas, R., Cardenas-Rodriguez, M., Irigoín, F., and Badano, J.L. (2015). Bardet-Biedl syndrome: Is it only cilia dysfunction? *FEBS Letters*, 589, pp. 3479–3491.

Nozawa, Y.I., Lin, C. and Chuang, P.T. (2013). Hedgehog signaling from the primary cilium to the nucleus: an emerging picture of ciliary localization, trafficking and transduction. *Current Opinion in Genetics & Development*, 23(4), pp. 429–437.

Nusse, R. and Clevers, H. (2017). Wnt/β-Catenin Signaling, Disease, and Emerging Therapeutic Modalities. *Cell*, 169(6), pp. 985–999.

Nyitrai, M. and Geeves, M.A. (2004). Adenosine diphosphate and strain sensitivity in myosin motors. *Philosophical Transactions of the Royal Society of London. Series B, Biological Sciences*, 359(1452), pp. 1867–1877.

O'Toole, J.F., Liu, Y., Davis, E.E., Westlake, C.J., Attanasio, M., Otto, E.A., Seelow, D., Nurnberg, G., Becker, C., Nuutinen, M., Kärppä, M., Ignatius, J., Uusimaa, J., Pakanen, S., Jaakkola, E., van den Heuvel, L.P., Fehrenbach, H., Wiggins, R., Goyal, M., Zhou, W., Wolf, M.T.F., Wise, E., Helou, J., Allen, S.J., Murga-Zamalloa, C.A., Ashraf, S., Chaki, M., Heeringa, S., Chernin, G., Hoskins, B.E., Chaib, H., Gleeson, J., Kusakabe, T., Suzuki, T., Isaac, R.E., Quarmby, L.M., Tennant, B., Fujioka, H., Tuominen, H., Hassinen, I., Lohi, H., van Houten, J.L., Rotig, A., Sayer, J.A., Rolinski, B., Freisinger, P., Madhavan, S.M., Herzer, M., Madignier, F., Prokisch, H., Nurnberg, P., Jackson, P.K., Jackson, P., Khanna, H., Katsanis, N. and Hildebrandt, F. (2010). Individuals with mutations in XPNPEP3, which encodes a

mitochondrial protein, develop a nephronophthisis-like nephropathy. *The Journal of Clinical Investigation*, 120(3), pp. 791–802.

Ocbina, P.J.R., Tuson, M. and Anderson, K.V (2009). Primary cilia are not required for normal canonical Wnt signaling in the mouse embryo. *PLOS ONE*, 4(8), e6839.

Oeffner, F., Moch, C., Neundorf, A., Hofmann, J., Koch, M., and Grzeschik, K.H. (2008). Novel interaction partners of Bardet-Biedl syndrome proteins. *Cell Motility and the Cytoskeleton*, 65, pp. 143–155.

Otto, E.A., Schermer, B., Obara, T., O'Toole, J.F., Hiller, K.S., Mueller, A.M., Ruf, R.G., Hoefele, J., Beekmann, F., Landau, D., Foreman, J.W., Goodship, J.A., Strachan, T., Kispert, A., Wolf, M.T., Gagnadoux, M.F., Nivet, H., Antignac, C., Walz, G., Drummond, I.A., Benzing, T. and Hildebrandt, F. (2003). Mutations in INVS encoding inversin cause nephronophthisis type 2, linking renal cystic disease to the function of primary cilia and left-right axis determination. *Nature Genetics*, 34(4), pp. 413–420.

Otto, E.A., Tory, K., Attanasio, M., Zhou, W., Chaki, M., Paruchuri, Y., Wise, E.L., Wolf, M.T.F., Utsch, B., Becker, C., Nurnberg, G., Nurnberg, P., Nayir, A., Saunier, S., Antignac, C. and Hildebrandt, F. (2009). Hypomorphic mutations in meckelin (MKS3/TMEM67) cause nephronophthisis with liver fibrosis (NPHP11). *Journal of Medical Genetics*, 46(10), pp. 663–670.

Palecek, S.P., Loftus, J.C., Ginsberg, M.H., Lauffenburger, D.A. and Horwitz, A.F. (1997). Integrin-ligand binding properties govern cell migration speed through cell-substratum adhesiveness. *Nature*, 385(6616), pp. 537–540.

Paluch, E.K. and Raz, E. (2013). The role and regulation of blebs in cell migration. *Current Opinion in Cell Biology*, 25(5), pp. 582–590.

Pampliega, O. and Cuervo, A.M. (2016). Autophagy and primary cilia: dual interplay. *Current Opinion in Cell Biology*, 39, pp. 1–7.

Parelkar, S.V, Kapadnis, S.P., Sanghvi, B.V., Joshi, P.B., Mundada, D. and Oak, S.N. (2013). Meckel-Gruber syndrome: A rare and lethal anomaly with review of literature. *Journal of Pediatric Neurosciences*, 8(2), pp. 154–157.

Patzke, S., Hauge, H., Sioud, M., Finne, E.F., Sivertsen, E.A., Delabie, J., Stokke, T. and Aasheim, H.-C. (2005). Identification of a novel centrosome/microtubule-associated coiled-coil protein involved in cell-cycle progression and spindle organization. *Oncogene*, 24(7), pp. 1159–1173.

Patzke, S., Stokke, T. and Aasheim, H.C. (2006). CSPP and CSPP-L associate with centrosomes and microtubules and differently affect microtubule organization. *Journal of Cellular Physiology*, 209(1), pp. 199–210.

Paulsson, M., Muller, M.E. and Edgar, D.H. (1992). Basement Membrane Proteins: Structure, Assembly, and Cellular Interactions. *Critical Reviews in Biochemistry and Molecular Biology*, 27(12), pp. 93–127.

Pelham, R.J., and Wang, Y. (1997). Cell locomotion and focal adhesions are regulated by substrate flexibility. *PNAS*, 94(25), pp. 13661–13665.

Pellegrin, S. and Mellor, H. (2007). Actin stress fibres. *Journal of Cell Science*, 120(20), pp. 3491–3499.

Piccolo, S., Dupont, S. and Cordenonsi, M. (2014). The Biology of YAP/TAZ: Hippo Signaling and Beyond. *Physiological Reviews*, 94(4), pp. 1287–1312.

Pitaval, A., Tseng, Q., Bornens, M. and Théry, M. (2010). Cell shape and contractility regulate ciliogenesis in cell cycle-arrested cells. *Journal of Cell Biology*, 191(2), pp. 303–312.

Plotnikova, O.V, Pugacheva, E.N. and Golemis, E. A. (2009). Primary cilia and the cell cycle. *Methods in Cell Biology*, 94, pp. 137–160.

Polakis, P. (2012). Wnt signaling in cancer. *Cold Spring Harbor Perspectives in Biology*, 4(5).

Pollard, T.D., Blanchoin, L. and Mullins, R.D. (2000). Molecular Mechanisms Controlling Actin Filament Dynamics in Nonmuscle Cells. *Annual Review of Biophysics and Biomolecular Stru*cture, 29(1), pp. 545–576.

Pollard, T.D. and Cooper, J.A. (1986). Actin and Actin-Binding Proteins. A Critical Evaluation of Mechanisms and Functions. *Annual Review of Biochemistry*, 55(1), pp. 987–1035.

Pollard, T.D. and Cooper, J.A. (2009). Actin, a Central Player in Cell Shape and Movement. Science, 326(5957), pp. 1208–1212.

Quarmby, L.M. and Parker, J.D.K. (2005). Cilia and the cell cycle? *The Journal of Cell Biology*, 169(5), pp. 707–710.

Ralston, E., Lu, Z., Biscocho, N., Soumaka, E., Mavroidis, M., Prats, C., Lømo, T., Capetanaki, Y. and Ploug, T. (2006). Blood vessels and desmin control the positioning of nuclei in skeletal muscle fibers. *Journal of Cellular Physiology*, 209(3), pp. 874–882.

Reiter, J.F. and Skarnes, W.C. (2006). Tectonic, a novel regulator of the Hedgehog pathway required for both activation and inhibition. *Genes & Development*, 20(1), pp. 22–27.

Ridley, A., Schwartz, M.A., Burridge, K., Firtel, R.A., Ginsberg, M.H., Borisy, G., Parsons, J.T. and Horwitz, A.R. (2003). Cell migration: integrating signals from front to back. *Science*, 302(5651), pp. 1704–1709.

Rimkus, T.K., Carpenter, R.L., Qasem, S., Chan, M. and Lo, H.W. (2016). Targeting the sonic hedgehog signaling pathway: Review of smoothened and GLI inhibitors. *Cancers*, 8(2), 22.

Ringo, D.L. (1967). Flagellar motion and fine structure of the flagellar apparatus in Chlamydomonas. *Journal of Cell Biology*, 33(3), pp. 543–571.

Roberson, E.C., Dowdle, W.E., Ozanturk, A., Garcia-Gonzalo, F.R., Li, C., Halbritter, J., Elkhartoufi, N., Porath, J.D., Cope, H., Ashley-Koch, A., Gregory, S., Thomas, S., Sayer, J.A., Saunier, S., Otto, E.A., Katsanis, N., Davis, E.E., Attié-Bitach, T., Hildebrandt, F., Leroux, M.R. and Reiter, J.F. (2015). TMEM231, mutated in orofaciodigital and Meckel syndromes, organizes the ciliary transition zone. *The Journal of Cell Biology*, 209(1), pp. 129–142.

Roberts, T.M. and Stewart, M. (1997). Nematode sperm: Amoeboid movement without actin. Trends in Cell Biology, 7(9), pp. 368–373.

Rosenbaum, J.L. and Witman, G.B. (2002). Intraflagellar transport. *Nature Reviews Molecular Cell Biology*, 3, pp. 813–825.

Rozario, T. and DeSimone, D.W. (2010). The extracellular matrix in development and morphogenesis: A dynamic view. Developmental Biology, 341(1), pp. 126–140.
Salonen, R. (1984). The Meckel syndrome: clinicopathological findings in 67 patients. *American Journal of Medical Genetics*, 18(4), pp. 671–689.

Sang, L., Miller, J.J., Corbit, K.C., Giles, R.H., Brauer, M.J., Otto, E.A., Baye, L.M., Wen, X., Scales, S.J., Kwong, M., Huntzicker, E.G., Sfakianos, M.K., Sandoval, W., Bazan, J.F., Kulkarni, P., Garcia-Gonzalo, F.R., Seol, A.D., O'Toole, J.F., Held, S., Reutter, H.M., Lane, W.S., Rafiq, M.A., Noor, A., Ansar, M., Devi, A.R.R., Sheffield, V.C., Slusarski, D.C., Vincent, J.B., Doherty, D.A., Hildebrandt, F., Reiter, J.F. and Jackson, P.K. (2011). Mapping the NPHP-JBTS-MKS protein network reveals ciliopathy disease genes and pathways. *Cell*, 145(4), pp. 513–528.

Sayer, J.A., Otto, E.A., Otoole, J.F., Nurnberg, G., Kennedy, M.A., Becker, C., Hennies, H.C., Helou, J., Attanasio, M., Fausett, B.V., Utsch, B., Khanna, H., Liu, Y., Drummond, I., Kawakami, I., Kusakabe, T., Tsuda, M., Ma, L., Lee, H., Larson, R. G., Allen, S.J., Wilkinson, C.J., Nigg, E.A., Shou, C., Lillo, C., Williams, D.S., Hoppe, B., Kemper, M.J., Neuhaus, T., Parisi, M.A., Glass, I.A., Petry, M., Kispert, A., Gloy, J., Ganner, A., Walz, G., Zhu, X., Goldman, D., Nurnberg, P., Swaroop, A., Leroux, M.R., and Hildebrandt, F. (2006). The centrosomal protein nephrocystin-6 is mutated in Joubert syndrome and activates transcription factor ATF4. *Nature Genetics*, 38, pp. 674–681.

Scholey, J.M. (2003). Intraflagellar Transport. *Annual Review of Cell and Developmental Biology*, 19(1), pp. 423–443.

Scholey, J.M. (2008). Intraflagellar transport motors in cilia: moving along the cell's antenna. *The Journal of Cell Biology*, 180(1), pp. 23–29.

Schwarzbauer, J.E., Tamkun, J.W., Lemischka, I.R. and Hynes, R.O. (1983). Three different fibronectin mRNAs arise by alternative splicing within the coding region. *Cell*, 35(2), pp. 421–431.

Shah, M.M., Sampogna, R.V., Sakurai, H., Bush, K.T. and Nigam, S.K. (2004). Branching morphogenesis and kidney disease. *Development*, 131(7), pp. 1449–1462.

Shaheen, R., Almoisheer, A., Faqeih, E., Babay, Z., Monies, D., Tassan, N., Abouelhoda, M., Kurdi, W., Al Mardawi, E., Khalil, M.M.I., Seidahmed, M.Z., Alnemer, M., Alsahan, N., Sogaty, S., Alhashem, A., Singh, A., Goyal, M., Kapoor, S., Alomar, R., Ibrahim, N. and Alkuraya, F.S. (2015). Identification of a novel MKS locus defined by TMEM107 mutation. *Human Molecular Genetics*, 24(18), pp. 5211–5218.

Shaheen, R., Ansari, S., Mardawi, E. Al, Alshammari, M.J. and Alkuraya, F.S. (2013). Mutations in TMEM231 cause Meckel-Gruber syndrome. *Journal of Medical Genetics*, 50(3), pp. 160–162.

Shaheen, R., Faqeih, E., Seidahmed, M.Z., Sunker, A., Alali, F.E., AlQahtani, K. and Alkuraya, F.S. (2011). A TCTN2 mutation defines a novel Meckel Gruber syndrome locus. *Human Mutation*, 32(6), pp. 573–578.

Shaheen, R., Shamseldin, H.E., Loucks, C.M., Seidahmed, M.Z., Ansari, S., Khalil, M.I., Al-Yacoub, N., Davis, E.E., Mola, N.A., Szymanska, K., Herridge, W., Chudley, A.E., Chodirker, B.N., Schwartzentruber, J., Majewski, J., Katsanis, N., Poizat, C., Johnson, C.A., Parboosingh, J., Boycott, K.M., Innes, A.M. and Alkuraya, F.S. (2014). REPORT Mutations in CSPP1, Encoding a Core Centrosomal Protein, Cause a Range of Ciliopathy Phenotypes in Humans. *The American Journal of Human Genetics*, 94, pp. 73–79.

Shi, X., Garcia, G., Van De Weghe, J.C., McGorty, R., Pazour, G.J., Doherty, D., Huang, B. and Reiter, J.F. (2017). Super-resolution microscopy reveals that disruption of ciliary transition-zone architecture causes Joubert syndrome. *Nature Cell Biology*, 19(10), pp. 1178–1188.

Simons, M., Gloy, J., Ganner, A., Bullerkotte, A., Bashkurov, M., Krönig, C., Schermer, B., Benzing, T., Cabello, O.A., Jenny, A., Mlodzik, M., Polok, B., Driever, W., Obara, T. and Walz, G. (2005). Inversin, the gene product mutated in nephronophthisis type II, functions as a molecular switch between Wnt signaling pathways. *Nature Genetics*, 37(5), pp. 537–543.

Singel, S.M., Cornelius, C., Zaganjor, E., Batten, K., Sarode, V.R., Buckley, D.L., Peng, Y., John, G.B., Li, H.C., Sadeghi, N., Wright, W.E., Lum, L., Corson, T.W. and Shay, J.W. (2014). KIF14 promotes AKT phosphorylation and contributes to chemoresistance in triple-negative breast cancer. *Neoplasia*, 16(3), pp. 247–256.

Singla, V. and Reiter, J.F. (2006). The primary cilium as the cell's antenna: Signaling at a sensory organelle. *Science*, 313(5787), pp. 629–633.

Smith, U.M., Consugar, M., Tee, L.J., McKee, B.M., Maina, E.N., Whelan, S., Morgan, N.V., Goranson, E., Gissen, P., Lilliquist, S., Aligianis, I.A., Ward, C.J., Pasha, S., Punyashthiti, R., Malik Sharif, S., Batman, P.A., Bennett, C.P., Woods, C.G., McKeown, C., Bucourt, M., Miller, C.A., Cox, P., Algazali, L., Trembath, R.C.,

Torres, V.E., Attie-Bitach, T., Kelly, D.A., Maher, E.R., Gattone, V.H., Harris, P.C. and Johnson, C.A. (2006). The transmembrane protein meckelin (MKS3) is mutated in Meckel-Gruber syndrome and the wpk rat. *Nature Genetics*, 38(2), pp. 191–196.

Sorokin, S. (1962). Centrioles and the formation of rudimentary cilia by fibroblasts and smooth muscle cells. *The Journal of Cell Biology*, 15(2), pp. 363–377.

Starr, D.A. and Fridolfsson, H.N. (2010). Interactions between nuclei and the cytoskeleton are mediated by SUN-KASH nuclear-envelope bridges. *Annual Review of Cell and Developmental Biology*, 26, pp. 421–444.

Starr, D.A. and Han, M. (2002). Role of ANC-1 in Tethering Nuclei to the Actin Cytoskeleton. *Science*, 298(5592), pp. 406–409.

Stowe, T.R., Wilkinson, C.J., Iqbal, A., and Stearns, T. (2012). The centriolar satellite proteins Cep72 and Cep290 interact and are required for recruitment of BBS proteins to the cilium. *Molecular Biology of the Cell*, 23, pp. 3322–3335.

Strachan, L.R. and Condic, M.L. (2003). Neural crest motility and integrin regulation are distinct in cranial and trunk populations. *Developmental Biology*, 259(2), pp. 288–302.

Stricker, J., Falzone, T. and Gardel, M.L. (2010). Mechanics of the F-actin cytoskeleton. *Journal of Biomechanics*, 43(1), pp. 9–14.

Sulston, J.E. and Horvitz, H.R. (1981). Abnormal cell lineages in mutants of the nematode Caenorhabditis elegans. *Developmental Biology*, 82(1), pp. 41–55.

Svensson, R.B., Hassenkam, T., Grant, C.A. and Magnusson, S.P. (2010). Tensile properties of human collagen fibrils and fascicles are insensitive to environmental salts. *Biophysical Journal*, 99(12), pp. 4020–4027.

Szymanska, K., Berry, I., Logan, C. V, Cousins, S.R., Lindsay, H., Jafri, H., Raashid, Y., Malik-Sharif, S., Castle, B., Ahmed, M., Bennett, C., Carlton, R. and Johnson, C.A. (2012). Founder mutations and genotype-phenotype correlations in Meckel-Gruber syndrome and associated ciliopathies. *Cilia*, 1(1), 18.

Tallila, J., Jakkula, E., Peltonen, L., Salonen, R. and Kestilä, M. (2008). Identification of CC2D2A as a Meckel syndrome gene adds an important piece to the ciliopathy puzzle. *American Journal of Human Genetics*, 82(6), pp. 1361–1367.

Tammachote, R., Hommerding, C.J., Sinders, R.M., Miller, C.A., Czarnecki, P.G., Leightner, A.C., Salisbury, J.L., Ward, C.J., Torres, V.E., Gattone, V.H. and Harris, P.C. (2009). Ciliary and centrosomal defects associated with mutation and depletion of the Meckel syndrome genes MKS1 and MKS3. *Human Molecular Genetics*, 18(17), pp. 3311–3323.

Tanos, B.E., Yang, H.-J., Soni, R., Wang, W.-J., Macaluso, F.P., Asara, J.M. and Tsou, M.-F.B. (2013). Centriole distal appendages promote membrane docking, leading to cilia initiation. *Genes & Development*, 27(2), pp. 163–168.

Thakar, K. and Carroll, C.W. (2017). Mkl1-dependent gene activation is sufficient to induce actin cap assembly. *Small GTPases*, [online]. Available at: http://www.tandfonline.com/doi/full/10.1080/21541248.2017.1328303 [Accessed 04/05/2019]

Thonghin, N., Kargas, V., Clews, J., Ford, R.C. (2018). Cryo-electron microscopy of membrane proteins. *Methods*, 147, pp. 176–186.

Timpl, R., Rohde, H., Robey, P.G., Rennard, S.I., Foidart, J.M. and Martin, G.R. (1979). Laminin- a glycoprotein from basement membranes. *The Journal of Biological Chemistry*, 254(19), pp. 9933–9937.

Toivola, D.M., Tao, G.-Z., Habtezion, A., Liao, J. and Omary, M.B. (2005). Cellular integrity plus: organelle-related and protein-targeting functions of intermediate filaments. *Trends in Cell Biology*, 15(11), pp. 608–617.

Tuxworth, R.I., Weber, I., Wessels, D., Addicks, G.C., Soll, D.R., Gerisch, G. and Titus, M.A. (2001). A role for myosin VII in dynamic cell adhesion. *Current Biology*, 11(5), pp. 318–329.

UniProt Consortium (2018). UniProt: a worldwide hub of protein knowledge. *Nucleic Acids Research*, 47(D1), pp. D506-D515.

Valente, E.M., Logan, C.V., Mougou-Zerelli, S., Lee, J.H., Silhavy, J.L., Brancati, F., Iannicelli, M., Travaglini, L., Romani, S., Illi, B., Adams, M., Szymanska, K., Mazzotta, A., Lee, J.E., Tolentino, J.C., Swistun, D., Salpietro, C.D., Fede, C., Gabriel, S., Russ, C., Cibulskis, K., Sougnez, C., Hildebrandt, F., Otto, E.A., Held, S., Diplas, B.H., Davis, E.E., Mikula, M., Strom, C.M., Ben-Zeev, B., Lev, D., Sagie, T.L., Michelson, M., Yaron, Y., Krause, A., Boltshauser, E., Elkhartoufi, N., Roume, J., Shalev, S., Munnich, A., Saunier, S., Inglehearn, C., Saad, A., Alkindy, A., Thomas, S., Vekemans, M., Dallapiccola, B., Katsanis, N., Johnson, C.A., Attié-Bitach, T. and Gleeson, J.G. (2010). Mutations in TMEM216 perturb ciliogenesis and cause Joubert, Meckel and related syndromes. *Nature Genetics*, 42(7), pp. 619–625.

Veland, I.R., Montjean, R., Eley, L., Pedersen, L.B., Schwab, A., Goodship, J., Kristiansen, K., Pedersen, S.F., Saunier, S. and Christensen, S.T. (2013). Inversin/Nephrocystin-2 Is Required for Fibroblast Polarity and Directional Cell Migration. *PLOS ONE*, 8(4), e60193.

Veleri, S., Manjunath, S.H., Fariss, R.N., May-Simera, H., Brooks, M., Foskett, T.A., Gao, C., Longo, T.A., Liu, P., Nagashima, K., Rachel, R.A., Li, T., Dong, L. and Swaroop, A. (2014). Ciliopathy-associated gene Cc2d2a promotes assembly of subdistal appendages on the mother centriole during cilia biogenesis. *Nature Communications*, 5, 4207.

Vicente-Manzanares, M., Ma, X., Adelstein, R.S. and Horwitz, A.R. (2009). Non-muscle myosin II takes centre stage in cell adhesion and migration. *Nature Reviews Molecular Cell Biology*, 10(11), pp. 778–790.

Vicente-Manzanares, M. and Horwitz, A.R. (2011). Adhesion dynamics at a glance. *Journal of Cell Science*, 124(23), pp. 3923–3927.

Vierkotten, J., Dildrop, R., Peters, T., Wang, B. and Ruther, U. (2007). Ftm is a novel basal body protein of cilia involved in Shh signalling. *Development*, 134(14), pp. 2569–2577.

Vorobjev, I.A. and Chentsov, YU. S. (1982). Centrioles in the cell cycle. I. Epithelial cells. *The Journal of Cell Biology*, 93(3), pp. 938–949.

Wallingford, J.B. and Mitchell, B. (2011). Strange as it may seem: the many links between Wnt signaling, planar cell polarity, and cilia. *Genes & Development*, 25(3), pp. 201–213.
Walz, G. (2017). Role of primary cilia in non-dividing and post-mitotic cells. *Cell and Tissue Research*, 369(1), pp. 11–25.

Wang, N., Tytell, J.D. and Ingber, D.E. (2009). Mechanotransduction at a distance: mechanically coupling the extracellular matrix with the nucleus. *Nature Reviews Molecular Cell Biology*, 10(1), pp. 75–82.

Watanabe, D., Saijoh, Y., Nonaka, S., Sasaki, G., Ikawa, Y., Yokoyama, T. and Hamada, H. (2003). The left-right determinant Inversin is a component of node monocilia and other 9+0 cilia. *Development*, 130(9), pp. 1725–1734.

Waters, A.M. and Beales, P.L. (2011). Ciliopathies: an expanding disease spectrum. *Pediatric Nephrology*, 26(7), pp. 1039–1056.

Weatherbee, S.D., Niswander, L.A. and Anderson, K.V. (2009). A mouse model for Meckel syndrome reveals Mks1 is required for ciliogenesis and Hedgehog signaling. *Human Molecular Genetics*, 18(23), pp. 4565–4575.

Wen, J.H., Choi, O., Taylor-Weiner, H., Fuhrmann, A., Karpiak, J.V., Almutrairi, A. and Engler, A.J. (2015). Haptotaxis is cell type specific and limited by substrate adhesiveness. *Cellular and Molecular Bioengineering*, 8(4), pp. 530–542.

Wen, Q. and Janmey, P.A. (2011). Polymer physics of the cytoskeleton. *Current Opinion in Solid State and Materials Science*, 15(5), pp. 177–182.

Wheway, G., Abdelhamed, Z., Natarajan, S., Toomes, C., Inglehearn, C. and Johnson, C.A. (2013). Aberrant Wnt signalling and cellular over-proliferation in a novel mouse model of Meckel-Gruber syndrome. *Developmental Biology*, 377(1), pp. 55–66.

Wheway, G., Schmidts, M., Mans, D.A., Szymanska, K., Nguyen, T.M.T., Racher, H., Phelps, I.G., Toedt, G., Kennedy, J., Wunderlich, K.A., Sorusch, N., Abdelhamed, Z.A., Natarajan, S., Herridge, W., Van Reeuwijk, J., Horn, N., Boldt, K., Parry, D.A., Letteboer, S.J.F., Roosing, S., Adams, M., Bell, S.M., Bond, J., Higgins, J., Morrison, E.E., Tomlinson, D.C., Slaats, G.G., Van Dam, T.J.P., Huang, L., Kessler, K., Giessl, A., Logan, C. V., Boyle, E.A., Shendure, J., Anazi, S., Aldahmesh, M., Al Hazzaa, S., Hegele, R.A., Ober, C., Frosk, P., Mhanni, A.A., Chodirker, B.N., Chudley, A.E.,

Lamont, R., Bernier, F.P., Beaulieu, C.L., Gordon, P., Pon, R.T., Donahue, C., Barkovich, A.J., Wolf, L., Toomes, C., Thiel, C.T., Boycott, K.M., McKibbin, M., Inglehearn, C.F., Stewart, F., Omran, H., Huynen, M.A., Sergouniotis, P.I., Alkuraya, F.S., Parboosingh, J.S., Innes, A.M., Willoughby, C.E., Giles, R.H., Webster, A.R., Ueffing, M., Blacque, O., Gleeson, J.G., Wolfrum, U., Beales, P.L., Gibson, T., Doherty, D., Mitchison, H.M., Roepman, R. and Johnson, C.A. (2015). An siRNA-based functional genomics screen for the identification of regulators of ciliogenesis and ciliopathy genes. *Nature Cell Biology*, 17(8), pp. 1074–1087.

Wheway, G., Nazlamova, L. and Hancock, J.T. (2018). Signaling through the Primary Cilium. *Frontiers in Cell and Developmental Biology*, 6, 8.

Williams, C.L., Li, C., Kida, K., Inglis, P.N., Mohan, S., Semenec, L., Bialas, N.J., Stupay, R.M., Chen, N., Blacque, O.E., Yoder, B.K. and Leroux, M.R. (2011). MKS and NPHP modules cooperate to establish basal body/transition zone membrane associations and ciliary gate function during ciliogenesis. *The Journal of Cell Biology*, 192(6), pp. 1023–1041.

Winder, S.J. and Ayscough, K.R. (2005). Actin-binding proteins. *Journal of Cell Science*, 118(Pt 4), pp. 651–654.

Woroniuk, A., Porter, A., White, G., Newman, D.T., Diamantopoulou, Z., Waring, T., Rooney, C., Strathdee, D., Marston, D.J., Hahn, K.M., Sansom, O.J., Zech, T., and Malliri, A. (2018). STEF/TIAM2-mediated Rac1 activity at the nuclear envelope regulates the perinuclear actin cap. *Nature Communications*, 9, 2124.

Wozniak, M.A., Modzelewska, K., Kwong, L. and Keely, P.J. (2004). Focal adhesion regulation of cell behavior. *Biochimica et Biophysica Acta*, 1692(2–3), pp. 103–119.

Xu, H., Choe, C., Shin, S.-H., Park, S.-W., Kim, H.-S., Jung, S.-H., Yim, S.-H., Kim, T.-M. and Chung, Y.-J. (2014). Silencing of KIF14 interferes with cell cycle progression and cytokinesis by blocking the p27Kip1 ubiquitination pathway in hepatocellular carcinoma. *Experimental & Molecular Medicine*, 46, e97.

Yang, H., Ganguly, A. and Cabral, F. (2010). Inhibition of cell migration and cell division correlates with distinct effects of microtubule inhibiting drugs. *The Journal of Biological Chemistry*, 285(42), pp. 32242–32250.

Yang, T.T., Su, J., Wang, W.J., Craige, B., Witman, G.B., Bryan Tsou, M.F. and Liao, J.C. (2015). Superresolution pattern recognition reveals the architectural map of the ciliary transition zone. *Scientific Reports*, 5, 14096.

Yu, H., Ye, X., Guo, N. and Nathans, J. (2012). Frizzled 2 and frizzled 7 function redundantly in convergent extension and closure of the ventricular septum and palate: evidence for a network of interacting genes. *Development*, 139(23), pp. 4383–4394.

Yunoki, S., Sugiura, H., Ikoma, T., Kondo, E., Yasuda, K. and Tanaka, J. (2011). Effects of increased collagen-matrix density on the mechanical properties and in vivo

absorbability of hydroxyapatite–collagen composites as artificial bone materials. *Biomedical Materials*, 6(1), 015012.

Zaidel-Bar, R., Cohen, M., Addadi, L. and Geiger, B. (2004). Hierarchical assembly of cell–matrix adhesion complexes. *Biochemical Society Transactions*, 32(3), pp. 416–420.

Zhang, H., Berg, J.S., Li, Z., Wang, Y., Lang, P., Sousa, A.D., Bhaskar, A., Cheney, R.E. and Stromblad, S. (2004). Myosin-X provides a motor-based link between integrins and the cytoskeleton. *Nature Cell Biology*, 6(6), pp. 523–531.

Zhang, X., Xu, R., Zhu, B., Yang, X., Ding, X., Duan, S., Xu, T., Zhuang, Y. and Han, M. (2007). Syne-1 and Syne-2 play crucial roles in myonuclear anchorage and motor neuron innervation. *Development*, 134(5), pp. 901–908.

Zhou, K., Rolls, M.M., Hall, D.H., Malone, C.J. and Hanna-Rose, W. (2009). A ZYG-12–dynein interaction at the nuclear envelope defines cytoskeletal architecture in the C. elegans gonad. *The Journal of Cell Biology*, 186(2), pp. 229–241.

Zhu, C., Zhao, J., Bibikova, M., Leverson, J.D., Bossy-Wetzel, E., Fan, J.-B., Abraham, R.T. and Jiang, W. (2005). Functional analysis of human microtubule-based motor proteins, the kinesins and dyneins, in mitosis/cytokinesis using RNA interference*. Molecular Biology of the Cell*, 16(7), pp. 3187–3199.

Zigmond, S.H., Otto, J.J. and Bryan, J. (1979). Organization of myosin in a submembranous sheath in well-spread human fibroblasts. *Experimental Cell Research*, 119(2), pp. 205–219.

6 Supplementary Information

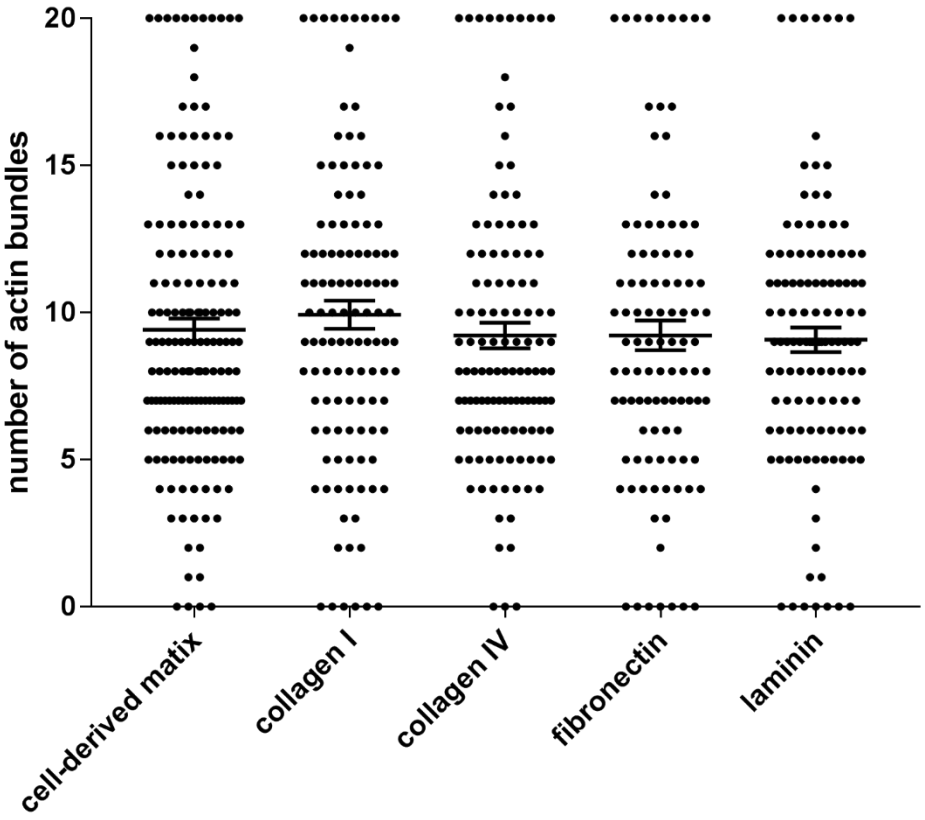

Supplementary Figure 1 There was no significant different between non-diseased control fibroblasts on their CDM and non-diseased control cells plated on collagen I, collagen IV, fibronectin or laminin.

```
>sp|Q5HYA8|MKS3_HUMAN Meckelin OS=Homo sapiens OX=9606 GN=TMEM67 PE=1 SV=2
MATRGGAGVAMAVWSLLSARAVTAFLLLFLPRFLQAQTFSFPFQQPEKCDNNQYFDISAL
SCVPCGANQRQDARGTSCVCLPGFQMISNNGGPAIICKKCPENMKGVTEDGWNCISCPSD
LTAEGKCHCPIGHILVERDINGTLLSQATCELCDGNENSFMVVNALGDRCVRCEPTFVNT
SRSCACSEPNILTGGLCFSSTGNFPLRRISAARYGEVGMSLTSEWFAKYLQSSAAACWVY
ANLTSCQALGNMCVMNMNSYDFATFDACGLFQFIFENTAGLSTVHSISFWRQNLPWLFYG
DQLGLAPQVLSSTSLPTNFSFKGENQNTKLKFVAASYDIRGNFLKWQTLEGGVLQLCPDT
ETRLNAAYSFGTTYQQNCEIPISKILIDFPTPIFYDVYLEYTDENQHQYILAVPVLNLNL
QHNKIFVNQDSNSGKWLLTRRIFLVDAVSGRENDLGTQPRVIRVATQISLSVHLVPNTIN
GNIYPPLITIAYSDIDIKDANSQSVKVSFSVTYEMDHGEAHVQTDIALGVLGGLAVLASL
LKTAGWKRRIGSPMIDLQTVVKFLVYYAGDLANVFFIITVGTGLYWLIFFKAQKSVSVLL
PMPIQEERFVTYVGCAFALKALQFLHKLISQITIDVFFIDWERPKGKVLKAVEGEGGVRS
ATVPVSIWRTYFVANEWNEIQTVRKINSLFQVLTVLFFLEVVGFKNLALMDSSSSLSRNP
PSYIAPYSCILRYAVSAALWLAIGIIQVVFFAVFYERFIEDKIRQFVDLCSMSNISVFLL
SHKCFGYYIHGRSVHGHADTNMEEMNMNLKREAENLCSQRGLVPNTDGQTFEIAISNQMR
QHYDRIHETLIRKNGPARLLSSSASTFEQSIKAYHMMNKFLGSFIDHVHKEMDYFIKDKL
LLERILGMEFMEPMEKSIFYNDEGYSFSSVLYYGNEATLLIFDLLFFCVVDLACQNFILA
SFLTYLQQEIFRYIRNTVGQKNLASKTLVDQRFLI
```

Supplementary Figure 2 The amino acid sequence of TMEM67 isoform 1 (Uniprot: Q5HYA8-1)

Supplementary Table 1 Dilutions and fixation conditions for primary and secondary antibodies used.

Antigen	Host species	Company	IF fixation condition	IF dilution	WB dilution
Primary antibodies					
HA (7C9)	rat	Chromotek	2% PFA	1:100	
TMEM67	rabbit	ProteinTech	2% PFA	1:500	
GFP	mouse	Roche	4% PFA	1:200	1:1000
Secondary antibodies					
anti-rabbit Alexa Fluor 488 Fab fragment	goat	Molecular Probes		1:500	
anti-mouse Alexa Fluor 488 Fab fragment	goat	Molecular Probes		1:500	
anti-rat Alexa Fluor 488 Fab fragment	goat	Molecular Probes		1:500	
Anti-mouse IGG	goat	Sigma Aldrich			1:40 000

Alexa Fluor 594 phallotoxin phalloidin (Molecular Probes) was used at a dilution of 1:250, in 4% PFA for isolated filamentous actin staining, and in 2% PFA for experiments when co-stained with anti-HA for IF.

DAPI was used at 1 μg ml^{-1} to counterstain nuclei in all IF experiments.

Supplementary Table 2 Primer details for sequencing HA-TMEM67 plasmids (sequence in pCMV plasmid).

Primer name	Primer sequence
CMVfor	CGCAAATGGGCGGTAGGCGTG
M13rev (-29)	CAGGAAACAGCTATGACC
TMEM67-Seq1 (for)	GAAGATGGCTGGAACTGCAT
TMEM67-Seq2 (for)	CAGCTTTGTCCAGACACAGA
TMEM67-Seq3 (for)	CATCACAGTGGGAACAGGTC

Supplementary Table 3 Full double positive lists of proteins identified in GFP-Trap® of (a) GFP-TMEM67 full length and (b) GFP-TMEM67 ΔECL.

(a) GFP-TMEM67 full length

Uniprot Accession	Description
Q8VDD5	Myosin-9 OS=Mus musculus GN=Myh9 PE=1 SV=4 - [MYH9_MOUSE]
P60710	Actin, cytoplasmic 1 OS=Mus musculus GN=Actb PE=1 SV=1 - [ACTB_MOUSE]
Q3UBP6	Putative uncharacterized protein OS=Mus musculus GN=Actb PE=2 SV=1 - [Q3UBP6_MOUSE]
Q9QXS1	Plectin OS=Mus musculus GN=Plec PE=1 SV=3 - [PLEC_MOUSE]
Q61879	Myosin-10 OS=Mus musculus GN=Myh10 PE=1 SV=2 - [MYH10_MOUSE]
P20152	Vimentin OS=Mus musculus GN=Vim PE=1 SV=3 - [VIME_MOUSE]
Q9WTI7	Unconventional myosin-Ic OS=Mus musculus GN=Myo1c PE=1 SV=2 - [MYO1C_MOUSE]
Q6ZWQ9	MCG5400 OS=Mus musculus GN=Myl12a PE=1 SV=1 - [Q6ZWQ9_MOUSE]
P68033	Actin, alpha cardiac muscle 1 OS=Mus musculus GN=Actc1 PE=1 SV=1 - [ACTC_MOUSE]
E9QPE7	Myosin-11 OS=Mus musculus GN=Myh11 PE=1 SV=1 - [E9QPE7_MOUSE]
Q5SYD0	Unconventional myosin-Id OS=Mus musculus GN=Myo1d PE=1 SV=1 - [MYO1D_MOUSE]
Q8BFZ3	Beta-actin-like protein 2 OS=Mus musculus GN=Actbl2 PE=1 SV=1 - [ACTBL_MOUSE]
Q5SWZ5	Myosin phosphatase Rho-interacting protein OS=Mus musculus GN=Mprip PE=1 SV=1 - [Q5SWZ5_MOUSE]
P97434	Myosin phosphatase Rho-interacting protein OS=Mus musculus GN=Mprip PE=1 SV=2 - [MPRIP_MOUSE]
Q05CR3	Plec1 protein (Fragment) OS=Mus musculus GN=Plec PE=2 SV=1 - [Q05CR3_MOUSE]
A0A0R4J221	Plectin (Fragment) OS=Mus musculus GN=Plec PE=1 SV=1 - [A0A0R4J221_MOUSE]
Q3THE2	Myosin regulatory light chain 12B OS=Mus musculus GN=Myl12b PE=1 SV=2 - [ML12B_MOUSE]
Q6PAC1	Gelsolin, isoform CRA_c OS=Mus musculus GN=Gsn PE=2 SV=1 - [Q6PAC1_MOUSE]
Q60605	Myosin light polypeptide 6 OS=Mus musculus GN=Myl6 PE=1 SV=3 - [MYL6_MOUSE]
D3YZ62	Unconventional myosin-Va OS=Mus musculus GN=Myo5a PE=1 SV=1 - [D3YZ62_MOUSE]
P46735	Unconventional myosin-Ib OS=Mus musculus GN=Myo1b PE=1 SV=3 - [MYO1B_MOUSE]
E9Q634	Unconventional myosin-Ie OS=Mus musculus GN=Myo1e PE=1 SV=1 - [MYO1E_MOUSE]
E9QNH6	Unconventional myosin-Ib OS=Mus musculus GN=Myo1b PE=1 SV=1 - [E9QNH6_MOUSE]
A0A0J9YUQ8	Gelsolin (Fragment) OS=Mus musculus GN=Gsn PE=1 SV=1 - [A0A0J9YUQ8_MOUSE]
B9EHJ3	Tight junction protein ZO-1 OS=Mus musculus GN=Tjp1 PE=1 SV=1 - [B9EHJ3_MOUSE]
Q642K0	MCG140959, isoform CRA_a OS=Mus musculus GN=Myl6 PE=2 SV=1 - [Q642K0_MOUSE]
E9Q175	Unconventional myosin-VI OS=Mus musculus GN=Myo6 PE=1 SV=1 - [E9Q175_MOUSE]
Q9JJ28	Protein flightless-1 homolog OS=Mus musculus GN=Flii PE=1 SV=1 - [FLII_MOUSE]
K3W4R2	Myosin-14 OS=Mus musculus GN=Myh14 PE=1 SV=1 - [K3W4R2_MOUSE]
Q9EP71	Ankycorbin OS=Mus musculus GN=Rai14 PE=1 SV=1 - [RAI14_MOUSE]
Q2KN98	Cytospin-A OS=Mus musculus GN=Specc1l PE=1 SV=1 - [CYTSA_MOUSE]
Q9ERG0	LIM domain and actin-binding protein 1 OS=Mus musculus GN=Lima1 PE=1 SV=3 - [LIMA1_MOUSE]
Q61553	Fascin OS=Mus musculus GN=Fscn1 PE=1 SV=4 - [FSCN1_MOUSE]
Q8VCQ8	Caldesmon 1 OS=Mus musculus GN=Cald1 PE=1 SV=1 - [Q8VCQ8_MOUSE]
K3W4L0	Unconventional myosin-XVIIIa OS=Mus musculus GN=Myo18a PE=1 SV=1 - [K3W4L0_MOUSE]
Q7TPR4	Alpha-actinin-1 OS=Mus musculus GN=Actn1 PE=1 SV=1 - [ACTN1_MOUSE]
P27659	60S ribosomal protein L3 OS=Mus musculus GN=Rpl3 PE=1 SV=3 - [RL3_MOUSE]
A0A0U1RNK7	Dedicator of cytokinesis protein 7 OS=Mus musculus GN=Dock7 PE=1 SV=1 - [A0A0U1RNK7_MOUSE]
Q9D8E6	60S ribosomal protein L4 OS=Mus musculus GN=Rpl4 PE=1 SV=3 - [RL4_MOUSE]
E9Q3Z5	Supervillin OS=Mus musculus GN=Svil PE=1 SV=1 - [E9Q3Z5_MOUSE]
E9PYF4	LIM domain only 7 OS=Mus musculus GN=Lmo7 PE=1 SV=1 - [E9PYF4_MOUSE]
P62141	Serine/threonine-protein phosphatase PP1-beta catalytic subunit OS=Mus musculus GN=Ppp1cb PE=1 SV=3 - [PP1B_MOUSE]
P08752	Guanine nucleotide-binding protein G(i) subunit alpha-2 OS=Mus musculus GN=Gnai2 PE=1 SV=5 - [GNAI2_MOUSE]

Q62261	Spectrin beta chain, non-erythrocytic 1 OS=Mus musculus GN=Sptbn1 PE=1 SV=2 - [SPTB2_MOUSE]
P62137	Serine/threonine-protein phosphatase PP1-alpha catalytic subunit OS=Mus musculus GN=Ppp1ca PE=1 SV=1 - [PP1A_MOUSE]
Q8R422	CD109 antigen OS=Mus musculus GN=Cd109 PE=1 SV=1 - [CD109_MOUSE]
E9PX70	Collagen alpha-1(XII) chain OS=Mus musculus GN=Col12a1 PE=1 SV=1 - [E9PX70_MOUSE]
F6TFN2	LIM domain only 7 (Fragment) OS=Mus musculus GN=Lmo7 PE=1 SV=1 - [F6TFN2_MOUSE]
Q9DBR7	Protein phosphatase 1 regulatory subunit 12A OS=Mus musculus GN=Ppp1r12a PE=1 SV=2 - [MYPT1_MOUSE]
B2CY77	Laminin receptor (Fragment) OS=Mus musculus GN=Rpsa PE=2 SV=1 - [B2CY77_MOUSE]
Q9QZF2	Glypican-1 OS=Mus musculus GN=Gpc1 PE=1 SV=1 - [GPC1_MOUSE]
F6SVV1	Uncharacterized protein OS=Mus musculus GN=Gm9493 PE=4 SV=1 - [F6SVV1_MOUSE]
Q5SQB0	Nucleophosmin OS=Mus musculus GN=Npm1 PE=1 SV=1 - [Q5SQB0_MOUSE]
Q08509	Epidermal growth factor receptor kinase substrate 8 OS=Mus musculus GN=Eps8 PE=1 SV=2 - [EPS8_MOUSE]
Q3TRK3	Putative uncharacterized protein OS=Mus musculus GN=Dbn1 PE=2 SV=1 - [Q3TRK3_MOUSE]
P62880	Guanine nucleotide-binding protein G(I)/G(S)/G(T) subunit beta-2 OS=Mus musculus GN=Gnb2 PE=1 SV=3 - [GBB2_MOUSE]
Q9DC51	Guanine nucleotide-binding protein G(k) subunit alpha OS=Mus musculus GN=Gnai3 PE=1 SV=3 - [GNAI3_MOUSE]
Q8R0W0	Epiplakin OS=Mus musculus GN=Eppk1 PE=1 SV=2 - [EPIPL_MOUSE]
Q9Z0U1	Tight junction protein ZO-2 OS=Mus musculus GN=Tjp2 PE=1 SV=2 - [ZO2_MOUSE]
B1AZ46	Brain-specific angiogenesis inhibitor 1-associated protein 2 OS=Mus musculus GN=Baiap2 PE=1 SV=1 - [B1AZ46_MOUSE]
Q8BK67	Protein RCC2 OS=Mus musculus GN=Rcc2 PE=1 SV=1 - [RCC2_MOUSE]
Q3TFA9	Putative uncharacterized protein OS=Mus musculus GN=Tmod3 PE=2 SV=1 - [Q3TFA9_MOUSE]
G3X9T8	Ceruloplasmin OS=Mus musculus GN=Cp PE=1 SV=1 - [G3X9T8_MOUSE]
E9Q3E2	Synaptopodin OS=Mus musculus GN=Synpo PE=1 SV=1 - [E9Q3E2_MOUSE]
A0A1L1SUX8	Thy-1 membrane glycoprotein (Fragment) OS=Mus musculus GN=Thy1 PE=1 SV=1 - [A0A1L1SUX8_MOUSE]
Q6IRU2	Tropomyosin alpha-4 chain OS=Mus musculus GN=Tpm4 PE=1 SV=3 - [TPM4_MOUSE]
Q3U561	Ribosomal protein OS=Mus musculus GN=Rpl10a PE=2 SV=1 - [Q3U561_MOUSE]
Q9CVB6	Actin-related protein 2/3 complex subunit 2 OS=Mus musculus GN=Arpc2 PE=1 SV=3 - [ARPC2_MOUSE]
D3Z2H9	Uncharacterized protein OS=Mus musculus GN=Tpm3-rs7 PE=3 SV=1 - [D3Z2H9_MOUSE]
P50580	Proliferation-associated protein 2G4 OS=Mus musculus GN=Pa2g4 PE=1 SV=3 - [PA2G4_MOUSE]
F7DBB3	AHNAK nucleoprotein 2 (Fragment) OS=Mus musculus GN=Ahnak2 PE=1 SV=1 - [F7DBB3_MOUSE]
Q0KL02	Triple functional domain protein OS=Mus musculus GN=Trio PE=1 SV=3 - [TRIO_MOUSE]
Q3THB3	Putative uncharacterized protein OS=Mus musculus GN=Hnrnpm PE=1 SV=1 - [Q3THB3_MOUSE]
Q3TZU7	Sorting nexin OS=Mus musculus GN=Snx9 PE=2 SV=1 - [Q3TZU7_MOUSE]
Q3TEU8	Coronin OS=Mus musculus GN=Coro1c PE=2 SV=1 - [Q3TEU8_MOUSE]
P28301	Protein-lysine 6-oxidase OS=Mus musculus GN=Lox PE=1 SV=1 - [LYOX_MOUSE]
A0A1D5RLW5	60S ribosomal protein L18a OS=Mus musculus GN=Rpl18a PE=1 SV=1 - [A0A1D5RLW5_MOUSE]
G3X9J0	Signal-induced proliferation-associated 1-like protein 3 OS=Mus musculus GN=Sipa1l3 PE=1 SV=1 - [SI1L3_MOUSE]
P67984	60S ribosomal protein L22 OS=Mus musculus GN=Rpl22 PE=1 SV=2 - [RL22_MOUSE]
P62270	40S ribosomal protein S18 OS=Mus musculus GN=Rps18 PE=1 SV=3 - [RS18_MOUSE]
P31001	Desmin OS=Mus musculus GN=Des PE=1 SV=3 - [DESM_MOUSE]
Q60597	2-oxoglutarate dehydrogenase, mitochondrial OS=Mus musculus GN=Ogdh PE=1 SV=3 - [ODO1_MOUSE]
Q3TCE7	Putative uncharacterized protein OS=Mus musculus GN=Arpc1b PE=2 SV=1 - [Q3TCE7_MOUSE]
Q3TJ01	tRNA-splicing ligase RtcB homolog OS=Mus musculus GN=Rtcb PE=2 SV=1 - [Q3TJ01_MOUSE]
Q3TF41	Nucleosome assembly protein 1-like 1, isoform CRA_d OS=Mus musculus GN=Nap1l1 PE=2 SV=1 - [Q3TF41_MOUSE]
Q60598	Src substrate cortactin OS=Mus musculus GN=Cttn PE=1 SV=2 - [SRC8_MOUSE]
Q01721	Growth arrest-specific protein 1 OS=Mus musculus GN=Gas1 PE=2 SV=2 - [GAS1_MOUSE]
P31230	Aminoacyl tRNA synthase complex-interacting multifunctional protein 1 OS=Mus musculus GN=Aimp1 PE=1 SV=2 - [AIMP1_MOUSE]
P28352	DNA-(apurinic or apyrimidinic site) lyase OS=Mus musculus GN=Apex1 PE=1 SV=2 - [APEX1_MOUSE]
A0A0R4J169	Leucine-rich repeat flightless-interacting protein 2 OS=Mus musculus GN=Lrrfip2 PE=1 SV=1 - [A0A0R4J169_MOUSE]

Q4VBF8	Sipa1l1 protein OS=Mus musculus GN=Sipa1l1 PE=2 SV=1 - [Q4VBF8_MOUSE]
Q6R891	Neurabin-2 OS=Mus musculus GN=Ppp1r9b PE=1 SV=1 - [NEB2_MOUSE]
Q8CBM2	Aspartyl/asparaginyl beta-hydroxylase OS=Mus musculus GN=Asph PE=1 SV=1 - [Q8CBM2_MOUSE]
Q8K173	Col3a1 protein (Fragment) OS=Mus musculus GN=Col3a1 PE=2 SV=1 - [Q8K173_MOUSE]
Q3TJZ6	Protein FAM98A OS=Mus musculus GN=Fam98a PE=1 SV=1 - [FA98A_MOUSE]
Q8BR76	Meckelin OS=Mus musculus GN=Tmem67 PE=1 SV=2 - [MKS3_MOUSE]
Q9D0P6	Putative uncharacterized protein OS=Mus musculus PE=2 SV=1 - [Q9D0P6_MOUSE]
P14115	60S ribosomal protein L27a OS=Mus musculus GN=Rpl27a PE=1 SV=5 - [RL27A_MOUSE]
P32067	Lupus La protein homolog OS=Mus musculus GN=Ssb PE=1 SV=1 - [LA_MOUSE]
Q3TWV4	AP-2 complex subunit mu OS=Mus musculus GN=Ap2m1 PE=1 SV=1 - [Q3TWV4_MOUSE]
P51655	Glypican-4 OS=Mus musculus GN=Gpc4 PE=1 SV=2 - [GPC4_MOUSE]
P42669	Transcriptional activator protein Pur-alpha OS=Mus musculus GN=Pura PE=1 SV=1 - [PURA_MOUSE]
A0A1L1SVG0	Uveal autoantigen with coiled-coil domains and ankyrin repeats OS=Mus musculus GN=Uaca PE=1 SV=1 - [A0A1L1SVG0_MOUSE]
P63037	DnaJ homolog subfamily A member 1 OS=Mus musculus GN=Dnaja1 PE=1 SV=1 - [DNJA1_MOUSE]
Q3U026	Putative uncharacterized protein OS=Mus musculus GN=Mogs PE=2 SV=1 - [Q3U026_MOUSE]
A0A0J9YTU3	Cytospin-B OS=Mus musculus GN=Specc1 PE=1 SV=1 - [A0A0J9YTU3_MOUSE]
Q3TAH3	Putative uncharacterized protein OS=Mus musculus GN=Npm3 PE=2 SV=1 - [Q3TAH3_MOUSE]
P54823	Probable ATP-dependent RNA helicase DDX6 OS=Mus musculus GN=Ddx6 PE=1 SV=1 - [DDX6_MOUSE]
Q3TQY2	Putative uncharacterized protein OS=Mus musculus GN=Dctn4 PE=2 SV=1 - [Q3TQY2_MOUSE]
Q6PDM2	Serine/arginine-rich splicing factor 1 OS=Mus musculus GN=Srsf1 PE=1 SV=3 - [SRSF1_MOUSE]
A0A0J9YUR2	Cytospin-B OS=Mus musculus GN=Specc1 PE=1 SV=1 - [A0A0J9YUR2_MOUSE]
Q8BG95	Protein phosphatase 1 regulatory subunit 12B OS=Mus musculus GN=Ppp1r12b PE=1 SV=2 - [MYPT2_MOUSE]
B2RQQ7	CDC42 binding protein kinase beta OS=Mus musculus GN=Cdc42bpb PE=2 SV=1 - [B2RQQ7_MOUSE]
Q925B0	PRKC apoptosis WT1 regulator protein OS=Mus musculus GN=Pawr PE=1 SV=2 - [PAWR_MOUSE]
Q9CX86	Heterogeneous nuclear ribonucleoprotein A0 OS=Mus musculus GN=Hnrnpa0 PE=1 SV=1 - [ROA0_MOUSE]
Q3UDS4	Putative uncharacterized protein OS=Mus musculus GN=Sqrdl PE=2 SV=1 - [Q3UDS4_MOUSE]
B2RSW8	Pericentriolar material 1 OS=Mus musculus GN=Pcm1 PE=2 SV=1 - [B2RSW8_MOUSE]
Q8K258	Srp68 protein OS=Mus musculus GN=Srp68 PE=2 SV=1 - [Q8K258_MOUSE]
E9Q0Y4	Signal-induced proliferation-associated protein 1 OS=Mus musculus GN=Sipa1 PE=1 SV=1 - [E9Q0Y4_MOUSE]
Q3TQP7	Putative uncharacterized protein OS=Mus musculus GN=Acat1 PE=2 SV=1 - [Q3TQP7_MOUSE]
Q3UMU9	Hepatoma-derived growth factor-related protein 2 OS=Mus musculus GN=Hdgfrp2 PE=1 SV=1 - [HDGR2_MOUSE]
Q3UFZ6	Putative uncharacterized protein (Fragment) OS=Mus musculus GN=Caprin1 PE=2 SV=1 - [Q3UFZ6_MOUSE]
Z4YJL4	182 kDa tankyrase-1-binding protein OS=Mus musculus GN=Tnks1bp1 PE=1 SV=1 - [Z4YJL4_MOUSE]
P27641	X-ray repair cross-complementing protein 5 OS=Mus musculus GN=Xrcc5 PE=1 SV=4 - [XRCC5_MOUSE]
Q8CI43	Myosin light chain 6B OS=Mus musculus GN=Myl6b PE=1 SV=1 - [MYL6B_MOUSE]
Q91XV3	Brain acid soluble protein 1 OS=Mus musculus GN=Basp1 PE=1 SV=3 - [BASP1_MOUSE]
E9Q740	Signal recognition particle 72 OS=Mus musculus GN=Srp72 PE=1 SV=1 - [E9Q740_MOUSE]
Q8BGH2	Sorting and assembly machinery component 50 homolog OS=Mus musculus GN=Samm50 PE=1 SV=1 - [SAM50_MOUSE]
Q3TGL4	Fibulin 2, isoform CRA_b OS=Mus musculus GN=Fbln2 PE=2 SV=1 - [Q3TGL4_MOUSE]
E9QAH1	Golgi autoantigen, golgin subfamily b, macrogolgin 1 OS=Mus musculus GN=Golgb1 PE=1 SV=1 - [E9QAH1_MOUSE]
Q05DU4	Msn protein (Fragment) OS=Mus musculus GN=Msn PE=2 SV=1 - [Q05DU4_MOUSE]
P05533	Lymphocyte antigen 6A-2/6E-1 OS=Mus musculus GN=Ly6a PE=1 SV=1 - [LY6A_MOUSE]
P0DP27	Calmodulin-2 OS=Mus musculus GN=Calm2 PE=1 SV=1 - [CALM2_MOUSE]
A0A0G2JDW7	40S ribosomal protein S27 (Fragment) OS=Mus musculus GN=Rps27 PE=1 SV=1 - [A0A0G2JDW7_MOUSE]
P49817	Caveolin-1 OS=Mus musculus GN=Cav1 PE=1 SV=1 - [CAV1_MOUSE]
Q8R081	Heterogeneous nuclear ribonucleoprotein L OS=Mus musculus GN=Hnrnpl PE=1 SV=2 - [HNRPL_MOUSE]

P59999	Actin-related protein 2/3 complex subunit 4 OS=Mus musculus GN=Arpc4 PE=1 SV=3 - [ARPC4_MOUSE]
A0A0N4SV32	Plasminogen activator inhibitor 1 RNA-binding protein OS=Mus musculus GN=Serbp1 PE=1 SV=1 - [A0A0N4SV32_MOUSE]
F8WIT2	Annexin OS=Mus musculus GN=Anxa6 PE=1 SV=1 - [F8WIT2_MOUSE]
P51863	V-type proton ATPase subunit d 1 OS=Mus musculus GN=Atp6v0d1 PE=1 SV=2 - [VA0D1_MOUSE]
G3UXT7	RNA-binding protein FUS (Fragment) OS=Mus musculus GN=Fus PE=1 SV=1 - [G3UXT7_MOUSE]
Q9D699	Putative uncharacterized protein OS=Mus musculus GN=Gas2 PE=2 SV=1 - [Q9D699_MOUSE]
A0A0N5E9G7	Replication factor C subunit 1 OS=Mus musculus GN=Rfc1 PE=1 SV=1 - [A0A0N5E9G7_MOUSE]
Q9WUM5	Succinate--CoA ligase [ADP/GDP-forming] subunit alpha, mitochondrial OS=Mus musculus GN=Suclg1 PE=1 SV=4 - [SUCA_MOUSE]
G5E8E1	Leucine rich repeat (In FLII) interacting protein 1, isoform CRA_e OS=Mus musculus GN=Lrrfip1 PE=1 SV=1 - [G5E8E1_MOUSE]
E9QN08	Elongation factor 1-delta (Fragment) OS=Mus musculus GN=Eef1d PE=1 SV=1 - [E9QN08_MOUSE]
F8VQB6	Unconventional myosin-X OS=Mus musculus GN=Myo10 PE=1 SV=1 - [MYO10_MOUSE]
O88398	Advillin OS=Mus musculus GN=Avil PE=1 SV=2 - [AVIL_MOUSE]
Q9D7S7	60S ribosomal protein L22-like 1 OS=Mus musculus GN=Rpl22l1 PE=1 SV=1 - [RL22L_MOUSE]
A0A0H3XWX3	Insulin-like growth factor 2 mRNA binding protein 1 dN CRDBP-2 OS=Mus musculus GN=Igf2bp1 PE=2 SV=1 - [A0A0H3XWX3_MOUSE]
P50396	Rab GDP dissociation inhibitor alpha OS=Mus musculus GN=Gdi1 PE=1 SV=3 - [GDIA_MOUSE]
F8VPU2	FERM, RhoGEF and pleckstrin domain-containing protein 1 OS=Mus musculus GN=Farp1 PE=1 SV=1 - [FARP1_MOUSE]
Q99JY0	Trifunctional enzyme subunit beta, mitochondrial OS=Mus musculus GN=Hadhb PE=1 SV=1 - [ECHB_MOUSE]
E9Q9H2	DnaJ homolog subfamily C member 2 OS=Mus musculus GN=Dnajc2 PE=1 SV=1 - [E9Q9H2_MOUSE]
Q8K335	Glutamate-rich WD repeat containing 1 OS=Mus musculus GN=Grwd1 PE=2 SV=1 - [Q8K335_MOUSE]
Q02013	Aquaporin-1 OS=Mus musculus GN=Aqp1 PE=1 SV=3 - [AQP1_MOUSE]
O89086	RNA-binding protein 3 OS=Mus musculus GN=Rbm3 PE=1 SV=1 - [RBM3_MOUSE]
Q3TFP8	Putative uncharacterized protein OS=Mus musculus GN=Pgrmc1 PE=2 SV=1 - [Q3TFP8_MOUSE]
B7ZMP1	Probable Xaa-Pro aminopeptidase 3 OS=Mus musculus GN=Xpnpep3 PE=1 SV=1 - [XPP3_MOUSE]
Q99LS8	Pbx1 protein OS=Mus musculus GN=Pbx1 PE=2 SV=1 - [Q99LS8_MOUSE]
O35682	Myeloid-associated differentiation marker OS=Mus musculus GN=Myadm PE=1 SV=2 - [MYADM_MOUSE]
P49718	DNA replication licensing factor MCM5 OS=Mus musculus GN=Mcm5 PE=1 SV=1 - [MCM5_MOUSE]
Q9DB77	Cytochrome b-c1 complex subunit 2, mitochondrial OS=Mus musculus GN=Uqcrc2 PE=1 SV=1 - [QCR2_MOUSE]
A1L0U3	Histone H3 (Fragment) OS=Mus musculus GN=Hist1h3e PE=2 SV=1 - [A1L0U3_MOUSE]
A2AW05	FACT complex subunit SSRP1 (Fragment) OS=Mus musculus GN=Ssrp1 PE=1 SV=1 - [A2AW05_MOUSE]
B2RXP1	Leucine-rich repeat and calponin homology domain-containing protein 3 OS=Mus musculus GN=Lrch3 PE=1 SV=1 - [B2RXP1_MOUSE]
Q3TP69	Putative uncharacterized protein OS=Mus musculus GN=Gpc6 PE=2 SV=1 - [Q3TP69_MOUSE]
Q922K7	Probable 28S rRNA (cytosine-C(5))-methyltransferase OS=Mus musculus GN=Nop2 PE=1 SV=1 - [NOP2_MOUSE]
Q8R5L1	Complement component 1 Q subcomponent-binding protein, mitochondrial OS=Mus musculus GN=C1qbp PE=1 SV=1 - [Q8R5L1_MOUSE]
E9QL13	MCG8382, isoform CRA_c OS=Mus musculus GN=Rbm14 PE=1 SV=2 - [E9QL13_MOUSE]
P60122	RuvB-like 1 OS=Mus musculus GN=Ruvbl1 PE=1 SV=1 - [RUVB1_MOUSE]
Q9CYL5	Golgi-associated plant pathogenesis-related protein 1 OS=Mus musculus GN=Glipr2 PE=1 SV=3 - [GAPR1_MOUSE]
Q8BG67	Protein EFR3 homolog A OS=Mus musculus GN=Efr3a PE=1 SV=1 - [EFR3A_MOUSE]
Q08288	Cell growth-regulating nucleolar protein OS=Mus musculus GN=Lyar PE=1 SV=2 - [LYAR_MOUSE]
A0A067XG53	Peripheral plasma membrane protein CASK (Fragment) OS=Mus musculus GN=Cask PE=1 SV=1 - [A0A067XG53_MOUSE]
Q9DCW4	Electron transfer flavoprotein subunit beta OS=Mus musculus GN=Etfb PE=1 SV=3 - [ETFB_MOUSE]
Q60737	Casein kinase II subunit alpha OS=Mus musculus GN=Csnk2a1 PE=1 SV=2 - [CSK21_MOUSE]
P10605	Cathepsin B OS=Mus musculus GN=Ctsb PE=1 SV=2 - [CATB_MOUSE]
Q3UA95	Histone H2A OS=Mus musculus GN=H2afz PE=2 SV=1 - [Q3UA95_MOUSE]
O35646	Calpain-6 OS=Mus musculus GN=Capn6 PE=1 SV=2 - [CAN6_MOUSE]
Q9QWJ3	Alpha-1-globin (Fragment) OS=Mus musculus PE=2 SV=1 - [Q9QWJ3_MOUSE]
H7BWZ3	Actin-related protein 2/3 complex subunit 3 OS=Mus musculus GN=Arpc3 PE=1 SV=1 - [H7BWZ3_MOUSE]

G3UYU4	Flotillin-1 OS=Mus musculus GN=Flot1 PE=1 SV=1 - [G3UYU4_MOUSE]
A0A1D5RM23	Cleavage and polyadenylation-specificity factor subunit 5 OS=Mus musculus GN=Nudt21 PE=1 SV=1 - [A0A1D5RM23_MOUSE]
Q6ZPF4	Formin-like protein 3 OS=Mus musculus GN=Fmnl3 PE=1 SV=2 - [FMNL3_MOUSE]
P26231	Catenin alpha-1 OS=Mus musculus GN=Ctnna1 PE=1 SV=1 - [CTNA1_MOUSE]
P01027	Complement C3 OS=Mus musculus GN=C3 PE=1 SV=3 - [CO3_MOUSE]
Q03963	Interferon-induced, double-stranded RNA-activated protein kinase OS=Mus musculus GN=Eif2ak2 PE=1 SV=2 - [E2AK2_MOUSE]
Q3UGJ5	Putative uncharacterized protein OS=Mus musculus GN=Rasa3 PE=2 SV=1 - [Q3UGJ5_MOUSE]
Q3THA0	Eukaryotic translation initiation factor 3 subunit G OS=Mus musculus GN=Eif3g PE=2 SV=1 - [Q3THA0_MOUSE]
Q99JX4	Eukaryotic translation initiation factor 3 subunit M OS=Mus musculus GN=Eif3m PE=1 SV=1 - [EIF3M_MOUSE]
Q04736	Tyrosine-protein kinase Yes OS=Mus musculus GN=Yes1 PE=1 SV=3 - [YES_MOUSE]
Q9D4P2	Putative uncharacterized protein OS=Mus musculus GN=Spag16 PE=2 SV=1 - [Q9D4P2_MOUSE]
Q3TCX4	Putative uncharacterized protein OS=Mus musculus GN=Zfp622 PE=2 SV=1 - [Q3TCX4_MOUSE]
Q99M31	Heat shock 70 kDa protein 14 OS=Mus musculus GN=Hspa14 PE=1 SV=2 - [HSP7E_MOUSE]
Q8R346	Aars protein (Fragment) OS=Mus musculus GN=Aars PE=2 SV=2 - [Q8R346_MOUSE]
E9PZJ8	Activating signal cointegrator 1 complex subunit 3 OS=Mus musculus GN=Ascc3 PE=1 SV=1 - [ASCC3_MOUSE]
P70199	ERF1 (Fragment) OS=Mus musculus GN=Etf1 PE=2 SV=1 - [P70199_MOUSE]
Q64339	Ubiquitin-like protein ISG15 OS=Mus musculus GN=Isg15 PE=1 SV=4 - [ISG15_MOUSE]
Q80VD1	Protein FAM98B OS=Mus musculus GN=Fam98b PE=1 SV=1 - [FA98B_MOUSE]
Q8C8X9	Putative uncharacterized protein OS=Mus musculus GN=Camk2d PE=2 SV=1 - [Q8C8X9_MOUSE]
A0A0G2JG59	Nexilin (Fragment) OS=Mus musculus GN=Nexn PE=1 SV=1 - [A0A0G2JG59_MOUSE]
B8JJM3	Complement factor B (Fragment) OS=Mus musculus GN=Cfb PE=3 SV=1 - [B8JJM3_MOUSE]
Q9ERU9	E3 SUMO-protein ligase RanBP2 OS=Mus musculus GN=Ranbp2 PE=1 SV=2 - [RBP2_MOUSE]
Q8BWX1	Putative uncharacterized protein OS=Mus musculus GN=Atxn10 PE=2 SV=1 - [Q8BWX1_MOUSE]
Q3UC76	Putative uncharacterized protein OS=Mus musculus GN=Eif1a PE=2 SV=1 - [Q3UC76_MOUSE]
Q3UF75	Alpha-parvin OS=Mus musculus GN=Parva PE=1 SV=1 - [Q3UF75_MOUSE]
P62315	Small nuclear ribonucleoprotein Sm D1 OS=Mus musculus GN=Snrpd1 PE=1 SV=1 - [SMD1_MOUSE]
Q5SS83	Flotillin 2, isoform CRA_a OS=Mus musculus GN=Flot2 PE=1 SV=1 - [Q5SS83_MOUSE]
Q543N4	Putative uncharacterized protein OS=Mus musculus GN=Bysl PE=2 SV=1 - [Q543N4_MOUSE]
A0A1D5RM32	Dipeptidase (Fragment) OS=Mus musculus GN=Dpep1 PE=1 SV=1 - [A0A1D5RM32_MOUSE]
H7BX99	Prothrombin OS=Mus musculus GN=F2 PE=1 SV=1 - [H7BX99_MOUSE]
Q3TN28	Putative uncharacterized protein OS=Mus musculus GN=Xrcc1 PE=2 SV=1 - [Q3TN28_MOUSE]
Q99KA3	Atp6v1b1 protein (Fragment) OS=Mus musculus GN=Atp6v1b1 PE=2 SV=1 - [Q99KA3_MOUSE]
Q3UXI9	Putative uncharacterized protein OS=Mus musculus GN=Ilf2 PE=2 SV=1 - [Q3UXI9_MOUSE]
P30412	Peptidyl-prolyl cis-trans isomerase C OS=Mus musculus GN=Ppic PE=1 SV=1 - [PPIC_MOUSE]
Q62446	Peptidyl-prolyl cis-trans isomerase FKBP3 OS=Mus musculus GN=Fkbp3 PE=1 SV=2 - [FKBP3_MOUSE]
Q8CAQ9	Putative uncharacterized protein OS=Mus musculus GN=Exoc4 PE=2 SV=1 - [Q8CAQ9_MOUSE]
F6UY19	Islet cell autoantigen 1 (Fragment) OS=Mus musculus GN=Ica1 PE=1 SV=1 - [F6UY19_MOUSE]
D3Z765	Putative RNA-binding protein Luc7-like 1 (Fragment) OS=Mus musculus GN=Luc7l PE=1 SV=1 - [D3Z765_MOUSE]
Q3TJA9	DnaJ (Hsp40) homolog, subfamily A, member 3, isoform CRA_b OS=Mus musculus GN=Dnaja3 PE=2 SV=1 - [Q3TJA9_MOUSE]
Q9D1R9	60S ribosomal protein L34 OS=Mus musculus GN=Rpl34 PE=1 SV=2 - [RL34_MOUSE]
A0A0G2JDL9	MCG10748, isoform CRA_b OS=Mus musculus GN=Rap1a PE=1 SV=1 - [A0A0G2JDL9_MOUSE]
Q3TXS7	26S proteasome non-ATPase regulatory subunit 1 OS=Mus musculus GN=Psmd1 PE=1 SV=1 - [PSMD1_MOUSE]
A0A0G2JDI9	ATP-binding cassette sub-family D member 3 OS=Mus musculus GN=Abcd3 PE=1 SV=1 - [A0A0G2JDI9_MOUSE]
A0A0U1RPX7	Unconventional myosin-VIIa OS=Mus musculus GN=Myo7a PE=1 SV=1 - [A0A0U1RPX7_MOUSE]
E9Q7G6	RNA-binding motif, single-stranded-interacting protein 2 OS=Mus musculus GN=Rbms2 PE=1 SV=1 - [E9Q7G6_MOUSE]
Q91ZU6	Dystonin OS=Mus musculus GN=Dst PE=1 SV=2 - [DYST_MOUSE]
Q07417	Short-chain specific acyl-CoA dehydrogenase, mitochondrial OS=Mus musculus GN=Acads PE=1 SV=2 - [ACADS_MOUSE]

D3Z1B9	V-type proton ATPase catalytic subunit A (Fragment) OS=Mus musculus GN=Atp6v1a PE=1 SV=1 - [D3Z1B9_MOUSE]
Q6A075	MKIAA0394 protein (Fragment) OS=Mus musculus GN=Gas7 PE=2 SV=1 - [Q6A075_MOUSE]
Q3U5K8	Putative uncharacterized protein OS=Mus musculus GN=Ifit1 PE=2 SV=1 - [Q3U5K8_MOUSE]
P62965	Cellular retinoic acid-binding protein 1 OS=Mus musculus GN=Crabp1 PE=1 SV=2 - [RABP1_MOUSE]
F8VQ42	Kinesin-like protein (Fragment) OS=Mus musculus GN=Kif2a PE=1 SV=1 - [F8VQ42_MOUSE]
V9GXA5	Zinc finger transcription factor Trps1 OS=Mus musculus GN=Trps1 PE=1 SV=1 - [V9GXA5_MOUSE]
Q6P9Q4	FH1/FH2 domain-containing protein 1 OS=Mus musculus GN=Fhod1 PE=1 SV=3 - [FHOD1_MOUSE]
Q3UUU0	Putative uncharacterized protein OS=Mus musculus GN=Emilin1 PE=2 SV=1 - [Q3UUU0_MOUSE]
Q80TP6	MKIAA0890 protein (Fragment) OS=Mus musculus GN=mKIAA0890 PE=4 SV=3 - [Q80TP6_MOUSE]
F6RB63	PC4 and SFRS1-interacting protein (Fragment) OS=Mus musculus GN=Psip1 PE=1 SV=1 - [F6RB63_MOUSE]
Q99JY8	Phospholipid phosphatase 3 OS=Mus musculus GN=Plpp3 PE=1 SV=1 - [PLPP3_MOUSE]
K7Q751	Focal ashension kinase 1 OS=Mus musculus GN=Ptk2 PE=2 SV=1 - [K7Q751_MOUSE]
O08842	GDNF family receptor alpha-2 OS=Mus musculus GN=Gfra2 PE=1 SV=2 - [GFRA2_MOUSE]
Q99J62	Replication factor C subunit 4 OS=Mus musculus GN=Rfc4 PE=1 SV=1 - [RFC4_MOUSE]
H3BLG5	Syntenin-1 (Fragment) OS=Mus musculus GN=Sdcbp PE=1 SV=1 - [H3BLG5_MOUSE]
Q8BGU5	Cyclin-Y OS=Mus musculus GN=Ccny PE=1 SV=1 - [CCNY_MOUSE]
F6YRQ2	DnaJ homolog subfamily B member 6 (Fragment) OS=Mus musculus GN=Dnajb6 PE=1 SV=1 - [F6YRQ2_MOUSE]
P26516	26S proteasome non-ATPase regulatory subunit 7 OS=Mus musculus GN=Psmd7 PE=1 SV=2 - [PSMD7_MOUSE]
Q80UU9	Membrane-associated progesterone receptor component 2 OS=Mus musculus GN=Pgrmc2 PE=1 SV=2 - [PGRC2_MOUSE]
Q4VAA7	Sorting nexin-33 OS=Mus musculus GN=Snx33 PE=1 SV=1 - [SNX33_MOUSE]
Q99M55	V-type proton ATPase subunit a OS=Mus musculus GN=Atp6v0a1 PE=2 SV=1 - [Q99M55_MOUSE]
Q8R2U0	Nucleoporin SEH1 OS=Mus musculus GN=Seh1l PE=2 SV=1 - [SEH1_MOUSE]
Q9DBR1	5'-3' exoribonuclease 2 OS=Mus musculus GN=Xrn2 PE=1 SV=1 - [XRN2_MOUSE]
P10833	Ras-related protein R-Ras OS=Mus musculus GN=Rras PE=1 SV=1 - [RRAS_MOUSE]
Q8R2X0	Ehd2 protein OS=Mus musculus GN=Ehd2 PE=2 SV=1 - [Q8R2X0_MOUSE]
Q8C1L7	40S ribosomal protein S21 OS=Mus musculus GN=mCG_6739 PE=2 SV=1 - [Q8C1L7_MOUSE]
A0A0R4J2A5	Suprabasin OS=Mus musculus GN=Sbsn PE=1 SV=1 - [A0A0R4J2A5_MOUSE]
Q8CD98	Putative uncharacterized protein OS=Mus musculus GN=Pfkl PE=2 SV=1 - [Q8CD98_MOUSE]
Q5XJX8	Mrps9 protein (Fragment) OS=Mus musculus GN=Mrps9 PE=2 SV=1 - [Q5XJX8_MOUSE]
A0A1D5RM74	Casein kinase II subunit alpha' (Fragment) OS=Mus musculus GN=Csnk2a2 PE=1 SV=1 - [A0A1D5RM74_MOUSE]
Q3UJP8	Trifunctional purine biosynthetic protein adenosine-3 OS=Mus musculus GN=Gart PE=2 SV=1 - [Q3UJP8_MOUSE]
P28660	Nck-associated protein 1 OS=Mus musculus GN=Nckap1 PE=1 SV=2 - [NCKP1_MOUSE]
B7ZP28	Dennd2a protein OS=Mus musculus GN=Dennd2a PE=2 SV=1 - [B7ZP28_MOUSE]
Q6PAH8	Gatad2b protein (Fragment) OS=Mus musculus GN=Gatad2b PE=2 SV=1 - [Q6PAH8_MOUSE]
Q9QZB9	Dynactin subunit 5 OS=Mus musculus GN=Dctn5 PE=1 SV=1 - [DCTN5_MOUSE]
Q9EP69	Phosphatidylinositide phosphatase SAC1 OS=Mus musculus GN=Sacm1l PE=1 SV=1 - [SAC1_MOUSE]
Q3TK56	Actin-related protein 2/3 complex subunit 5 (Fragment) OS=Mus musculus GN=Arpc5 PE=2 SV=1 - [Q3TK56_MOUSE]
E9PZC4	Flavin reductase (NADPH) OS=Mus musculus GN=Blvrb PE=1 SV=1 - [E9PZC4_MOUSE]
S4R294	Protein PRRC2C OS=Mus musculus GN=Prrc2c PE=1 SV=1 - [S4R294_MOUSE]
Q3UT80	Putative uncharacterized protein OS=Mus musculus GN=Gm1587 PE=2 SV=1 - [Q3UT80_MOUSE]
O08543	Ephrin-A5 OS=Mus musculus GN=Efna5 PE=1 SV=1 - [EFNA5_MOUSE]
A2AG47	Melanoma antigen, family D, 2 (Fragment) OS=Mus musculus GN=Maged2 PE=1 SV=1 - [A2AG47_MOUSE]
Q9CZX0	Elongator complex protein 3 OS=Mus musculus GN=Elp3 PE=1 SV=1 - [ELP3_MOUSE]
B7ZN65	Il5ra protein OS=Mus musculus GN=Il5ra PE=2 SV=1 - [B7ZN65_MOUSE]
Q91YN9	BAG family molecular chaperone regulator 2 OS=Mus musculus GN=Bag2 PE=1 SV=1 - [BAG2_MOUSE]
Q922M3	BTB/POZ domain-containing adapter for CUL3-mediated RhoA degradation protein 3 OS=Mus musculus GN=Kctd10 PE=1 SV=1 - [BACD3_MOUSE]
Q45VK5	Interleukin enhancer-binding factor 3 OS=Mus musculus GN=Ilf3 PE=1 SV=1 - [Q45VK5_MOUSE]

Q3UX26	Putative uncharacterized protein (Fragment) OS=Mus musculus GN=Pak1ip1 PE=2 SV=1 - [Q3UX26_MOUSE]
B1AXI9	5-azacytidine induced gene 1 OS=Mus musculus GN=Cep131 PE=1 SV=1 - [B1AXI9_MOUSE]
A0A0G2JF66	Coiled-coil domain-containing 149 OS=Mus musculus GN=Ccdc149 PE=4 SV=1 - [A0A0G2JF66_MOUSE]
Q3TLT9	Putative uncharacterized protein OS=Mus musculus GN=Cd44 PE=2 SV=1 - [Q3TLT9_MOUSE]
Q9EPK2	Protein XRP2 OS=Mus musculus GN=Rp2 PE=1 SV=3 - [XRP2_MOUSE]
Q91Y95	Thioredoxin reductase 1 (Fragment) OS=Mus musculus GN=Txnrd1 PE=4 SV=1 - [Q91Y95_MOUSE]
Q9CQ62	2,4-dienoyl-CoA reductase, mitochondrial OS=Mus musculus GN=Decr1 PE=1 SV=1 - [DECR_MOUSE]
Q99L68	Stom protein OS=Mus musculus GN=Stom PE=2 SV=1 - [Q99L68_MOUSE]
Q6ZQM3	cDNA fis, clone TRACH3010757, highly similar to Interferon-gamma inducible protein MG11 OS=Mus musculus GN=Samhd1 PE=2 SV=1 - [Q6ZQM3_MOUSE]
Q3ULP8	Putative uncharacterized protein OS=Mus musculus GN=Pus7 PE=2 SV=1 - [Q3ULP8_MOUSE]
A0A0U1RPS0	AP-2 complex subunit sigma OS=Mus musculus GN=Ap2s1 PE=1 SV=1 - [A0A0U1RPS0_MOUSE]
Q5XG71	Small subunit processome component 20 homolog OS=Mus musculus GN=Utp20 PE=1 SV=2 - [UTP20_MOUSE]
D6RET7	GRAM domain-containing protein 4 OS=Mus musculus GN=Gramd4 PE=1 SV=1 - [D6RET7_MOUSE]
Q9D4G5	Processing of precursor 1, ribonuclease P/MRP family, (S. cerevisiae) OS=Mus musculus GN=Pop1 PE=1 SV=1 - [Q9D4G5_MOUSE]
Q6PFQ7	Ras GTPase-activating protein 4 OS=Mus musculus GN=Rasa4 PE=1 SV=1 - [RASL2_MOUSE]
Q9CR32	Putative uncharacterized protein (Fragment) OS=Mus musculus GN=Snrnp70 PE=2 SV=3 - [Q9CR32_MOUSE]
Q9QZB7	Actin-related protein 10 OS=Mus musculus GN=Actr10 PE=1 SV=2 - [ARP10_MOUSE]
P27048	Small nuclear ribonucleoprotein-associated protein B OS=Mus musculus GN=Snrpb PE=1 SV=1 - [RSMB_MOUSE]
Q9D898	Actin-related protein 2/3 complex subunit 5-like protein OS=Mus musculus GN=Arpc5l PE=1 SV=1 - [ARP5L_MOUSE]
Q9WTX2	Interferon-inducible double-stranded RNA-dependent protein kinase activator A OS=Mus musculus GN=Prkra PE=1 SV=1 - [PRKRA_MOUSE]
B1AQR8	Galectin OS=Mus musculus GN=Lgals9 PE=1 SV=1 - [B1AQR8_MOUSE]
Q3TZG4	Putative uncharacterized protein OS=Mus musculus GN=Elmo3 PE=2 SV=1 - [Q3TZG4_MOUSE]
Q3TT24	Putative uncharacterized protein (Fragment) OS=Mus musculus GN=Ptprf PE=2 SV=1 - [Q3TT24_MOUSE]
Q3TGN4	Putative uncharacterized protein (Fragment) OS=Mus musculus GN=Arhgap6 PE=2 SV=1 - [Q3TGN4_MOUSE]
Q3UAP7	S-adenosylmethionine synthase OS=Mus musculus GN=Mat2a PE=2 SV=1 - [Q3UAP7_MOUSE]
O54784	Death-associated protein kinase 3 OS=Mus musculus GN=Dapk3 PE=1 SV=1 - [DAPK3_MOUSE]
Q3UEW8	Putative uncharacterized protein (Fragment) OS=Mus musculus GN=Pdpk1 PE=2 SV=1 - [Q3UEW8_MOUSE]
A2AFI4	RNA-binding motif protein, X chromosome (Fragment) OS=Mus musculus GN=Rbmx PE=1 SV=1 - [A2AFI4_MOUSE]
Q3U8N1	Putative uncharacterized protein OS=Mus musculus GN=Sars PE=2 SV=1 - [Q3U8N1_MOUSE]
Q3TIV5	Zinc finger CCCH domain-containing protein 15 OS=Mus musculus GN=Zc3h15 PE=1 SV=2 - [ZC3HF_MOUSE]
Q5MJS3	Extracellular serine/threonine protein kinase FAM20C OS=Mus musculus GN=Fam20c PE=1 SV=1 - [FA20C_MOUSE]
D3Z710	Kinesin light chain 3 OS=Mus musculus GN=Klc3 PE=1 SV=1 - [D3Z710_MOUSE]
G3UXX5	DNA-directed RNA polymerases I and III subunit RPAC1 (Fragment) OS=Mus musculus GN=Polr1c PE=1 SV=1 - [G3UXX5_MOUSE]
Q3TJP6	Putative uncharacterized protein OS=Mus musculus GN=Cd34 PE=2 SV=1 - [Q3TJP6_MOUSE]
Q8HW98	IgLON family member 5 OS=Mus musculus GN=Iglon5 PE=2 SV=2 - [IGLO5_MOUSE]
Q3U1G4	Putative uncharacterized protein OS=Mus musculus GN=Exoc1 PE=2 SV=1 - [Q3U1G4_MOUSE]
Q9D4I1	Putative uncharacterized protein OS=Mus musculus GN=Myo18b PE=2 SV=1 - [Q9D4I1_MOUSE]
Q3TLK3	Putative uncharacterized protein OS=Mus musculus GN=Ncbp1 PE=2 SV=1 - [Q3TLK3_MOUSE]
Q3UPF5	Zinc finger CCCH-type antiviral protein 1 OS=Mus musculus GN=Zc3hav1 PE=1 SV=1 - [ZCCHV_MOUSE]
E0CZH6	Mitochondrial amidoxime reducing component 2 (Fragment) OS=Mus musculus GN=Marc2 PE=1 SV=1 - [E0CZH6_MOUSE]
F6V8R7	Replication protein A 32 kDa subunit (Fragment) OS=Mus musculus GN=Rpa2 PE=1 SV=1 - [F6V8R7_MOUSE]
D3YUY3	Phosphatidylinositol 4-phosphate 5-kinase type-1 alpha OS=Mus musculus GN=Pip5k1a PE=1 SV=1 - [D3YUY3_MOUSE]
P30677	Guanine nucleotide-binding protein subunit alpha-14 OS=Mus musculus GN=Gna14 PE=1 SV=2 - [GNA14_MOUSE]
Q9CRB5	Prolactin-7C1 OS=Mus musculus GN=Prl7c1 PE=2 SV=1 - [PR7C1_MOUSE]

Q8K314	Atp2b1 protein (Fragment) OS=Mus musculus GN=Atp2b1 PE=2 SV=1 - [Q8K314_MOUSE]
A3KG81	Multiple PDZ domain protein OS=Mus musculus GN=Mpdz PE=1 SV=1 - [A3KG81_MOUSE]
Q80U19	Disheveled-associated activator of morphogenesis 2 OS=Mus musculus GN=Daam2 PE=1 SV=4 - [DAAM2_MOUSE]
F6U8X4	Serine/threonine-protein kinase SIK3 (Fragment) OS=Mus musculus GN=Sik3 PE=1 SV=1 - [F6U8X4_MOUSE]
Q61425	Hydroxyacyl-coenzyme A dehydrogenase, mitochondrial OS=Mus musculus GN=Hadh PE=1 SV=2 - [HCDH_MOUSE]
Q0KK56	Protein FAM184B OS=Mus musculus GN=Fam184b PE=2 SV=1 - [F184B_MOUSE]
P62869	Elongin-B OS=Mus musculus GN=Elob PE=1 SV=1 - [ELOB_MOUSE]
A2BDX3	Adenylyltransferase and sulfurtransferase MOCS3 OS=Mus musculus GN=Mocs3 PE=1 SV=1 - [MOCS3_MOUSE]
P62915	Transcription initiation factor IIB OS=Mus musculus GN=Gtf2b PE=1 SV=1 - [TF2B_MOUSE]
A0A0A6YXS8	Antithrombin-III OS=Mus musculus GN=Serpinc1 PE=1 SV=1 - [A0A0A6YXS8_MOUSE]
Q8CI33	CWF19-like protein 1 OS=Mus musculus GN=Cwf19l1 PE=1 SV=2 - [C19L1_MOUSE]
Q6ZQK4	MKIAA0044 protein (Fragment) OS=Mus musculus GN=Ppp2r5c PE=2 SV=1 - [Q6ZQK4_MOUSE]
D3Z2D9	Peroxisome proliferator-activated receptor gamma coactivator-related protein 1 (Fragment) OS=Mus musculus GN=Pprc1 PE=4 SV=8 - [D3Z2D9_MOUSE]
Q6LAL7	Beta-2 glycoprotein I (Fragment) OS=Mus musculus PE=4 SV=1 - [Q6LAL7_MOUSE]
Q2M4I5	Sp3 (Fragment) OS=Mus musculus GN=Sp3 PE=4 SV=1 - [Q2M4I5_MOUSE]
B2RWU2	Immunodeficiency virus type I enhancer binding protein 2 OS=Mus musculus GN=Hivep2 PE=2 SV=1 - [B2RWU2_MOUSE]
P43267	Protein SOX-15 OS=Mus musculus GN=Sox15 PE=1 SV=3 - [SOX15_MOUSE]
O09164	Extracellular superoxide dismutase [Cu-Zn] OS=Mus musculus GN=Sod3 PE=1 SV=1 - [SODE_MOUSE]
Q8R0S2	IQ motif and SEC7 domain-containing protein 1 OS=Mus musculus GN=Iqsec1 PE=1 SV=2 - [IQEC1_MOUSE]
Q14C53	Solute carrier family 39 (Zinc transporter), member 7 OS=Mus musculus GN=Slc39a7 PE=2 SV=1 - [Q14C53_MOUSE]
E9Q5I9	26S proteasome non-ATPase regulatory subunit 13 OS=Mus musculus GN=Psmd13 PE=1 SV=1 - [E9Q5I9_MOUSE]
B7FAT3	CDNA sequence BC005537 (Fragment) OS=Mus musculus GN=BC005537 PE=4 SV=1 - [B7FAT3_MOUSE]
Q8BU35	Putative uncharacterized protein OS=Mus musculus GN=Rbm25 PE=2 SV=1 - [Q8BU35_MOUSE]
Q3TJI4	Putative uncharacterized protein (Fragment) OS=Mus musculus GN=Amd1 PE=2 SV=1 - [Q3TJI4_MOUSE]
A0A0A6YY78	Serine/threonine-protein kinase MARK1 (Fragment) OS=Mus musculus GN=Mark1 PE=1 SV=1 - [A0A0A6YY78_MOUSE]
A2ADN1	Frem1 protein OS=Mus musculus GN=Frem1 PE=2 SV=1 - [A2ADN1_MOUSE]
P61082	NEDD8-conjugating enzyme Ubc12 OS=Mus musculus GN=Ube2m PE=1 SV=1 - [UBC12_MOUSE]
Q9EQY0	Serine/threonine-protein kinase/endoribonuclease IRE1 OS=Mus musculus GN=Ern1 PE=1 SV=1 - [ERN1_MOUSE]
Q3V415	Putative uncharacterized protein (Fragment) OS=Mus musculus GN=Mtmr2 PE=2 SV=1 - [Q3V415_MOUSE]
Q91W97	Putative hexokinase HKDC1 OS=Mus musculus GN=Hkdc1 PE=2 SV=1 - [HKDC1_MOUSE]
D6RHA2	N-acylglucosamine 2-epimerase OS=Mus musculus GN=Renbp PE=1 SV=2 - [D6RHA2_MOUSE]
D3K2X3	Truncated DJ-1 variant SV4,5DEL OS=Mus musculus GN=Park7 PE=2 SV=1 - [D3K2X3_MOUSE]

(b) GFP-TMEM67 ΔECL

Uniprot Accession	**Description**
Q9QXS1	Plectin OS=Mus musculus GN=Plec PE=1 SV=3 - [PLEC_MOUSE]
Q6S385	Plectin 10 OS=Mus musculus GN=Plec PE=2 SV=1 - [Q6S385_MOUSE]
Q8VDD5	Myosin-9 OS=Mus musculus GN=Myh9 PE=1 SV=4 - [MYH9_MOUSE]
Q3UBP6	Putative uncharacterized protein OS=Mus musculus GN=Actb PE=2 SV=1 - [Q3UBP6_MOUSE]
Q61879	Myosin-10 OS=Mus musculus GN=Myh10 PE=1 SV=2 - [MYH10_MOUSE]
Q3UFT0	Putative uncharacterized protein (Fragment) OS=Mus musculus GN=Myh9 PE=2 SV=1 - [Q3UFT0_MOUSE]
P20152	Vimentin OS=Mus musculus GN=Vim PE=1 SV=3 - [VIME_MOUSE]
Q9WTI7	Unconventional myosin-Ic OS=Mus musculus GN=Myo1c PE=1 SV=2 - [MYO1C_MOUSE]

Q05CR3	Plec1 protein (Fragment) OS=Mus musculus GN=Plec PE=2 SV=1 - [Q05CR3_MOUSE]
A0A0R4J221	Plectin (Fragment) OS=Mus musculus GN=Plec PE=1 SV=1 - [A0A0R4J221_MOUSE]
E9Q634	Unconventional myosin-Ie OS=Mus musculus GN=Myo1e PE=1 SV=1 - [MYO1E_MOUSE]
Q5SWZ5	Myosin phosphatase Rho-interacting protein OS=Mus musculus GN=Mprip PE=1 SV=1 - [Q5SWZ5_MOUSE]
Q5SYD0	Unconventional myosin-Id OS=Mus musculus GN=Myo1d PE=1 SV=1 - [MYO1D_MOUSE]
P46735	Unconventional myosin-Ib OS=Mus musculus GN=Myo1b PE=1 SV=3 - [MYO1B_MOUSE]
B9EHJ3	Tight junction protein ZO-1 OS=Mus musculus GN=Tjp1 PE=1 SV=1 - [B9EHJ3_MOUSE]
E9QNH6	Unconventional myosin-Ib OS=Mus musculus GN=Myo1b PE=1 SV=1 - [E9QNH6_MOUSE]
Q7TPR4	Alpha-actinin-1 OS=Mus musculus GN=Actn1 PE=1 SV=1 - [ACTN1_MOUSE]
Q8BFZ3	Beta-actin-like protein 2 OS=Mus musculus GN=Actbl2 PE=1 SV=1 - [ACTBL_MOUSE]
P11087	Collagen alpha-1(I) chain OS=Mus musculus GN=Col1a1 PE=1 SV=4 - [CO1A1_MOUSE]
Q6PAC1	Gelsolin, isoform CRA_c OS=Mus musculus GN=Gsn PE=2 SV=1 - [Q6PAC1_MOUSE]
Q9EP71	Ankycorbin OS=Mus musculus GN=Rai14 PE=1 SV=1 - [RAI14_MOUSE]
P62737	Actin, aortic smooth muscle OS=Mus musculus GN=Acta2 PE=1 SV=1 - [ACTA_MOUSE]
A3KGU5	Spectrin alpha chain, non-erythrocytic 1 OS=Mus musculus GN=Sptan1 PE=1 SV=1 - [A3KGU5_MOUSE]
A0A0J9YUQ8	Gelsolin (Fragment) OS=Mus musculus GN=Gsn PE=1 SV=1 - [A0A0J9YUQ8_MOUSE]
E9Q175	Unconventional myosin-VI OS=Mus musculus GN=Myo6 PE=1 SV=1 - [E9Q175_MOUSE]
Q61553	Fascin OS=Mus musculus GN=Fscn1 PE=1 SV=4 - [FSCN1_MOUSE]
Q2KN98	Cytospin-A OS=Mus musculus GN=Specc1l PE=1 SV=1 - [CYTSA_MOUSE]
E9PX70	Collagen alpha-1(XII) chain OS=Mus musculus GN=Col12a1 PE=1 SV=1 - [E9PX70_MOUSE]
Q9ERG0	LIM domain and actin-binding protein 1 OS=Mus musculus GN=Lima1 PE=1 SV=3 - [LIMA1_MOUSE]
Q8K4L3	Supervillin OS=Mus musculus GN=Svil PE=1 SV=1 - [SVIL_MOUSE]
E9Q3Z5	Supervillin OS=Mus musculus GN=Svil PE=1 SV=1 - [E9Q3Z5_MOUSE]
Q6ZWQ9	MCG5400 OS=Mus musculus GN=Myl12a PE=1 SV=1 - [Q6ZWQ9_MOUSE]
Q62261	Spectrin beta chain, non-erythrocytic 1 OS=Mus musculus GN=Sptbn1 PE=1 SV=2 - [SPTB2_MOUSE]
E9Q3E2	Synaptopodin OS=Mus musculus GN=Synpo PE=1 SV=1 - [E9Q3E2_MOUSE]
B7ZND7	2310014H01Rik protein OS=Mus musculus GN=Ppp1r18 PE=2 SV=1 - [B7ZND7_MOUSE]
A0A1B0GX25	Histone deacetylase 6 (Fragment) OS=Mus musculus GN=Hdac6 PE=1 SV=1 - [A0A1B0GX25_MOUSE]
Q60605	Myosin light polypeptide 6 OS=Mus musculus GN=Myl6 PE=1 SV=3 - [MYL6_MOUSE]
Q9DBR7	Protein phosphatase 1 regulatory subunit 12A OS=Mus musculus GN=Ppp1r12a PE=1 SV=2 - [MYPT1_MOUSE]
Q642K0	MCG140959, isoform CRA_a OS=Mus musculus GN=Myl6 PE=2 SV=1 - [Q642K0_MOUSE]
P07901	Heat shock protein HSP 90-alpha OS=Mus musculus GN=Hsp90aa1 PE=1 SV=4 - [HS90A_MOUSE]
K3W4R2	Myosin-14 OS=Mus musculus GN=Myh14 PE=1 SV=1 - [K3W4R2_MOUSE]
Q3URM4	Putative uncharacterized protein OS=Mus musculus GN=Erp44 PE=2 SV=1 - [Q3URM4_MOUSE]
Q3THE2	Myosin regulatory light chain 12B OS=Mus musculus GN=Myl12b PE=1 SV=2 - [ML12B_MOUSE]
P08752	Guanine nucleotide-binding protein G(i) subunit alpha-2 OS=Mus musculus GN=Gnai2 PE=1 SV=5 - [GNAI2_MOUSE]
Q8R422	CD109 antigen OS=Mus musculus GN=Cd109 PE=1 SV=1 - [CD109_MOUSE]
Q9QZF2	Glypican-1 OS=Mus musculus GN=Gpc1 PE=1 SV=1 - [GPC1_MOUSE]
Q3TRK3	Putative uncharacterized protein OS=Mus musculus GN=Dbn1 PE=2 SV=1 - [Q3TRK3_MOUSE]
A0A1D5RLD8	Glyceraldehyde-3-phosphate dehydrogenase OS=Mus musculus GN=Gm10358 PE=1 SV=1 - [A0A1D5RLD8_MOUSE]
Q3TQW3	Putative uncharacterized protein OS=Mus musculus GN=Ptbp1 PE=2 SV=1 - [Q3TQW3_MOUSE]
P62137	Serine/threonine-protein phosphatase PP1-alpha catalytic subunit OS=Mus musculus GN=Ppp1ca PE=1 SV=1 - [PP1A_MOUSE]
Q8VCQ8	Caldesmon 1 OS=Mus musculus GN=Cald1 PE=1 SV=1 - [Q8VCQ8_MOUSE]
K3W4L0	Unconventional myosin-XVIIIa OS=Mus musculus GN=Myo18a PE=1 SV=1 - [K3W4L0_MOUSE]
Q9JJ28	Protein flightless-1 homolog OS=Mus musculus GN=Flii PE=1 SV=1 - [FLII_MOUSE]

A0A0U1RNK7	Dedicator of cytokinesis protein 7 OS=Mus musculus GN=Dock7 PE=1 SV=1 - [A0A0U1RNK7_MOUSE]
B2CY77	Laminin receptor (Fragment) OS=Mus musculus GN=Rpsa PE=2 SV=1 - [B2CY77_MOUSE]
Q08509	Epidermal growth factor receptor kinase substrate 8 OS=Mus musculus GN=Eps8 PE=1 SV=2 - [EPS8_MOUSE]
Q6R891	Neurabin-2 OS=Mus musculus GN=Ppp1r9b PE=1 SV=1 - [NEB2_MOUSE]
Q3TZU7	Sorting nexin OS=Mus musculus GN=Snx9 PE=2 SV=1 - [Q3TZU7_MOUSE]
P62141	Serine/threonine-protein phosphatase PP1-beta catalytic subunit OS=Mus musculus GN=Ppp1cb PE=1 SV=3 - [PP1B_MOUSE]
Q3TGE1	Putative uncharacterized protein OS=Mus musculus GN=Actr3 PE=2 SV=1 - [Q3TGE1_MOUSE]
Q03265	ATP synthase subunit alpha, mitochondrial OS=Mus musculus GN=Atp5a1 PE=1 SV=1 - [ATPA_MOUSE]
Q4VBF8	Sipa1l1 protein OS=Mus musculus GN=Sipa1l1 PE=2 SV=1 - [Q4VBF8_MOUSE]
Q0KL02	Triple functional domain protein OS=Mus musculus GN=Trio PE=1 SV=3 - [TRIO_MOUSE]
P62880	Guanine nucleotide-binding protein G(I)/G(S)/G(T) subunit beta-2 OS=Mus musculus GN=Gnb2 PE=1 SV=3 - [GBB2_MOUSE]
Q9Z0U1	Tight junction protein ZO-2 OS=Mus musculus GN=Tjp2 PE=1 SV=2 - [ZO2_MOUSE]
E9QAH1	Golgi autoantigen, golgin subfamily b, macrogolgin 1 OS=Mus musculus GN=Golgb1 PE=1 SV=1 - [E9QAH1_MOUSE]
Q3TFD0	Serine hydroxymethyltransferase OS=Mus musculus GN=Shmt2 PE=2 SV=1 - [Q3TFD0_MOUSE]
Q69ZN7	Myoferlin OS=Mus musculus GN=Myof PE=1 SV=2 - [MYOF_MOUSE]
Q99L75	Heat shock protein 4 OS=Mus musculus GN=Hspa4 PE=2 SV=1 - [Q99L75_MOUSE]
Q9DC51	Guanine nucleotide-binding protein G(k) subunit alpha OS=Mus musculus GN=Gnai3 PE=1 SV=3 - [GNAI3_MOUSE]
P80314	T-complex protein 1 subunit beta OS=Mus musculus GN=Cct2 PE=1 SV=4 - [TCPB_MOUSE]
P35979	60S ribosomal protein L12 OS=Mus musculus GN=Rpl12 PE=1 SV=2 - [RL12_MOUSE]
P56480	ATP synthase subunit beta, mitochondrial OS=Mus musculus GN=Atp5b PE=1 SV=2 - [ATPB_MOUSE]
E9Q452	Tropomyosin alpha-1 chain OS=Mus musculus GN=Tpm1 PE=1 SV=1 - [E9Q452_MOUSE]
Q8BK67	Protein RCC2 OS=Mus musculus GN=Rcc2 PE=1 SV=1 - [RCC2_MOUSE]
Q6IRU2	Tropomyosin alpha-4 chain OS=Mus musculus GN=Tpm4 PE=1 SV=3 - [TPM4_MOUSE]
P05064	Fructose-bisphosphate aldolase A OS=Mus musculus GN=Aldoa PE=1 SV=2 - [ALDOA_MOUSE]
P47754	F-actin-capping protein subunit alpha-2 OS=Mus musculus GN=Capza2 PE=1 SV=3 - [CAZA2_MOUSE]
P18872	Guanine nucleotide-binding protein G(o) subunit alpha OS=Mus musculus GN=Gnao1 PE=1 SV=3 - [GNAO_MOUSE]
G3X9T8	Ceruloplasmin OS=Mus musculus GN=Cp PE=1 SV=1 - [G3X9T8_MOUSE]
E9Q450	Tropomyosin alpha-1 chain OS=Mus musculus GN=Tpm1 PE=1 SV=1 - [E9Q450_MOUSE]
G3X9J0	Signal-induced proliferation-associated 1-like protein 3 OS=Mus musculus GN=Sipa1l3 PE=1 SV=1 - [SI1L3_MOUSE]
P80313	T-complex protein 1 subunit eta OS=Mus musculus GN=Cct7 PE=1 SV=1 - [TCPH_MOUSE]
A0A1L1SUX8	Thy-1 membrane glycoprotein (Fragment) OS=Mus musculus GN=Thy1 PE=1 SV=1 - [A0A1L1SUX8_MOUSE]
Q8BH78	Reticulon OS=Mus musculus GN=Rtn4 PE=1 SV=1 - [Q8BH78_MOUSE]
Q61344	Beta-tropomyosin OS=Mus musculus GN=Tpm2 PE=2 SV=1 - [Q61344_MOUSE]
P28301	Protein-lysine 6-oxidase OS=Mus musculus GN=Lox PE=1 SV=1 - [LYOX_MOUSE]
E9Q133	T-complex protein 1 subunit gamma OS=Mus musculus GN=Cct3 PE=1 SV=1 - [E9Q133_MOUSE]
Q3TCE7	Putative uncharacterized protein OS=Mus musculus GN=Arpc1b PE=2 SV=1 - [Q3TCE7_MOUSE]
Q3TFA9	Putative uncharacterized protein OS=Mus musculus GN=Tmod3 PE=2 SV=1 - [Q3TFA9_MOUSE]
Q5SF07	Insulin-like growth factor 2 mRNA-binding protein 2 OS=Mus musculus GN=Igf2bp2 PE=1 SV=1 - [IF2B2_MOUSE]
Q61753	D-3-phosphoglycerate dehydrogenase OS=Mus musculus GN=Phgdh PE=1 SV=3 - [SERA_MOUSE]
F7DBB3	AHNAK nucleoprotein 2 (Fragment) OS=Mus musculus GN=Ahnak2 PE=1 SV=1 - [F7DBB3_MOUSE]
Q7TPV4	Myb-binding protein 1A OS=Mus musculus GN=Mybbp1a PE=1 SV=2 - [MBB1A_MOUSE]
O54724	Polymerase I and transcript release factor OS=Mus musculus GN=Ptrf PE=1 SV=1 - [PTRF_MOUSE]

P31001	Desmin OS=Mus musculus GN=Des PE=1 SV=3 - [DESM_MOUSE]
Q8QZY1	Eukaryotic translation initiation factor 3 subunit L OS=Mus musculus GN=Eif3l PE=1 SV=1 - [EIF3L_MOUSE]
Q3TEU8	Coronin OS=Mus musculus GN=Coro1c PE=2 SV=1 - [Q3TEU8_MOUSE]
Q925B0	PRKC apoptosis WT1 regulator protein OS=Mus musculus GN=Pawr PE=1 SV=2 - [PAWR_MOUSE]
D0VYV7	Erythrocyte protein band 4.1-like 3 isoform C OS=Mus musculus GN=Epb41l3 PE=2 SV=1 - [D0VYV7_MOUSE]
O89079	Coatomer subunit epsilon OS=Mus musculus GN=Cope PE=1 SV=3 - [COPE_MOUSE]
P51410	60S ribosomal protein L9 OS=Mus musculus GN=Rpl9 PE=2 SV=2 - [RL9_MOUSE]
Q9R0P3	S-formylglutathione hydrolase OS=Mus musculus GN=Esd PE=1 SV=1 - [ESTD_MOUSE]
Q63844	Mitogen-activated protein kinase 3 OS=Mus musculus GN=Mapk3 PE=1 SV=5 - [MK03_MOUSE]
G5E8R0	Tropomyosin 1, alpha, isoform CRA_i OS=Mus musculus GN=Tpm1 PE=1 SV=1 - [G5E8R0_MOUSE]
P47753	F-actin-capping protein subunit alpha-1 OS=Mus musculus GN=Capza1 PE=1 SV=4 - [CAZA1_MOUSE]
Q8BG95	Protein phosphatase 1 regulatory subunit 12B OS=Mus musculus GN=Ppp1r12b PE=1 SV=2 - [MYPT2_MOUSE]
P67778	Prohibitin OS=Mus musculus GN=Phb PE=1 SV=1 - [PHB_MOUSE]
Q8BMA4	Putative uncharacterized protein OS=Mus musculus PE=2 SV=1 - [Q8BMA4_MOUSE]
A2AL12	Heterogeneous nuclear ribonucleoprotein A3 OS=Mus musculus GN=Hnrnpa3 PE=1 SV=1 - [A2AL12_MOUSE]
P31230	Aminoacyl tRNA synthase complex-interacting multifunctional protein 1 OS=Mus musculus GN=Aimp1 PE=1 SV=2 - [AIMP1_MOUSE]
P42208	Septin-2 OS=Mus musculus GN=Sept2 PE=1 SV=2 - [SEPT2_MOUSE]
P54823	Probable ATP-dependent RNA helicase DDX6 OS=Mus musculus GN=Ddx6 PE=1 SV=1 - [DDX6_MOUSE]
A2AMW0	Capping protein (Actin filament) muscle Z-line, beta, isoform CRA_a OS=Mus musculus GN=Capzb PE=1 SV=1 - [A2AMW0_MOUSE]
Q3TF41	Nucleosome assembly protein 1-like 1, isoform CRA_d OS=Mus musculus GN=Nap1l1 PE=2 SV=1 - [Q3TF41_MOUSE]
Q4VA93	Protein kinase C OS=Mus musculus GN=Prkca PE=1 SV=1 - [Q4VA93_MOUSE]
Q9CVB6	Actin-related protein 2/3 complex subunit 2 OS=Mus musculus GN=Arpc2 PE=1 SV=3 - [ARPC2_MOUSE]
Q60598	Src substrate cortactin OS=Mus musculus GN=Cttn PE=1 SV=2 - [SRC8_MOUSE]
Q01721	Growth arrest-specific protein 1 OS=Mus musculus GN=Gas1 PE=2 SV=2 - [GAS1_MOUSE]
Q3TGL4	Fibulin 2, isoform CRA_b OS=Mus musculus GN=Fbln2 PE=2 SV=1 - [Q3TGL4_MOUSE]
B0LAA8	Nucleoside diphosphate kinase (Fragment) OS=Mus musculus GN=Nme2 PE=2 SV=1 - [B0LAA8_MOUSE]
E9QN08	Elongation factor 1-delta (Fragment) OS=Mus musculus GN=Eef1d PE=1 SV=1 - [E9QN08_MOUSE]
Q5DTS3	MKIAA4020 protein (Fragment) OS=Mus musculus GN=Sept7 PE=2 SV=1 - [Q5DTS3_MOUSE]
Q60865	Caprin-1 OS=Mus musculus GN=Caprin1 PE=1 SV=2 - [CAPR1_MOUSE]
Q9CQV8	14-3-3 protein beta/alpha OS=Mus musculus GN=Ywhab PE=1 SV=3 - [1433B_MOUSE]
Q3TIP8	Chloride intracellular channel protein OS=Mus musculus GN=Clic1 PE=2 SV=1 - [Q3TIP8_MOUSE]
Q9CX86	Heterogeneous nuclear ribonucleoprotein A0 OS=Mus musculus GN=Hnrnpa0 PE=1 SV=1 - [ROA0_MOUSE]
E9Q0U7	Heat shock protein 105 kDa OS=Mus musculus GN=Hsph1 PE=1 SV=1 - [E9Q0U7_MOUSE]
Q922R8	Protein disulfide-isomerase A6 OS=Mus musculus GN=Pdia6 PE=1 SV=3 - [PDIA6_MOUSE]
P54071	Isocitrate dehydrogenase [NADP], mitochondrial OS=Mus musculus GN=Idh2 PE=1 SV=3 - [IDHP_MOUSE]
Q3TKR5	Putative uncharacterized protein OS=Mus musculus GN=Rpl5 PE=2 SV=1 - [Q3TKR5_MOUSE]
Q9DBJ1	Phosphoglycerate mutase 1 OS=Mus musculus GN=Pgam1 PE=1 SV=3 - [PGAM1_MOUSE]
P0DP27	Calmodulin-2 OS=Mus musculus GN=Calm2 PE=1 SV=1 - [CALM2_MOUSE]
Q3TWN8	Putative uncharacterized protein OS=Mus musculus GN=Aldh18a1 PE=2 SV=1 - [Q3TWN8_MOUSE]
Q91XV3	Brain acid soluble protein 1 OS=Mus musculus GN=Basp1 PE=1 SV=3 - [BASP1_MOUSE]
Q8K173	Col3a1 protein (Fragment) OS=Mus musculus GN=Col3a1 PE=2 SV=1 - [Q8K173_MOUSE]
A0A0J9YUR2	Cytospin-B OS=Mus musculus GN=Specc1 PE=1 SV=1 - [A0A0J9YUR2_MOUSE]

Q5SQB0	Nucleophosmin OS=Mus musculus GN=Npm1 PE=1 SV=1 - [Q5SQB0_MOUSE]
F8VPU2	FERM, RhoGEF and pleckstrin domain-containing protein 1 OS=Mus musculus GN=Farp1 PE=1 SV=1 - [FARP1_MOUSE]
Q3UAG2	6-phosphogluconate dehydrogenase, decarboxylating OS=Mus musculus GN=Pgd PE=2 SV=1 - [Q3UAG2_MOUSE]
A0A0R4J169	Leucine-rich repeat flightless-interacting protein 2 OS=Mus musculus GN=Lrrfip2 PE=1 SV=1 - [A0A0R4J169_MOUSE]
Q3TQY2	Putative uncharacterized protein OS=Mus musculus GN=Dctn4 PE=2 SV=1 - [Q3TQY2_MOUSE]
A0A0J9YTU3	Cytospin-B OS=Mus musculus GN=Specc1 PE=1 SV=1 - [A0A0J9YTU3_MOUSE]
Q3UPL0	Protein transport protein Sec31A OS=Mus musculus GN=Sec31a PE=1 SV=2 - [SC31A_MOUSE]
P05202	Aspartate aminotransferase, mitochondrial OS=Mus musculus GN=Got2 PE=1 SV=1 - [AATM_MOUSE]
E9Q035	Uncharacterized protein OS=Mus musculus GN=Gm20425 PE=4 SV=1 - [E9Q035_MOUSE]
P28352	DNA-(apurinic or apyrimidinic site) lyase OS=Mus musculus GN=Apex1 PE=1 SV=2 - [APEX1_MOUSE]
Q02013	Aquaporin-1 OS=Mus musculus GN=Aqp1 PE=1 SV=3 - [AQP1_MOUSE]
Q3TJ01	tRNA-splicing ligase RtcB homolog OS=Mus musculus GN=Rtcb PE=2 SV=1 - [Q3TJ01_MOUSE]
A0A171KXD3	Protein arginine N-methyltransferase 1 OS=Mus musculus GN=Prmt1 PE=1 SV=1 - [A0A171KXD3_MOUSE]
Q6P5F9	Exportin-1 OS=Mus musculus GN=Xpo1 PE=1 SV=1 - [XPO1_MOUSE]
P67984	60S ribosomal protein L22 OS=Mus musculus GN=Rpl22 PE=1 SV=2 - [RL22_MOUSE]
A0A0J9YTY0	Septin-11 OS=Mus musculus GN=Sept11 PE=1 SV=1 - [A0A0J9YTY0_MOUSE]
Q6ZQE7	MKIAA0270 protein (Fragment) OS=Mus musculus GN=Palm PE=2 SV=1 - [Q6ZQE7_MOUSE]
D3Z0S1	Annexin (Fragment) OS=Mus musculus GN=Anxa4 PE=1 SV=1 - [D3Z0S1_MOUSE]
P32067	Lupus La protein homolog OS=Mus musculus GN=Ssb PE=1 SV=1 - [LA_MOUSE]
Q8BL36	Putative uncharacterized protein OS=Mus musculus GN=Fam98a PE=2 SV=1 - [Q8BL36_MOUSE]
Q80UE5	Epb4.1l2 protein OS=Mus musculus GN=Epb41l2 PE=2 SV=1 - [Q80UE5_MOUSE]
P60122	RuvB-like 1 OS=Mus musculus GN=Ruvbl1 PE=1 SV=1 - [RUVB1_MOUSE]
Q3ULZ3	Phosphoserine aminotransferase OS=Mus musculus GN=Psat1 PE=2 SV=1 - [Q3ULZ3_MOUSE]
O08807	Peroxiredoxin-4 OS=Mus musculus GN=Prdx4 PE=1 SV=1 - [PRDX4_MOUSE]
Q9Z1Z2	Serine-threonine kinase receptor-associated protein OS=Mus musculus GN=Strap PE=1 SV=2 - [STRAP_MOUSE]
O35682	Myeloid-associated differentiation marker OS=Mus musculus GN=Myadm PE=1 SV=2 - [MYADM_MOUSE]
P63330	Serine/threonine-protein phosphatase 2A catalytic subunit alpha isoform OS=Mus musculus GN=Ppp2ca PE=1 SV=1 - [PP2AA_MOUSE]
P63037	DnaJ homolog subfamily A member 1 OS=Mus musculus GN=Dnaja1 PE=1 SV=1 - [DNJA1_MOUSE]
Q3TDD8	Putative uncharacterized protein OS=Mus musculus GN=Eif4b PE=2 SV=1 - [Q3TDD8_MOUSE]
O35295	Transcriptional activator protein Pur-beta OS=Mus musculus GN=Purb PE=1 SV=3 - [PURB_MOUSE]
Q6ZQ58	La-related protein 1 OS=Mus musculus GN=Larp1 PE=1 SV=3 - [LARP1_MOUSE]
A0A0R4J1Y7	Thioredoxin domain-containing protein 5 OS=Mus musculus GN=Txndc5 PE=1 SV=1 - [A0A0R4J1Y7_MOUSE]
Q8BG67	Protein EFR3 homolog A OS=Mus musculus GN=Efr3a PE=1 SV=1 - [EFR3A_MOUSE]
Q3UGJ5	Putative uncharacterized protein OS=Mus musculus GN=Rasa3 PE=2 SV=1 - [Q3UGJ5_MOUSE]
Q3UDS4	Putative uncharacterized protein OS=Mus musculus GN=Sqrdl PE=2 SV=1 - [Q3UDS4_MOUSE]
Q8R010	Aminoacyl tRNA synthase complex-interacting multifunctional protein 2 OS=Mus musculus GN=Aimp2 PE=1 SV=2 - [AIMP2_MOUSE]
A2AW05	FACT complex subunit SSRP1 (Fragment) OS=Mus musculus GN=Ssrp1 PE=1 SV=1 - [A2AW05_MOUSE]
P26043	Radixin OS=Mus musculus GN=Rdx PE=1 SV=3 - [RADI_MOUSE]
Q9DB77	Cytochrome b-c1 complex subunit 2, mitochondrial OS=Mus musculus GN=Uqcrc2 PE=1 SV=1 - [QCR2_MOUSE]
F6QYF8	Aminopeptidase (Fragment) OS=Mus musculus GN=Npepps PE=1 SV=1 - [F6QYF8_MOUSE]
Q3TCL2	Putative uncharacterized protein (Fragment) OS=Mus musculus GN=Akr1b3 PE=2 SV=1 - [Q3TCL2_MOUSE]
Q8BGH2	Sorting and assembly machinery component 50 homolog OS=Mus musculus GN=Samm50 PE=1 SV=1 - [SAM50_MOUSE]

E9PWY9	Phenylalanine--tRNA ligase alpha subunit OS=Mus musculus GN=Farsa PE=1 SV=1 - [E9PWY9_MOUSE]
A0A0J9YUD8	High mobility group protein B1 OS=Mus musculus GN=Hmgb1 PE=1 SV=1 - [A0A0J9YUD8_MOUSE]
P26231	Catenin alpha-1 OS=Mus musculus GN=Ctnna1 PE=1 SV=1 - [CTNA1_MOUSE]
Q921M3	Splicing factor 3B subunit 3 OS=Mus musculus GN=Sf3b3 PE=1 SV=1 - [SF3B3_MOUSE]
P29758	Ornithine aminotransferase, mitochondrial OS=Mus musculus GN=Oat PE=1 SV=1 - [OAT_MOUSE]
P28658	Ataxin-10 OS=Mus musculus GN=Atxn10 PE=1 SV=2 - [ATX10_MOUSE]
Q9D051	Pyruvate dehydrogenase E1 component subunit beta, mitochondrial OS=Mus musculus GN=Pdhb PE=1 SV=1 - [ODPB_MOUSE]
Q3TTX0	Putative uncharacterized protein OS=Mus musculus GN=Matr3 PE=2 SV=1 - [Q3TTX0_MOUSE]
B7ZMP1	Probable Xaa-Pro aminopeptidase 3 OS=Mus musculus GN=Xpnpep3 PE=1 SV=1 - [XPP3_MOUSE]
Q80WJ7	Protein LYRIC OS=Mus musculus GN=Mtdh PE=1 SV=1 - [LYRIC_MOUSE]
Q3TNN6	Putative uncharacterized protein OS=Mus musculus GN=Capg PE=2 SV=1 - [Q3TNN6_MOUSE]
A0A0J9YUN4	Dynamin-1 OS=Mus musculus GN=Dnm1 PE=1 SV=1 - [A0A0J9YUN4_MOUSE]
Q3UK68	Putative uncharacterized protein OS=Mus musculus GN=Naca PE=2 SV=1 - [Q3UK68_MOUSE]
Q641N8	Nedd4l protein (Fragment) OS=Mus musculus GN=Nedd4l PE=2 SV=1 - [Q641N8_MOUSE]
A0A0H3XWX3	Insulin-like growth factor 2 mRNA binding protein 1 dN CRDBP-2 OS=Mus musculus GN=Igf2bp1 PE=2 SV=1 - [A0A0H3XWX3_MOUSE]
Q3TYZ4	Putative uncharacterized protein (Fragment) OS=Mus musculus GN=Arhgef2 PE=2 SV=1 - [Q3TYZ4_MOUSE]
P26443	Glutamate dehydrogenase 1, mitochondrial OS=Mus musculus GN=Glud1 PE=1 SV=1 - [DHE3_MOUSE]
Z4YKV1	Guanine nucleotide-binding protein G(s) subunit alpha isoforms short OS=Mus musculus GN=Gnas PE=1 SV=1 - [Z4YKV1_MOUSE]
A0A0A0MQF1	Kalirin OS=Mus musculus GN=Kalrn PE=1 SV=1 - [A0A0A0MQF1_MOUSE]
Q9QZD9	Eukaryotic translation initiation factor 3 subunit I OS=Mus musculus GN=Eif3i PE=1 SV=1 - [EIF3I_MOUSE]
Q8BR76	Meckelin OS=Mus musculus GN=Tmem67 PE=1 SV=2 - [MKS3_MOUSE]
Q3V2Z4	Annexin OS=Mus musculus PE=2 SV=1 - [Q3V2Z4_MOUSE]
Q922Z3	Trap1 protein (Fragment) OS=Mus musculus GN=Trap1 PE=2 SV=1 - [Q922Z3_MOUSE]
P49718	DNA replication licensing factor MCM5 OS=Mus musculus GN=Mcm5 PE=1 SV=1 - [MCM5_MOUSE]
H7BWZ3	Actin-related protein 2/3 complex subunit 3 OS=Mus musculus GN=Arpc3 PE=1 SV=1 - [H7BWZ3_MOUSE]
H7BX23	Prolyl 4-hydroxylase subunit alpha-3 OS=Mus musculus GN=P4ha3 PE=1 SV=1 - [H7BX23_MOUSE]
Q9QWJ3	Alpha-1-globin (Fragment) OS=Mus musculus PE=2 SV=1 - [Q9QWJ3_MOUSE]
P60335	Poly(rC)-binding protein 1 OS=Mus musculus GN=Pcbp1 PE=1 SV=1 - [PCBP1_MOUSE]
Q9DCW4	Electron transfer flavoprotein subunit beta OS=Mus musculus GN=Etfb PE=1 SV=3 - [ETFB_MOUSE]
O35326	Serine/arginine-rich splicing factor 5 OS=Mus musculus GN=Srsf5 PE=1 SV=2 - [SRSF5_MOUSE]
O89086	RNA-binding protein 3 OS=Mus musculus GN=Rbm3 PE=1 SV=1 - [RBM3_MOUSE]
Q3TW74	Putative uncharacterized protein OS=Mus musculus GN=Mthfd1 PE=2 SV=1 - [Q3TW74_MOUSE]
Q7TMI0	Psmd11 protein (Fragment) OS=Mus musculus GN=Psmd11 PE=2 SV=1 - [Q7TMI0_MOUSE]
Q00612	Glucose-6-phosphate 1-dehydrogenase X OS=Mus musculus GN=G6pdx PE=1 SV=3 - [G6PD1_MOUSE]
Q3U026	Putative uncharacterized protein OS=Mus musculus GN=Mogs PE=2 SV=1 - [Q3U026_MOUSE]
O70251	Elongation factor 1-beta OS=Mus musculus GN=Eef1b PE=1 SV=5 - [EF1B_MOUSE]
A0A0N4SVP8	Predicted pseudogene 5580 OS=Mus musculus GN=Gm5580 PE=3 SV=1 - [A0A0N4SVP8_MOUSE]
P46471	26S protease regulatory subunit 7 OS=Mus musculus GN=Psmc2 PE=1 SV=5 - [PRS7_MOUSE]
Q9WUM5	Succinate--CoA ligase [ADP/GDP-forming] subunit alpha, mitochondrial OS=Mus musculus GN=Suclg1 PE=1 SV=4 - [SUCA_MOUSE]
K9JA74	Glutathione S-transferase pi 2 (Fragment) OS=Mus musculus GN=Gstp2 PE=2 SV=1 - [K9JA74_MOUSE]
P51655	Glypican-4 OS=Mus musculus GN=Gpc4 PE=1 SV=2 - [GPC4_MOUSE]
Q9CZU6	Citrate synthase, mitochondrial OS=Mus musculus GN=Cs PE=1 SV=1 - [CISY_MOUSE]

F6ZV59	Heterogeneous nuclear ribonucleoprotein D0 (Fragment) OS=Mus musculus GN=Hnrnpd PE=1 SV=1 - [F6ZV59_MOUSE]
A0A0A6YXZ1	CLIP-associating protein 1 OS=Mus musculus GN=Clasp1 PE=1 SV=2 - [A0A0A6YXZ1_MOUSE]
Q3UEB3	Poly(U)-binding-splicing factor PUF60 OS=Mus musculus GN=Puf60 PE=1 SV=2 - [PUF60_MOUSE]
Q3TXF9	Sodium/potassium-transporting ATPase subunit alpha OS=Mus musculus GN=Atp1a1 PE=2 SV=1 - [Q3TXF9_MOUSE]
Q78ZA7	Nucleosome assembly protein 1-like 4 OS=Mus musculus GN=Nap1l4 PE=1 SV=1 - [NP1L4_MOUSE]
P35486	Pyruvate dehydrogenase E1 component subunit alpha, somatic form, mitochondrial OS=Mus musculus GN=Pdha1 PE=1 SV=1 - [ODPA_MOUSE]
Q8K335	Glutamate-rich WD repeat containing 1 OS=Mus musculus GN=Grwd1 PE=2 SV=1 - [Q8K335_MOUSE]
P50247	Adenosylhomocysteinase OS=Mus musculus GN=Ahcy PE=1 SV=3 - [SAHH_MOUSE]
Q8BUM1	Putative uncharacterized protein OS=Mus musculus GN=Tardbp PE=2 SV=1 - [Q8BUM1_MOUSE]
P10605	Cathepsin B OS=Mus musculus GN=Ctsb PE=1 SV=2 - [CATB_MOUSE]
Q7TN20	Ythdf3 protein (Fragment) OS=Mus musculus GN=Ythdf3 PE=2 SV=1 - [Q7TN20_MOUSE]
Q8R5L1	Complement component 1 Q subcomponent-binding protein, mitochondrial OS=Mus musculus GN=C1qbp PE=1 SV=1 - [Q8R5L1_MOUSE]
D3Z3E8	Putative helicase MOV-10 OS=Mus musculus GN=Mov10 PE=1 SV=1 - [D3Z3E8_MOUSE]
Q6ZPF4	Formin-like protein 3 OS=Mus musculus GN=Fmnl3 PE=1 SV=2 - [FMNL3_MOUSE]
Q8R2X0	Ehd2 protein OS=Mus musculus GN=Ehd2 PE=2 SV=1 - [Q8R2X0_MOUSE]
Q9CYL5	Golgi-associated plant pathogenesis-related protein 1 OS=Mus musculus GN=Glipr2 PE=1 SV=3 - [GAPR1_MOUSE]
A0A0A6YY29	Calcyclin-binding protein (Fragment) OS=Mus musculus GN=Cacybp PE=1 SV=1 - [A0A0A6YY29_MOUSE]
Q1L6K5	Apoptosis-inducing factor short isoform 2 OS=Mus musculus GN=Aifm1 PE=2 SV=1 - [Q1L6K5_MOUSE]
Q99MR6	Serrate RNA effector molecule homolog OS=Mus musculus GN=Srrt PE=1 SV=1 - [SRRT_MOUSE]
Q9CPY7	Cytosol aminopeptidase OS=Mus musculus GN=Lap3 PE=1 SV=3 - [AMPL_MOUSE]
P61027	Ras-related protein Rab-10 OS=Mus musculus GN=Rab10 PE=1 SV=1 - [RAB10_MOUSE]
E9QAT0	Synaptic functional regulator FMR1 OS=Mus musculus GN=Fmr1 PE=1 SV=1 - [E9QAT0_MOUSE]
Q9D4P2	Putative uncharacterized protein OS=Mus musculus GN=Spag16 PE=2 SV=1 - [Q9D4P2_MOUSE]
A0A067XG53	Peripheral plasma membrane protein CASK (Fragment) OS=Mus musculus GN=Cask PE=1 SV=1 - [A0A067XG53_MOUSE]
Q3UDN8	Putative uncharacterized protein (Fragment) OS=Mus musculus GN=Trim28 PE=2 SV=1 - [Q3UDN8_MOUSE]
Q7TT37	Elongator complex protein 1 OS=Mus musculus GN=Ikbkap PE=1 SV=2 - [ELP1_MOUSE]
Q9ERK4	Exportin-2 OS=Mus musculus GN=Cse1l PE=1 SV=1 - [XPO2_MOUSE]
P51660	Peroxisomal multifunctional enzyme type 2 OS=Mus musculus GN=Hsd17b4 PE=1 SV=3 - [DHB4_MOUSE]
Q6IRT4	Eukaryotic translation initiation factor 3 subunit F OS=Mus musculus GN=Eif3f PE=2 SV=1 - [Q6IRT4_MOUSE]
Q9WUM3	Coronin-1B OS=Mus musculus GN=Coro1b PE=1 SV=1 - [COR1B_MOUSE]
F8VQB6	Unconventional myosin-X OS=Mus musculus GN=Myo10 PE=1 SV=1 - [MYO10_MOUSE]
P24547	Inosine-5'-monophosphate dehydrogenase 2 OS=Mus musculus GN=Impdh2 PE=1 SV=2 - [IMDH2_MOUSE]
Q9CRS5	Putative uncharacterized protein (Fragment) OS=Mus musculus GN=Ewsr1 PE=2 SV=1 - [Q9CRS5_MOUSE]
G3UYU4	Flotillin-1 OS=Mus musculus GN=Flot1 PE=1 SV=1 - [G3UYU4_MOUSE]
Q9CT37	Putative uncharacterized protein (Fragment) OS=Mus musculus GN=Hnrnpr PE=2 SV=3 - [Q9CT37_MOUSE]
Q3THA0	Eukaryotic translation initiation factor 3 subunit G OS=Mus musculus GN=Eif3g PE=2 SV=1 - [Q3THA0_MOUSE]
Q3TWV4	AP-2 complex subunit mu OS=Mus musculus GN=Ap2m1 PE=1 SV=1 - [Q3TWV4_MOUSE]
E9PYT3	Atlastin-3 OS=Mus musculus GN=Atl3 PE=1 SV=1 - [E9PYT3_MOUSE]
Q8VHY0	Chondroitin sulfate proteoglycan 4 OS=Mus musculus GN=Cspg4 PE=1 SV=3 - [CSPG4_MOUSE]
Q3U890	Putative uncharacterized protein OS=Mus musculus GN=Hars PE=2 SV=1 - [Q3U890_MOUSE]
C6EQH3	Succinate--CoA ligase [GDP-forming] subunit beta, mitochondrial OS=Mus musculus GN=Suclg2 PE=2 SV=1 - [C6EQH3_MOUSE]

P01027	Complement C3 OS=Mus musculus GN=C3 PE=1 SV=3 - [CO3_MOUSE]
E9Q740	Signal recognition particle 72 OS=Mus musculus GN=Srp72 PE=1 SV=1 - [E9Q740_MOUSE]
A0A0G2JG59	Nexilin (Fragment) OS=Mus musculus GN=Nexn PE=1 SV=1 - [A0A0G2JG59_MOUSE]
Q9D0F3	Protein ERGIC-53 OS=Mus musculus GN=Lman1 PE=1 SV=1 - [LMAN1_MOUSE]
P49817	Caveolin-1 OS=Mus musculus GN=Cav1 PE=1 SV=1 - [CAV1_MOUSE]
O35646	Calpain-6 OS=Mus musculus GN=Capn6 PE=1 SV=2 - [CAN6_MOUSE]
Q3U1H7	Sorting nexin OS=Mus musculus GN=Snx18 PE=2 SV=1 - [Q3U1H7_MOUSE]
Q3U8N2	Putative uncharacterized protein (Fragment) OS=Mus musculus GN=Gas7 PE=2 SV=1 - [Q3U8N2_MOUSE]
E9QL13	MCG8382, isoform CRA_c OS=Mus musculus GN=Rbm14 PE=1 SV=2 - [E9QL13_MOUSE]
O08842	GDNF family receptor alpha-2 OS=Mus musculus GN=Gfra2 PE=1 SV=2 - [GFRA2_MOUSE]
B1ARU1	Microtubule-actin cross-linking factor 1 OS=Mus musculus GN=Macf1 PE=1 SV=1 - [B1ARU1_MOUSE]
Q3TD51	Putative uncharacterized protein OS=Mus musculus GN=Picalm PE=2 SV=1 - [Q3TD51_MOUSE]
S4R238	MICOS complex subunit OS=Mus musculus GN=Chchd3 PE=1 SV=1 - [S4R238_MOUSE]
Q3UT02	Putative uncharacterized protein OS=Mus musculus GN=Larp4 PE=2 SV=1 - [Q3UT02_MOUSE]
Q99JY0	Trifunctional enzyme subunit beta, mitochondrial OS=Mus musculus GN=Hadhb PE=1 SV=1 - [ECHB_MOUSE]
A0A0R4J083	Long-chain-specific acyl-CoA dehydrogenase, mitochondrial OS=Mus musculus GN=Acadl PE=1 SV=1 - [A0A0R4J083_MOUSE]
Q0VGU9	Rbm39 protein OS=Mus musculus GN=Rbm39 PE=2 SV=1 - [Q0VGU9_MOUSE]
Q3TUI9	Proteasome subunit alpha type OS=Mus musculus GN=Psma5 PE=2 SV=1 - [Q3TUI9_MOUSE]
Q6PHN9	Ras-related protein Rab-35 OS=Mus musculus GN=Rab35 PE=1 SV=1 - [RAB35_MOUSE]
Q3TN31	Proteasome subunit alpha type OS=Mus musculus GN=Psma7 PE=2 SV=1 - [Q3TN31_MOUSE]
Q04736	Tyrosine-protein kinase Yes OS=Mus musculus GN=Yes1 PE=1 SV=3 - [YES_MOUSE]
Q61599	Rho GDP-dissociation inhibitor 2 OS=Mus musculus GN=Arhgdib PE=1 SV=3 - [GDIR2_MOUSE]
Q5SX49	Profilin OS=Mus musculus GN=Pfn1 PE=1 SV=1 - [Q5SX49_MOUSE]
Q62418	Drebrin-like protein OS=Mus musculus GN=Dbnl PE=1 SV=2 - [DBNL_MOUSE]
E0CXA0	Hepatoma-derived growth factor (Fragment) OS=Mus musculus GN=Hdgf PE=1 SV=1 - [E0CXA0_MOUSE]
Q3V3R1	Monofunctional C1-tetrahydrofolate synthase, mitochondrial OS=Mus musculus GN=Mthfd1l PE=1 SV=2 - [C1TM_MOUSE]
Q3TYK3	Nuclear factor 1 OS=Mus musculus GN=Nfix PE=1 SV=1 - [Q3TYK3_MOUSE]
Q8K258	Srp68 protein OS=Mus musculus GN=Srp68 PE=2 SV=1 - [Q8K258_MOUSE]
Q571A1	MKIAA0765 splice variant 1 (Fragment) OS=Mus musculus GN=Cpne1 PE=2 SV=1 - [Q571A1_MOUSE]
Q9D2G2	Dihydrolipoyllysine-residue succinyltransferase component of 2-oxoglutarate dehydrogenase complex, mitochondrial OS=Mus musculus GN=Dlst PE=1 SV=1 - [ODO2_MOUSE]
P61164	Alpha-centractin OS=Mus musculus GN=Actr1a PE=1 SV=1 - [ACTZ_MOUSE]
Q8BWT1	3-ketoacyl-CoA thiolase, mitochondrial OS=Mus musculus GN=Acaa2 PE=1 SV=3 - [THIM_MOUSE]
Q8R539	WD-repeat protein p122 OS=Mus musculus GN=Wdr6 PE=2 SV=1 - [Q8R539_MOUSE]
Q3UNJ3	Peptidylprolyl isomerase OS=Mus musculus GN=Fkbp10 PE=2 SV=1 - [Q3UNJ3_MOUSE]
Q6PGC1	ATP-dependent RNA helicase DHX29 OS=Mus musculus GN=Dhx29 PE=1 SV=1 - [DHX29_MOUSE]
L0HCN1	Ifi202b OS=Mus musculus PE=2 SV=1 - [L0HCN1_MOUSE]
G3XA25	Acetyl-CoA acetyltransferase, cytosolic OS=Mus musculus GN=Acat2 PE=1 SV=1 - [G3XA25_MOUSE]
Q3TFC2	Putative uncharacterized protein OS=Mus musculus GN=Nono PE=2 SV=1 - [Q3TFC2_MOUSE]
Q3TLE8	Putative uncharacterized protein OS=Mus musculus GN=Cyb5b PE=2 SV=1 - [Q3TLE8_MOUSE]
P27641	X-ray repair cross-complementing protein 5 OS=Mus musculus GN=Xrcc5 PE=1 SV=4 - [XRCC5_MOUSE]
A0A068BFR3	RAS oncogene family protein OS=Mus musculus GN=Rab11b PE=2 SV=1 - [A0A068BFR3_MOUSE]
Q8BSI4	Putative uncharacterized protein OS=Mus musculus GN=Gpc6 PE=2 SV=1 - [Q8BSI4_MOUSE]

B7ZWM8	Leucine-rich repeat and calponin homology domain-containing protein 3 OS=Mus musculus GN=Lrch3 PE=1 SV=1 - [B7ZWM8_MOUSE]
A0A0G2JDW7	40S ribosomal protein S27 (Fragment) OS=Mus musculus GN=Rps27 PE=1 SV=1 - [A0A0G2JDW7_MOUSE]
Q3ULG5	DNA helicase OS=Mus musculus GN=Mcm6 PE=1 SV=1 - [Q3ULG5_MOUSE]
A0A0N4SW34	V-type proton ATPase subunit E 1 (Fragment) OS=Mus musculus GN=Atp6v1e1 PE=1 SV=1 - [A0A0N4SW34_MOUSE]
E9Q715	Putative RNA-binding protein Luc7-like 2 OS=Mus musculus GN=Luc7l2 PE=1 SV=1 - [E9Q715_MOUSE]
B2RQQ7	CDC42 binding protein kinase beta OS=Mus musculus GN=Cdc42bpb PE=2 SV=1 - [B2RQQ7_MOUSE]
Q9CQE8	UPF0568 protein C14orf166 homolog OS=Mus musculus PE=1 SV=1 - [CN166_MOUSE]
A2BE93	Protein SET (Fragment) OS=Mus musculus GN=Set PE=1 SV=1 - [A2BE93_MOUSE]
E0CXB1	Proteasome endopeptidase complex OS=Mus musculus GN=Psma6 PE=1 SV=1 - [E0CXB1_MOUSE]
Q9D7S7	60S ribosomal protein L22-like 1 OS=Mus musculus GN=Rpl22l1 PE=1 SV=1 - [RL22L_MOUSE]
Q8CGI9	Psmd1 protein (Fragment) OS=Mus musculus GN=Psmd1 PE=2 SV=1 - [Q8CGI9_MOUSE]
O70194	Eukaryotic translation initiation factor 3 subunit D OS=Mus musculus GN=Eif3d PE=1 SV=2 - [EIF3D_MOUSE]
G3X909	Slit homolog 2 protein OS=Mus musculus GN=Slit2 PE=1 SV=1 - [G3X909_MOUSE]
A2AFI9	Histone-binding protein RBBP7 OS=Mus musculus GN=Rbbp7 PE=1 SV=1 - [A2AFI9_MOUSE]
B1AQR8	Galectin OS=Mus musculus GN=Lgals9 PE=1 SV=1 - [B1AQR8_MOUSE]
G5E829	Plasma membrane calcium-transporting ATPase 1 OS=Mus musculus GN=Atp2b1 PE=1 SV=1 - [AT2B1_MOUSE]
Q99JI4	26S proteasome non-ATPase regulatory subunit 6 OS=Mus musculus GN=Psmd6 PE=1 SV=1 - [PSMD6_MOUSE]
E9QL12	Dysferlin OS=Mus musculus GN=Dysf PE=1 SV=1 - [E9QL12_MOUSE]
S4R294	Protein PRRC2C OS=Mus musculus GN=Prrc2c PE=1 SV=1 - [S4R294_MOUSE]
Q9CRL8	Putative uncharacterized protein (Fragment) OS=Mus musculus GN=Gm10817 PE=2 SV=1 - [Q9CRL8_MOUSE]
K7Q751	Focal ashension kinase 1 OS=Mus musculus GN=Ptk2 PE=2 SV=1 - [K7Q751_MOUSE]
O08583	THO complex subunit 4 OS=Mus musculus GN=Alyref PE=1 SV=3 - [THOC4_MOUSE]
B8JJM3	Complement factor B (Fragment) OS=Mus musculus GN=Cfb PE=3 SV=1 - [B8JJM3_MOUSE]
Q9WVJ2	26S proteasome non-ATPase regulatory subunit 13 OS=Mus musculus GN=Psmd13 PE=1 SV=1 - [PSD13_MOUSE]
Q5SUW3	Growth factor receptor-bound protein 10 OS=Mus musculus GN=Grb10 PE=1 SV=1 - [Q5SUW3_MOUSE]
Q8BH80	Putative uncharacterized protein OS=Mus musculus GN=Vapb PE=1 SV=1 - [Q8BH80_MOUSE]
D3Z7K0	Ubiquitin thioesterase OTUB1 (Fragment) OS=Mus musculus GN=Otub1 PE=1 SV=1 - [D3Z7K0_MOUSE]
Q3US65	Putative uncharacterized protein (Fragment) OS=Mus musculus GN=Srpk1 PE=2 SV=1 - [Q3US65_MOUSE]
P97807	Fumarate hydratase, mitochondrial OS=Mus musculus GN=Fh PE=1 SV=3 - [FUMH_MOUSE]
A0A0R4J119	Cytoplasmic FMR1-interacting protein 1 OS=Mus musculus GN=Cyfip1 PE=1 SV=1 - [A0A0R4J119_MOUSE]
Q64339	Ubiquitin-like protein ISG15 OS=Mus musculus GN=Isg15 PE=1 SV=4 - [ISG15_MOUSE]
Q4VAA7	Sorting nexin-33 OS=Mus musculus GN=Snx33 PE=1 SV=1 - [SNX33_MOUSE]
B1AU76	Nuclear autoantigenic sperm protein OS=Mus musculus GN=Nasp PE=1 SV=1 - [B1AU76_MOUSE]
B1AZ26	Cordon-bleu protein-like 1 (Fragment) OS=Mus musculus GN=Cobll1 PE=1 SV=8 - [B1AZ26_MOUSE]
P55012	Solute carrier family 12 member 2 OS=Mus musculus GN=Slc12a2 PE=1 SV=2 - [S12A2_MOUSE]
P62965	Cellular retinoic acid-binding protein 1 OS=Mus musculus GN=Crabp1 PE=1 SV=2 - [RABP1_MOUSE]
Q9D1R9	60S ribosomal protein L34 OS=Mus musculus GN=Rpl34 PE=1 SV=2 - [RL34_MOUSE]
Q9R1P1	Proteasome subunit beta type-3 OS=Mus musculus GN=Psmb3 PE=1 SV=1 - [PSB3_MOUSE]
Q8C1L7	40S ribosomal protein S21 OS=Mus musculus GN=mCG_6739 PE=2 SV=1 - [Q8C1L7_MOUSE]
A0A0N4SVT3	Guanine nucleotide-binding protein subunit gamma (Fragment) OS=Mus musculus GN=Gng12 PE=1 SV=1 - [A0A0N4SVT3_MOUSE]
Q99KR1	Psmc5 protein (Fragment) OS=Mus musculus GN=Psmc5 PE=2 SV=1 - [Q99KR1_MOUSE]

P09671	Superoxide dismutase [Mn], mitochondrial OS=Mus musculus GN=Sod2 PE=1 SV=3 - [SODM_MOUSE]
P42125	Enoyl-CoA delta isomerase 1, mitochondrial OS=Mus musculus GN=Eci1 PE=1 SV=2 - [ECI1_MOUSE]
P30412	Peptidyl-prolyl cis-trans isomerase C OS=Mus musculus GN=Ppic PE=1 SV=1 - [PPIC_MOUSE]
D3Z0E7	Rabenosyn-5 (Fragment) OS=Mus musculus GN=Rbsn PE=1 SV=1 - [D3Z0E7_MOUSE]
Q3TJA9	DnaJ (Hsp40) homolog, subfamily A, member 3, isoform CRA_b OS=Mus musculus GN=Dnaja3 PE=2 SV=1 - [Q3TJA9_MOUSE]
F6U8X4	Serine/threonine-protein kinase SIK3 (Fragment) OS=Mus musculus GN=Sik3 PE=1 SV=1 - [F6U8X4_MOUSE]
P32233	Developmentally-regulated GTP-binding protein 1 OS=Mus musculus GN=Drg1 PE=1 SV=1 - [DRG1_MOUSE]
Q3U6K8	Putative uncharacterized protein OS=Mus musculus GN=Vdac1 PE=2 SV=1 - [Q3U6K8_MOUSE]
Q8BGU5	Cyclin-Y OS=Mus musculus GN=Ccny PE=1 SV=1 - [CCNY_MOUSE]
Q3UJW1	Putative uncharacterized protein OS=Mus musculus GN=Aldh2 PE=2 SV=1 - [Q3UJW1_MOUSE]
Q5SX46	Mitochondrial 2-oxoglutarate/malate carrier protein (Fragment) OS=Mus musculus GN=Slc25a11 PE=1 SV=1 - [Q5SX46_MOUSE]
Q9CW59	Putative uncharacterized protein (Fragment) OS=Mus musculus GN=Aox3 PE=2 SV=1 - [Q9CW59_MOUSE]
F6USD5	Mesencephalic astrocyte-derived neurotrophic factor (Fragment) OS=Mus musculus GN=Manf PE=1 SV=1 - [F6USD5_MOUSE]
Q6PB52	Lrpap1 protein (Fragment) OS=Mus musculus GN=Lrpap1 PE=2 SV=1 - [Q6PB52_MOUSE]
P54923	[Protein ADP-ribosylarginine] hydrolase OS=Mus musculus GN=Adprh PE=1 SV=1 - [ADPRH_MOUSE]
Q3UAZ7	Putative uncharacterized protein (Fragment) OS=Mus musculus GN=Hmgb2 PE=2 SV=1 - [Q3UAZ7_MOUSE]
Q9D0M3	Cytochrome c1, heme protein, mitochondrial OS=Mus musculus GN=Cyc1 PE=1 SV=1 - [CY1_MOUSE]
Q3UXI9	Putative uncharacterized protein OS=Mus musculus GN=Ilf2 PE=2 SV=1 - [Q3UXI9_MOUSE]
Q8R2Q8	Bone marrow stromal antigen 2 OS=Mus musculus GN=Bst2 PE=1 SV=1 - [BST2_MOUSE]
O08614	Cytoskeletal protein OS=Mus musculus GN=Utrn PE=2 SV=1 - [O08614_MOUSE]
P68181	cAMP-dependent protein kinase catalytic subunit beta OS=Mus musculus GN=Prkacb PE=1 SV=2 - [KAPCB_MOUSE]
F8WI90	Tyrosine-protein kinase OS=Mus musculus GN=Src PE=1 SV=1 - [F8WI90_MOUSE]
P62315	Small nuclear ribonucleoprotein Sm D1 OS=Mus musculus GN=Snrpd1 PE=1 SV=1 - [SMD1_MOUSE]
A0A1B0GS13	Apoptosis regulator BAX (Fragment) OS=Mus musculus GN=Bax PE=1 SV=1 - [A0A1B0GS13_MOUSE]
P42669	Transcriptional activator protein Pur-alpha OS=Mus musculus GN=Pura PE=1 SV=1 - [PURA_MOUSE]
Q8HW98	IgLON family member 5 OS=Mus musculus GN=Iglon5 PE=2 SV=2 - [IGLO5_MOUSE]
Q3KQQ1	Nsfl1c protein (Fragment) OS=Mus musculus GN=Nsfl1c PE=2 SV=1 - [Q3KQQ1_MOUSE]
Q05CM5	Eif5 protein (Fragment) OS=Mus musculus GN=Eif5 PE=2 SV=1 - [Q05CM5_MOUSE]
Q3TCX4	Putative uncharacterized protein OS=Mus musculus GN=Zfp622 PE=2 SV=1 - [Q3TCX4_MOUSE]
E9PZJ8	Activating signal cointegrator 1 complex subunit 3 OS=Mus musculus GN=Ascc3 PE=1 SV=1 - [ASCC3_MOUSE]
A0A1D5RLE4	Casein kinase II subunit alpha' (Fragment) OS=Mus musculus GN=Csnk2a2 PE=1 SV=1 - [A0A1D5RLE4_MOUSE]
Q3U3L3	Putative uncharacterized protein OS=Mus musculus GN=Serpinb6a PE=2 SV=1 - [Q3U3L3_MOUSE]
Q9Z2I0	LETM1 and EF-hand domain-containing protein 1, mitochondrial OS=Mus musculus GN=Letm1 PE=1 SV=1 - [LETM1_MOUSE]
Q5SS83	Flotillin 2, isoform CRA_a OS=Mus musculus GN=Flot2 PE=1 SV=1 - [Q5SS83_MOUSE]
Q61081	Hsp90 co-chaperone Cdc37 OS=Mus musculus GN=Cdc37 PE=1 SV=1 - [CDC37_MOUSE]
Q3TPM3	Cullin-1 (Fragment) OS=Mus musculus GN=Cul1 PE=1 SV=1 - [Q3TPM3_MOUSE]
Q5SWD9	Pre-rRNA-processing protein TSR1 homolog OS=Mus musculus GN=Tsr1 PE=1 SV=1 - [TSR1_MOUSE]
A0JLR3	Dhx36 protein (Fragment) OS=Mus musculus GN=Dhx36 PE=2 SV=1 - [A0JLR3_MOUSE]
P28660	Nck-associated protein 1 OS=Mus musculus GN=Nckap1 PE=1 SV=2 - [NCKP1_MOUSE]
A0A1D5RLW4	Unconventional myosin-IXb (Fragment) OS=Mus musculus GN=Myo9b PE=1 SV=1 - [A0A1D5RLW4_MOUSE]

Q543N4	Putative uncharacterized protein OS=Mus musculus GN=Bysl PE=2 SV=1 - [Q543N4_MOUSE]
A2ARI4	Leucine-rich repeat-containing G-protein coupled receptor 4 OS=Mus musculus GN=Lgr4 PE=1 SV=1 - [LGR4_MOUSE]
Q6P4T2	U5 small nuclear ribonucleoprotein 200 kDa helicase OS=Mus musculus GN=Snrnp200 PE=1 SV=1 - [U520_MOUSE]
Q61425	Hydroxyacyl-coenzyme A dehydrogenase, mitochondrial OS=Mus musculus GN=Hadh PE=1 SV=2 - [HCDH_MOUSE]
P23949	mRNA decay activator protein ZFP36L2 OS=Mus musculus GN=Zfp36l2 PE=1 SV=2 - [TISD_MOUSE]
P51863	V-type proton ATPase subunit d 1 OS=Mus musculus GN=Atp6v0d1 PE=1 SV=2 - [VA0D1_MOUSE]
P21981	Protein-glutamine gamma-glutamyltransferase 2 OS=Mus musculus GN=Tgm2 PE=1 SV=4 - [TGM2_MOUSE]
Q9DBS1	Transmembrane protein 43 OS=Mus musculus GN=Tmem43 PE=1 SV=1 - [TMM43_MOUSE]
Q8R2U0	Nucleoporin SEH1 OS=Mus musculus GN=Seh1l PE=2 SV=1 - [SEH1_MOUSE]
Q3TLT9	Putative uncharacterized protein OS=Mus musculus GN=Cd44 PE=2 SV=1 - [Q3TLT9_MOUSE]
B1AQG7	Zinc finger protein 207 (Fragment) OS=Mus musculus GN=Zfp207 PE=1 SV=1 - [B1AQG7_MOUSE]
Q05BC6	Sucla2 protein OS=Mus musculus GN=Sucla2 PE=2 SV=1 - [Q05BC6_MOUSE]
O08582	GTP-binding protein 1 OS=Mus musculus GN=Gtpbp1 PE=1 SV=2 - [GTPB1_MOUSE]
Q6P5D8	Structural maintenance of chromosomes flexible hinge domain-containing protein 1 OS=Mus musculus GN=Smchd1 PE=1 SV=2 - [SMHD1_MOUSE]
P50136	2-oxoisovalerate dehydrogenase subunit alpha, mitochondrial OS=Mus musculus GN=Bckdha PE=1 SV=1 - [ODBA_MOUSE]
Q4G0C2	Prss3 protein (Fragment) OS=Mus musculus GN=Prss3 PE=2 SV=1 - [Q4G0C2_MOUSE]
F7ALS6	Aspartate aminotransferase, cytoplasmic (Fragment) OS=Mus musculus GN=Got1 PE=1 SV=1 - [F7ALS6_MOUSE]
Q3UZD8	Putative uncharacterized protein OS=Mus musculus GN=Rangap1 PE=2 SV=1 - [Q3UZD8_MOUSE]
B7ZNW0	Pgam5 protein OS=Mus musculus GN=Pgam5 PE=2 SV=1 - [B7ZNW0_MOUSE]
E9Q7G6	RNA-binding motif, single-stranded-interacting protein 2 OS=Mus musculus GN=Rbms2 PE=1 SV=1 - [E9Q7G6_MOUSE]
O35648	Centrin-3 OS=Mus musculus GN=Cetn3 PE=1 SV=1 - [CETN3_MOUSE]
Q9DCL1	Putative uncharacterized protein OS=Mus musculus GN=Dhrs4 PE=2 SV=1 - [Q9DCL1_MOUSE]
Q9WTX2	Interferon-inducible double-stranded RNA-dependent protein kinase activator A OS=Mus musculus GN=Prkra PE=1 SV=1 - [PRKRA_MOUSE]
F7D909	Paraspeckle component 1 (Fragment) OS=Mus musculus GN=Pspc1 PE=1 SV=1 - [F7D909_MOUSE]
P04925	Major prion protein OS=Mus musculus GN=Prnp PE=1 SV=2 - [PRIO_MOUSE]
Q9EPK2	Protein XRP2 OS=Mus musculus GN=Rp2 PE=1 SV=3 - [XRP2_MOUSE]
Q80TP6	MKIAA0890 protein (Fragment) OS=Mus musculus GN=mKIAA0890 PE=4 SV=3 - [Q80TP6_MOUSE]
O08604	Retinoic acid early-inducible protein 1-gamma OS=Mus musculus GN=Raet1c PE=1 SV=1 - [RAE1C_MOUSE]
Q9D832	DnaJ homolog subfamily B member 4 OS=Mus musculus GN=Dnajb4 PE=1 SV=1 - [DNJB4_MOUSE]
Q64669	NAD(P)H dehydrogenase [quinone] 1 OS=Mus musculus GN=Nqo1 PE=1 SV=3 - [NQO1_MOUSE]
D3Z3B8	Disks large homolog 1 OS=Mus musculus GN=Dlg1 PE=1 SV=1 - [D3Z3B8_MOUSE]
B8JJI9	COUP transcription factor 1 OS=Mus musculus GN=Nr2f1 PE=1 SV=1 - [B8JJI9_MOUSE]
Q8K354	Carbonyl reductase [NADPH] 3 OS=Mus musculus GN=Cbr3 PE=1 SV=1 - [CBR3_MOUSE]
A0A0A6YVU8	MCG119397 OS=Mus musculus GN=Gm9774 PE=4 SV=1 - [A0A0A6YVU8_MOUSE]
Q9CY29	Putative uncharacterized protein OS=Mus musculus GN=Psmd4 PE=2 SV=1 - [Q9CY29_MOUSE]
G3UXY0	Proteasome activator complex subunit 1 OS=Mus musculus GN=Psme1 PE=1 SV=1 - [G3UXY0_MOUSE]
Q91VA7	Isocitrate dehydrogenase [NAD] subunit, mitochondrial OS=Mus musculus GN=Idh3b PE=1 SV=1 - [Q91VA7_MOUSE]
A0A0R4J0C8	3'-5' exoribonuclease 1 OS=Mus musculus GN=Eri1 PE=1 SV=1 - [A0A0R4J0C8_MOUSE]
Q8C3X8	Lipase maturation factor 2 OS=Mus musculus GN=Lmf2 PE=1 SV=1 - [LMF2_MOUSE]
Q9CSF9	Putative uncharacterized protein (Fragment) OS=Mus musculus GN=Rsl1d1 PE=2 SV=1 - [Q9CSF9_MOUSE]
D3Z1B9	V-type proton ATPase catalytic subunit A (Fragment) OS=Mus musculus GN=Atp6v1a PE=1 SV=1 - [D3Z1B9_MOUSE]

P57784	U2 small nuclear ribonucleoprotein A' OS=Mus musculus GN=Snrpa1 PE=1 SV=2 - [RU2A_MOUSE]
E9Q9H2	DnaJ homolog subfamily C member 2 OS=Mus musculus GN=Dnajc2 PE=1 SV=1 - [E9Q9H2_MOUSE]
Q8R1H1	Nrd1 protein (Fragment) OS=Mus musculus GN=Nrd1 PE=2 SV=1 - [Q8R1H1_MOUSE]
P16675	Lysosomal protective protein OS=Mus musculus GN=Ctsa PE=1 SV=1 - [PPGB_MOUSE]
Q5NC05	Transcription termination factor 2 OS=Mus musculus GN=Ttf2 PE=1 SV=2 - [TTF2_MOUSE]
A0A0G2JDI9	ATP-binding cassette sub-family D member 3 OS=Mus musculus GN=Abcd3 PE=1 SV=1 - [A0A0G2JDI9_MOUSE]
Q80ZR5	Rtf1 protein (Fragment) OS=Mus musculus GN=Rtf1 PE=2 SV=1 - [Q80ZR5_MOUSE]
Q9CTR1	Histone H2A (Fragment) OS=Mus musculus GN=H2afy2 PE=2 SV=1 - [Q9CTR1_MOUSE]
Q3UNU2	Putative uncharacterized protein (Fragment) OS=Mus musculus GN=Smc3 PE=2 SV=1 - [Q3UNU2_MOUSE]
Q7TQJ8	Wilms tumor protein 1-interacting protein OS=Mus musculus GN=Wtip PE=1 SV=1 - [WTIP_MOUSE]
Q6P1B9	Bin1 protein OS=Mus musculus GN=Bin1 PE=1 SV=1 - [Q6P1B9_MOUSE]
Q9D8Z1	Activating signal cointegrator 1 complex subunit 1 OS=Mus musculus GN=Ascc1 PE=1 SV=1 - [ASCC1_MOUSE]
P0C6F1	Dynein heavy chain 2, axonemal OS=Mus musculus GN=Dnah2 PE=1 SV=1 - [DYH2_MOUSE]
F7DFQ2	WD repeat-containing protein 26 (Fragment) OS=Mus musculus GN=Wdr26 PE=1 SV=1 - [F7DFQ2_MOUSE]
Q80UK4	MICAL-like 2 OS=Mus musculus GN=Micall2 PE=2 SV=1 - [Q80UK4_MOUSE]
A0A087WQ23	TRMT1-like protein OS=Mus musculus GN=Trmt1l PE=1 SV=1 - [A0A087WQ23_MOUSE]
Q7TNC9	Inositol polyphosphate-5-phosphatase A OS=Mus musculus GN=Inpp5a PE=1 SV=1 - [Q7TNC9_MOUSE]
A0A0A6YXK7	Centrosomal protein of 170 kDa (Fragment) OS=Mus musculus GN=Cep170 PE=1 SV=1 - [A0A0A6YXK7_MOUSE]
Q8BJY1	26S proteasome non-ATPase regulatory subunit 5 OS=Mus musculus GN=Psmd5 PE=1 SV=4 - [PSMD5_MOUSE]
Q3UQ81	Putative uncharacterized protein (Fragment) OS=Mus musculus GN=P4ha2 PE=2 SV=1 - [Q3UQ81_MOUSE]
Q8CFZ0	SUMO-conjugating enzyme UBC9 OS=Mus musculus GN=Ube2i PE=1 SV=1 - [Q8CFZ0_MOUSE]
Q8BPA1	Putative uncharacterized protein OS=Mus musculus GN=Stom PE=2 SV=1 - [Q8BPA1_MOUSE]
Q2XSQ4	TIP47 protein isoform 2 OS=Mus musculus GN=Plin3 PE=2 SV=1 - [Q2XSQ4_MOUSE]
P60670	Nuclear protein localization protein 4 homolog OS=Mus musculus GN=Nploc4 PE=1 SV=3 - [NPL4_MOUSE]
Q91ZE0	Trimethyllysine dioxygenase, mitochondrial OS=Mus musculus GN=Tmlhe PE=1 SV=2 - [TMLH_MOUSE]
Q3TGI0	Putative uncharacterized protein OS=Mus musculus GN=Xrcc1 PE=2 SV=1 - [Q3TGI0_MOUSE]
Q8K274	Ketosamine-3-kinase OS=Mus musculus GN=Fn3krp PE=1 SV=2 - [KT3K_MOUSE]
F6V4G5	Alpha-adducin (Fragment) OS=Mus musculus GN=Add1 PE=1 SV=1 - [F6V4G5_MOUSE]
Q3UGL3	Putative uncharacterized protein OS=Mus musculus GN=Clint1 PE=2 SV=1 - [Q3UGL3_MOUSE]
F7B6X4	Ataxin-2 (Fragment) OS=Mus musculus GN=Atxn2 PE=1 SV=1 - [F7B6X4_MOUSE]
Q07417	Short-chain specific acyl-CoA dehydrogenase, mitochondrial OS=Mus musculus GN=Acads PE=1 SV=2 - [ACADS_MOUSE]
Q9R0X4	Acyl-coenzyme A thioesterase 9, mitochondrial OS=Mus musculus GN=Acot9 PE=1 SV=1 - [ACOT9_MOUSE]
Q4FJY5	Ltb4dh protein OS=Mus musculus GN=Ptgr1 PE=2 SV=1 - [Q4FJY5_MOUSE]
G3X939	Sodium/hydrogen exchanger 3 OS=Mus musculus GN=Slc9a3 PE=1 SV=1 - [SL9A3_MOUSE]
P63321	Ras-related protein Ral-A OS=Mus musculus GN=Rala PE=1 SV=1 - [RALA_MOUSE]
F8VQ42	Kinesin-like protein (Fragment) OS=Mus musculus GN=Kif2a PE=1 SV=1 - [F8VQ42_MOUSE]
F7ARZ1	28S ribosomal protein S23, mitochondrial (Fragment) OS=Mus musculus GN=Mrps23 PE=1 SV=1 - [F7ARZ1_MOUSE]
Q9CSH0	Putative uncharacterized protein (Fragment) OS=Mus musculus GN=Hnrnpll PE=2 SV=1 - [Q9CSH0_MOUSE]
A0A0A6YXS8	Antithrombin-III OS=Mus musculus GN=Serpinc1 PE=1 SV=1 - [A0A0A6YXS8_MOUSE]
Q9QYB1	Chloride intracellular channel protein 4 OS=Mus musculus GN=Clic4 PE=1 SV=3 - [CLIC4_MOUSE]
A0A087WP98	Prothymosin alpha OS=Mus musculus GN=Ptma PE=1 SV=1 - [A0A087WP98_MOUSE]
Q8CDZ6	Putative uncharacterized protein OS=Mus musculus GN=Wls PE=2 SV=1 - [Q8CDZ6_MOUSE]

Q3UTB8	GrpE protein homolog OS=Mus musculus GN=Grpel1 PE=2 SV=1 - [Q3UTB8_MOUSE]
E9Q6G0	Microtubule-associated serine/threonine-protein kinase 4 (Fragment) OS=Mus musculus GN=Mast4 PE=1 SV=1 - [E9Q6G0_MOUSE]
Q3TTY6	Putative uncharacterized protein (Fragment) OS=Mus musculus GN=Lin7c PE=2 SV=1 - [Q3TTY6_MOUSE]
D3YTS3	RIKEN cDNA D630045J12 gene OS=Mus musculus GN=D630045J12Rik PE=1 SV=2 - [D3YTS3_MOUSE]
Q3TT24	Putative uncharacterized protein (Fragment) OS=Mus musculus GN=Ptprf PE=2 SV=1 - [Q3TT24_MOUSE]
Q921E4	Receptor expression-enhancing protein OS=Mus musculus GN=Reep5 PE=2 SV=1 - [Q921E4_MOUSE]
Q8BU18	Putative uncharacterized protein (Fragment) OS=Mus musculus GN=Tpr PE=2 SV=1 - [Q8BU18_MOUSE]
D3Z7P4	Glutaminase kidney isoform, mitochondrial OS=Mus musculus GN=Gls PE=1 SV=1 - [D3Z7P4_MOUSE]
B0R029	Synaptosomal-associated protein 23 (Fragment) OS=Mus musculus GN=Snap23 PE=1 SV=8 - [B0R029_MOUSE]
Q3UHM4	Putative uncharacterized protein OS=Mus musculus GN=Gm10723 PE=2 SV=1 - [Q3UHM4_MOUSE]
S4R2U9	Rho guanine nucleotide exchange factor 40 OS=Mus musculus GN=Arhgef40 PE=1 SV=1 - [S4R2U9_MOUSE]
A2A4W9	RNA-binding protein fox-1 homolog 3 (Fragment) OS=Mus musculus GN=Rbfox3 PE=1 SV=1 - [A2A4W9_MOUSE]
Q922T9	Lamp1 protein (Fragment) OS=Mus musculus GN=Lamp1 PE=2 SV=1 - [Q922T9_MOUSE]
Q3UZV3	Putative uncharacterized protein OS=Mus musculus GN=Pcsk2 PE=2 SV=1 - [Q3UZV3_MOUSE]
O88653	Ragulator complex protein LAMTOR3 OS=Mus musculus GN=Lamtor3 PE=1 SV=1 - [LTOR3_MOUSE]
P23591	GDP-L-fucose synthase OS=Mus musculus GN=Tsta3 PE=1 SV=3 - [FCL_MOUSE]
B7ZWC4	Insulin-like growth factor 2 receptor OS=Mus musculus GN=Igf2r PE=2 SV=1 - [B7ZWC4_MOUSE]
Q3UE11	Putative uncharacterized protein OS=Mus musculus PE=2 SV=1 - [Q3UE11_MOUSE]
P32020	Non-specific lipid-transfer protein OS=Mus musculus GN=Scp2 PE=1 SV=3 - [NLTP_MOUSE]
P70199	ERF1 (Fragment) OS=Mus musculus GN=Etf1 PE=2 SV=1 - [P70199_MOUSE]
D6RII3	Echinoderm microtubule-associated protein-like 1 OS=Mus musculus GN=Eml1 PE=1 SV=1 - [D6RII3_MOUSE]
Q14B70	Highly divergent homeobox OS=Mus musculus GN=Hdx PE=2 SV=1 - [HDX_MOUSE]
A0A0J9YVG0	Protein phosphatase 1G OS=Mus musculus GN=Ppm1g PE=1 SV=1 - [A0A0J9YVG0_MOUSE]
Q3U6X6	Putative uncharacterized protein OS=Mus musculus GN=Pgm2 PE=2 SV=1 - [Q3U6X6_MOUSE]
Q6A096	MKIAA0264 protein (Fragment) OS=Mus musculus GN=Mrps27 PE=2 SV=1 - [Q6A096_MOUSE]
F6XYA0	SUN domain-containing protein 1 (Fragment) OS=Mus musculus GN=Sun1 PE=1 SV=8 - [F6XYA0_MOUSE]
D3Z7B1	Run domain Beclin-1-interacting and cysteine-rich domain-containing protein OS=Mus musculus GN=Rubcn PE=1 SV=1 - [D3Z7B1_MOUSE]
P20918	Plasminogen OS=Mus musculus GN=Plg PE=1 SV=3 - [PLMN_MOUSE]
Q58EV2	Apoa1 protein OS=Mus musculus GN=Apoa1 PE=2 SV=1 - [Q58EV2_MOUSE]
Q8BRU6	Synaptic vesicular amine transporter OS=Mus musculus GN=Slc18a2 PE=1 SV=1 - [VMAT2_MOUSE]
Q9Z1Z5	Succinate dehydrogenase Ip subunit (Fragment) OS=Mus musculus GN=Sdhb PE=2 SV=1 - [Q9Z1Z5_MOUSE]
Q8K2C9	Very-long-chain (3R)-3-hydroxyacyl-CoA dehydratase 3 OS=Mus musculus GN=Hacd3 PE=1 SV=2 - [HACD3_MOUSE]
Q679P5	Histone-lysine N-methyltransferase, H3 lysine-79 specific OS=Mus musculus GN=Dot1l PE=2 SV=1 - [Q679P5_MOUSE]
A2BDX3	Adenylyltransferase and sulfurtransferase MOCS3 OS=Mus musculus GN=Mocs3 PE=1 SV=1 - [MOCS3_MOUSE]
P49182	Heparin cofactor 2 OS=Mus musculus GN=Serpind1 PE=1 SV=1 - [HEP2_MOUSE]
E9Q5Q0	Ataxin-2-like protein (Fragment) OS=Mus musculus GN=Atxn2l PE=1 SV=2 - [E9Q5Q0_MOUSE]
O09164	Extracellular superoxide dismutase [Cu-Zn] OS=Mus musculus GN=Sod3 PE=1 SV=1 - [SODE_MOUSE]
Q9CTI8	Putative uncharacterized protein (Fragment) OS=Mus musculus GN=Atp6v1d PE=2 SV=1 - [Q9CTI8_MOUSE]
Q3TUQ7	Non-specific serine/threonine protein kinase OS=Mus musculus GN=Prkaa1 PE=2 SV=1 - [Q3TUQ7_MOUSE]
B7FAT3	CDNA sequence BC005537 (Fragment) OS=Mus musculus GN=BC005537 PE=4 SV=1 - [B7FAT3_MOUSE]

P39749	Flap endonuclease 1 OS=Mus musculus GN=Fen1 PE=1 SV=1 - [FEN1_MOUSE]
D3YZE6	UDP-glucuronosyltransferase (Fragment) OS=Mus musculus GN=Ugt1a6a PE=3 SV=1 - [D3YZE6_MOUSE]
Q3TUN7	Putative uncharacterized protein OS=Mus musculus GN=Hbb-bh1 PE=2 SV=1 - [Q3TUN7_MOUSE]
D3Z7R6	Calponin OS=Mus musculus GN=Cnn2 PE=1 SV=1 - [D3Z7R6_MOUSE]
Q99JZ9	Signal recognition particle 54 kDa protein OS=Mus musculus GN=Srp54c PE=2 SV=1 - [Q99JZ9_MOUSE]
G5E850	Cytochrome b-5, isoform CRA_a OS=Mus musculus GN=Cyb5a PE=1 SV=1 - [G5E850_MOUSE]
D3YUY3	Phosphatidylinositol 4-phosphate 5-kinase type-1 alpha OS=Mus musculus GN=Pip5k1a PE=1 SV=1 - [D3YUY3_MOUSE]
Q3U617	Putative uncharacterized protein OS=Mus musculus GN=Psmd8 PE=2 SV=1 - [Q3U617_MOUSE]
D3YXG0	Hemicentin-1 OS=Mus musculus GN=Hmcn1 PE=1 SV=1 - [HMCN1_MOUSE]
E9Q8K5	Titin OS=Mus musculus GN=Ttn PE=1 SV=1 - [E9Q8K5_MOUSE]
H3BKD4	Arf-GAP with SH3 domain, ANK repeat and PH domain-containing protein 1 OS=Mus musculus GN=Asap1 PE=1 SV=1 - [H3BKD4_MOUSE]
B1AXI9	5-azacytidine induced gene 1 OS=Mus musculus GN=Cep131 PE=1 SV=1 - [B1AXI9_MOUSE]
Q8VCK2	Ctsd protein (Fragment) OS=Mus musculus GN=Ctsd PE=2 SV=1 - [Q8VCK2_MOUSE]
Q8BJ75	Putative uncharacterized protein OS=Mus musculus GN=Chd6 PE=2 SV=1 - [Q8BJ75_MOUSE]
Q920A5	Retinoid-inducible serine carboxypeptidase OS=Mus musculus GN=Scpep1 PE=1 SV=2 - [RISC_MOUSE]
E9PUC2	Long-chain-fatty-acid--CoA ligase 3 OS=Mus musculus GN=Acsl3 PE=1 SV=1 - [E9PUC2_MOUSE]
A0A087WNV6	5'-3' exoribonuclease 1 OS=Mus musculus GN=Xrn1 PE=1 SV=1 - [A0A087WNV6_MOUSE]

Supplementary Table 4 Full data lists of proteins identified in GFP-Trap® of (a) GFP-only, (b) GFP-TMEM67 full length and (c) GFP-TMEM67 ΔECL before the filtering steps used to create the double positive lists. (Lists included as separate excel files.)